LIÈGE université
GIGA

Faculty of Medicine

GIGA Neurosciences / GIGA Stem-Cells

Laboratory of the Molecular Regulation of Neurogenesis

Pr. Laurent Nguyen (Promotor)

Dr. Carla G. Silva (Co-promotor)

Microtubule post-translational modifications and their impact on axonal transport

Romain Le Bail

Academic year 2022-2023

Thesis presented to obtain the Doctorate degree in Biomedical and Pharmaceutical Sciences

Abstract

Neurons are polarized cells with a dendritic tree that specialize in receiving inputs and a long, ramified axon that conveys electrical signals. The transport of mitochondria, protein-containing vesicles, lysosomes and other organelles is essential for the maintenance of neuronal homeostasis and synaptic function. Cargoes are transported along microtubules (MTs) by molecular motors and alterations to their motility are associated to neurological disorders. In the last years, the "tubulin code" concept emerged, referring to the role of MT posttranslational modifications (PTMs) in cellular function. PTMs, such as acetylation and polyglutamylation can change the properties of intracellular transport, subsequently altering the properties of synaptic communication and neuronal circuit function. Since the enzymes performing PTMs are cell-type and developmental stage-dependent, it is essential to consider these aspects when exploring the functional and physiological significance of PTMs. In my doctoral work I used several experimental models, notably the fly and the mouse to explore how MT acetylation and polyglutamylation modulate neuronal transport and how alterations in these PTMs perturbs cellular function. I contributed to several research projects exploring the molecular regulation of MT acetylation and developed the project exploring the functional consequences of hyperglutamylation in interneurons.

We found that αTAT1, the enzyme catalyzing microtubule acetylation, is required for physiological axonal transport in neurons. We further demonstrate that αTAT1 is transported at the cytosolic side of vesicles and uses acetyl-CoA mainly produced by a vesicular pool of ATP-citrate lyase (Acly) to catalyze microtubule acetylation. These results reinforce the link between MT acetylation and the regulation of axonal transport and suggest that cargoes modulate MT acetylation by delivering αTAT1 and its substrate acetyl-CoA.

We also demonstrate that parvalbumin (PV) interneurons (INs) of the hippocampus are hyperglutamylated following the loss of cytosolic carboxypeptidase A (CCP1), an enzyme that catalyzes the removal of polyglutamate side chains from tubulin. Hyperglutamylation of PV INs is associated with transport defects *in vitro* and a reduction of inhibitory synapses and miniature inhibitory post-synaptic currents in the adult mice. Our results demonstrate that CCP1 loss is sufficient to induce hyperglutamylation and circuitry alterations in a subtype of hippocampal interneuron.

Together, these studies improve our understanding of the mechanisms that underlie MT acetylation and extend the scope of neuronal subtypes sensitive to CCP1 loss and hyperglutamylation. Since hyperglutamylation is strongly associated with neurodegeneration, deciphering the dynamics of polyglutamylation in a neuron subtype dependent manner might lead to the discovery of treatments to rescue the function of specific types of neurons.

Résumé

Les neurones sont des cellules polarisées avec un arbre dendritique spécialisé dans la réception de signaux et un long axone ramifié qui transmet les signaux électriques. Le transport des mitochondries, des vésicules contenant des protéines, des lysosomes et d'autres organelles est essentiel au maintien de l'homéostasie neuronale et de la fonction synaptique. Les cargos sont transportés le long des microtubules (MT) par des moteurs moléculaires et des altérations de leur motilité sont associées à des troubles neurologiques. Au cours des dernières années, le concept de « code de la tubuline » a émergé, faisant référence au rôle des modifications post-traductionnelles (PTM) des MTs dans la fonction cellulaire. Les PTMs, telles que l'acétylation et la polyglutamylation, peuvent modifier les propriétés du transport intracellulaire, altérant ainsi les propriétés de la communication synaptique et la fonction du circuit neuronal. Étant donné que les enzymes catalysant les PTMs dépendent du type de cellule et du stade de développement, il est essentiel de prendre en compte ces aspects lors de l'exploration de la signification fonctionnelle et physiologique des PTMs. Dans mon travail de doctorat, j'ai utilisé plusieurs modèles expérimentaux, notamment la mouche et la souris, pour explorer comment l'acétylation et la polyglutamylation des MTs modulent le transport neuronal et comment les altérations de ces PTMs perturbent la fonction cellulaire. J'ai contribué à plusieurs projets de recherche explorant la régulation moléculaire de l'acétylation de la MT et développé le projet explorant les conséquences fonctionnelles de l'hyperglutamylation dans les interneurones.

Nous avons découvert qu'αTAT1, l'enzyme catalysant l'acétylation des microtubules, est nécessaire pour le maintien du transport axonal physiologique dans les neurones. Nous démontrons en outre qu'αTAT1 est transporté du côté cytosolique des vésicules et utilise l'acétyl-CoA principalement produit par un pool vésiculaire d'ATP-citrate lyase (Acly) pour catalyser l'acétylation des microtubules. Ces résultats renforcent le lien entre l'acétylation des MTs et la régulation du transport axonal et suggèrent que les cargos modulent l'acétylation des MTs en délivrant αTAT1 et son cofacteur acétyl-CoA.

Nous démontrons également que les interneurones (IN) à parvalbumine (PV) de l'hippocampe sont hyperglutamylés suite à la perte de la carboxypeptidase cytosolique 1 (CCP1), une enzyme qui catalyse l'élimination des chaînes latérales de polyglutamate de la tubuline.

L'hyperglutamylation des INs PV est associée à des défauts de transport *in vitro* et à une réduction des synapses inhibitrices et des courants post-synaptiques inhibiteurs miniatures chez les souris adultes. Nos résultats démontrent que la perte de CCP1 est suffisante pour induire une hyperglutamylation et des altérations des circuits dans un sous-type d'interneurone hippocampique.

Ensemble, ces études améliorent notre compréhension des mécanismes qui sous-tendent l'acétylation des MTs et élargissent le spectre des sous-types neuronaux sensibles à la perte de CCP1 suivie d'hyperglutamylation. Étant donné que l'hyperglutamylation est fortement associée à la neurodégénérescence, déchiffrer la dynamique de la polyglutamylation d'une manière dépendante du sous-type neuronal pourrait conduire à la découverte de traitements pour restaurer la fonction de types spécifiques de neurones.

Acknowledgments

I would first like to thank the members of my thesis committee who accompanied throughout this journey and provided critical feedback during the rapidly changing landscape of my PhD: **Stéphane Schurmans, Brigitte Malgrange, Denis Mottet, Bernard Rogister**. It must have been surprising to discover a new project almost every year but I am thankful for your guidance and support. I extend special thanks to Bernard Rogister, president of the thesis committee**,** for the help you provided at every step of the thesis program**.** I would also like to thank my external jury members, **Carsten Janke and Patrik Verstreken,** for kindly taking the time to read my manuscript and taking part in the thesis defense. I would like to highlight that the work of the laboratory of Carsten Janke has been at the foundation of the project on which I worked for the last years and lit our way as we were building the project. Thank you for that, for providing some of the tools for this project and for your critical advice during our few interactions.

These past years have been an amazing personal and professional adventure that made me grow as a scientist but also as a person. The time I spent here was so beneficial only because of the great people I have met along the way.

Thank you **Laurent** for accompanying me for the past 6 years from the master to this day. I was given the freedom to explore many different projects and you often helped me find the way when my work tended to branch out a bit too much ! If I think back on my early years as a PhD student, I realize that you successfully made me grasp that biology and the brain in all their complexity can only be described as “shades of grey” as you often reminded me when I tended to interpret data in a binary fashion. Thank you also for giving me the opportunity to attend conferences, the amazing stem-cell course in Venice and travel to the laboratory of Silvia Cappello for a month, those helped me feed my curiosity for the various fields of Neuroscience that I explored during my PhD. Thank you also to **Carla** without whom the CCP1 project would have never taken flight. You set the foundation for this work and kindly offered me to work with you when my previous project fell apart. I am extremely thankful for the trust you gave me at the time and even more so for all the time you have invested in mentoring me while still performing some experiments for the project. I learnt a lot from you, especially that during the exploratory phase of a project, what seems like a shot in the dark

may turn out to be an amazing discovery. I remain impressed by your ability to build projects, your unlimited curiosity and tenacity in the face of adversity. I like to think that with all the problems that we had with the project, I managed to develop a bit of this tenacity myself !

The last year of the PhD was not easy since we were finally getting somewhere but were running out of time. Thank you **Ira,** for giving me the opportunity to continue the adventure a bit longer and finish some crucial experiments that tied the story together. You did not only allow me to continue my PhD but you also welcomed me in your own team with **Mathilde** and **Gérald** where I took a lot pleasure in working with organoids again. Special shoutout to Mathilde for the long afternoons we spent together live-imaging transport or calcium oscillations. The time was passing very fast with the stimulating conversations with you and I loved playing a little part in your project. I will remember for a long time the hours we spent staring at the screen, convincing ourselves we just saw a cell blinking until we finally managed to observe beautiful calcium oscillations ! I am sure you will do great, you have the mindset and persistence required to succeed as a PhD student and I wish you all the luck in the future.

The hippocampal electrophysiology experiments would not have been possible without the considerable efforts of **Dominique.** Thank you so much for taking the time to participate in this project. You are a master of your craft and I felt that I could rely completely on your expertise. I felt like you needed to know about the project to understand where your experiments fit and I loved sharing our results and progress with you which often led to stimulating conversations. Thank you also for your consistent positive attitude and smile which contributed in making this experience great. Although the hard work of **Bernard L.** is not displayed in the results of the thesis, he dedicated a giant of time to heroically perform behavioral experiments and generate plasmids. The results did not turn out as we had hoped but I want to thank you sincerely for all your time and efforts. I also particularly enjoyed our conversations and the few beers we shared. You are truly a kind hearted person and I always felt like you were looking out for me, Silvia and all the students that pass by your office ! Thank you for your positive attitude and the occasional pep talk !

The optogenetic experiments were only possible thanks to the contribution of **Jean-Bernard Manent** and his talented post-doc **Delphine Hardy** who worked tirelessly when receiving batches of electroporated animals to ensure that all experiments were done in a few days.

Thank you very much for taking part in this project and for your great contribution that gave me confidence in the results I had acquired before. I believe this is a start of a very interesting project and I am curious to see which direction it will take.

My master thesis and the beginning of my PhD were probably the most stimulating time in my life and I owe this in great part to the mentoring of **Ivan.** I wouldn't be the same person today if hadn't crossed your path and I'm extremely thankful for all the science and life lessons you've given me (and continue to give me …). You are probably one of the kindest hearted person I met, with an altruism that rivals the most accomplished monks. The amount of time you've given me, simply taking out for yourself the pleasure to help someone is unbelievable. Thank you also **Giovanni** who taught me everything I know about fly work and axonal transport. You played the role of both a friend and a supervisor for the acetylation projects and I am truly thankful for the time we've had working together. I would also like to thank **Christian** for working with me in the early days of my PhD thesis before we had to change project. I learnt a lot from you and will remember fondly our philosophical conversations in Ivan's office at night.

All the friends who joined the GIGA Neuroscience with me or that I met along the way transformed the last years to make it the great experience that it was. Shoutout to **Fanny** and **Ron** the wonder couple, we met 11 years ago and sailed the tumultuous waters of university years together. It was a great adventure and I will cherish the time we spent together. Thank you Fanny for the times when you truly helped me stay afloat when the boat was sinking ! Although I came to Belgium a long time ago, the French touch was never very far with the unique and amazing **Lucas**. We spent a long time not knowing each other until you invited me to share some crisps on a fateful day at the Boverie park ! Since then we spent a lot of time there together, or cycling about or just hanging out. You were truly a best friend and confident and it has been hard to adjust to your return to the homeland but it was only difficult because of how great the time we spent together was. I hope we will manage to keep seeing each other on occasions, I count on you to bring me on a sailing trip as soon as you are a captain. The french team wouldn't be complete without **Julie** who brings her smile, positive attitude and desire to help every day at the lab. Thank you for being such a good friend, I hope we have many other dinners and adventures to come ! Thank you also to **Sébastien** for all the great analytical conversations and the support throughout the thesis. Finally, a big thank you

to **Cyrine, Bilal, Margaux, Badr, Laurence, Nathalie, Sofian** and all the others who made every day fun at the lab !

Although I have been working in the laboratory of Laurent for 6 years, I have been sharing my office with the laboratory of neuroendocrinology of **Julie B.** The reason takes root in history since as Julie eloquently put sit I have become “part of the furniture” since I first joined the GIGA Neuroscience as a research student in 2015. Thank you Julie for welcoming me in the lab and providing me with my first research experience but also for all the conversations and laughs that we had over the last years. You have helped amplify my love for cycling and taught me a lot, it was a pleasure to be part of your office furniture ! A big thank you to **Sonia, Vini, Yassine, Jessica** and **Vincent H.** with whom I have shared the office for many years. The day was punctuated and made better by all our little interactions ! Hang on tight Sonia, your time will come too, you have shown so much resilience in these past years and you truly deserve to make it to the end. I wish you all the best Vini, thank you for all your wise advice, you have been my neuro endocrinology consultant and a great friend, I can’t wait to see what is next on your scientific journey and I am sure you will do great ! Thank you also to the **Cornil lab, and** in particular to **Charlotte, Jacques, Catherine** and **Delphine,** I often relied on you when statistics were over my head and you have always been willing to give me some time for my neuro-endocrinology questions.

A big thank you to all my lab mates **Laura, Antonela, Miriam, Jolien, Nico, Martin, Max, Sylvia, Nath, Bernard C., Sophie, Loic…** I think one defining characteristic of the Nguyen lab is the close relationship between its members. Thank you for all being such great team players and for creating the great work atmosphere that we have had. We lost a little bit of sunshine in our days when you left the lab Laura but I am very happy that you found your way and I am sure you will do great ! It was pleasure to work with you Antonela, you are the true organoid wizard and I will remember for a long time when you showed me your first movies of migrating interneurons from assembloids ! Congrats for all you have accomplished and thank you for sharing some of it with me ! Thank you Miriam for all the good moments we’ve spent at the lab or elsewhere, if I think about it, when you first got your cat (won’t say the name here it would be confusing in this sentence), I think it was the catalyst that convinced Silvia to do the same… So you can also take credit for that too ! I had a great time sharing a few years at the lab with you Jolien ! It was truly special and I will remember it fondly. The way you

managed to take a turn in your PhD and succeed through pure grit was inspiring to me and you deserve everything you got ! It was a pleasure to work with you in the stem cell lab Bernard. I was still figuring stuff out at the time but I feel like I have learnt a lot from your organizational skills. Your hard work and dedication are inspiring ! Thank you also to Nath for all the little things you have done in these many years, from taking care of the flies, to helping with plasmids and orders. You have made every day a bit easier and provided us with amazing experiences through your outstanding skills in lab retreat organization ! I would like to write a little paragraph for each of you but I realize that the page count on this thing is increasing rapidly and so I will deliver some of my thoughts face to face !

Il y a des gens au GIGA Neuroscience sur qui on peut toujours compter lorsqu'on a besoin d'aide. Ce ne serait vraiment pas la même chose sans vous **Lari, Jess, Alex, Laurent M. and PB.** Merci pour m'avoir aidé à chaque étape et pour faire en sorte que tout fonctionne correctement dans notre petite communauté. Merci aussi pour vos efforts qui font du GIGA Neuro un endroit où il fait bon vivre grâce à vos talents de pâtisserie entre autres. Alex, tu m'as beaucoup appris et a fait que le laboratoire d'histologie était toujours un endroit dans lequel j'aimais travailler grâce à ta remarquable attention pour l'organisation et ton attitude positive. Comme Vincent S. l'a dit, nous serions perdu sans Laurent M. et en effet ça aurait été mon cas. Tu m'as aidé d'innombrables fois lorsque j'avais besoin d'un outil particulier ou que les électrodes d'électroporation étaient cassées pour la énième fois ! Merci d'avoir été aussi disponible et toujours prêt à aider.

J'ai passé des jours à la **plateforme d'imagerie** et j'ai toujours été bien accueilli et aidé par son équipe. Merci à **Sandra, Alexandre** et **Gaëtan** pour votre travail qui nous permet de bénéficier des derniers outils disponibles et maintenus dans un parfait état. Merci spécialement à Alexandre et Gaëtan pour toutes les fois où vous m'avez dépanné au microscope et les bons conseils que vous m'avez fourni au cours de ces dernières années.

J'ai aussi eu la chance de bénéficier d'un super slide scanner et de toute l'aide dont j'avais besoin grâce à **Didier Cataldo** et son équipe, en particulier **Fabienne** et **Damien.** Merci pour tout le temps que vous m'avoir donné accès à votre équipement et pour tout le temps que vous m'avez accordé.

Les jours que j'ai passé au Cyclotron avec **Mohamed** ne sont pas reflétés dans la thèse car malheureusement nous n'avons pas réussi à faire marcher ces expériences mais ce n'était pas faute d'avoir essayé. Merci beaucoup pour ta persistance Mohamed et pour tous les moments que nous avons partagé à deux, j'ai beaucoup appris !

Un grand merci à ma **famille** pour m'avoir soutenu pendant toute la thèse mais aussi avant… Je ne serais pas arrivé jusque-là sans vous. Merci **Maman** pour avoir souvent fait l'effort de prétendre être intéressée par mes expériences et pour m'avoir remonté le moral quand ça ne se passait pas comme prévu. Merci P**apa** d'avoir été toujours disponible pour discuter quand j'en avais besoin. On a passé de belles aventures pendant ma thèse et d'autres à venir ! Merci aussi à toute ma famille qui a supporté mes monologues sur les organoïdes à Noël et à ma **Mamie** pour s'être toujours souciée de l'avancement de ma thèse !

I kept the best for the end and I dedicate this paragraph to **Silvia**. You've been my pillar for the last 4 years, made every tough moment bearable and every other moment a great memory. You are a model of hard work, dedication and an inspiration. But most importantly you have an infectious enthusiasm with which you lighten every room you enter. I feel very lucky to have met you and I'm looking forward to the following years together. Thank you for being yourself, you make me happy.

List of abbreviations

AAV	Adeno-associated virus
Acetyl-CoA	Acetyl coenzyme A
ACLY	ATP-citrate lyase
ACSS2	acyl-CoA synthetase short-chain family member 2
AD	Alzheimer's disease
ALS	Amyotrophic lateral sclerosis
ASD	Autism spectrum disorder
BC	Basket cell
BMP	Bone morphogenic protein
BSA	Bovine serum albumin
CA	Cornu Ammonis
CCP	Cytosolic-carboxypeptidase
CGE	Caudal ganglionic eminence
CH	Cortical hem
ChR2	Channel rhodopsin 2
cIN	cortical interneuron
cKO	conditional knockout
CLIP	cytoplasmic linker protein
CNS	Central nervous system
CSP	Cysteine string protein
DG	Dentate gyrus
DMSO	Dimethyl sulfoxide
DNE	Dentate neuroepithelium
DP	Dorsal pallium
EC	Entorhinal cortex
EPSC	Excitatory post-synaptic current
FD	Familial Dysautonomia
GAPDH	Glyceraldehyde-3-phosphate dehydrogenase
GFP	Green fluorescent protein
HD	Huntington disease
HDAC6	Histonde deacetylase 6
hIPSC	Human induced pluripotent stem cells
HRP	Horseradish peroxidase
I-LTD	Inhibitory long-term depression
IN	Interneuron
KD	Knockdown
KO	Knockout
L2/3	Layers 2 and 3
LGE	Lateral ganglionic eminence
LP	Lateral pallium
LPP	Lateral perforant pathway
MAP	Microtubule-associated protein
MCAK	Mitotic-centromere associated
mcm^5	5-methoxycarbonylmethyl
MEF	Mouse embryonic fibroblast
MGE	Medial ganglionic eminence

MIP	Microtubule inner protein
mIPSC	Miniature inhibitory post-synaptic current
MLCK	Myosin light-chain kinase
MP	Medial pallium
MPP	Medial perforant pathway
MT	Microtubule
NAP	Nucleosome assembly protein
ncm^5	5-carbamoylmethyl
NHE	Hippocampal neuroepithelium
NMJ	Neuro-muscular junction
OCT	Optimal cutting temperature
p27	$p27^{kip1}$
Pcd	Purkinje cell degeneration
PCR	Polymerase chain reaction
PDH	Pyruvate dehydrogenase
PFA	Paraformaldehyde
PLA	Puromycin-ligation assay
PN	Pyramidal neuron
PNS	Peripheral nervous system
PP	Perforant pathway
PTM	Post-translational modification
PV	Parvalbumin
RNAi	RNA interference
SIRT2	Sirtuin 2
SO	Stratum oriens
SP	Stratum pyramidale
SRL	Stratum radiatum/lacunosum
SST	Somatostatin
SVP	Synaptic vesicle precursor
SVZ	Sub-ventricular zone
TBA	Tubastatin A
TIRK	Total internal reflection fluorescence
TRN	Touch receptor neuron
TSA	Trichostatin A
TTL	Tubulin-tyrosine ligase
TTLL	Tubulin-tyrosine ligase-like
TTX	Tetrodotoxine
U34	Uridine 34
UPR	Unfolded protein response
VASH	vasohibin
VGAT	Vesicular GABA transporter
VNC	Ventral nerve cord
VP	Ventral pallium
VZ	Ventricular zone
WFA	Wisteria floribunda lectin
Wnt	Wingless/Int
WT	Wild type
αK40	α-tubulin lysine 40
αTAT	α-tubulin N-acetyltransferase

Table of contents

INTRODUCTION

The human brain is a fascinating structure, made of about 86 billion neurons, which together compute electrical signals to allow us to sense, think and act. Neurons connect in complex ways through synapses and sometimes over long distances to set up networks that enable all brain functions. Neurons in the brain are diverse and rely on multiple finely tuned processes to maintain their homeostasis and to provide the characteristic plasticity of brain networks.

Neurons are polarized structures displaying dendrites which receive inputs from other neurons and the axon that projects over long distances to convey electrical signals. Dendrites emerge from the cell-body in a tree-like fashion while the single axon can develop remarkable complexity to create synaptic connections with thousands of other neurons. The morphological polarization of neurons also extends to the intracellular makeup of each compartment. Protein synthesis is mainly restricted to the cell body, except for local mRNA translation which occurs for specific proteins in the dendrites and in the axon. The cytoskeleton also exhibits molecular signatures specific to its compartment. This compartmentalization is essential to provide neurons with the ability to function as input/output units but also raises the need for a cellular machinery that enables efficient exchanges of cargoes from one compartment to another.

Microtubules (MTs) are dynamic, polarized structures with a +end and a -end and they serve as “rails” for intracellular transport. Cargoes are carried along MTs by molecular motors which use ATP to fuel bidirectional transport over long distances (Vallee, McKenney and Ori-Mckenney, 2012; Qin *et al.*, 2020). Kinesins are the motors responsible for the transport towards the +end while dynein carries cargoes towards the -end of MTs. In the axons, MTs are oriented +end out and therefore, kinesins mediate anterograde transport away from the cell soma while dynein carry cargoes in the retrograde direction, towards the cell soma. In dendrites however, the polarity of MTs is mixed and consequently both the anterograde and retrograde transport are mediated by both types of motors (Baas *et al.*, 1988; Kapitein *et al.*, 2010; Yang *et al.*, 2019) **(Figure 1 A)**.

Distance is not the only challenge for axonal transport since specific cargoes also have specific transport requirements. Anterograde transport typically carries cargoes such as newly synthesized proteins that need to be delivered to their final compartment, RNA for fueling local translation or organelles such as mitochondria to distribute energy at specific sites.

Conversely, retrograde transport is typically involved in the transport of acidic organelles for the degradation and recycling of molecular components or the transport of signaling molecules from neurites to the cell body to inform the cell on its environment (Cosker and Segal, 2014; Cason and Holzbaur, 2022) **(Figure 1 C)**.

To achieve cargo-specific delivery to appropriate sites, neurons rely on a complex regulation machinery that combines: **1)** Cargo-specific motors and adaptor proteins; 2**)** MT diversity in its elementary units, tubulins, together with chemical modifications named post-translational modifications (PTMs), constitute the "tubulin code", which can fine-tune motor motility to ensure adequate spatial and temporal delivery of cargoes **(Figure 1 B-C)**.

The aim of my doctoral work is to increase our understanding of MT PTMs and how they contribute to intracellular transport and thereby neuronal function. Therefore, in this introduction, I will especially focus on the tubulin code with an emphasis on the role of several PTMs in neuronal trafficking.

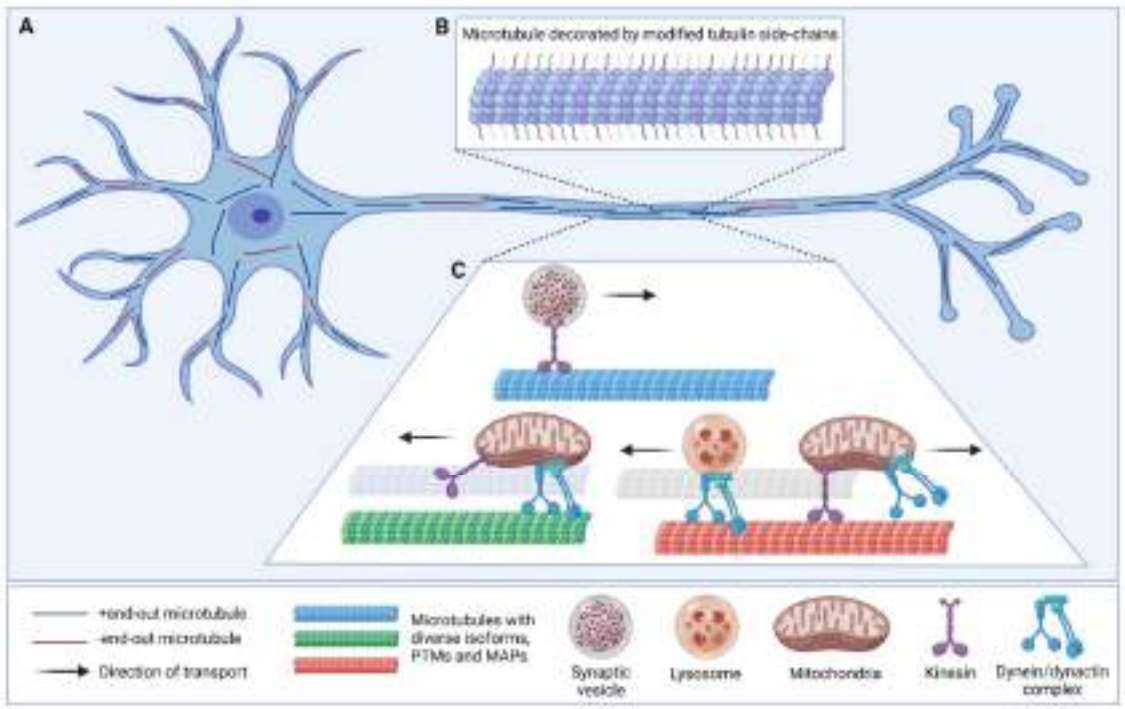

Figure 1: Overview of microtubule diversity and axonal transport
A. Microtubules (MTs) are polarized structures and are typically oriented with the +end facing away from the soma in axon whereas they have a mixed polarity in dendrites.

B. The C-terminal tail of tubulin protrudes from the microtubule lattice and is modified by several post-translational modifications (PTMs) that generate extensive MT diversity which subsequently tunes MT function.
C. Cargos are transported on MTs by molecular motors. Kinesins transport cargos from the -end to the +end while dynein moves from the +end to -end. The concept of "tubulin code" postulates that MTs are diverse due to their tubulin isoform makeup, the PTMs they harbor, and the microtubule associated proteins they bind to. The molecular diversity of MTs is essential for the regulation of transport. Lysosomes, synaptic vesicles, mitochondria and other cargos are transported along MTs to maintain neuronal homeostasis and synaptic function.

1. MTs are the "rails" of axonal transport

MTs are highly evolutionary conserved cytoskeletal structures that provide and maintain the polarized morphology of neurons but also serve other critical functions in the brain. These tubulin polymers are involved in neuronal motility during migration, the segregation of homologous chromosomes during mitosis and serve as the substrate for intracellular transport. The versatility of MTs is made possible by their dynamic nature (Akhmanova and Steinmetz, 2015), their remarkable functional specialization via the "tubulin code" (Janke and Magiera, 2020) and their interaction with MT-associated proteins (MAPs) .

1.1 MT structure and dynamics

MTs are polymers containing α and β tubulin heterodimers, which together form a hollow tubular structure of about 25nm diameter. Since α/β tubulin heterodimers polymerize in a head-to-tail fashion, MTs are intrinsically polarized with β tubulin at the +end and α tubulin at the – end. Soluble heterodimers bound to GTP on the β-tubulin monomer are added to the +end of MTs to drive polymerization. β-tubulin monomers included to the MT lattice briefly maintain their GTP, thus forming a stabilizing GTP-cap at the +end through conformational changes in α-tubulin. GTP is progressively hydrolyzed so that most of the MT polymer is composed of GDP α/β heterodimers except for the GTP-cap at the +end. GDP α/β heterodimers are less stable than their counterpart and exert forces on the MT lattice that eventually lead to a depolymerization event known as "catastrophe" (Mitchison and Kirschner, 1984; Desai and Mitchison, 1997). During catastrophe, MTs quickly depolymerize and can, in some circumstances, be rescued to stabilize the MT and prevent

depolymerization. Rescue may be induced by "GTP islands" within the MT lattice where GTP-bound β monomers remain and therefore stabilize the lattice or they may be rescued by MAPs (Dimitrov *et al.*, 2008). The cycle of polymerization/depolymerization of MTs is termed "dynamic instability" and enables rapid remodeling of the cytoskeleton (**Figure 2**).

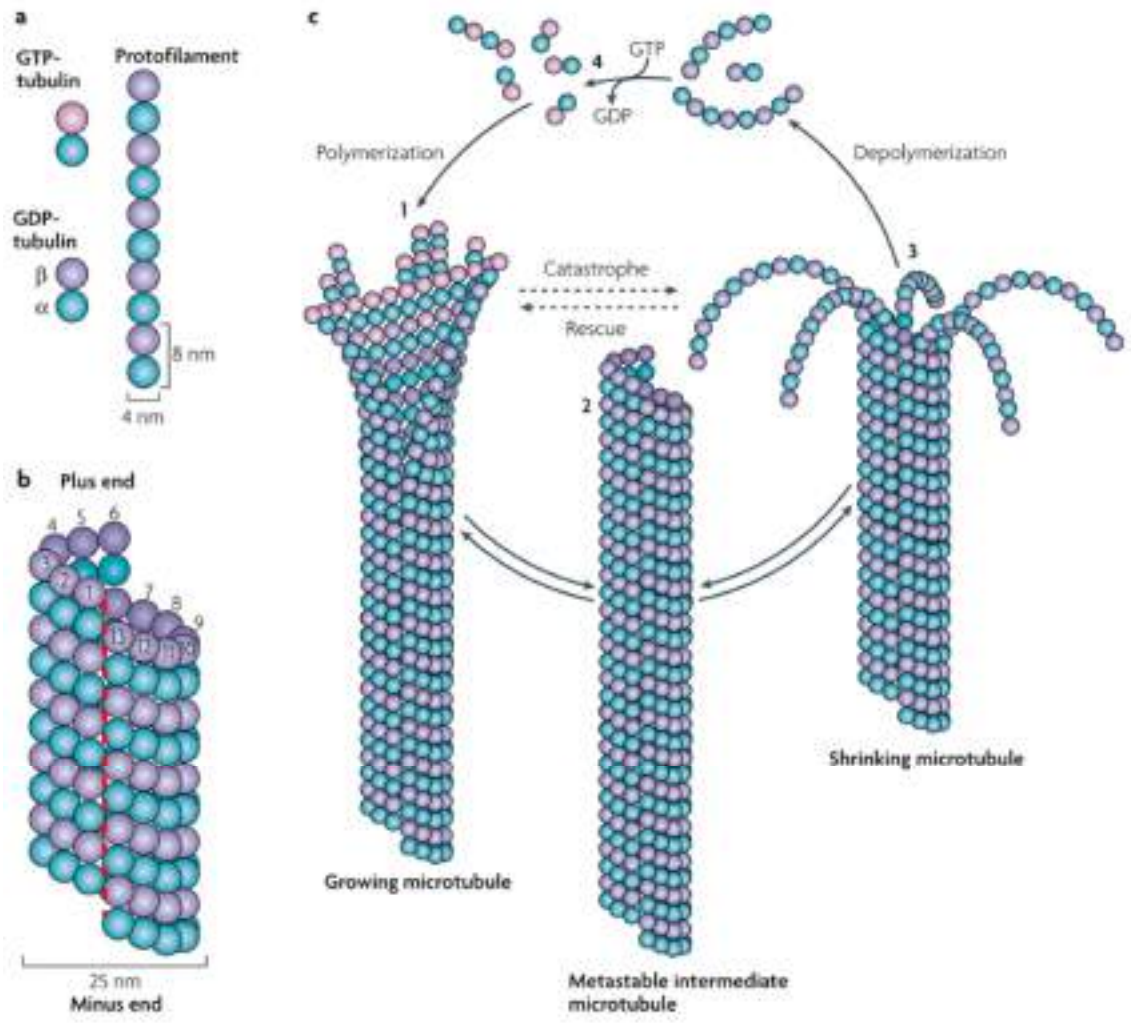

Figure 2: MT structure and dynamic instability
A. Protofilaments are formed by the head-to-tail addition of α/β heterodimers.
B. MTs in mammalian cells are typically made of 13 parallel protofilaments.
C. Schematic representation of MT dynamic instability.
Figure adapted from (Akhmanova and Steinmetz, 2008).

1.2 The multifaceted roles of microtubule associated proteins

MAPs are organizers of the MT network and the diversity within this family of protein reflects their multiple functions within cells **1)** Structural MAPs regulate the polymerization,

stabilization and bundling of MTS (Bodakuntla *et al.*, 2019); **2)** Enzymatic MAPs sever or depolymerize MTs (McNally and Roll-Mecak, 2018); **3)** End-binding MAPs help in MT guidance, MT attachment, MT stabilization and signaling (Akhmanova and Steinmetz, 2015); **4)** Motor proteins are MAPs that generate the forces that drive intracellular transport (Cason and Holzbaur, 2022).

Microtubule plus-end tracking proteins (+TIPs) bind to the GTP-cap at the growing + end of MTs. The end-binding (EB) protein family can be used to track the growing +end of MTs and interact with various other players to regulate the MT network (Xia *et al.*, 2014). For instance, +TIPs proteins such as cytoplasmic linker protein (CLIP) CLIP-170 and the large subunit of dynactin (p150Glued) both bind to EBs promote MT stability and can rescue catastrophes (Komarova et al., 2002; Lazarus et al., 2013). Interaction of EBs with actin or other cytoskeletal elements can also guide MT growth. Spectraplakins are a family of actin-MT linker proteins that regulate axonal growth. EB1 binds to spectraplakins to promote axonal growth through directed MT polymerization (Alves-Silva *et al.*, 2012).

MT-severing enzymes such as spastin and katanin can release MTs from neuronal centrosome to promote axonal growth (Ahmad *et al.*, 1999). Spastin mutations have also been linked to axonal transport defects with accumulation of cargoes in axonal swellings (Kasher *et al.*, 2009). Interestingly, structural MAPs such as MAP2 and tau can also inhibit microtubule severing, potentially by covering the surface of MTs and preventing access to katanin (Qiang *et al.*, 2006).

Structural MAPs such as MAP2, MAP1B and tau appear to stabilize MTs (Takemura *et al.*, 1992). More recently, it was shown that tau dynamically binds to the MT lattice (Janning *et al.*, 2014) and seems to enable labile domains on MTs (Qiang *et al.*, 2018). Doublecortin (DCX), a neuronal MAP helps in stabilizing MTs into 13 protofilaments structure, which may explain the highly consistent number of protofilaments in cells (Fourniol *et al.*, 2010). DCX is particularly expressed in migrating neurons and mutations in this gene can lead to lissencephaly, through the disruption of neuronal migration and axonal outgrowth (Gleeson *et al.*, 1999; Bahi-buisson *et al.*, 2013). Interestingly, structural MAPs can also affect intracellular transport, as overexpression of tau can induce “road blocks” and impair transport

(Ebneth *et al.*, 1998; Mandelkow, 2003). Consequently, downregulation of tau can prevent axonal transport defects in mouse models of Alzheimer's disease (Vossel *et al.*, 2010).

Finally, the drivers of intracellular transport are MAPs which use ATP to induce conformational changes that drive movement along MTs (Vallee, McKenney and Ori-Mckenney, 2012; Qin *et al.*, 2020). Kinesins are a superfamily of 44 proteins in humans and are classified according to their similarity into 14 subclasses (Cason and Holzbaur, 2022). In this introduction, I will mainly focus on the role played by kinesin-1 (KIF5A, KIF5B, KIF5C) and kinesin-3 family members (KIF1A, KIF1B, KIF13, KIF6B) (Cason and Holzbaur, 2022). Dynein 1 on the other hand single handedly carries cargoes towards the -end, albeit with the help of adaptor proteins that vary from one cargo to another (Reck-Peterson *et al.*, 2018). Interestingly, some kinesins preferentially localize to dendrites (KIF17, KIF13A) or axons (KIF5C, KIF13B) and some kinesins are specific to particular cargoes (Chen *et al.*, 1992; Trinczek *et al.*, 1999; Cason and Holzbaur, 2022).

1.3 Cargo delivery mediated by MT organization

In some instances, the structure and dynamics of MTs can influence intracellular transport and play a key role in the delivery of specific cargoes to cellular sub-compartments. Interestingly, the +end of MTs is almost always oriented away from the cell soma in axons and consequently, anterograde transport is driven by kinesins and retrograde transport by dynein in this compartment. In hippocampal neuron dendrites however, the proximal region shows a mixed distribution of MT polarity with only half of +ends pointing away from the cell soma (Baas *et al.*, 1988). Interestingly, the mixed polarity of MTs in dendrites may contribute to cargo-specific delivery in this sub compartment (Kapitein *et al.*, 2010). Indeed, KIF5 and KIF17 predominantly target cargoes to the axon whereas dynein selectively drives cargoes into dendrites. Inhibition of dynein consequently impairs the dendritic localization of AMPA receptors (Kapitein *et al.*, 2010). The density of MTs also plays an important part in the regulation of axonal transport. Synaptic vesicle precursors (SVPs) transported in the retrograde direction tend to pause when they reach the -end of MTs. The duration of pauses is inversely correlated with the density of MT tracks, suggesting that a higher number of MTs increases the efficiency of transport by enabling SVPs to switch tracks more rapidly after reaching a -end (Yogev *et al.*, 2016).

In addition to setting molecular transport directionality, MT polarity influences transport by modifying the affinity of specific motors at + and -ends. KIF5 has been shown bind more strongly to GTP-bound tubulin in MTs, whether on +ends or GTP islands within the MT lattice (Nakata *et al.*, 2011). In addition, motors can modify the tracks on which they travel to subsequently regulate their motility. KIF5 triggers allosteric conformational changes in GDP-tubulins to increase their resemblance with GTP-tubulin which stabilizes and straightens MTs. Additionally, MTs modified by the run of KIF5 show improved binding affinity for the next KIF5 motors (Peet, Burroughs and Cross, 2018; Shima *et al.*, 2018). This mechanism may contribute to the preference of KIF5 for specific cellular sub-compartments since KIF5 may promote the preferential attachment of other KIF5 motors to the same MT tracks (Jacobson, Schnapp and Banker, 2006). Contrary to KIF5, KIF1A shows a low binding affinity for GTP-rich MT +ends which tends to lead to the pausing of the cargo it carries (Guedes-Dias *et al.*, 2019). The distribution of MTs and affinity of molecular motors for +ends may therefore contribute to the spatiotemporal delivery of cargoes. Along this line, *en passant* synapses exhibit an enrichment in MTs +ends bound to GTP, which enables SVP delivery to these sub-compartments, carried by KIF1A. Conversely, LAMP1+ late endosomes-lysosomes carried by KIF5 or KIF1C do not pause at *en passant* synapses. Of note, a disease-causing mutation of KIF1A results in a higher affinity of this motor to MT +ends which subsequently impairs the delivery of SVPs to presynaptic sites and reduces synaptic efficiency (Guedes-Dias *et al.*, 2019).

2. Tubulin isotypes in the brain

2.1 Diversity and cell-type specificity of tubulin isotypes

One element of the tubulin code that contributes to MT diversity is the expression of various α- and β- tubulin isotypes with slight differences in their primary amino acid sequences. The expression of tubulin isotypes is tissue-dependent and contributes to the versatility of MT functions.

In MTs, the C-terminal tail of tubulin monomers protrudes from the lattice and is susceptible to modifications by PTMs and interaction with MAPs. Although the percentage of identity between tubulin isotypes is very high, the C-terminal tail is a hotspot for amino acid changes

and therefore confers different opportunities for regulation by PTMs depending on the tubulin isotypes (Khodiyar *et al.*, 2007; Sirajuddin, Rice and Vale, 2014), (**Figure 3**). At least 9 α-tubulin isotypes and 9 β-tubulin isotypes have been described in mammals and show remarkable conservation across evolution (see the nomenclature here: https://www.genenames.org/data/genegroup/#!/group/778).

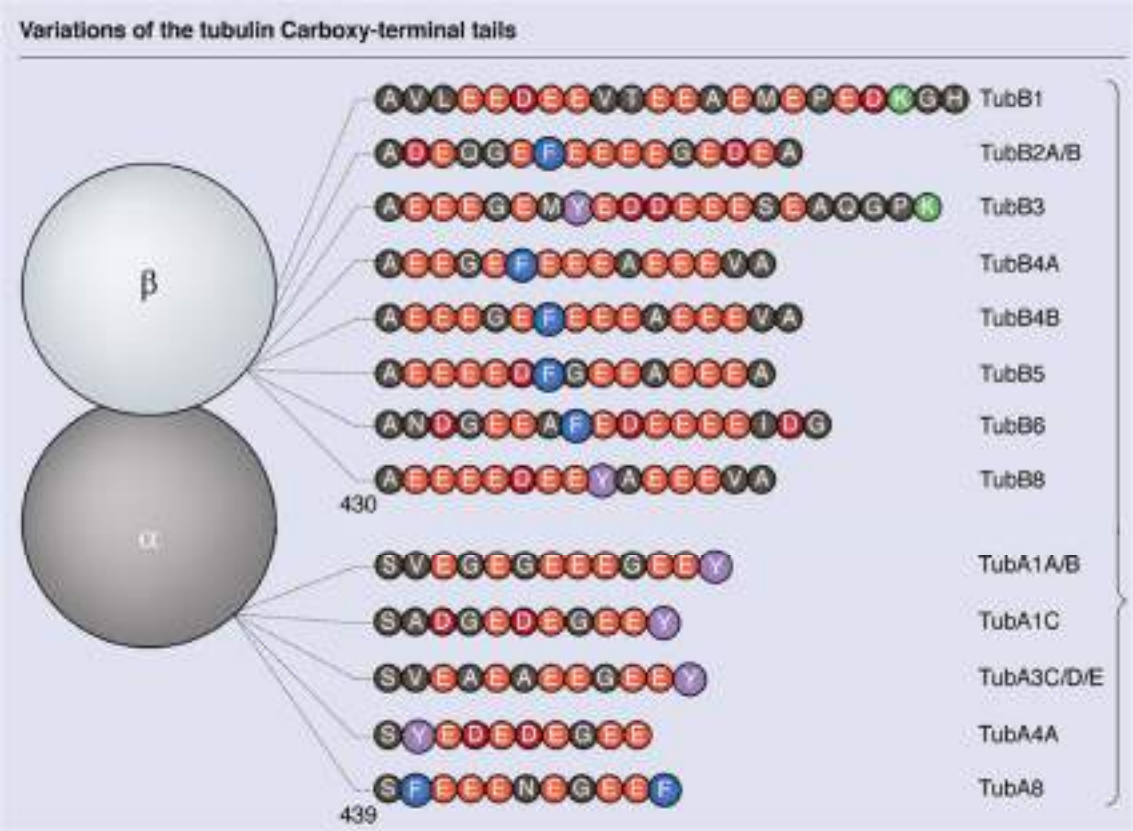

Figure 3: C-terminal heterogeneity in α and β tubulin isotypes
Tubulin isotypes show differences in the length and amino-acid composition of their C-terminal tail. The heterogeneity of the C-terminal tail may translate into different patterns of PTMs or interaction with MAPs and therefore provide tubulin isotypes with specific functional properties. For instance, TUBA8 is immune to detyrosination since it does encode for a final tyrosine residue. Figure adapted from (Gadadhar, Bodakuntla, *et al.*, 2017).

The high degree of conservation and tissue-specific expression of tubulin isotypes suggests that they exert different functions despite their relative similarity. TUBA1A is the most prevalent α-tubulin isotype in the brain (Hall and Cowan, 1985; Aiken *et al.*, 2017). TUBB3 is a neuron-specific tubulin isotype (also named Tuj1 or β3-tubulin) and is used as a marker of neurons (Latremoliere *et al.*, 2018). TUBB3 shares the β-tubulin landscape in the brain with TUBB2B, TUBB2C, TUBB4 and TUBB5 (Zhang *et al.*, 2014; Aiken *et al.*, 2020). Interestingly

single MT tracks can include various tubulin isotypes, therefore making it possible for each MT to have a unique and adaptable composition (Lewis, Gu and Cowan, 1987).

To understand if the brain-specific expression of tubulin isotypes relates to specific functions, researchers have either, mutated, removed or replaced one tubulin isotype by another. TUBB3 knockdown (KD) in mice results in alterations in cortical development by delaying projection neuron migration and morphology. Replacement of TUBB3 with other β-tubulins fail to rescue the alterations which highlights the specific function of TUBB3 in radial migrating neurons (Saillour *et al.*, 2014). In a TUBB3 knockout (KO) mouse, researchers found that other β-tubulin isotypes are upregulated in neurons to maintain physiological levels of β-tubulin. However, growth cone function and consequently axonal growth were impaired in this model, suggesting again an isotype-specific regulation of MT dynamics (Latremoliere *et al.*, 2018). The most prevalent α-tubulin in the brain, TUBA1A is also important for ensuring proper regulation of neuronal migration. A mutation in this tubulin isotype increases the branching and slows the migration of INs in the rostral migratory stream (Belvindrah *et al.*, 2017). Interestingly, this effect occurs when expressing the mutant TUBA1A via electroporation, which highlights the fact that mutant tubulin isotypes can induce pathogenesis through gain of function. Consistent with this, numerous tubulinopathies arise from dominant negative mutations (Chakraborti *et al.*, 2016). Together, these findings suggest that single tubulin isotypes enable unique MT functions in a cell-type specific manner.

2.2 Tubulin isotypes may contribute to the regulation of transport

GTP-bound β-tubulin and conformational changes in MTs alter the binding affinity of motors to the lattice of MTs (Nakata *et al.*, 2011; Peet, Burroughs and Cross, 2018; Shima *et al.*, 2018). Some studies suggest that tubulin isotypes modulate the binding affinity of several motors and as such may serve as a regulatory mechanism for the spatiotemporal delivery of cargoes.

In *C. elegans*, the α-tubulin isotype TBA-6 is particularly expressed in sensory neurons. It regulates the transport speed of cargoes carried by kinesin-2 but not kinesin-3 motors (Silva *et al.*, 2017). In yeast, the G436R mutation in α-tubulin mimics a variant of TUBA1A described in tubulinopathies. Interestingly, the G436R mutation in yeast is responsible for a dramatic increase in dynein activity induced by an impaired interaction with the MAP she1, a dynein

inhibitor (Denarier *et al.*, 2021). Similarly, a study generating yeast/human tubulin chimera through the expression of various human β-tubulin C-terminal chains suggest that the velocity and processivity of motors was dependent on tubulin isotype side-chains (Sirajuddin, Rice and Vale, 2014). For instance, the processivity of kinesin-1 on TUBB3 or TUBB1 is significantly lower than on TUBB2. This effect is specific to kinesin-1 because kinesin-2 processivity remains unchanged. Interestingly, TUBB1 and TUBB3 possess a positively-charged lysine residue on their C-terminal tail and removing this single residue increased the processivity of kinesin-1 on these isotypes (Sirajuddin, Rice and Vale, 2014). Together, these studies suggest that slight differences between tubulin isotypes are sufficient to induce meaningful changes in the binding and motility of motors on MTs.

Recent studies suggest that changes to the binding of motors on specific tubulin isotypes may modulate intracellular transport. As previously mentioned, TUBB4A mutations are associated with tubulinopathies in patients. At the molecular level, some mutations in the TUBB4A isotype result in increased KIF5 binding to MTs (Vulinovic *et al.*, 2018). In neurons derived from human induced pluripotent stem cells (hIPSCs), heterozygous loss of TUBB4A resulted in a disruption of mitochondrial transport (Vulinovic *et al.*, 2018). The mechanism through which these transport defects occur are unclear and may result from changes in the binding of molecular motors or other modifications in the MT structure and dynamics. The proportion of TUBB3 in neuronal MTs may also contribute to the regulation of intracellular transport. TUBB3 KD is compensated by an increased expression of TUBB4 which results in similar levels of total β-tubulin. However, the velocity of KIF5C is increased in TUBB3 KD hippocampal neurons, suggesting that the proportion of this isotype can regulate transport (Radwitz *et al.*, 2022). This effect may be mediated by PTMs since TUBB3 KD was also responsible for a significant decrease in MT polyglutamylation which has been shown to regulate the motility of various cargoes (Magiera *et al.*, 2018; Bodakuntla *et al.*, 2020). Interestingly, the levels of TUBB3 in hippocampal neurons can physiologically fluctuate in correlation with neuronal activity, suggesting that the expression of tubulin isotypes may be involved in some neuronal plasticity processes (Radwitz *et al.*, 2022).

2.3 Neurological diseases associated with tubulin isotype mutations

The critical importance of tubulin isotypes is exemplified by mutations in specific tubulin isotypes that underlie neurological disorders, also referred to as "tubulinopathies" (reviewed in Chakraborti et al., 2016). Tubulinopathies often alter MT functions by modifying their structure and dynamics (Panda *et al.*, 1994; Geyer *et al.*, 2015; Ti *et al.*, 2016), or mutating the C-terminal tail which is involved in interaction with MAPs and regulation by PTMs (Cowan *et al.*, 1988; Fiore, Goulas and Pillois, 2017; Hebebrand *et al.*, 2019). Mutations in tubulin isotypes whose expression is not restricted to the brain still lead to neurological disorders, which suggests that the brain is particularly sensitive to changes in its tubulin isotypes. Tubulinopathies can lead to cortical malformations such as lissencephaly, pachygyria, polymicrogyria or microcephaly (Chang, 2015; Chakraborti *et al.*, 2016). Interestingly, tubulinopathies often arise from missense mutations rather than truncation mutations. This, together with the observation that most tubulinopathies emerge from spontaneous mutations that lead to dominant negative effects, suggests that tubulinopathies are caused by gain of function mutations rather than haploinsufficiency (Chakraborti *et al.*, 2016).

Mutations in TUBA1A, TUBA4A, TUBB2B, TUBB3, TUBB2A, TUBB5, TUBB4A and TUBG1 have been identified and cause neurodevelopmental or neurodegenerative diseases (Chakraborti *et al.*, 2016). Mutations can occur throughout the tubulin isotype sequence, with effects on microtubule dynamics, interaction between protofilaments or interaction with MAPs. For instance, at least 121 variants of TUBA1A have been described, with mutations spanning the whole sequence. Interestingly, 38.6% of disease-causing variants are concentrated in the C-terminal region and are predicted to affect MAP binding (Hebebrand *et al.*, 2019). For instance the TUBA1A R402H variant which causes lissencephaly and cerebellar phenotypes leads to perturbed binding of several MAPs including dynein (Aiken, Moore and Bates, 2019; Leca *et al.*, 2020). Dynein binding impairment is correlated with the abundance of the mutant R402H variant and it is therefore hypothesized that dominant negative phenotypes are induced by the partial population of mutant TUB1A1 that disrupts the continuous motion of dynein along microtubules (Aiken, Moore and Bates, 2019).

Similarly, mutations thourghout the TUBB3 sequence can alter microtubule dynamics, interactions with kinesin as well as axon guidance (Tischfield *et al.*, 2010). This highlights the

multifunctionality of tubulins and the fact that different mutations in one isotype may alter the physiology of cells in different ways. All 8 mutations considered in a study of TUBB3 syndromes induced alterations to dynamic instability but only some disrupted interaction with motors (Tischfield *et al.*, 2010). Mutations in TUBB4A also lead to very different clinical outcomes (Blumkin *et al.*, 2014), with some variants causing an hypomyelination with an atrophy of the basal ganglia and cerebellum in patients (Alata *et al.*, 2021). TUBB4A represents up to 60% of all β-tubulin in oligodendrocytes and granule cells of the cerebellum. These cells are also those that degenerate in a cell-autonomous manner in a mouse model of dominant TUBB4A mutation (Fertuzinhos *et al.*, 2022). This suggests that cell-type specific expression levels of tubulin isotypes within the brain correlate to sensitivity to tubulin mutations.

3. Post-translational modifications of MTs

Together with tubulin isotypes, PTMs endow MTs with an extraordinary versatility. MTs can be modified by a variety of PTMs including acetylation, methylation, glutamylation, glycylation, detyrosination, Δ2 and Δ3-tubulin generation, polyamination, phosphorylation, ubiquitinylation, sumoylation and palmitoylation (reviewed in Janke and Magiera, 2020) (**Figure 4**). Although MT PTMs have been studied for decades it remains an important field of study. Methylation of α-tubulin lysine 40 (K40) was only discovered recently (Park, Powell, *et al.*, 2016), some of the enzymes catalyzing MT PTMs are still unknown and the function and regulation of some PTMs remains unclear. Some MT PTMs seem irreversible such as the generation of Δ2 and Δ3-tubulin (Paturle-Lafanechere *et al.*, 1991; Prota *et al.*, 2013), while others exist in an equilibrium state regulated by the balance of “forward enzymes” which catalyze the addition of a group and “reverse enzymes” which catalyze the removal.

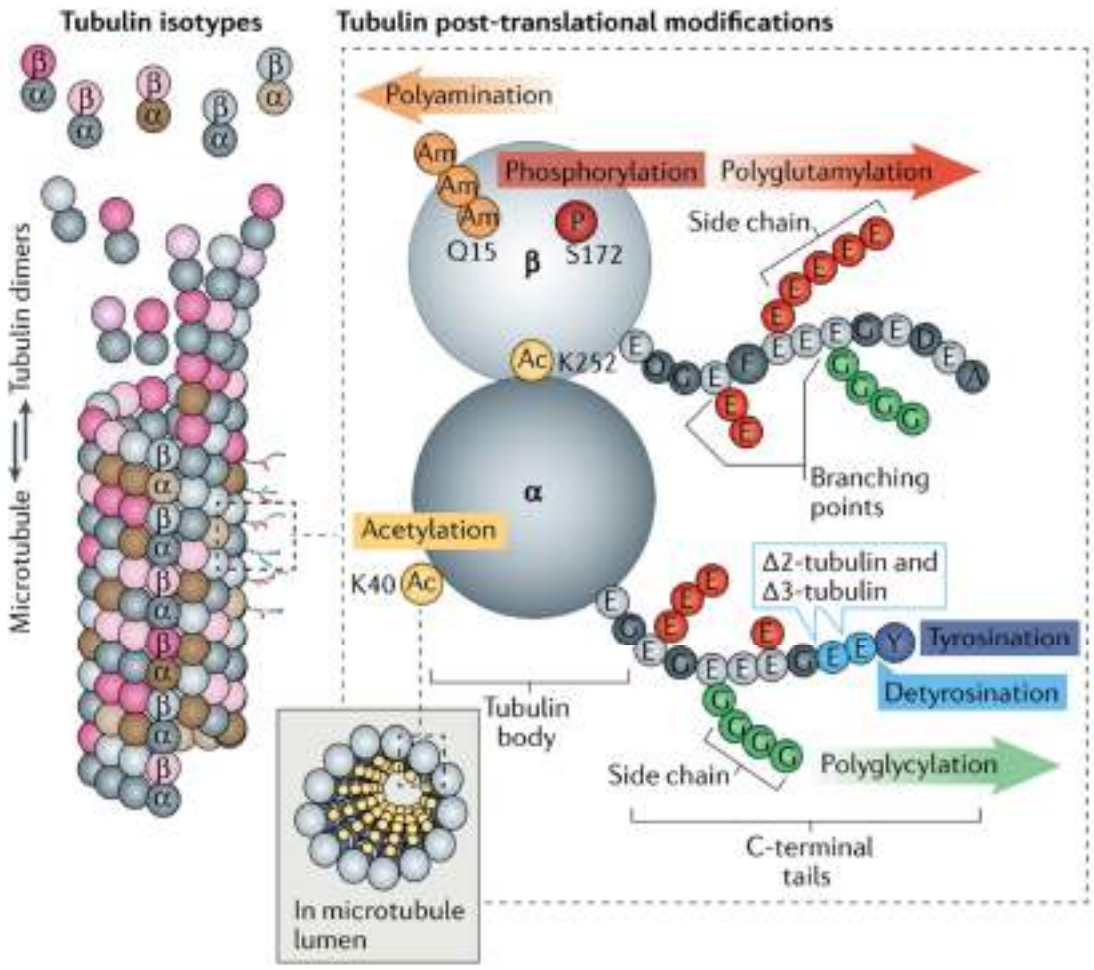

Figure 4: Overview of the main MT PTMs

The C-terminal tail of tubulins protrudes from the lattice and is a hotspot for PTMs. Polyglutamylation and glycylation modifies glutamate residues by creating a branching point followed by elongation of the side chain with glutamate or glycine residues. Most α-tubulin isotypes encode for a tyrosine as the last residue of the C-terminal chain. This residue can be removed by detyrosination which exposes the two glutamates to deglutamylation. Removal of one or two glutamates after detyrosination generates Δ2-tubulin and Δ3-tubulin respectively. Aside from the C-terminal chain, Serine 172 (S172) of β-tubulin can be phosphorylated and Glutamine 15 (Q15) can be polyaminated. Interestingly, Lysine 40 (K40) is modified by acetylation but this amino acid is present on a loop inside the MT lumen. Figure from (Janke and Magiera, 2020).

The PTM profile of MTs changes interactions with MAPs and therefore the function of MTs. PTMs of MTs are particularly abundant in neurons which may be explained by the spatio-temporal constraints of cargo delivery in these complex cells. In the following section I will review the two PTMs which are the focus of this thesis: acetylation and glutamylation. In

addition, I will provide an overview of glycylation, detyrosination and the generation of Δ2 and Δ3-tubulin.

3.1 Acetylation

3.1.1 Enzymes implicated in the regulation of acetylation

Acetylation of tubulin was discovered some time ago (L'Hernault and Rosenbaum, 1985; LeDizet and Piperno, 1987) but the enzymes responsible for adding the acetyl group have only been discovered recently. In C. *elegans* and *Drosophila Melanogaster*, MEC-17 or α-tubulin N-acetyltransferase 1 (αTAT1) and αTAT2 are the enzymes that acetylate MTs (Akella *et al.*, 2010; Shida *et al.*, 2010; Even *et al.*, 2019). In mammals, αTAT1 is the only enzyme catalyzing the transfer of acetyl groups from acetyl-CoA to the K40 of α-tubulin and consequently, its deletion leads to undetectable levels of MT acetylation (Kalebic, Sorrentino, *et al.*, 2013). Histone deacetylase 6 (HDAC6) and sirtuin 2 (SIRT2) are the two reverse enzymes responsible for the deacetylation of tubulin K40 (Hubbert *et al.*, 2002; North *et al.*, 2003). Interestingly, αTAT1 preferentially acetylates α-tubulin in MTs rather than free tubulin, while deacetylation seems to occur on tubulin regardless of its polymerization state (Hubbert *et al.*, 2002; Skultetyova *et al.*, 2017). Interestingly, acetylation of α-tubulin can occur on multiple sites (Weinert *et al.*, 2011; Lundby *et al.*, 2012; Liu, Xiong, Li, *et al.*, 2015; Liu, Xiong, Ren, *et al.*, 2015) and acetylation of K394 of α-tubulin is linked to MT stability in a fly model (Saunders *et al.*, 2022). While HDAC6 promotes the deacetylation of at least some of these sites, it is unclear which enzymes are catalyzing their acetylation (Liu, Xiong, Li, *et al.*, 2015; Saunders *et al.*, 2022). β-tubulin also possesses at least one acetylation site on K252, which can be acetylated by San and which regulates MT polymerization (Chu *et al.*, 2011). K252 acetylation appears to reduce the rate of microtubule polymerization after catastrophe *in vitro* (Chu *et al.*, 2011). However, K252 acetylation and other alternative sites of acetylation remain poorly studied and we will therefore focus on K40 acetylation of α-tubulin (αK40) which has gathered most of the interest relating to MT acetylation.

3.1.2 Functions of MT acetylation

3.1.2.1 MT dynamics

First experiments on αK40 acetylation led to the observation that high levels of acetylation correlated with long-lived MTs (Webster and Borisy, 1989). This led to two main hypotheses: **1)** Acetylation may stabilize MTs and therefore delay depolymerization; **2)** Acetylation slowly and progressively accumulates in MTs without affecting stabilization, which results in long-lived MTs showing high levels of acetylation. Although some early observations suggested that acetylation increases MT stability (L'Hernault and Rosenbaum, 1985; LeDizet and Piperno, 1986; Webster and Borisy, 1989), others have suggested that it was not the case (Palazzo, Ackerman and Gundersen, 2003).

On one hand, αTAT1 has been shown to destabilize MTs and intriguingly, this effect was independent of its catalytic activity, suggesting non-canonical functions of this enzyme on MT dynamics (Kalebic, Martinez, *et al.*, 2013). On the other hand however, recent evidence supports a role of acetylation in the stabilization of MTs (Portran *et al.*, 2017; Xu *et al.*, 2017; Eshun-Wilson *et al.*, 2019). Acetylation would increase the flexibility of the MT lattice by weakening the bonds between protofilaments, therefore protecting MTs from mechanical stress (Portran *et al.*, 2017; Xu *et al.*, 2017). Indeed, acetylation of αK40 changes the structure of the loop that carries this amino acid which may affect lateral contact sites and therefore provide MTs with more flexibility (Eshun-Wilson *et al.*, 2019). Interestingly, loss of αTAT1 leads to MT instability with a reduction in MT numbers in touch receptor neurons (TRNs) of *C. elegans,* which subsequently leads to axonal degeneration (Cueva *et al.*, 2012; Neumann and Hilliard, 2014; Yan *et al.*, 2018). TRNs are subject to mechanical flexion due to the peristaltic movements of the animal and consequently, paralysis of the animal prevents MT loss and degeneration (Neumann and Hilliard, 2014). αK40 acetylation may therefore protect MTs in contexts of repeated mechanical stress.

Acetylation may also affect MT dynamics in other ways since acetylated MTs seem to be the preferred substrate of katanin, a MT severing enzyme (Sudo and Baas, 2010). Additionally, acetylation promotes the bundling of MTs and consequently, loss of αTAT1 debundles MTs (Wei *et al.*, 2018; Yang *et al.*, 2022). MT acetylation may also regulate MT polymerization since

loss of αTAT1 increases +end dynamics which results in axon overbranching during cortical development (Wei *et al.*, 2018).

3.1.2.2 Intracellular transport

MT acetylation also modulates intracellular transport. Loss of αK40 in a neuronal cell line *in vitro* influences the binding and motility of kinesin-1. Interestingly, increasing MT acetylation with an HDAC6 inhibitor, redirected JNK-interacting protein 1 to sub-compartments in which it is normally absent (Reed *et al.*, 2006). This observation was the first suggestion that MT acetylation may regulate intracellular transport by modulating molecular motor binding affinity. Another study found that kinesin-1 and dynein are more efficiently recruited on acetylated tubulin in a purified system *in vitro* (Jim P Dompierre *et al.*, 2007).

Neurodegenerative diseases are often associated with axonal transport defects (Sleigh *et al.*, 2019a) and in some cases to alterations in MT acetylation levels, such as in the brain of patients suffering from Alzheimer (AD) or Huntington disease (HD) (Bart and Jean-Pierre, 1996; Jim P Dompierre *et al.*, 2007; Andreu-Carbó *et al.*, 2022). HDAC6 inhibition in a mouse model of AD increased αK40 acetylation and mitochondrial trafficking (Kim *et al.*, 2012; Govindarajan *et al.*, 2013) while it also ameliorated cognitive deficits (Govindarajan *et al.*, 2013). Similarly, HDAC6 inhibition had positive effects on amyotrophic lateral sclerosis (ALS) in mouse models where it rescued axonal transport defects (d'Ydewalle *et al.*, 2011; Taes *et al.*, 2013) and in hIPSC-derived neurons (Guo *et al.*, 2017). In a mouse model of Huntington disease, HDAC6 inhibition appears to rescue acetylation levels and intracellular transport as well (Jim P Dompierre *et al.*, 2007), however, subsequent studies failed to demonstrate a positive effect of HDAC6 inhibition on behavioral symptoms in mouse (Bobrowska *et al.*, 2011; Ragot *et al.*, 2015). Together these studies suggest that MT acetylation, via its ability to modulate intracellular transport, is a potential therapeutic target to rescue cargo motility and, in some cases, improve the symptoms of the disease. Most studies performed to date on the regulation of transport by changes of MT acetylation consist in rescues of existing axonal transport defects by HDAC6 inhibitors. Although HDAC6 inhibition increases αK40 acetylation, it can also deacetylate other substrates (Gomes, Ariyaratne and Pflum, 2021) and therefore, further research is needed to reinforce the causative link between MT acetylation and intracellular transport. For instance, one alternative mechanism by which HDAC6 inhibition

may regulate mitochondrial motility is through the deacetylation of Miro1, an adaptor protein that helps linking mitochondria to molecular motors (Kalinski *et al.*, 2019).

3.1.2.3 Consequences for brain development and function

MT acetylation has been linked to several physiological defects. In *C. Elegans*, *Drosophila* and mouse loss of αTAT1 or its paralog αTAT2 leads to defects in touch sensation, highlighting a highly conserved regulation of sensory neuron physiology mediated by the acetylating enzymes (Shida *et al.*, 2010; Morley *et al.*, 2016; Yan *et al.*, 2018). Loss of αTAT1 in mice also leads to impaired migration of cortical neurons, mild hippocampal malformation and increased cortico-cortical projections (Li *et al.*, 2012; Kim *et al.*, 2013; Wei *et al.*, 2018). Despite these morphological changes to brain development, no severe behavioral defects have been highlighted in αTAT1 KO mice aside from reduced mechanosensation and a mild increase in anxiety (Kalebic, Sorrentino, *et al.*, 2013; Morley *et al.*, 2016; Wei *et al.*, 2018).

3.1.3 Upstream regulators of MT acetylation

Although we focused so far on the enzymes directly involved in MT acetylation, other proteins act upstream to finely tune the balance of acetylation and deacetylation. These enzymes either **1)** generate the acetyl-CoA which provides the acetyl group in the acetylation reaction or **2)** interact with acetylation enzymes to regulate their activity.

3.1.3.1 Acly/Acss2

Acetyltransferases utilize acetyl-coenzyme A (acetyl-CoA) as a donor of an acetyl-group to catalyze lysine acetylation (Choudhary *et al.*, 2014). As such, a close relationship between the abundance of acetyl-CoA and the efficiency of post-translational acetylation has been demonstrated (Sivanand, Viney and Wellen, 2018). MT and histone acetylation levels are correlated to acetyl-CoA availability which highlights the crucial importance of the regulation of acetyl-CoA production to modulate the balance of MT acetylation/deacetylation (Wellen *et al.*, 2009; Cai *et al.*, 2011; Siudeja *et al.*, 2011; Lee *et al.*, 2014).

Acetyl-CoA is essential in several metabolic pathways in mitochondria and therefore multiple pathways converge to produce Acetyl-CoA in this organelle (Pietrocola et al., 2015; Corbet and Feron, 2017). The main mechanisms of acetyl-CoA production in mitochondria are the conversion of pyruvate originating from glycolysis into acetyl-CoA by pyruvate dehydrogenase

(PDH) and the break-down of fatty-acids by the β-oxidation pathway. However, it is noteworthy that in neurons, the breakdown of fatty acids does not contribute to acetyl-CoA production since these cells rely solely on carbohydrates as their primary energy source and are unable to oxidize fatty acids (Schönfeld and Reiser, 2017, 2021). Despite the production of acetyl-CoA within the mitochondria, this metabolite cannot be utilized as a substrate for microtubule acetylation since it is unable to traverse the mitochondrial membranes. Therefore, other sources of acetyl-CoA are required to enable post-translational acetylation (Pietrocola *et al.*, 2015). ATP-citrate lyase (Acly) and acyl-CoA synthetase short-chain family member 2 (Acss2) are the two major sources of acetyl-CoA outside of mitochondria and are therefore the enzymes supplying acetyltransferases with their substrate (Watson, Fang and Lowenstein, 1969; Luong *et al.*, 2000; Zaidi, Swinnen and Smans, 2012). These two enzymes appear to function in a coordinated way since loss of Acly results in the upregulation of Acss2 to partially rescue histone acetylation (Sivanand, Viney and Wellen, 2018).

Acly is present in both the nucleus and cytosol and uses citrate as substrate to produce acetyl-CoA. Citrate originates from the cytosol or mitochondria. In the cytosol, the glutamine metabolism results in the production of citrate. In mitochondria, citrate synthase combines acetyl CoA with oxaloacetate to produce citrate which can be exported to the cytosol. Citrate is then cleaved by Acly to produce acetyl-CoA (Sivanand, Viney and Wellen, 2018). Acss2 is also present in both the nucleus and cytoplasm but contrary to Acly it uses acetate as a substrate for acetyl-CoA production. Acetate can come from the extracellular milieu but is also the byproduct of deacetylation by HDACs. Acss2 therefore ensures that acetate is recycled by converting back into acetyl-CoA (Sivanand, Viney and Wellen, 2018) (**Figure 5**).

Since acetylation levels are strongly correlated to acetyl-CoA availability, it is tempting to hypothesize that regulating Acly or Acss2 activity may indirectly regulate MT acetylation (Wellen *et al.*, 2009; Cai *et al.*, 2011; Siudeja *et al.*, 2011; Lee *et al.*, 2014). However, the mechanisms regulating Acly and Acss2 are still unclear and therefore additional research is needed to understand whether these two enzymes could be upstream regulators of MT acetylation.

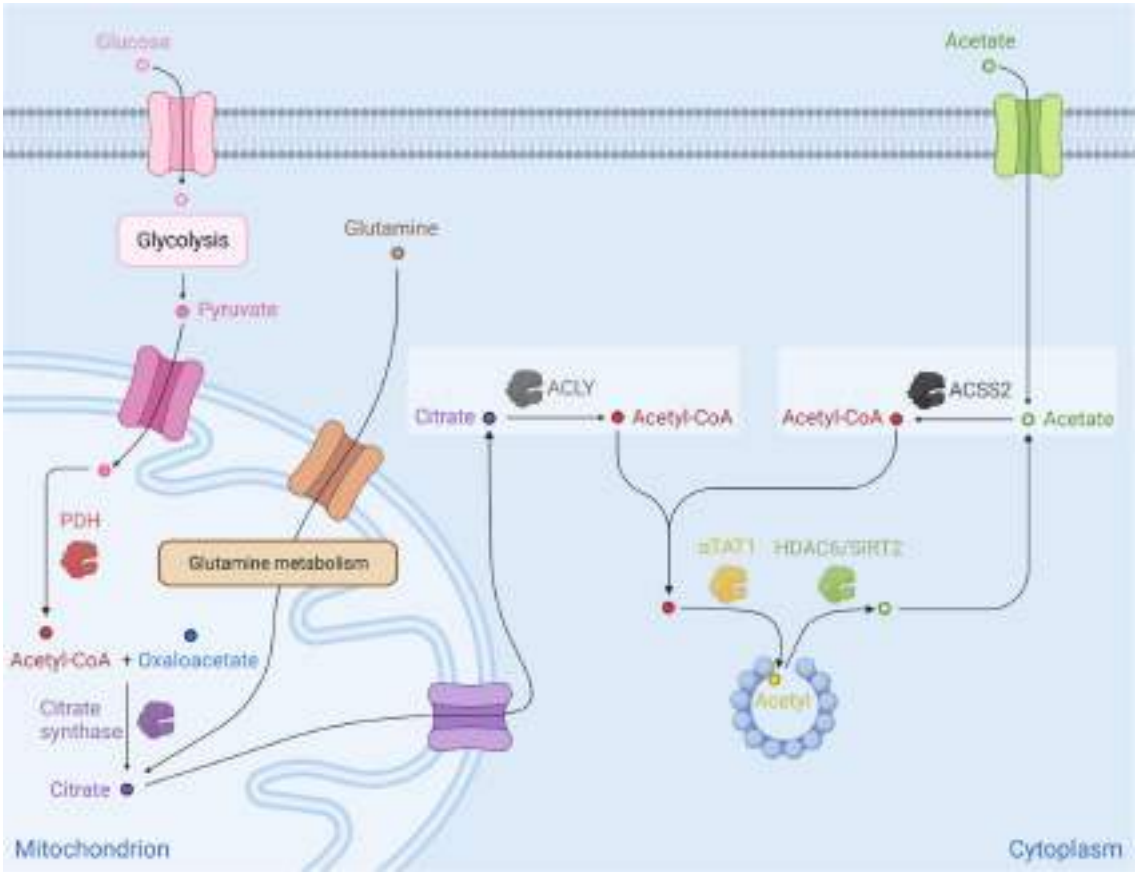

Figure 5: Cytoplasmic origin of acetyl-CoA in neurons

Acetyl-CoA is the substrate that provides the acetyl group added to the lysine 40 of α-tubulin by αTAT1. Acetyl-CoA is produced within mitochondria through the conversion of pyruvate into acetyl-CoA by pyruvate dehydrogenase (PDH). However, acetyl-CoA cannot cross the mitochondrial membrane and therefore, cytoplasmic acetyl-CoA originates from the conversion of citrate or acetate into Acetyl-CoA by ACLY and ACSS2 respectively. Citrate originates from mitochondria and can be produced by **1)** the condensation of acetyl-CoA and oxaloacetate, catalyzed by citrate synthase; **2)** the glutamine metabolism. Citrate is then transported into the cytoplasm to be converted into acetyl-CoA by Acly. Acetate, the substrate of Acss2 is the byproduct of deacetylation catalyzed by deacetylating enzymes such as HDAC6 and SIRT2 and originates from the extracellular space as well.

3.1.3.2 p27^{kip1}

p27^{kip1} (p27) is a protein of the Cip/Kip family originally discovered as a cell cycle regulator able to inhibit the G1/S phase transition through the blockade of multiple cyclin-dependent kinases (Toyoshima and Hunter, 1994; Lacy *et al.*, 2004). As such it has been extensively studied in the field of cancer, where it acts as a tumor suppressor (McKay and White, 2021). Since these original discoveries however, multiple functions of p27 have emerged, including in the brain (Godin and Nguyen, 2014). p27 owes its myriad of functions to its intrinsically

disordered nature (Russo *et al.*, 1996; Bienkiewicz, Adkins and Lumb, 2002; Bencivenga *et al.*, 2021). Indeed, p27 lacks a 3D structure and instead possesses multiple binding sites which allow it to adopt different conformations depending on its interactor.

Some early evidence suggested that one of the non-canonical function of p27 is the regulation of MT dynamics and MT acetylation (Baldassarre *et al.*, 2005; Godin *et al.*, 2012). p27 can bind to MTs and promote their polymerization thereby controlling the tangential migration of cortical interneurons (Godin *et al.*, 2012). Additionally, p27 binds and inhibits the MT-destabilizing protein stathmin, therefore increasing MT stability in a human epithelial cell-line (Baldassarre *et al.*, 2005). Interestingly, this was associated with an increase of acetylation although whether it was due to a greater accumulation of acetylation in stable MTs or to the regulation of acetylation by p27 itself remained unclear (Baldassarre *et al.*, 2005).

A study from our laboratory aimed to clarify the role of p27 in MT acetylation and assessed whether it may indirectly modulate neuronal transport (Morelli *et al.*, 2018). Loss of p27 in mouse and flies resulted in reduced MT acetylation levels in axons and was correlated with transport deficits for multiple cargoes. Interestingly, transport defects in mouse cortical neurons were rescued by expression of a p27 variant unable to bind to MTs, suggesting that p27 function as a MAP is not involved in the regulation of axonal transport. Instead, restoration of MT acetylation levels by HDAC6 inhibition rescued transport defects in both flies and mouse neurons, suggesting that p27 regulates transport through the modulation of MT acetylation levels. αTAT1 and HDAC6 mRNA levels were unchanged in p27 KO mice but αTAT1 protein levels were reduced. Immuno-precipitation and cycloheximide assays demonstrated that p27 binds to αTAT1 leading to its stabilization and protection from proteasomal degradation. Therefore, p27 acts as an upstream regulator of MT acetylation by controlling the balance of acetylation/deacetylation through the stabilization of αTAT1 (Morelli *et al.*, 2018) (**Figure 6**). A recent study led to similar findings in mouse embryonic fibroblast (MEFs) where p27 loss leads to reduced MT acetylation and abnormal distribution of autophagosomes. In MEFs, p27 also binds to αTAT1 and increases its stability, consequently, inhibition of deacetylases restores MT acetylation and autophagosome distribution (Bencivenga *et al.*, 2021).

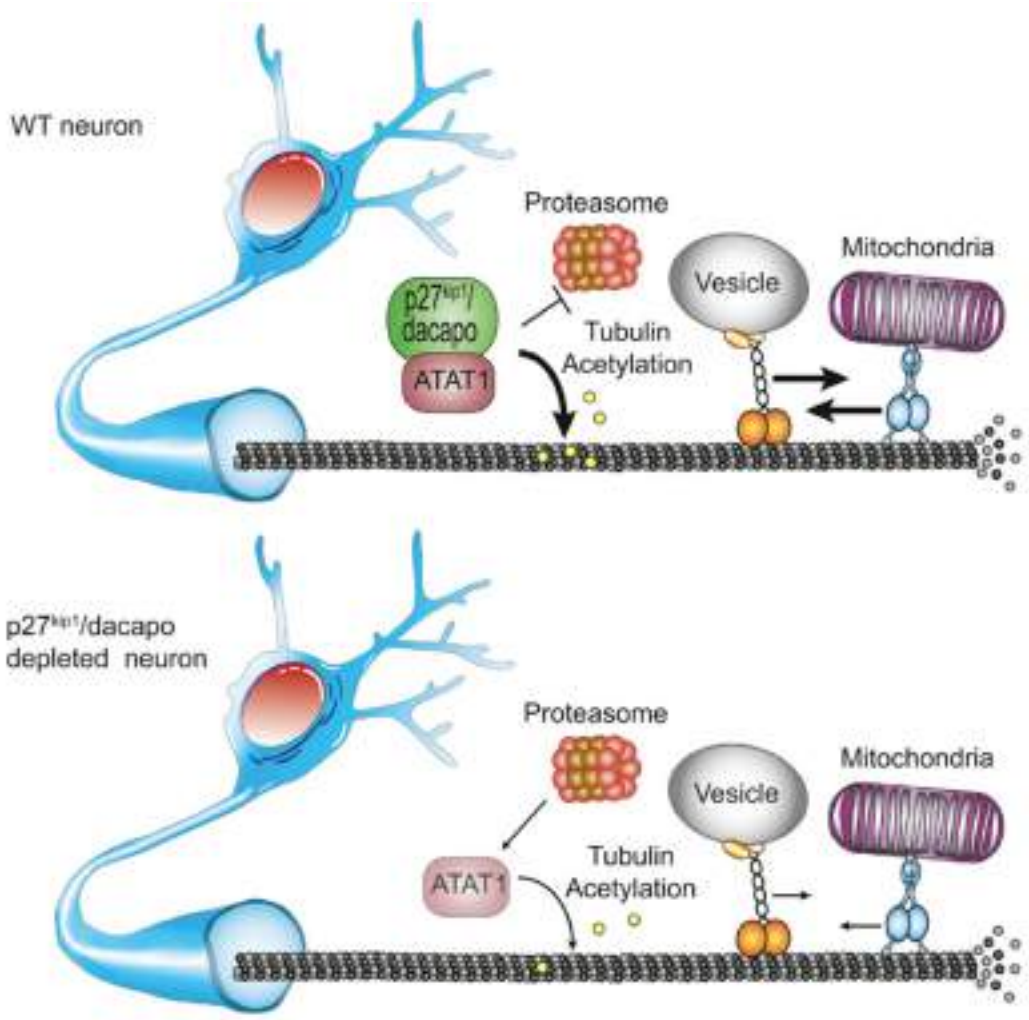

Figure 6: Model of the regulation of MT acetylation and transport by p27
In physiological conditions, p27 binds to αTAT1 protecting it from proteasomal degradation. Upon p27 loss, αTAT1 levels are reduced thereby reducing MT acetylation and transport efficiency. Figure from (Morelli *et al.*, 2018).

3.1.3.3 Elongator

Elongator is a complex comprised of two copies of each of its six subunits named Elp1-Elp6. It is conserved across species and deletion of any of the six subunits that constitutes the complex leads to its dysfunction (Jablonowski *et al.*, 2001; Krogan and Greenblatt, 2001; Huang, Joanhsson and Byström, 2005; Chen, Tuck and Byström, 2009; Mehlgarten *et al.*, 2010; Walker *et al.*, 2011). Further highlighting the importance of Elongator, loss of function studies have demonstrated major alterations in the brain such as microcephaly due to impaired progenitor specification, defects in neuronal migration or neuritogenesis (Creppe *et al.*, 2009;

Laguesse *et al.*, 2015; Tielens *et al.*, 2016; Shilian *et al.*, 2022). Consistent with this, mutations in multiple Elongator subunits have been linked to neurological diseases and of particular interest to **Chapter 1**, recessive mutations in *Elp1* can cause familial dysautonomia (FD) (Nguyen *et al.*, 2010; Gaik *et al.*, 2022). FD is caused by a single nucleotide mutation that induces mis-splicing and skipping of exon 20 resulting in a frameshift and generation of unstable or undetectable Elp1 (Slaugenhaupt *et al.*, 2001; Cuajungco *et al.*, 2003). Most FD cases are caused by the same mutation that likely originates from a common ancestor (Anderson *et al.*, 2001; Slaugenhaupt *et al.*, 2001). Interestingly, the reduction in splicing efficiency is tissue-dependent, meaning that different cells express various ratios of WT and mutant *Elp1*. As a consequence, the peripheral nervous system (PNS) where almost only the mutant form is found is most affected (Slaugenhaupt *et al.*, 2001; Cuajungco *et al.*, 2003). Peripheral nerves of the sensory and autonomic system show developmental abnormalities and degeneration in FD patients (Riley and Day, 1949; Rubin and Anderson, 2017).

The broad range of alterations caused by Elongator loss correlates with the observation that this complex is multifunctional and required to fulfill many cellular roles (Svejstrup, 2007; Kolaj-Robin and Séraphin, 2017; Dalwadi and Yip, 2018). They include DNA methylation, tRNA modification, regulation of acto-myosin/MT dynamics and acetylation of multiple substrates (Creppe *et al.*, 2009; Okada *et al.*, 2010; Solinger *et al.*, 2010; Tielens *et al.*, 2016; Johansson, Xu and Byström, 2018; Planelles-Herrero *et al.*, 2022). The main function of the complex is to drive tRNA modifications. A subset of tRNAs encode for a wobble uridine at position 34 (U34) which can be modified by a cascade of enzymatic reactions that requires Elongator and results in the formation of 5-methoxycarbonylmethyl (mcm^5) and 5-carbamoylmethyl (ncm^5) side chains on U34 (Huang, Joanhsson and Byström, 2005). tRNA modification by Elongator is necessary for accurate and efficient protein translation and consequently tRNA modification by Elongator has a wide range of cellular effects (Yarian *et al.*, 2000; Murphy *et al.*, 2004). In yeast, the cellular processes regulated by Elongator appear to rely exclusively on its role as a tRNA modifier. Indeed, supplementation with modified U34 tRNAs rescues all cellular processes in those cells, suggesting that tRNA modification and its effect on protein translation mediates Elongator cellular functions (Esberg *et al.*, 2006; Chen *et al.*, 2011; Karlsborn *et al.*, 2014). The lack of the mcm^5 and ncm^5 modified U34 results in a slowdown of translation and accumulation of protein aggregates in both yeasts and mammals. Aggregates

may trigger the unfolded response protein (UPR) in cortical neurons of Elp3 KO mice which subsequently leads to microcephaly (Laguesse *et al.*, 2015). *Elp3* mutations have also been linked to ALS, where protein aggregates are believed to precede the degeneration of motor neurons (Simpson *et al.*, 2009; Bento-Abreu *et al.*, 2018). Finally, tumor cells in melanoma can acquire resistance to targeted therapy by increasing the activity of Elongator to promote tRNA modifications, suggesting a critical role of tRNA modification in cancer pathogenesis (Rapino *et al.*, 2018).

In eukaryotic organisms, it is likely that Elongator harbors additional functions. The acetyltransferase domain of *Elp3* has been shown to catalyze the acetylation of histone H3, Bruchpilot at the fly neuromuscular junction and connexin-43 in the cerebral cortex (Winkler *et al.*, 2002; Miśkiewicz *et al.*, 2011; Laguesse *et al.*, 2017). Interestingly, early studies also identified Elp3 as a potential acetyltransferase of α-tubulin in mouse and *C. elegans* (Creppe *et al.*, 2009; Solinger *et al.*, 2010). HT29 cells depleted in Elp1 or Elp3 showed reduced MT acetylation levels and low acetylation levels induced by HDAC6 overexpression could be partially restored by Elp3 overexpression (Creppe *et al.*, 2009). Similarly in *C. elegans*, *Elp1* or *Elp3* deletion reduced α-tubulin acetylation and interestingly it was also correlated to a reduced velocity of synaptic dense core vesicles (Solinger *et al.*, 2010). However, since these original discoveries, αTAT1 has been discovered as the major α-tubulin acetyltransferase in mouse and together, αTAT1 and αTAT2 are responsible for αK40 acetylation in *C. elegans* (Akella *et al.*, 2010; Shida *et al.*, 2010; Kalebic, Sorrentino, *et al.*, 2013). These findings suggest that Elongator does not directly acetylate α-tubulin through its Elp3 catalytic subunit but rather may act upstream of the enzymes regulating acetylation. Further studies are therefore required to clarify how Elp1 and Elp3 loss leads to α-tubulin acetylation deficiency.

3.2 Polyglutamylation

Polyglutamylation consists in the addition of glutamate amino acids to other glutamate residues on the C-terminal tail of α and β tubulin. Contrary to acetylation, multiple residues can be added sequentially to form side chains of polyglutamate. This modification was discovered on MTs (Eddé *et al.*, 1990; Rüdiger *et al.*, 1992) but can also occur on other substrates (Regnard *et al.*, 2000; van Dijk *et al.*, 2008). Interestingly, polyglutamylation is enriched in the brain and particularly in neurons, suggesting that it plays an essential role in

these cells (Wolff *et al.*, 1992). Consequently, the Purkinje cell degeneration (pcd) mouse in which polyglutamylation is dramatically increased suffers from degeneration of multiple cell types in the brain (Mullen, Eichert and Sidman, 1976; Landis and Mullen, 1978; Greer and Shepherd, 1982; O'Gorman and Sidman, 1985; Fernandez-Gonzalez, 2002). The enzyme responsible for the phenotype is a deglutamylase whose loss triggers similar neurodegeneration in human patients (Shashi *et al.*, 2018).

3.2.1 Enzymes implicated in the regulation of polyglutamylation

Glutamylation is catalyzed by enzymes sharing similarities with the tubulin-tyrosine ligase (TTL) that catalyzes tyrosination and have therefore been named tubulin-tyrosine ligase-like (TTLL) (Janke *et al.*, 2005; van Dijk *et al.*, 2007). The enzymes of the TTLL family exhibit substrate specificity and preferentially target α- or β- tubulin. For instance, TTLL1 and TTLL7, the main TTLLs in the brain, exclusively target MTs with preference for α- and β- tubulin respectively. Also, some TTLLs are responsible for the initiation of polyglutamylation, adding only one glutamate to the C-terminal tail while others catalyze the elongation of the polyglutamate side chains by adding more residues (Janke *et al.*, 2005; van Dijk *et al.*, 2007). The specificity of TTLLs and whether they tend to initiate or elongate side chains is summarized in (**Table 1**). Like acetylation, polyglutamylation of tubulin is reversible and the removal of glutamate residues is catalyzed by enzymes of the cytosolic-carboxypeptidase (CCP) family. Their discovery led to the identification of multiple enzymes that, like TTLLs, exhibit specific patterns of activity (Kimura *et al.*, 2010; Rogowski *et al.*, 2010). CCP1, CCP4 and CCP6 typically deglutamylate side chains without removing the branching point glutamate while CCP5 preferentially removes the last glutamate at the branching point (Rogowski *et al.*, 2010; Berezniuk *et al.*, 2013) (**Figure 7**). The specificity in the function of TTLLs and CCPs likely enables a complex regulation of polyglutamylation patterns in cells, increasing the possible combinations of this PTM on MTs to provide a diversity of functions.

	Substrate Specificity			Reaction Specificity	
	α-Tubulin	β-Tubulin	NAP	Initiation	Elongation
TTLL4	+	+++	+++	+++	–
TTLL5	+++	+	–	+++	+
TTLL6	+++	+	–	+	+++
TTLL7	+	+++	–	+++	+
TTLL11	++	+	–	+	+++
TTLL13	++	+	–	–	++

Table 1: Substrate and reaction specificity of some of the TTLLs.
TTLL4 preferentially initiates glutamylation on β-tubulin but can also target nucleosome assembly proteins (NAP). Table adapted from (van Dijk *et al.*, 2007).

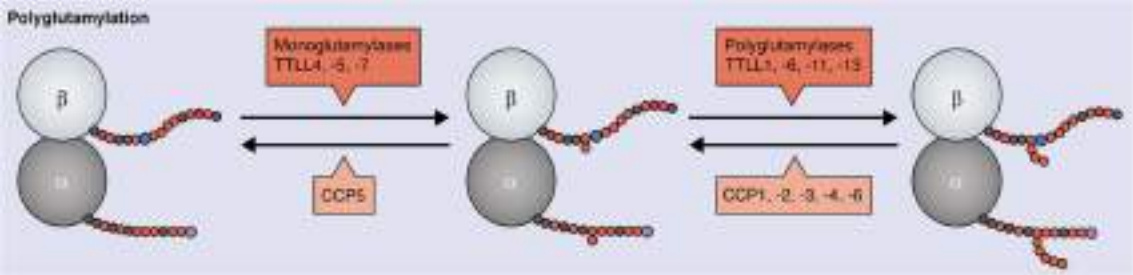

Figure 7: Enzymes regulating the initiation and elongation of polyglutamylation
Monoglutamylases initiate the addition of the side chains by adding a first branch point glutamate and polyglutamylases elongate the side chains by adding multiple glutamate residues. Both glutamylases and carboxypeptidases preferentially initiate or elongate polyglutamate side chains (Gadadhar, Bodakuntla, *et al.*, 2017).

3.2.2 Functions of MT polyglutamylation

3.2.2.1 MT severing

Because of its localization at the C-terminal tail of tubulins, polyglutamylation is in a prime position to modulate interactions with MAPs. Consistent with this, the binding of Tau, MAP1A, MAP1B and MAP2 are affected by the polyglutamylation status of MTs (Boucher *et al.*, 1994; Bonnet *et al.*, 2001). The activity of the severing enzymes spastin and katanin is also mediated by the polyglutamylation levels of MTs (Lacroix *et al.*, 2010; Valenstein and Roll-Mecak, 2016; Shin *et al.*, 2019). Hela cells natively express low levels of glutamylation, and when transfected with various TTLLs, show increased levels of either branching point glutamate or polyglutamate side chains (**Table 1**). Spastin activity is increased in Hela cells following transfection of TTLL6 and TTLL11 but not TTLL4, TTLL5 or TTLL7 (Lacroix *et al.*, 2010). This suggests that elongated polyglutamate chains on α-tubulin specifically regulate spastin

activity and therefore highlight the fact that different polyglutamylation modifications modulate MAPs in different ways. Neurons have high levels of polyglutamylation and relatively stable MTs which seems contradictory with the observation that spastin activity is increased by polyglutamylation level. However, a non-linear relation between polyglutamylation level and spastin activity ensures that highly polyglutamylated MTs are protected from spastin severing activity (Valenstein and Roll-Mecak, 2016). Similarly, the activity of katanin was also increased by TTLL6 and TTLL11 specifically. Interestingly, TTLL11 only moderately increased katanin activity compared to spastin activity, suggesting that TTLL6 and TTLL11 may generate side chains of different lengths or on different residues, therefore affecting the affinity of spastin and katanin differently (Lacroix *et al.*, 2010).

3.2.2.2 Intracellular transport

Consistent with its role in modulating the affinity of MAPs, polyglutamylation also appears to affect the binding of molecular motors. Some studies suggested that kinesin motors preferentially bind to polyglutamylated tubulin and some kinesin families show increased processivity and velocity on polyglutamylated MTs *in vitro* (Larcher *et al.*, 1996; Sirajuddin, Rice and Vale, 2014). Since then, additional evidence suggests that similar to acetylation, polyglutamylation helps to regulate the motility and the sub-compartment-specific delivery of cargoes. In a mouse model in which polyglutamylation of α-tubulin is low, the distribution of KIF1A was less abundant in neurites which correlated with a decreased synaptic vesicle density and impaired synaptic transmission (Ikegami *et al.*, 2007). Polyglutamylation levels are also sensitive to neuronal activity since administration of antagonists of glycine receptors leads to increased MT polyglutamylation (Maas *et al.*, 2009). Interestingly, this also led to reduced motility of KIF5 and the presynaptic protein gephyrin, both of which could be rescued by restoring normal polyglutamylation levels (Maas *et al.*, 2009). Together, these studies suggest that changing levels of MT polyglutamylation results in alterations of intracellular transport which can have consequences for synaptic function.

The link between polyglutamylation and intracellular transport was reinforced by a series of recent studies driven by the observation that degeneration in the pcd mouse results from MT hyperglutamylation. These mice suffer from neurodegeneration of multiple neuronal populations that includes cerebellar neurons, mitral cells of the olfactory bulb and some

subpopulations of thalamic neurons (Mullen, Eichert and Sidman, 1976; Landis and Mullen, 1978; Greer and Shepherd, 1982; O'Gorman, 1985; O'Gorman and Sidman, 1985). The phenotype is due to CCP1 loss which results in severe accumulation of polyglutamylation in the cell types suffering from neurodegeneration (Fernandez-Gonzalez, 2002; Rogowski *et al.*, 2010). Purkinje cell degeneration can be rescued by the downregulation of TTLL1 which rescues polyglutamylation levels (Rogowski *et al.*, 2010; Magiera *et al.*, 2018). Interestingly, conditional CCP1 loss restricted to Purkinje cells is sufficient to induce the neurodegeneration, highlighting the cell-autonomous nature of the phenotype (Magiera *et al.*, 2018). Excessive MT polyglutamylation is associated with a decreased overall motility of multiple cargoes in hippocampal neurons including mitochondria, lysosomes, LAMP1-endosomes and BDNF vesicles (Magiera *et al.*, 2018; Bodakuntla *et al.*, 2020). Mitochondria transport is also impaired in cerebellar neurons but surprisingly lysosomes motility was not, suggesting cell-type specific regulation of transport by polyglutamylation (Gilmore-Hall *et al.*, 2019). The transport defects caused by hyperglutamylation may be specifically driven by α-tubulin polyglutamylation since knockout of the α-tubulin specific TTLL1 enhances overall motility but the knockout of β-tubulin specific TTLL7 does not (Bodakuntla *et al.*, 2021). Consistent with this, TTLL1 KD but not TTLL7 KD rescues neurodegeneration in the cerebellum of pcd mice, hinting that hyperglutamylation of α-tubulin may drive neurodegeneration (Bodakuntla *et al.*, 2021). Together, these studies strongly suggest that hyperglutamylation of α-tubulin alters intracellular transport through mechanisms that remain unclear. More research is needed to understand whether transport defects have a causal relationship with neurodegeneration.

3.3 Polyglycylation

Polyglycylation is similar to polyglutamylation in nature but can lead to very different outcomes (Grau *et al.*, 2013; Szczesna *et al.*, 2022). It consists in the addition of glycine to tubulin instead of glutamate residues and similar to polyglutamylation, residues can be added sequentially to form elongated glycine side chains. The enzymes that catalyze glycylation also belong to the TTLL family and although removal of glycine residues is possible, the enzymes that catalyze this reaction are still unknown (Ikegami and Setou, 2009; Rogowski *et al.*, 2009; Wloga *et al.*, 2009). In mammals, TTLL3 and TTLL8 appear to be the initiating glycylases while TTLL1 elongates glycine chains (Rogowski *et al.*, 2009). Polyglycylation is almost exclusively found in the axoneme, the array of MTs at the center of motile cilia and flagella and on

primary cilia (Redeker *et al.*, 1994; Bre *et al.*, 1996; Xia *et al.*, 2000; Gadadhar, Dadi, *et al.*, 2017). Consistent with its localization, polyglycylation regulates flagellar beat and primary cilia length (Gadadhar, Dadi, *et al.*, 2017; Gadadhar *et al.*, 2021). Loss of glycylation in the flagella of mouse sperm results in impaired flagellar beat and hypofertility (Gadadhar *et al.*, 2021). In the developing cilia, polyglutamylation is detected before glycylation and the former seems to regulate beating while the latter glycylation is required for cilia stability (Grau *et al.*, 2013). Despite its similarity with polyglutamylation, these two modifications complement each other to increase the complexity of PTMs and therefore modulate MT interactions in different ways. As mentioned before, moderate increases in polyglutamylation stimulates the activity of the severing enzyme katanin (Lacroix *et al.*, 2010; Valenstein and Roll-Mecak, 2016). Increased glycylation has the opposite effect and reduces the binding and activity of katanin on MTs (Szczesna *et al.*, 2022).

3.4 Tyrosination/Detyrosination

Tyrosine is genetically-encoded as the last amino-acid in the primary sequence of most α-tubulin isotypes (Gadadhar, Bodakuntla, *et al.*, 2017; Nieuwenhuis and Brummelkamp, 2019) and it can be removed in a process called detyrosination (Hallak *et al.*, 1977). Interestingly, the removal of tyrosine is a reversible process and tyrosine can be added in a reaction catalyzed by TTL (Arce *et al.*, 1975; Murofushi, 1980; Schröder, Wehland and Weber, 1985). The discovery of the enzymes responsible for catalyzing detyrosination is a relatively recent development, with their identification ultimately credited to the VASH family of enzymes (VASHs) (Aillaud et al., 2017; Nieuwenhuis et al., 2017) and to MT associated tyrosine carboxypeptidase (MATCAP) (Landskron *et al.*, 2022) (**Figure 8**). VASH1 and VASH2, complexed with small vasohibin binding protein (SVBP) act as carboxypeptidases for the tyrosine residues on tubulin side-chains, without specificity for tubulin isotypes (Aillaud *et al.*, 2017; N. Wang *et al.*, 2019). Down regulation of vasohibins or SVPB results in impaired migration of cortical projection neurons and defects in axon specification (Aillaud *et al.*, 2017; N. Wang *et al.*, 2019). Similarly, MATCAP is capable of MT detyrosination and co-deletion of MATCAP and SVBP leads to microcephaly an abnormal behavior (Landskron *et al.*, 2022).

Long-lived MTs tend to accumulate detyrosinated α-tubulin while dynamic MTs undergoing fast cycles of polymerization and depolymerization tend to show higher levels of tyrosination

(Slepecky, Henderson and Saha, 1995). This observation could be explained by the fact that TTL can only add tyrosine on soluble tubulin dimers (Beltramo, Arce and Barra, 1987) while VASHs have a preference for polymerized MTs (Kumar and Flavin, 1981; Arce and Barra, 1985). As a result, dimers newly incorporated in MTs tend to be tyrosinated while long-lived MTs tend to irreversibly accumulate detyrosinated tubulin until a catastrophe event occurs (Slepecky, Henderson and Saha, 1995). The accumulation of detyrosination itself does not seem to improve MT stability (Khawaja, Gundersen and Bulinski, 1988; Webster, 1990). However, detyrosinated MTs appear more resistant to depolymerization, an effect that may result from the high affinity of kinesin mitotic-centromere associated kinesin (MCAK) for tyrosinated MTs (Peris *et al.*, 2009; Sirajuddin, Rice and Vale, 2014). MCAK is a type of kinesin motor that uses ATP to pull on tubulin dimers and depolymerize the MT lattice.

MT tyrosination also affects the binding of motors involved in intracellular transport. For instance, the dynein-dynactin complex which drives retrograde transport shows a higher processivity on tyrosinated compared to detyrosinated MTs (McKenney *et al.*, 2016). In one study, KIF5 processivity was decreased on detyrosinated compared to tyrosinated MTs *in vitro* (Sirajuddin, Rice and Vale, 2014) but in other studies, KIF5 preferred associating with detyrosinated tubulin in cells (Dunn *et al.*, 2008; Konishi and Setou, 2009; Hammond *et al.*, 2010). KIF5 tends to be localized in axons where detyrosinated MTs are more abundant than in dendrites (Nakata and Hirokawa, 2003; Konishi and Setou, 2009). Interestingly, in dendrites, detyrosinated MTs tend to be oriented -end out which may contribute to the axonal localization of KIF5 since this motor travels towards the +end of MTs (Tas *et al.*, 2017). Together, these studies suggest that the tyrosination status of MTs may help driving the delivery of specific to cargos to their sub-compartment while also affecting the processivity of motors. Consistent with these functions of tyrosination, mice in which TTL is knocked-out suffer from severe alterations in neuronal development and die perinatally (Erck *et al.*, 2005).

3.5 Δ2/Δ3-tubulin

The tyrosine residue at the C-terminal tail of tubulin is preceded by two glutamates (Gadadhar, Bodakuntla, *et al.*, 2017; Nieuwenhuis and Brummelkamp, 2019) which can be removed by carboxypeptidases acting on detyrosinated tubulin. Δ2-tubulin and Δ3-tubulin refers to α-tubulin in which respectively one or two glutamates have been removed following

detyrosination (**Figure 8**). Interestingly, the removal of glutamate prevents the tyrosination of α-tubulin, therefore locking it in a detyrosinated state (Paturle-Lafanechere *et al.*, 1991). Removal of glutamates is catalyzed by proteins from the CCP family and it is still unclear whether it is reversible (Rogowski *et al.*, 2010). Consistent with this observation, mice lacking TTL tend to accumulate Δ2-tubulin since the genetically encoded tyrosine residue is rapidly removed by VASHs enzymes which exposes the glutamate residues to carboxypeptidases (Erck *et al.*, 2005). The function of Δ2/ Δ3-tubulin is still unclear and deserves further study. Patients suffering from Alzheimer disease show increased levels of α-tubulin that is concomitantly Δ2-tubulin and polyglutamylated in the hippocampus and in apical dendrites of projection neurons (PNs) (Vu *et al.*, 2017). Interestingly, the chemotherapy drug bortezomib increases Δ2-tubulin expression, which appears sufficient and necessary to drive defects in mitochondria motility and leads to peripheral nerve neuropathy (Pero *et al.*, 2021).

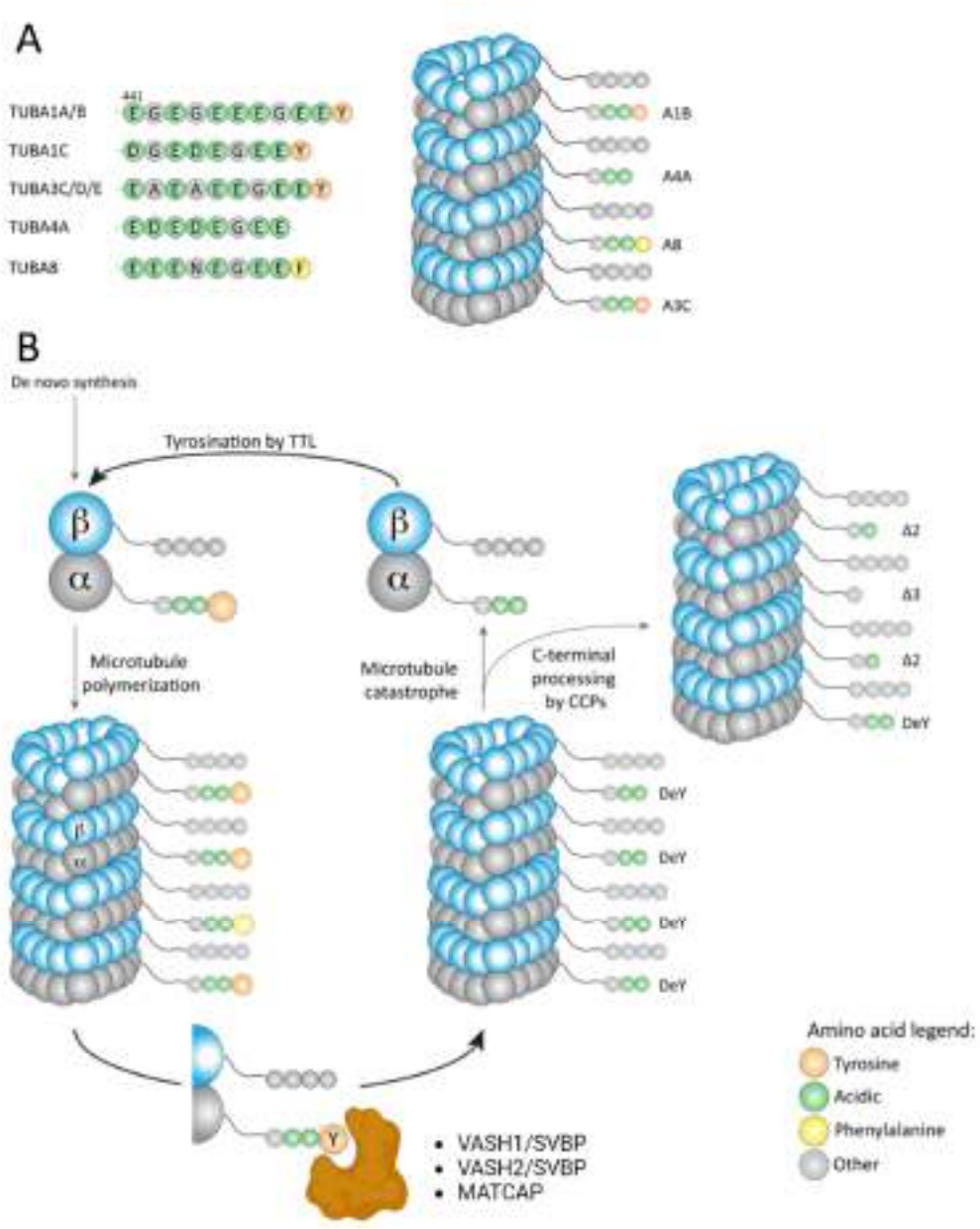

Figure 8: Tyrosination/Detyrosination cycle and generation of Δ2-tubulin/Δ3-tubulin

A. Primary sequence of the C-terminal tail of the main α-tubulin isotypes. Most α-tubulin isotypes genetically encode a tyrosine or phenylalanine as their last amino acid, preceded by two glutamates.

B. Isotypes terminated by a lysine (K) or phenylalanine (F) can be targeted by detyrosinating enzymes to have their last amino acid removed in a process called detyrosination. Detyrosinating enzymes are microtubule associated tyrosine carboxypeptidase (MATCAP) and the vasohibins 1 and 2 (VASH). The latter form a complex with small vasohibin binding protein (SVBP) which regulates their catalytic activity. TTL can revert this process by adding a new tyrosine residue in a process called tyrosination. Detyrosinated tubulin can be further cleaved by carboxypeptidases to remove one (Δ2-tubulin) or two (Δ3-tubulin) glutamate residues. Adapted from (Nieuwenhuis and Brummelkamp, 2019).

4. Methods to study axonal transport in neurons

In this section, I will give an overview of the methods to assess transport in *Drosophila* melanogaster (hereafter named flies) and rodent models. I will put a special emphasis on the former since my thesis work in chapter 2 was dedicated to this model.

4.1 *Drosophila melanogaster* as a model for axonal transport

Flies have long been used in research because of their short life cycle, economic and easy maintenance as well as the wide range of genetic tools available. In addition, basic pathways are remarkably conserved between invertebrates and mammals, and the human and fly genome show a high degree of homology, with about 70% of known disease-causing genes in humans being conserved in flies (Reiter *et al.*, 2001; Bonner and Boulianne, 2011). Consequently, flies have been widely used in the field of neurodegenerative diseases and have enabled major discoveries (Bolus *et al.*, 2020). The molecular tools developed to manipulate gene expression in flies makes it an ideal model for reverse genetic screens. In addition, the transparent body of larvae enables the recording of axonal transport *in vivo*, a feat which is much more challenging in rodent models (Greenspan, 1997).

Whole brain single cell RNA-sequencing studies have also flourished recently and provide critical information about neuronal diversity and ontogeny of the fly brain in larvae (Avalos, Brugmann and Sprecher, 2019; Corrales *et al.*, 2022) and adult flies (Davie *et al.*, 2018; Konstantinides *et al.*, 2018; Kurmangaliyev *et al.*, 2020; Özel *et al.*, 2021; Li *et al.*, 2022)

4.1.1 The Drosophila central nervous system

The development of the central nervous system (CNS) in flies is remarkably fast, taking less than 10 days to form from a single cell to the adult brain. The CNS is composed of an outer cortex and an inner neuropile, which is mostly comprised of axons and dendrites connected via synapses (Nassif, Noveen and Hartenstein, 2003). The brain is prolonged by the ventral nerve cord (VNC), a structure that is organized into neuromeres that correspond to the body segments. Each neuromere of the VNC connects with a segment to receive sensory input and send motor output (Niven, Graham and Burrows, 2008). The organization of the VNC corresponds to the arrangement of the body segments, so motor neurons emerging from the VNC along the antero-posterior axis connect with their respective muscles along the same

axis to form the neuromuscular junction (NMJ) (Ruiz-Cañada and Budnik, 2006). In *Drosophila* larvae, stereotyped sequences of movement such as feeding and crawling behavior are generated by the neuronal networks in the VNC (Cardona, Larsen and Hartenstein, 2009. However, goal-directed behavior such as chemotaxis are mainly driven by the brain (Berni *et al.*, 2012).

4.1.2 Drosophila as a model for axonal transport

Flies display a remarkable genetic homology with mammals, with an estimated 77% of human disease genes having an ortholog in flies and major signaling pathways being conserved (Reiter, 2001; Perrimon, Pitsouli and Shilo, 2012). The fly genome is smaller than its mammal counterparts as a result of gene duplications in the latter. The smaller genome of flies compared to mammals allows for easier interpretation of loss of function studies, making them a useful model for studying new regulatory pathways (McGurk, Berson and Bonini, 2015).

Flies have been a particularly attractive model for the study of axonal transport because of their anatomy and transparent bodies which allows the *in vivo* imaging of motor neurons in larvae (**Figure 10 A**) or in the wings of adult flies with a conventional confocal microscope (Vagnoni and Bullock, 2016; G. Morelli *et al.*, 2018). In addition, fly lines expressing recombinant green fluorescent protein (GFP) are readily available to visualize mitochondria (Pilling *et al.*, 2006), lysosomes (Pulipparacharuvil *et al.*, 2005), or synaptic vesicles (Zhang, Rodesch and Broadie, 2002) *in vivo*. For this reason, flies have been a popular model to study axonal transport regulation, especially in a disease context (Gunawardena *et al.*, 2003; Johnson *et al.*, 2013; Godena *et al.*, 2014; Janssens *et al.*, 2014; Turchetto *et al.*, 2022).

4.2 *In vitro* reconstitution assays

In vitro reconstitution assays allow the study of MT-dependent transport in a simplified system. They consist in the purification of polymerized MTs followed by the addition of molecular motors, organelles and possibly MT modifying enzymes. The recomposed system can then be imaged by total internal reflection fluorescence (TIRF) microscopy which allows the visualization of single motors or tagged cargoes moving along MTs (Reed *et al.*, 2006; Barisic *et al.*, 2015; M. V. Hinckelmann *et al.*, 2016). MTs of different source can be used, such as from Hela cells which display low levels of polyglutamylation or from neurons that on the

contrary are highly polyglutamylated. Additionally, MTs from transgenic mice with specific PTM patterns can be used (Even *et al.*, 2019) (**Figure 10 B**).

In vitro reconstitution assays enable easy manipulation of the system and can assist in the elucidation of single factors affecting transport to dissect the molecular mechanisms of transport. However, confirmation of the findings in cells which harbor the full complexity of the transport machinery are necessary to draw physiologically relevant conclusions.

4.3 Methods to study neuronal transport in rodents

Three main approaches can be used to study neuronal transport in rodents. The first consists in preparing a primary culture of the desired cell-type *in vitro*. Primary rodent cultures of neurons develop an axon, multiple dendrites and establish active synapse contacts that elicit spontaneous electrophysiological currents (Beaudoin *et al.*, 2012). The motility of specific organelles can then be assessed by adding dyes such as MitoTracker™ or LysoTracker™ to visualize mitochondria and acidic vesicles respectively. Alternatively, organelles can be fluorescently tagged by recombinant proteins expressed from a transgenic mouse or following plasmid deliver (Turchetto *et al.*, 2022). Cells *in vitro* can easily be manipulated genetically or pharmacologically to further dissect MT-dependent transport regulation and therefore this method has the advantage to be simple while providing versatility and physiologically relevant results but may not recapitulate the full complexity of *in vivo* systems. (**Figure 10 C**)

Axonal transport can also be measured *ex vivo* by electroporating recombinant fluorescent proteins marking specific organelles and recording their movement in the corpus callosum of organotypic slices. Because cortical neurons send projections to the contralateral cortex through the corpus callosum, unilateral electroporation allows the visualization of axons with a unique direction. Not only can axonal transport be assessed *ex vivo* but the information about the axon polarity is maintained (Even *et al.*, 2019; Turchetto, Broix and Nguyen, 2020a). (**Figure 10 D**)

Finally, neuronal transport can be recorded *in vivo* by using transgenic mouse lines or adeno-associated viruses (AAV) to express fluorescent proteins on specific organelles. The spinal cord or cortex can then be exposed by implementing a widow which allows the visualization

of moving organelles by two-photon microscopy on awake or anesthetized mice (Lewis *et al.*, 2016; Knabbe *et al.*, 2018; Knabbe, Protzmann and Kuner, 2022). (**Figure 10 E**)

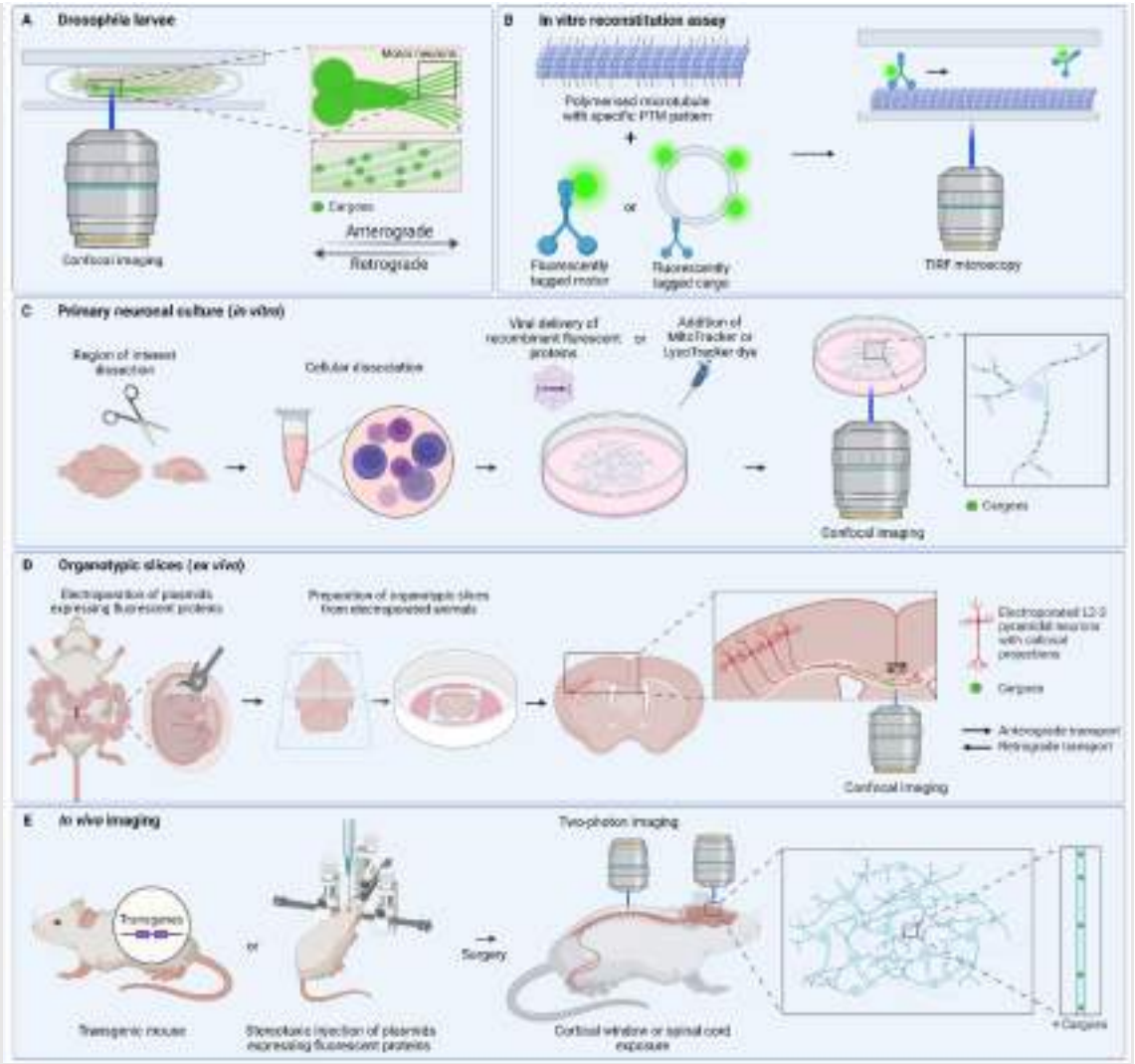

Figure 10: Methods for the study of neuronal transport

A. Transgenic D*rosophila* larvae expressing fluorescent recombinant proteins that tag specific cargoes can be used for the *in vivo* imaging of axonal transport. The larva is placed in a dorsal position on a coverslip and the motor neurons emerging from the brain can then be imaged through the cuticle to reveal moving cargoes.

B. *In vitro* reconstitution assays consist in mixing purified MTs harboring specific PTM signatures together with fluorescently tagged motors or cargoes to assess the dynamics of transport in a simplified system. Total internal reflection fluorescence (TIRF) microscopy is required for this type of imaging.

C. Primary cultures of rodent neurons enable easy genetic and pharmacological manipulation of neurons which helps in studying the regulation of transport mechanisms. Cultured neurons are typically imaged with a confocal microscope.

D. *Ex vivo* systems can be created by preparing organotypic slices following unilateral cortical electroporation of fluorescent proteins. The cortico-cortical projections of layer 2-3 neurons

that pass through the corpus callosum can then be imaged by confocal microscopy to reveal moving cargoes.
E. Transgenic mice or stereotaxic injection of adeno associated viruses allow the fluorescent labelling of cargoes in the central nervous system of living animals. *In vivo* imaging of neuronal transport can then be performed thanks to the development of innovative surgeries that exploit two-photon microscopy to image through a cortical window or after spinal cord exposure. Panels **(A)** and **(D)** are adapted from (Turchetto, Broix and Nguyen, 2020b; Turchetto *et al.*, 2022).

5. Development and anatomy of the hippocampus

The hippocampus is part of the limbic system and is particularly important for the generation of new memories and spatial navigation (Sprick, 1995; Burgess, Maguire and O'Keefe, 2002; Rudy and Matus-Amat, 2005). It is made up of three cortical layers called the archicortex, which is believed to be the phylogenetically oldest region of the cerebral cortex (Murray, Wise and Graham, 2018). The adjacent neocortex is composed of six cortical layers and may be the most recent product of evolution (Rakic, 2009). During embryonic development, the ventricular zone (VZ) and subventricular zone (SVZ) that borders the lateral ventricles is populated by stem cells that generate the wide diversity of neurons and glia in the brain (Gupta, Tsai and Wynshaw-Boris, 2002; Sultan, Brown and Shi, 2013). The proliferative region of the dorsal brain, also called pallium, will generate the glutamatergic neurons of the cortex and hippocampus while the ventral brain, also called subpallium, will generate GABAergic neurons that migrate tangentially into the pallium (**Figure 11**). In this section I will provide an overview of hippocampus development and anatomy with a special emphasis on the origin and diversity of hippocampal interneurons (INs) which are the focus of **Chapter 1**.

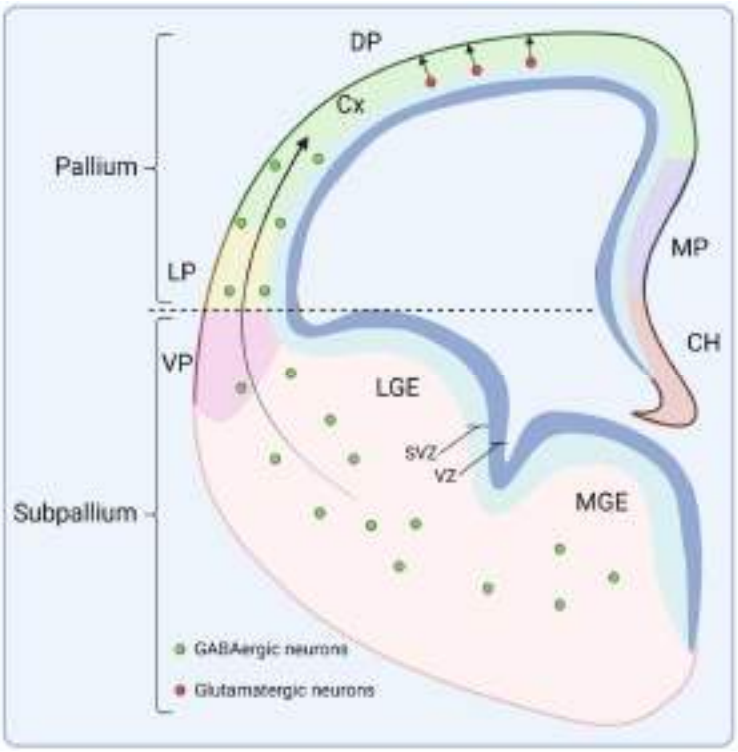

Figure 11: Overview of cortical development

Schematic representation of a coronal mouse brain slice at 14.5 days of gestation (E14.5). The ventricular zone (VZ) and subventricular zone (SVZ) are neurogenic zones that border the lateral ventricle of the developing brain. At this rostro-caudal level, the ventral part of the brain (subpallium) is made of the medial ganglionic eminence (MGE) and lateral ganglionic eminence (LGE). The former generates GABAergic neurons that migrate tangentially into the cortex. The dorsal part of the brain (pallium) generates glutamatergic neurons that migrate radially to settle in cortical layers. The pallium is divided in the ventral pallium (VP) and lateral pallium (LP) that will generate the piriform cortex, the dorsal pallium (DP) will generate the neocortex and finally the medial pallium (MP) will give rise to the hippocampus under the influence of cues from the cortical hem (CH).

5.1 Overview of hippocampus development

The development of the hippocampus is orchestrated by the cortical hem (CH) which directs the differentiation of the medial pallium (MP) into the hippocampus (Moore and Iulianella, 2021). The MP is further subdivided into the hippocampal neuroepithelium (NHE) and the dentate neuroepithelium (DNE) that will respectively give rise to the Ammon horn and the dentate gyrus. The development process by which PNs of Ammon's horn and granule neurons of the dentate gyrus (DG) are generated is explained in (**Figure 12**).

The CH expresses morphogens, including wingless/int (Wnt) and bone morphogenetic protein (BMP) to orchestrate hippocampal development (Grove *et al.*, 1998; Subramanian and Tole, 2009). Loss of Wnt3a in mice, one of the morphogen expressed by the CH, results in almost complete loss of the hippocampus whereas the rest of the pallium seems largely unaffected (Lee *et al.*, 2000). Similarly, chimeric mice in which Lhx2 is lost only in some cells develop patches of CH tissue in the pallium which results in the development of one hippocampal field per patch of CH (Mangale *et al.*, 2008). Together, these studies establish the CH as the organizing center of the hippocampus.

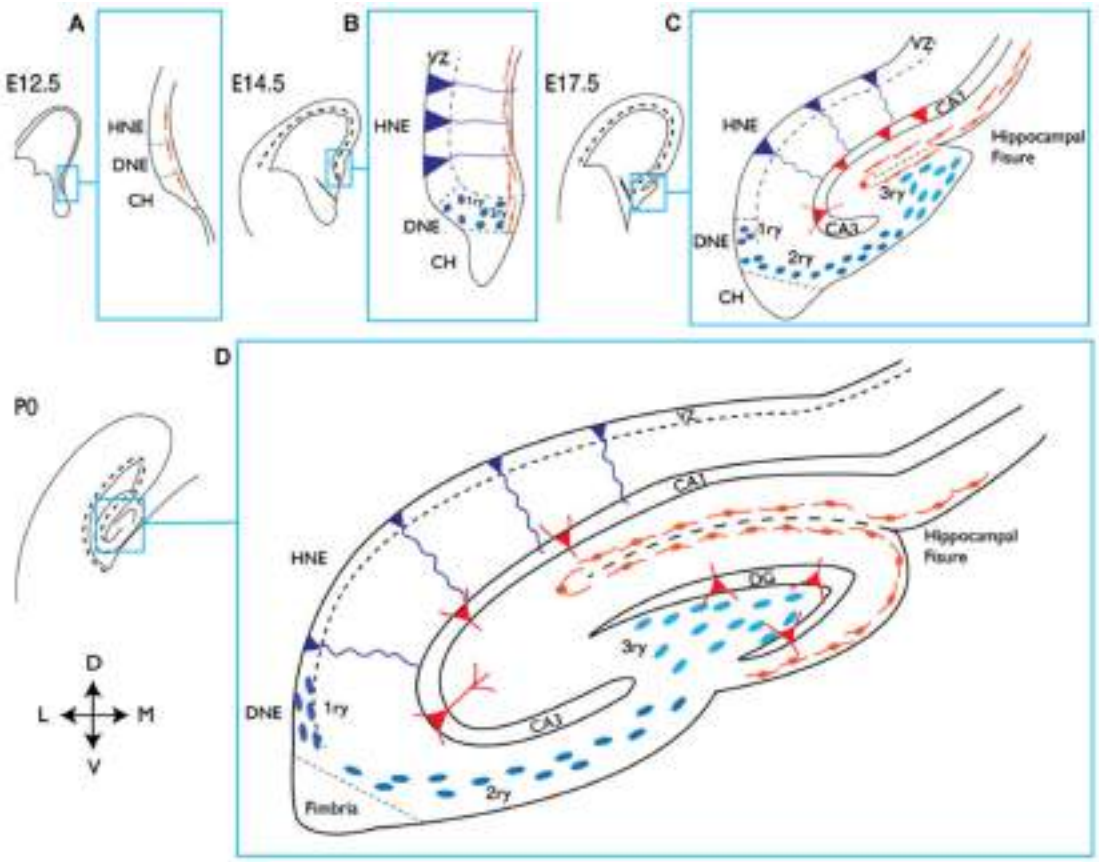

Figure 12: Development of the mouse hippocampus

Schematic representation of the mouse hippocampus development from E12.5 to P0. Figure from (Urbán and Guillemot, 2014).

A. The medial pallium (MP) is subdivided into the hippocampal neuroepithelium (HNE) and the dentate neuroepithelium (DNE) which will give rise to Cajal-Retzius cells (in orange).

B. At E14.5 radial glial cells (dark blue) of the HNE proliferate and start generating glutamatergic neurons. Precursor cells of the DNE migrate to form the primary and secondary matrix.

C. At E17.5, the nascent hippocampus starts to fold on itself to generate the hippocampal fissure where the stem cells of the tertiary matrix will migrate. Neurons (in red) are produced

from the radial glia of the HNE and settle in the pyramidal layer of Ammon's horn made up of the CA1, CA2 and CA3 fields.
D. At P0, numerous granule neurons (red) born from the primary, secondary and tertiary matrixes invade the dentate gyrus (DG). Cells in the tertiary matrix self-renew and maintain the production of granule neurons postnatally.

5.2 Organization of the hippocampal circuitry

The hippocampal circuitry has historically been a subject of intense study due to the relative simplicity of its organization. It is neatly organized in layers that delineate the neuronal cells and the zones of connectivity (Johnston and Amaral, 2004). The main hippocampal circuit forms a loop connecting the entorhinal cortex, dentate gyrus, CA3 and CA1 which projects back to the entorhinal cortex though the subiculum (Johnston and Amaral, 2004; Deng, Aimone and Gage, 2010) (**Figure 13**).

In addition to the trisynaptic circuit, the hippocampus is largely connected to the rest of the brain. Connections to the cingulate cortex, amygdala and thalamus modulate hippocampus function and tether it to emotional centers of the brain (Ghosh, Laxmi and Chattarji, 2013; Bubb, Kinnavane and Aggleton, 2017). The hippocampus is also strongly connected to the neocortex and interestingly, a large body of studies has demonstrated that although the hippocampus is critical for the generation and retrieval of memories, long-term memories tends to be stored in the cortex (Scoville and Milner, 1957; Squire and Zola-Morgan, 1991; Schacter, 1997).

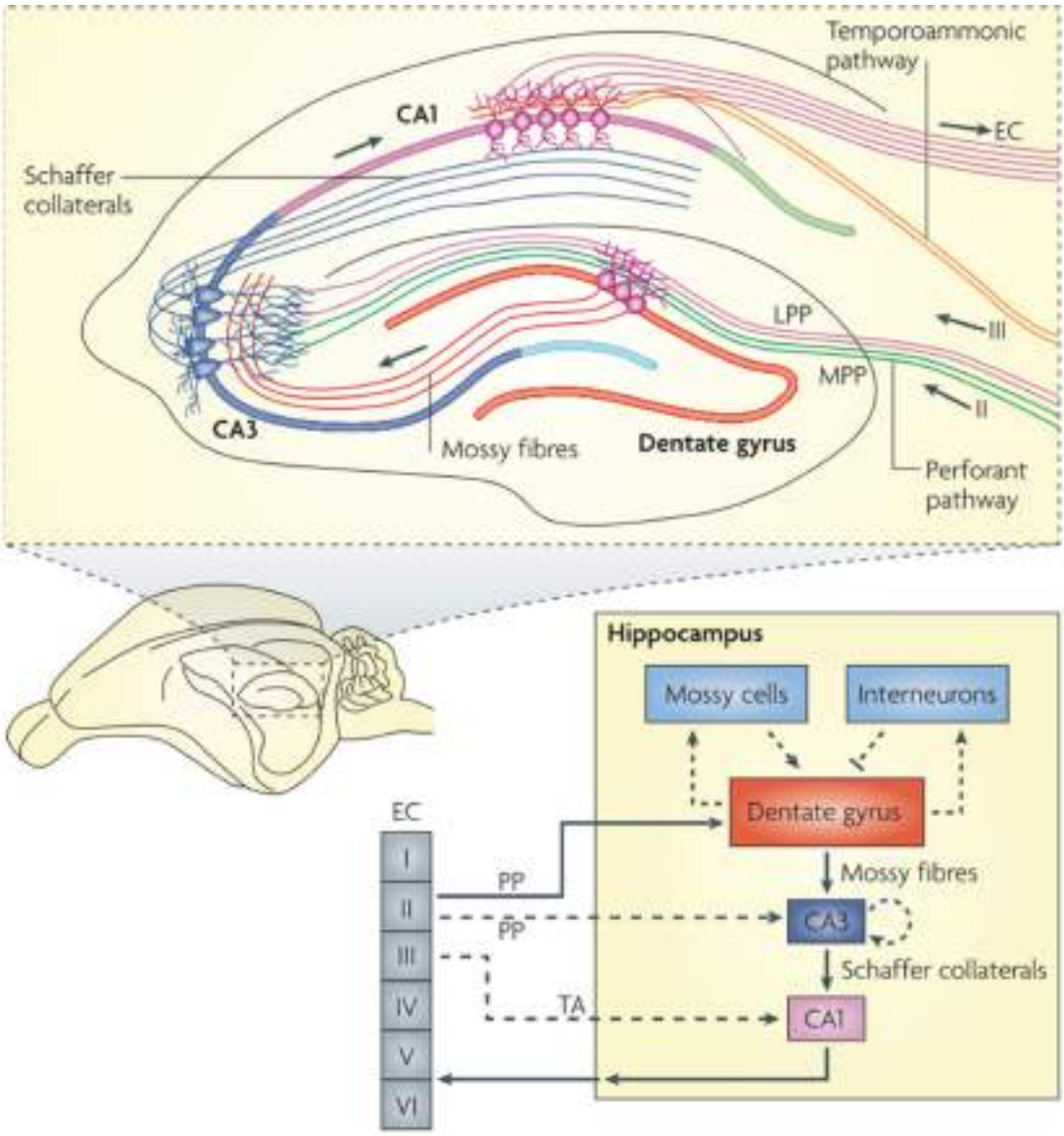

Figure 13: The trisynaptic circuit of the hippocampus

The dentate gyrus receives synaptic input from the perforant pathway (PP) which consists in axons from the lateral perforant pathway (LPP) and medial perforant pathway (MPP) that originate from the layer 2 of the entorhinal cortex (EC). Granule neurons of the dentate gyrus then project to CA3 neurons through the mossy fibers that in turn project to CA1 neurons through the Schaffer collaterals. This circuit is also termed the trisynaptic circuit. The loop is closed by the projection of CA1 neurons back to the layers 5 and 6 of the entorhinal cortex through the temporoammonic pathway that passes through the subiculum. Figure adapted from (Deng, Aimone and Gage, 2010).

Although the CA2 region of the hippocampus has historically been considered as a transition zone between CA3 and CA1 and has largely been ignored, recent discoveries have reignited interest in this atypical structure. Indeed, the CA2 region expresses specific biomarkers that

differentiate it from CA1 and CA3. RGS14 and PCP4 which are involved in calcium homeostasis are specifically expressed in CA2 PNs in the hippocampus (Kohara *et al.*, 2014). Additionally, some extracellular matrix proteoglycans which are usually detected only in the perineuronal-nets of parvalbumin (PV) INs are particularly abundant around PNs of the CA2 region (Carstens *et al.*, 2016; Noguchi *et al.*, 2017). This demonstrates that CA2 has a very specific molecular identity and interestingly it also correlates with specific electrophysiological properties as CA2 PNs typically show remarkably low synaptic plasticity in comparison to other hippocampal glutamatergic neurons (Zhao *et al.*, 2007). The lack of synaptic plasticity may in part be due to the strong expression of calcium-regulating proteins such as RGS14 and PCP4 but also to the complex extracellular matrix around CA2 PNs (Lee *et al.*, 2010; Carstens *et al.*, 2016; Robert *et al.*, 2018).

The discoveries of unique biomolecular signatures of CA2 PNs has allowed researchers to probe the function of these neurons using genetic models which led to the discovery that CA2 is crucial for social memory (Hitti and Siegelbaum, 2014; Meira *et al.*, 2018; Robert *et al.*, 2021). Interestingly, CA2 exhibits a specific pattern of connectivity with strong bilateral connections to the supramamillary nucleus and medial septum which are also involved in social memory (Hitti and Siegelbaum, 2014; Kohara *et al.*, 2014; Robert *et al.*, 2021). Additionally, CA2 receives modulatory input from vasopressin and oxytocin neurons from the periventricular nucleus which is also crucially involved in social interactions (Cui, Gerfen and Young, 2013; Smith *et al.*, 2016). CA2 PNs encode social memory by projecting to CA1 ventral cells that store social memory (Okuyama *et al.*, 2016). Together these studies suggest that instead of being a transition region between CA1 and CA3, CA2 may be a major hub integrating inputs from various brain regions involved in social interactions to enable the encoding of social memory in ventral CA1 neurons.

5.3 Hippocampal INs

GABAergic INs constitute the second major neuronal class of neurons in the hippocampus and form microcircuits with excitatory principal cells that typically project over longer distances. INs tend to innervate multiple neurons locally through an exquisitely complex and ramified axon and modulate neuronal activity through the release of the inhibitory neurotransmitter GABA. Although INs represent about 10-15% of hippocampal neurons, this diverse cell

population is essential for the appropriate computation of hippocampal circuits (Bezaire and Soltesz, 2013). Hippocampal INs are essential to regulate the excitability of PNs and the precise timing of inhibitory input enables the synchronization of PN activity which results in broad frequency waves measurable by electroencephalogram (Pelkey *et al.*, 2017). In this section I will highlight the diversity in the molecular features, hodology and function of the IN population, provide a brief overview of their origin and address their critical importance in pathological contexts.

5.3.1 IN diversity

INs can be subdivided in classes depending on the expression of class-specific proteins, their transcriptome, morphology, positioning within the hippocampal layers, pattern of projections and electrophysiological properties (Pelkey *et al.*, 2017; Booker and Vida, 2018). A single-cell RNA sequencing study of the neocortex and CA1 region of hippocampus has revealed 16 subclasses of INs that could be delineated from their transcriptomic profile. However, this likely does not even capture the full complexity of IN subtypes since multiple subclasses of PV and somatostatin (SST) can be differentiated by their morphology but only few could be identified through RNA sequencing (Zeisel *et al.*, 2015). Another study found that the PV class of INs could not be clustered into its various subtypes by single-cell RNA sequencing due to the limited transcriptomic changes between PV subtypes (Que *et al.*, 2021). This suggests that broad classes of INs can be clustered by single-cell RNA sequencing but a small number of changes in gene expression within a class of IN are enough to drive meaningful changes to their morphological and functional properties. Consequently, only the observation of a combination of IN features can appropriately delineate IN subtypes. At least 29 subtypes of INs can be recognized in the hippocampus by the combined observation of their morphological, molecular and hodological profiles (Booker and Vida, 2018) (**Figure 14**). IN subtypes and their properties are thoroughly reviewed in: (Pelkey *et al.*, 2017; Booker and Vida, 2018).

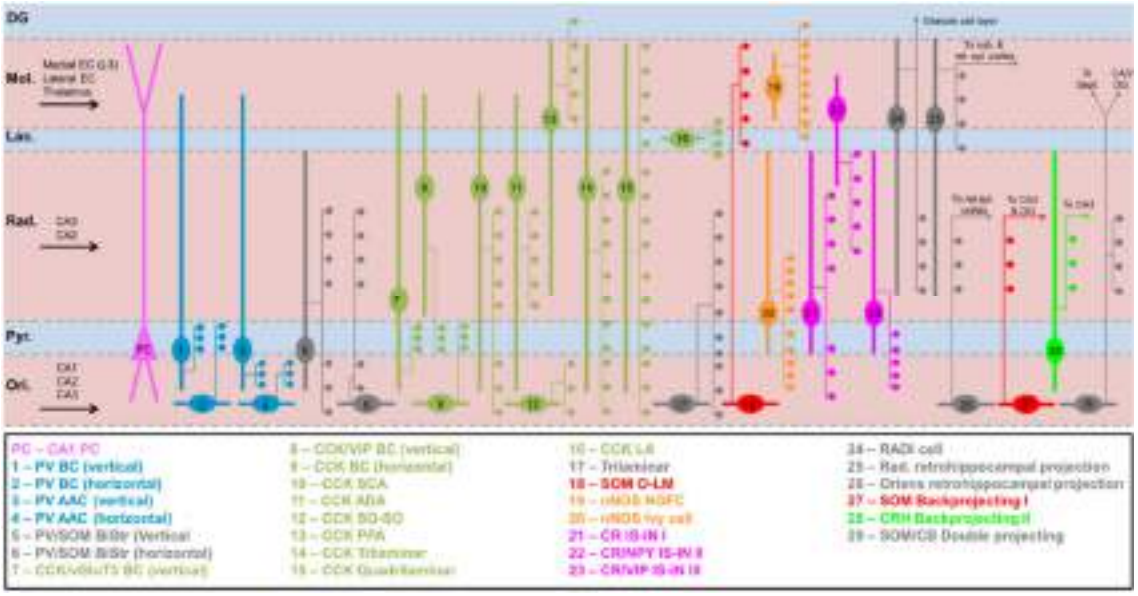

Figure 14: Schematic representation of known IN subtypes in the mouse hippocampus
The CA subfields of the hippocampus are divided in layers. The *stratum oriens* (*Ori*.), *stratum pyramidale* (*Pyr*.), *stratum radiatum* (*Rad*.), *stratum lacunosum* (*Lac*.), and *stratum moleculare* (*Mol*.). The *stratum pyramidale* harbors the pyramidal cells (PC) which are the excitatory neurons of the hippocampus. INs are dispersed within all layers and exhibit specific patterns of projection onto PCs and INs. Some INs mainly innervate the perisomatic region of PCs, such as PV and CCK basket cells while others innervate mostly the dendritic region of PCs or target INs.
Abbreviations; BC: Basket cells, AAC: axo-axonic cells, BiSTR: Bi-stratified, SOM: somatostatin, CCK: cholecystokinin, VIP: vasoactive intestinal peptide, SCA: schaffercollateral-associated, ADA: apical dendrite-associated, SO-SO: *str. oriens-str. oriens*, PPA: perforant path-associated, LA: lacunosum-associated, O-LM: *str. oriens-lacunosum moleculare*, NGFC: neurogliaform cells, CR: calretinin, NPY: neuropeptide Y, IS-IN: IN-specific INs, CRH: corticotropin-releasing hormone, CB: calbindin, Figure from (Booker and Vida, 2018).

Although IN subtypes largely overlap across the CA1, CA2 and CA3 fields, some differences can be noted. For instance, IN density is particularly high in the CA2 region where PV and SST neuron density is almost 2-fold higher (Botcher *et al.*, 2014). Additionally, PV basket cells (BCs) which mostly innervate the perisomatic region of PNs show much longer dendrites in the CA2/CA3 area as compared to the CA1 subfield (Tukker *et al.*, 2013). PV cells of the CA2 region exert a strong feedforward inhibition onto CA2 PNs which can be lifted by an inhibitory long-term depression (I-LTD) triggered by a tetanus in CA3 PNs. This I-LTD of PV neurons is unique to CA2 and defects in feedforward inhibition may be involved in schizophrenia (Piskorowski and Chevaleyre, 2013; Piskorowski *et al.*, 2016). Together these studies suggest that although IN subtypes are very similar across the CA fields, slight changes in the distribution and electrophysiological properties of INs may reflect meaningful functions specific to a subfield.

5.3.2 Hippocampal IN origins

The remarkable diversity of INs unfolds progressively as corticogenesis proceeds where some IN subclasses can already be identified based on their place and time of birth. Cortical INs are born in the ventral part of the brain in embryonic structures called the ganglionic eminences. They then undergo a long tangential migration to the pallium to reach their final destination and intermingle with excitatory neurons (Ayala, Shu and Tsai, 2007; Silva, Peyre and Nguyen, 2019). The ganglionic eminences are subdivided in three anatomical regions that develop sequentially in the following order: the medial ganglionic eminence (MGE) at E9, the lateral ganglionic eminence (LGE) at E10, and the caudal ganglionic eminence (CGE) at E11 (Pelkey *et al.*, 2017). Hippocampal INs originate from the MGE and CGE and each region specializes in the generation of specific IN subtypes (**Figure 15**).

At early stages, expression of transcription factors such as Dlx1,2 in progenitors and Dlx5,6 in post-mitotic INs derived from the GEs drives these cells towards a GABAergic IN fate (Panganiban and Rubenstein, 2002; Long *et al.*, 2009; Wang *et al.*, 2010). In addition to transcription factors shared across IN subtypes, evidence suggests that IN diversity already starts to emerge at the progenitor and early-postmitotic stage in GEs. Indeed, specific transcriptomic signatures anticipate the expression of IN-subtype biomarkers such as PV and SST which therefore allows researchers to predict the fate of INs at early stages of development (Mayer *et al.*, 2018; Mi *et al.*, 2018). Fine differences in IN subtypes remain hard to predict at early stages however and it is likely that a combination of cell-intrinsic genetic programs and environmental cues refine the identity of INs (Wamsley and Fishell, 2017; Lim *et al.*, 2018).

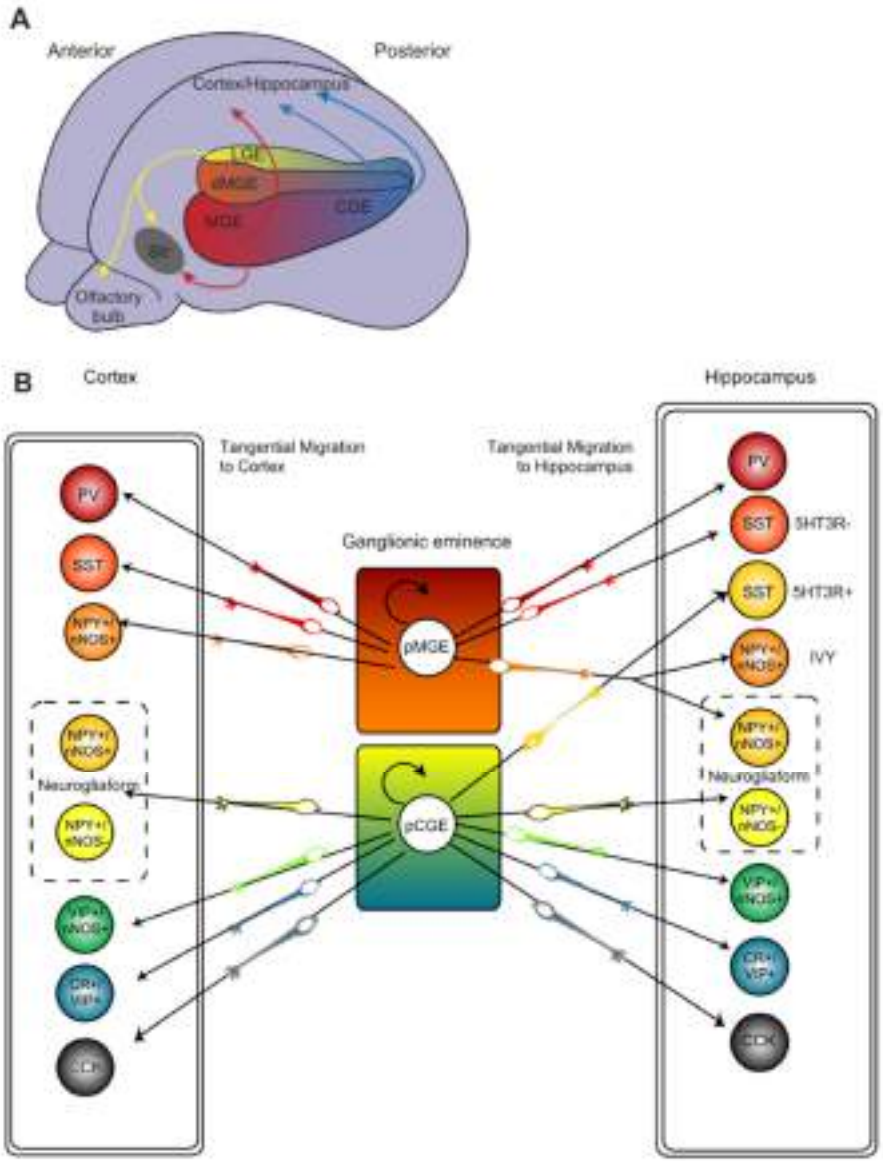

Figure 15: Origin of hippocampal IN diversity

A. The medial ganglionic eminence (MGE) and dorsal-MGE (dMGE) produce INs destined to the striatal (Str), neocortical and hippocampal regions. The lateral ganglionic eminence (LGE) contributes to the production of INs for the striatum and is responsible for the generation of most GABAergic olfactory neurons. INs from the caudal ganglionic eminence (CGE) specifically target the neocortex and hippocampus. A small number of INs are also produced by the preoptic area (POA). Hippocampal INs therefore originate primarily from the MGE and CGE.

B. In the cortex, all PV and SST neurons are generated from MGE progenitors (pMGE) while the rest of IN subtypes emerge from CGE progenitors (pCGE). The generation of hippocampal INs is slightly more complex since the CGE contributes to a pool of SST INs and some neuropeptide-Y (NPY) INs originate from the MGE.

Figure adapted from (Pelkey *et al.*, 2017).

5.3.3 Microcircuit disorders in neuropathology

Based on the critical function of microcircuits, it is not surprising that alterations in INs underly numerous neurological disorders such as autism spectrum disorder (ASD), schizophrenia, epilepsy or depression and in some cases hippocampal INs have also been linked to neurodegenerative disorders such as Alzheimer's disease (AD) (Pelkey *et al.*, 2017).

Dysfunctions in inhibitory transmission can arise from developmental defects which alter the production, migration and specification of INs therefore perturbing microcircuits. Mutations in the *Tsc1* gene can cause autism and epilepsy in human patients. In a mouse model where *Tsc1* is lost in INs, IN numbers in the hippocampus are reduced and IN migration is perturbed. Loss of *Tsc1* in INs is sufficient to reduce the threshold at which epileptic seizures are induced, suggesting an involvement of INs in the pathophysiology (Fu *et al.*, 2012). Similarly, mutations in *Cntnap2* gene are strongly associated with epilepsy and autism in human patients and *Cntnap2* KO mice recapitulate this phenotype (Peñagarikano *et al.*, 2011). Defects in neuronal migration may account for the reduction of INs observed in these mice and consequently, perisomatic inhibition on CA1 PNs is reduced (Peñagarikano *et al.*, 2011; Jurgensen and Castillo, 2015).

Mutations in genes that control synaptic function in INs are also commonly associated with neurological disorders. Mutations in *Epha7* can cause neurodevelopmental alterations in humans (Lévy *et al.*, 2021) and loss of *Epha7* in mice destabilizes GABAergic synapses in the hippocampus and results in impaired long-term potentiation and learning (Beuter *et al.*, 2016). The Shank family of proteins is also strongly linked to ASD in humans and Shank mice models recapitulate the behavioral hallmarks of ASD (Jiang and Ehlers, 2013). Shank are synapse scaffolding proteins and *Shank1* is strongly expressed in PV INs of the hippocampus. Consequently, loss of *Shank1* results in reduced firing of PV INs and a shift in the excitatory/inhibitory balance that has often been associated with ASD (Mao *et al.*, 2015; Lee, Lee and Kim, 2017). Together these studies suggest that alterations in the development and synaptogenesis of INs contribute to the pathophysiology of neurodevelopmental disorders.

Loss of hippocampal INs can also occur after birth which perturbs microcircuits thus resulting in behavioral alterations characteristic of schizophrenia or AD. In the 22q11.2 deletion model of schizophrenia, mice suffer from a progressive loss of PV in the hippocampus that results in

reduced feedforward inhibition and impaired social cognition. Interestingly, rescue of PV excitability improves the behavioral hallmarks of the disease (Piskorowski *et al.*, 2016; Marissal *et al.*, 2018). Hippocampal INs have also been studied in the context of AD and have yielded conflicting results which may reflect the diverse methodologies for IN detection, the various models of ADs and region-specific changes in IN numbers (Reid *et al.*, 2021). A meta-analysis combining studies of hippocampal IN numbers in human post-mortem AD brains and rodent AD models found that PV INs tend to degenerate early in the disease while NPY and CCK INs are affected later (Reid *et al.*, 2021). Transplantation of MGE progenitors in the hippocampus results in the functional integration of new INs into microcircuits which can reduce behavioral deficits in an AD mouse model overexpressing the human amyloid precursor protein (Martinez-Losa *et al.*, 2018). This suggests that loss of INs may contribute to the pathogenesis of some neurological disorders and INs may therefore constitute a therapeutic target in these contexts.

AIMS OF THE STUDY

MTs are the substrates for several PTMs which consists in the addition or subtraction of modifying groups (Janke and Magiera, 2020). Common modifications of tubulin include phosphorylation, acetylation, ubiquitylation or glutamylation among others and this thesis focuses on the role of MT acetylation and glutamylation on the regulation of intracellular transport.

The presentation of my thesis work will then be divided in two chapters:

Chapter 1: Microtubule polyglutamylation in GABAergic neurons: A key regulator of axonal transport and synaptic homeostasis

This chapter focuses on a detailed analysis of a model in which CCP1 is lost in hippocampal INs. We aim to answer the following questions:

1) Is CCP1 loss alone sufficient to induce hyperglutamylation in specific IN subtypes?
2) Since hyperglutamylation induces transport defects in projection neurons and cerebellar granule cells, does it extend to INs?
3) Does IN hyperglutamylation induce neurodegeneration and/or alterations in hippocampal circuitry?

Chapter 2: Uncovering the role of organelles in the regulation of microtubule acetylation and axonal transport dynamics

This chapter focuses on two studies that shed light on the tight link between MT acetylation and axonal transport. The questions we aim to answer are:

1) Is there a causal link between MT acetylation levels and transport efficiency of multiple cargoes across species?
2) By which mechanisms is αTAT1 activity regulated?
3) Do cargoes contribute to the regulation of MT acetylation and how is this accomplished?

CHAPTER 1:

Microtubule polyglutamylation in GABAergic neurons: A key regulator of axonal transport and synaptic homeostasis

1. Context of the study

Loss of CCP1 in the pcd mouse results in the degeneration of specific cell types of the brain, such as the Purkinje cells, while others appear largely unaffected (Mullen, Eichert and Sidman, 1976; Landis and Mullen, 1978; Greer and Shepherd, 1982; O'Gorman, 1985; O'Gorman and Sidman, 1985). It remains unclear why only specific cell subtypes die but it may in part result from the balance of expression of enzymes regulating glutamylation in Purkinje and mitral cells. Indeed, Purkinje cells express very low levels of CCP6 and degenerate while cortical neurons are susceptible to degeneration only after concomitant CCP1 and CCP6 loss (Kalinina *et al.*, 2007; Rogowski *et al.*, 2010; Magiera *et al.*, 2018). Susceptibility to CCP1 loss in the cortex and hippocampus has been studied with a specific focus on PNs. No previous studies addressed how polyglutamylation is regulated in interneurons and how these cells react to changes in the levels of glutamylation.

We have previously demonstrated that at embryonic stages, CCP1 is expressed in the GEs and migrating INs (Silva *et al.*, 2018). Using a conditional mouse model to invalidate CCP1 function specifically in newborn post-mitotic INs (CCP1 cKO), we uncovered a role for CCP1 in the regulation of the discontinuous (saltatory) migration. This regulation occured via deglutamylation of the myosin light chain kinase (MLCK). CCP1 loss in those neurons resulted in increased MLCK activity and changes of myosin-actin contractions that converted the IN mode of migration from saltatory to sliding. This subsequently increased the synchronicity of IN movement at the population level, resulting in higher numbers of INs in the cortex of CCP1 cKO as compared to WT mice at embryonic stages. However, IN numbers are normalized in the cortex of postnatal mice (Silva *et al.*, 2018).

Here we ask whether adult INs are sensitive to CCP1 loss by leveraging the CCP1 cKO model which allows the deletion of CCP1 specifically in INs. We focus on the hippocampus where CCP1 loss in PNs has already been studied and extend upon this study by looking specifically at hippocampal IN subtypes.

2. Results

2.1 Ccp1, Ccp6 and Ttll1 mRNA expression levels in PV and SST hippocampal INs

Evidence from CCP1 and CCP6 loss in the cortex shows that only a small proportion of neurons (about 20%) degenerate at 5 months in mice, contrary to the cerebellum where all Purkinje cells degenerate by the first month of life (Mullen, Eichert and Sidman, 1976; Magiera *et al.*, 2018). We hypothesized that specific neuronal types may be sensitive to CCP1 loss and leveraged public databases of RNA-sequencing to find differential expression of enzymes regulating polyglutamylation in IN subtypes. The HippoSeq database comprises a study of RNA expression in PV and SST interneurons database (Cembrowski *et al.*, 2016). PV-CRE and SST-CRE transgenic mice were injected with AAVs carrying a plasmid for conditional expression of eGFP within the hippocampus. GFP positive cells were manually sorted according to the method described in (Hempel, Sugino and Nelson, 2007) and bulk RNA-sequencing was performed. 3 male mice for each genotype (PV-CRE and SST-CRE) were used to generate the reference data that can be consulted with an interactive tool at https://hipposeq.janelia.org/int/.

Using the HippoSeq database (Cembrowski *et al.*, 2016), we compared the expression levels of the main enzymes regulating tubulin polyglutamylation in the brain. We found that PV and SST INs were enriched in *Pvalb* and *Sst* respectively which suggests appropriate sorting of the two subtypes. In addition, some differences in the expression of enzymes regulating polyglutamylation emerged and in particular, the *Agtpbp1* gene which encodes for CCP1 has a higher level of expression in PV compared to SST INs (**Figure 21**).

This preliminary analysis led us to investigate the expression levels of polyglutamylation enzymes in PV and SST INs from the adult hippocampus to reveal a putative sensitivity to CCP1 loss. We compared enzyme expression levels in 3 months old WT and CCP1 cKO mice using the BaseScope™ technology (Baker *et al.*, 2017; Y. Wang *et al.*, 2019). CCP1 cKO mice correspond to a double transgenic model that combines: **1)** CRE and GFP expression under an enhancer sequence common to *Dlx5* and *Dlx6* that are expressed embryonically in post-mitotic GABAergic neurons of the MGEs; **2)** Floxed exons 20 and 21 of the *Ccp1* gene for deletion of the catalytic site of CCP1 following CRE recombination. CCP1 cKO mice have been

characterized in a previous publication of the lab and show efficient loss of CCP1 function in post-mitotic GABAergic neurons specifically (Silva *et al.*, 2018). WT mice in this study refers to a model that also express CRE and GFP under the control of Dlx5,6 but carries two WT *Ccp1* alleles.

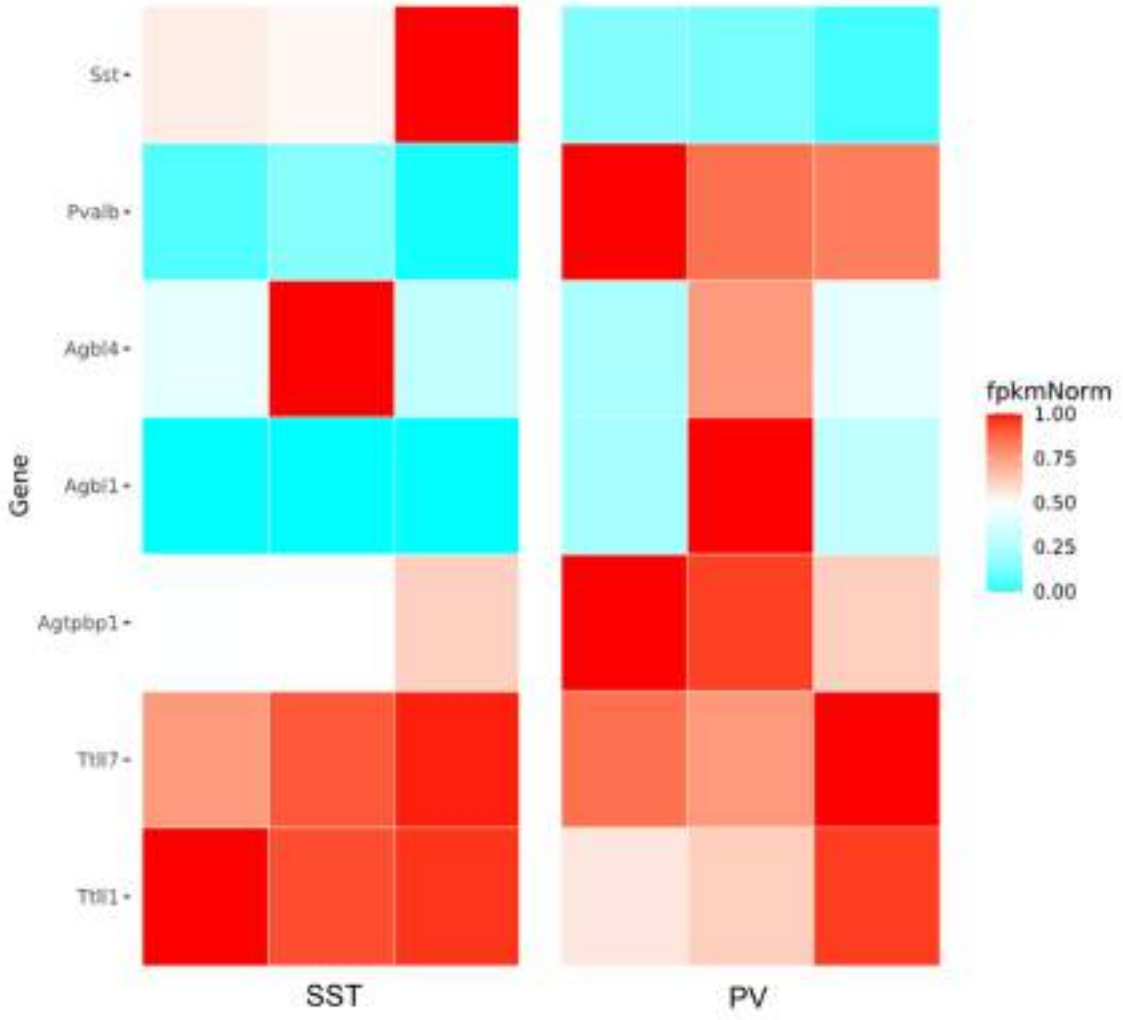

Figure 21: Expression levels of the enzymes regulating tubulin polyglutamylation in PV and SST hippocampal INs

We used the Hipposeq database to compare the expression levels of the major enzymes regulating tubulin polyglutamylation in PV and SST INs (Cembrowski *et al.*, 2016). Each square represents the normalized fragments per kilobase of exon per million reads (fpkmNorm) for one replicate and one gene. Expression levels of *Pvalb* and *Sst* accurately differentiate PV and SST INs. In addition, *Agtpbp1* (alternative name of *Ccp1*) appears to be more expressed in PV than SST INs. *Agbl1* encodes for CCP4, *Agbl4* encodes for CCP6.

We chose a technique that allows single RNA-molecule detection *in situ* to analyze the expression levels of *Ccp1*, *Ccp6* and *Ttll1* mRNA in PV and SST cells. BaseScope™ technology

is a variant of RNAScope™ which allows the quantification of single mRNA molecules on brain slices, combined with immunohistochemistry (Bunda and Andrade, 2022). It uses probes that hybridize to the target mRNA and multiple signal amplification steps to generate a punctate signal where each *puncta* represents a single mRNA of interest. Contrary to RNAScope™, BaseScope™ probes can identify target regions as small as 300bp which allowed us to design probes for *Ccp1* (*Agtpbp1*) that target specifically the exons 20 and 21, therefore controlling for the loss of these exons in CCP1 cKO INs. In addition, we designed probes for *Ttll1*, the major α-tubulin polyglutamylase in the brain and *Agbl4* which encodes for CCP6 and may compensate for CCP1 loss in the cortex and hippocampus (Rogowski *et al.*, 2010; Magiera *et al.*, 2018). We combined the detection of *Ccp1*, *Ccp6* and *Ttll1* mRNA with immunohistochemistry for PV and SST INs to count the number of *punctae* of each mRNA in the soma of these IN subtypes.

Consistent with the analysis of the Hipposeq database, we find that CCP1 mRNA levels are higher in PV as compared to SST INs in WT animals. As expected, no signal for *Ccp1* mRNA was detected in CCP1 cKO INs (**Figure 22 A-C**). *Ccp6* mRNA levels were also elevated in PV INs of WT animals and surprisingly, CCP1 cKO animals showed reduced *Ccp6* levels in PV INs as compared to WT animals (**Figure 22 D-F**). Finally, *Ttll1* mRNA levels were higher in PV INs compared to SST INs in both the WT and CCP1 cKO condition but a reduction in *Ttll1* levels could be detected between WT and CCP1 cKO PV INs (**Figure 22 G-I**). Together, these results suggest that PV INs may exhibit a particular sensitivity to CCP1 loss due to the high level of Ccp1 mRNA expression in those cells, the lack of compensation by *Ccp6* mRNA expression and the only moderate downregulation of *Ttll1*.

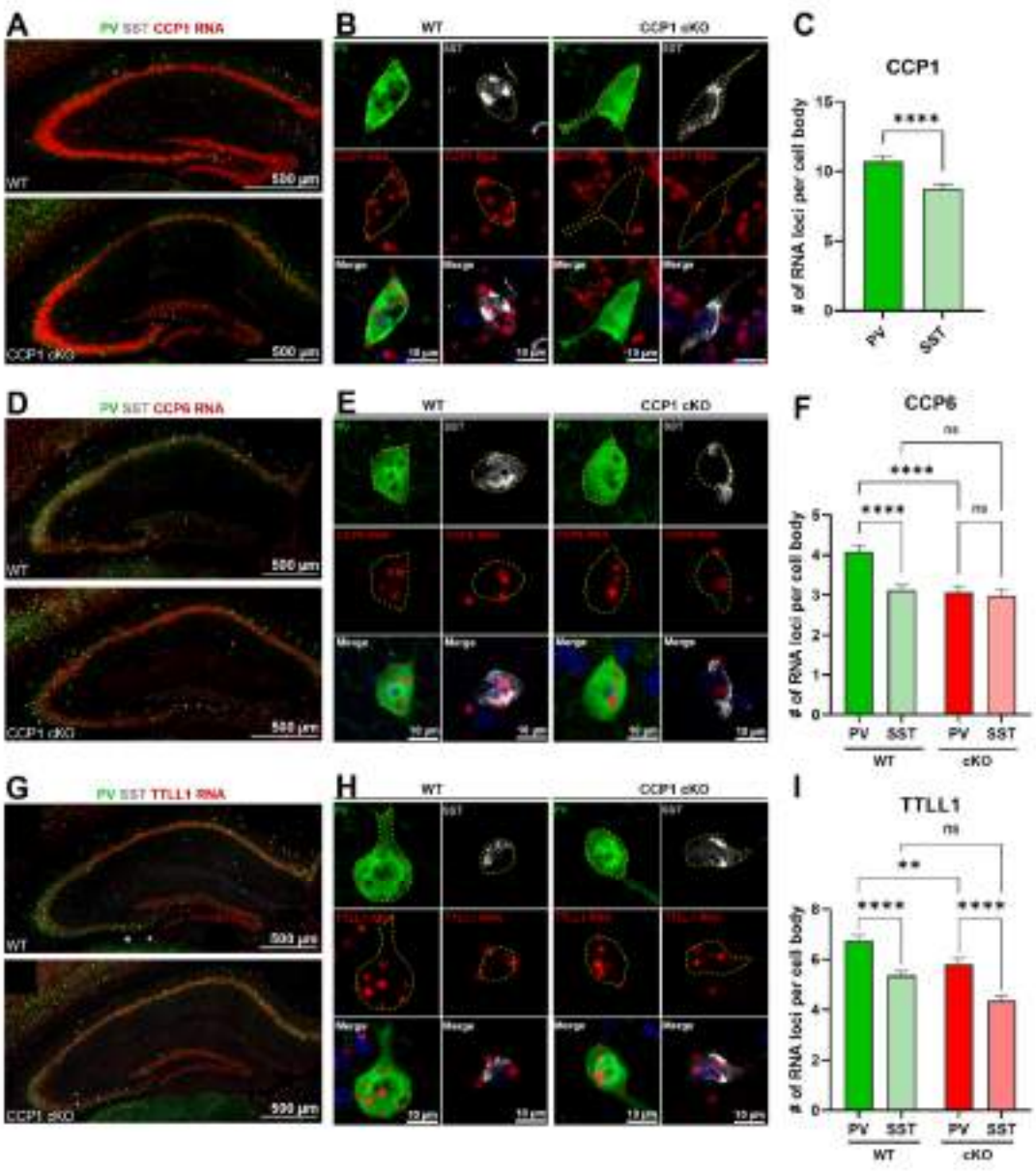

Figure 22: IN subtypes express different levels of polyglutamylation enzyme mRNA and respond differently to CCP1 loss.

A, D and G. Representative images of hippocampi slices from 3 months WT and CCP1 cKO showing expression of *Ccp1*, *Ccp6* and *Ttll1* mRNA together with co-detection of PV and SST immunoreactivity.

B, E and H. Magnification of hippocampal PV and SST INs showing representative BaseScope™ signal for *Ccp1*, *Ccp6* and *Ttll1* mRNA. Yellow doted lines represent the contours of the cell-body.

G. Quantification of the number of *Ccp1* mRNA loci within the cell bodies of WT PV and SST INs. Because no signal is present for CCP1 RNA in CCP1 cKO INs, quantification was only performed in WT animals. $n_{PV\text{-}WT}$ = 156 neurons, $n_{SST\text{-}WT}$ = 165 neurons from 3 WT mice. For statistical analysis, a Mann-Whitney analysis was conducted ($p < 0.0001$).

H-I. Quantification of the number of *Ccp6* or *Ttll1* mRNA loci within the cell bodies of WT and CCP1 cKO PV and SST INs. For CCP6, $n_{PV\text{-}WT}$ = 266 neurons, $n_{SST\text{-}WT}$ = 255 neurons, $n_{PV\text{-}cKO}$ = 171 neurons, $n_{SST\text{-}cKO}$ = 107 neurons from 4 WT and 3 CCP1 cKO mice. For TTLL1, $n_{PV\text{-}WT}$ = 225 neurons, $n_{SST\text{-}WT}$ = 234 neurons, $n_{PV\text{-}cKO}$ = 196 neurons, $n_{SST\text{-}cKO}$ = 201 neurons from 4 WT and 3 CCP1 cKO mice. For statistical analysis, data was transformed according to the formula Y = sqrt(Y+1) to obtain a normal distribution, then a two-way ANOVA analysis was conducted. ** = $p < 0.1$, *** = $p < 0.01$, **** = $p < 0.001$.

2.2 Measurement of PV and SST INs polyglutamylation levels

We observed that **1)** *Ccp1* mRNA levels are higher in PV compared to SST INs of WT animals; **2)** *Ccp6* mRNA levels are comparable between PV and SST INs of CCP1 cKO; **3)** *Ttll1* mRNA levels are higher in PV INs compared to SST INs in both WT and CCP1 cKO animals. This suggests that PV INs rely on high expression levels of *Ccp1* and *Ttll1* for the regulation of polyglutamylation and we therefore hypothesized that loss of CCP1 would particularly alter the balance of polyglutamylation in PV INs. We tested this hypothesis by measuring polyglutamylation levels in PV and SST hippocampal INs at 3 months, in brain slices of WT and CCP1 cKO mice. We used immunohistochemistry to identify PV and SST IN subtypes and to evaluate the polyglutamylation (PolyE) levels in the soma of those neurons. Bright PolyE signal was seen in sparse cells within the hippocampi of CCP1 cKO but not WT mice (**Figure 23 A**). Bright PolyE signal was detected specifically in PV^+ INs while SST^+ INs expressed PolyE levels similar to the surrounding tissue (**Figure 23 B**). We therefore analyzed the fluorescence intensity of PolyE signal in the soma of PV and SST INs normalized by the fluorescence intensity of the surrounding hippocampal neuropile, where PolyE intensity remains homogenous (**Figure 23 C**). Interestingly, we found that PolyE levels were increased in CCP1 cKO PV INS but not in SST INs (**Figure 23 C**). These findings suggest that PV INs particularly rely on CCP1 to maintain physiological polyglutamylation levels while SST INs can compensate for loss of CCP1 to maintain normal polyglutamylation. Interestingly, previous reports suggested that PolyE levels were slightly increased in the cortex and hippocampus of adult pcd mice and mice with deletion of exons 20-21 of CCP1 driven by the CMV promoter (Rogowski *et al.*, 2010; Magiera *et al.*, 2018). Theses studies conducted an analysis of PolyE levels using Western Blot on dissected cortex or hippocampus. However, it remained unclear whether the increased PolyE levels were due to a mild increase throughout all neuronal subtypes or a severe increase in specific subtypes. By using immunolabeling in a conditional CCP1 deletion,

we could highlight a specific sensitivity of PV INs to CCP1 loss that may partially drive the PolyE increase in dissociated tissues. We cannot exclude however that pyramidal neurons also contribute to the increased PolyE levels in CCP1 KO mice.

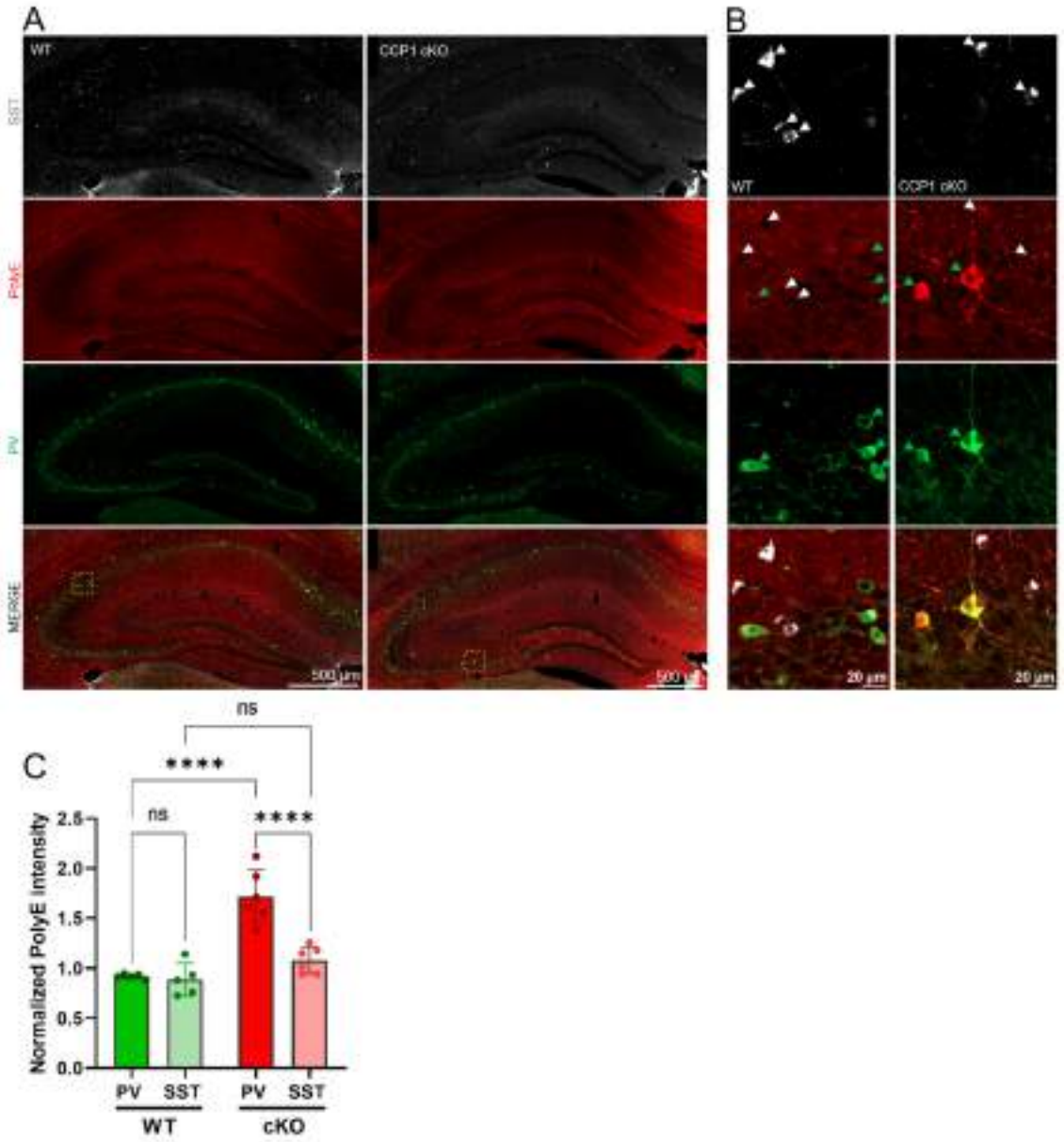

Figure 23: Hippocampal PV INs are hyperglutamylated in CCP1 cKO animals at 3 months.
A. Representative images of mouse hippocampi stained with SST, PolyE and PV in WT and CCP1 cKO in 3 month old mice. Red cell bodies that colocalize with PV^+ INs are visible in the CCP1 cKO condition. Yellow dotted square corresponds to the area magnified in panel (**B**).
B. Magnification of representative PV and SST INs stained with PolyE in the hippocampus of WT and CCP1 cKO mice. White and green arrows point to the cell bodies of SST and PV INs respectively. In CCP1 cKO, PV but not SST INs show strong PolyE immunoreactivity.

C. Average PolyE intensity in PV and SST INs of WT and CCP1 cKO mice. The PolyE intensity was normalized to the intensity of the surrounding hippocampal tissue. PV INs show a significant hyperglutamylation in CCP1 cKO. Each value on the graph represents the average PolyE intensity for all PV or SST INs analyzed in one animal. WT: n=5 CCP1cKO n= 6. A two-way ANOVA was conducted after confirmation of normal data distribution, **** = $p < 0.0001$

PV INs exhibit distinct variations in connectivity across CA fields (Booker and Vida, 2018) and may vary in their regulation of polyglutamylation as well. We therefore tested whether the increase in PV IN PolyE levels in CCP1 cKO mice is consistent across the CA1, CA2 and CA3 region of the hippocampus. We used RGS14 staining which specifically marks pyramidal cells of the CA2 field to define the anatomical boundaries of CA1, CA2 and CA3. We found an increase of somatic PolyE levels in PV INs across all hippocampal fields which suggests that PV INs are hyperglutamylated throughout the hippocampus (**Figure 24 A-B**).

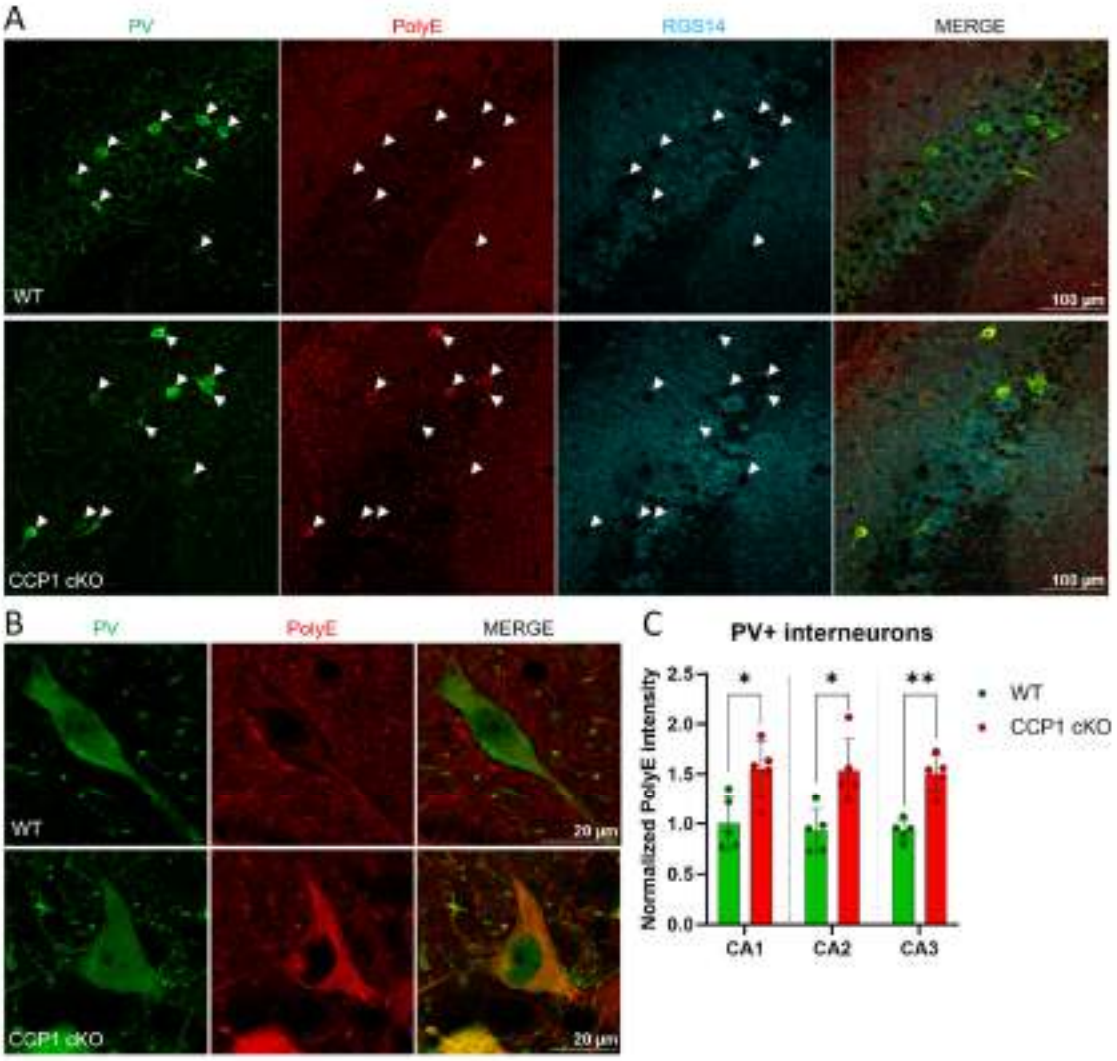

Figure 24: Hyperglutamylation of PV$^+$ INs is consistent across hippocampal fields

A. Representative images of PV, PolyE, RGS14 staining around the CA2 region of the hippocampus in 3 month old WT and CCP1 cKO mice. RGS14 is a marker of CA2 projections neurons and was used to delimit the CA1/CA2/CA3 areas. White arrows indicate PV+ INs to highlight their tendency to show strong PolyE signal in CCP1 cKO mice.

B. Representative images of PolyE staining in hippocampal PV INs of WT or CCP1 cKO mice. Although PV staining is visible in the nucleus and cytoplasm, PolyE staining is exclusively cytoplasmic and shows a fibrillar pattern reminiscent of microtubules.

C. Average PolyE intensity in PV INs of WT and CCP1 cKO mice. The PolyE intensity was normalized to the intensity of the surrounding hippocampal tissue. PV INs show a significant hyperglutamylation in CCP1 cKO across hippocampal regions. Each value on the graph represents the average PolyE intensity for the PV INs analyzed in the corresponding hippocampal region for one animal. WT: n=5 CCP1cKO n= 5. A Mann-Whitney test per region was conducted to compare PolyE levels between WT and CCP1 cKO, for CA1, CA2 and CA3, the p-values are respectively $p = 0.0317$, $p = 0.0159$, $p = 0.0079$.

2.3 Analysis of transport in PV$^+$ and PV$^-$ hippocampal INs

Hyperglutamylation has been correlated to neuronal transport defects in hippocampal and cerebellar neurons (Magiera *et al.*, 2018; Gilmore-Hall *et al.*, 2019; Bodakuntla *et al.*, 2020). Studies previously performed in the hippocampus showed that deletion of CCP1 alone or together with CCP6 lead to hyperglutamylation and altered neuronal transport in hippocampal cultures at DIV4. Interestingly, CCP1 loss alone is responsible for defects similar to CCP1 and CCP6 concomitant deletion, likely due to the low level of CCP6 expression at early postnatal stages (Rogowski *et al.*, 2010; Magiera *et al.*, 2018; Bodakuntla *et al.*, 2020). Indeed, PolyE levels are elevated in the cortex of perinatal pcd mice but normalized by P21 (Rogowski *et al.*, 2010). Transport was specifically analyzed in the axon but no distinction was made between IN subtype and consequently, most neurons analyzed were likely glutamatergic PNs since they are by far the most abundant in hippocampal primary cultures (Magiera *et al.*, 2018; Bodakuntla *et al.*, 2020).

We first characterized the hippocampal cultures of WT and CCP1 cKO mice. Dissociated E17.5 hippocampi were plated on coverslips and cultured *in vitro* for 15 days to allow their differentiation and the expression of PV protein (Alcantara, Ferrer and Soriano, 1993; Lecea, del Ri´o and Soriano, 1995). We then analyzed total neuronal numbers by assessing the expression of the pan-neuronal marker NeuN and calculated the proportion of GFP$^+$ INs and the proportion of GFP$^+$ INs expressing PV (**Figure 25 A-E**). As expected, the proportion of INs

relative to NeuN$^+$ neurons is low (3.4% in WT and 5.3% in CCP1 cKO) and lower than what has been described *in vivo* (**Figure 25 B-C**) (Bezaire and Soltesz, 2013). This may be because at E17.5, IN migration within the hippocampus is not yet completed and therefore some INs destined to integrate this region have not yet reached the hippocampus at this timepoint. In addition, progenitors of pyramidal cells are still producing neurons at E17.5 which may further bias the population of neurons towards the glutamatergic type (Bond *et al.*, 2020). These observations confirmed that previous studies of transport parameters in E17.5 hippocampal cultures were primarily focused on glutamatergic cells (Magiera *et al.*, 2018; Bodakuntla *et al.*, 2020). PV-expressing neurons represented 9.95% of GFP$^+$ INs in WT cultures and 13.79% in CCP1 cKO cultures (**Figure 25 D-E**). This proportion was also slightly lower than in previous *in vivo* measurement where PV$^+$ cells represented about 20% of total INs (Botcher *et al.*, 2014). This may result from the protracted timing of PV expression and it is therefore possible that a small proportion of GFP$^+$ PV$^-$ cells do not yet express detectable levels of PV. Similar to our observation *in vivo*, PolyE levels were markedly increased in CCP1 cKO PV INs (**Figure 25 F**).

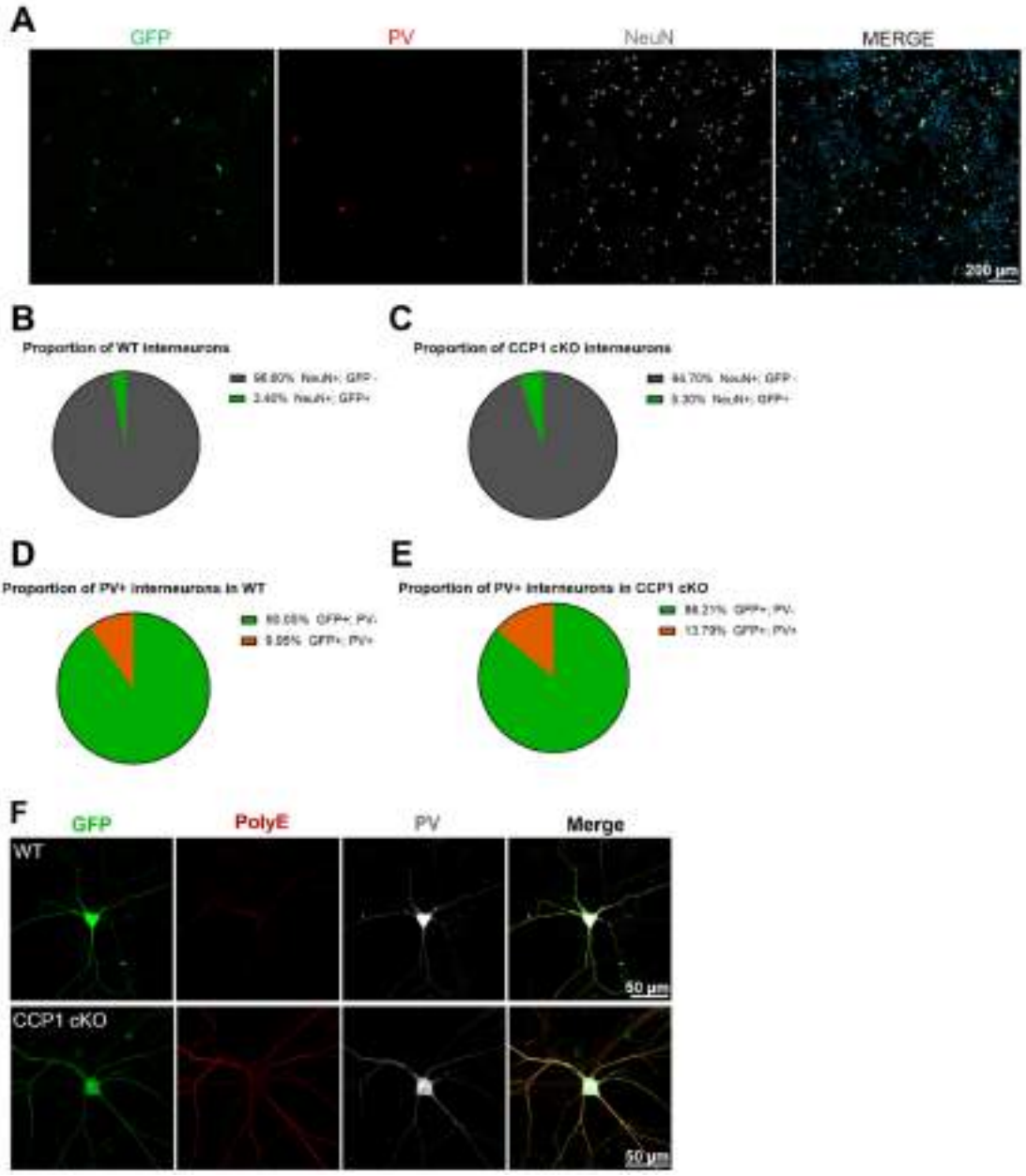

Figure 25: Characterization of DIV15 hippocampal cultures

A. Representative image of GFP, PV and NeuN staining in a DIV 15 hippocampal culture.
B-C. Proportion of WT and CCP1 cKO INs assessed as the ratio between $NeuN^+$; GFP^+ and $NeuN^+$; GFP- neurons. Data was collected from 3 independent experiments per genotype.
D-E. Proportion of PV^+ INs in WT and CCP1 cKO assessed as the ratio between GFP^+; PV^+ and GFP^+; PV^- neurons. Data was collected from 3 independent experiments per genotype.
F. Representative image of a WT and CCP1 cKO DIV15 IN after GFP, PolyE and PV staining. The CCP1 cKO IN shows hyperglutamylated tubulin.

Since we hypothesize that PV INs are sensitive to CCP1 loss, we designed an experimental paradigm that would allow us to measure the transport parameters specifically in PV^+ and PV^-

INs (**Material and Methods, Figure 35**). We used glass-bottom dishes with an embedded numbered grid which can be viewed under a microscope. This set up allows the user to mark down the location of neurons to retrieve them at a later date. Similar to the cultures used for the characterization of IN and PV proportions, we plated E17.5 dissociated hippocampi from both WT and CCP1 cKO and cultured the cells for 15 days. At DIV15, we labelled acidic vesicles with the LysoTracker^{TM} dye which has already been used to reveal transport alterations in the lysosomes of CCP1 KO hippocampal neurons (Bodakuntla *et al.*, 2020). Two-minute movies were recorded in multiple neurites of GFP^{+} INs and PV expression was then analyzed by immunohistochemistry after fixation and localization of the corresponding neurons on the grid. We therefore divided INs into the PV^{+} and PV^{-} subgroups for the analysis of transport parameters.

To characterize the transport parameters of lysosomes, we generated kymographs and traced the entire path of single vesicles. One path may be divided into multiple runs with changes in direction and velocity. A threshold was established (0.1µm/s) under which the vesicle was considered as immobile. For each vesicle, we extracted the runs when the vesicle is motile in the anterograde or retrograde direction and calculated the average velocity of the vesicle while in movement. Similar to previous findings in CCP1 KO hippocampal neurons, we found no difference in the anterograde and retrograde velocity of lysosomes in PV^{+} INs (**Figure 26 A-B**). We then analyzed the fraction of time during which vesicles move by calculating the proportion of time during which each vesicle exhibits a velocity > 0.1µm/s. This analysis also considered vesicles that are immobile for the whole duration of the movie and therefore had a fraction of time in movement equal to 0%. Interestingly, we found a robust reduction of time in movement for vesicles in CCP1 cKO PV^{+} INs, which is consistent with the observations made in hippocampal neurons at DIV4 (**Figure 26 C**) (Bodakuntla *et al.*, 2020). To further dissect the mechanism responsible for a reduction of time in movement, we calculated the fraction of time pausing in motile vesicles. Only vesicles that show movement in at least one run were considered in this analysis and the fraction of time spent with a velocity < 0.1 µm/s was measured. We find that CCP1 cKO PV^{+} INs exhibit an increase in their fraction of time pausing, indicating that lysosomes in CCP1 cKO animals tend to pause more between bouts of motility (**Figure 26 D**). In addition, we calculated the proportion of vesicles immobile for the whole duration of the movie in each IN and found a significantly higher proportion of

immobile lysosomes in CCP1 cKO PV^{+} INs (**Figure 26 E**). These findings suggest that the reduction in lysosomal motility may result from the combination of **1)** increased paused length that results in immobility for the duration of the movie; **2)** complete immobility of some lysosomes. Interestingly, our findings are remarkably similar to the transport defects that have been characterized in hyperglutamylated DIV4 hippocampal neurons which suggests that hyperglutamylation similarly affects lysosomal transport across neuronal subtypes (Magiera *et al.*, 2018; Bodakuntla *et al.*, 2020).

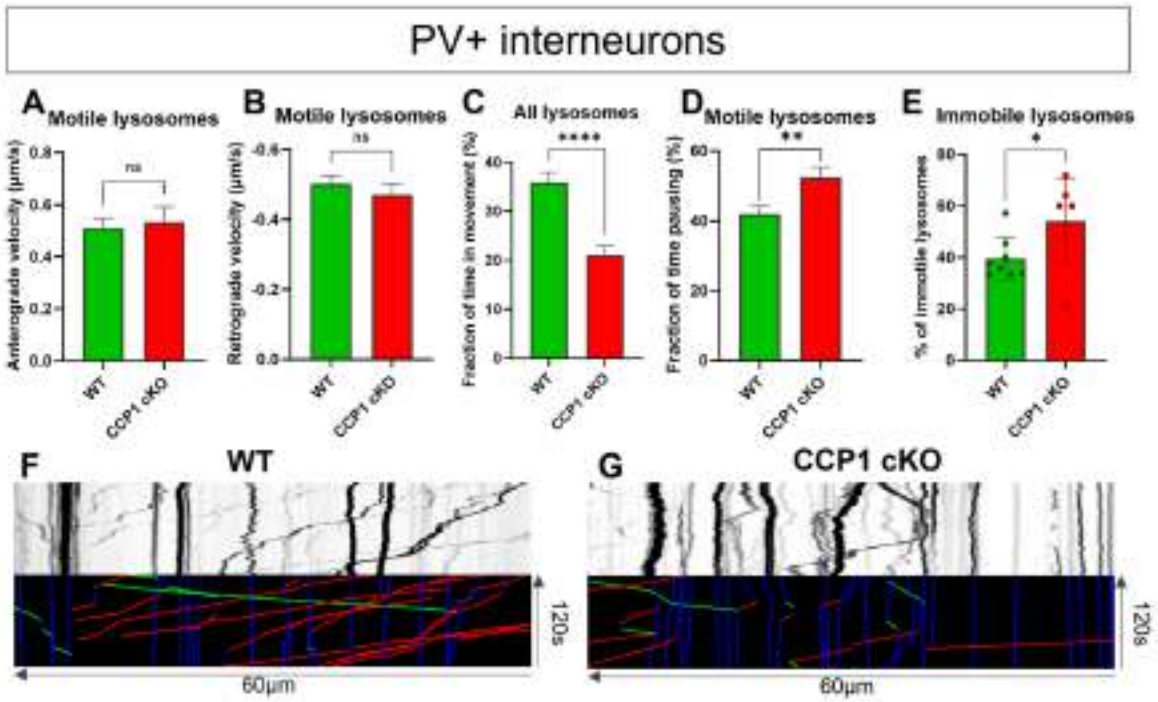

Figure 26: Vesicular transport is perturbed in PV IN neurites.

Dissociated hippocampi were seeded in glass-bottom gridded dishes and treated with LysoTracker^{TM} to label acidic vesicles at DIV15. Two minutes movies were acquired in the neurites of GFP^{+} INs and the position of each neuron on the grid was recorded. Neurons were fixed and immuno-labelled after the imaging session to identify PV INs.

A. Measurement of the anterograde velocity in both genotypes. Only the fractions of movement when vesicles travel away from the cell body are considered. When vesicles are moving in the anterograde direction, no change in velocity was detected in CCP1 cKO PV INs. The number of vesicles with anterograde movement in this analysis is 99 for WT and 79 for CCP1 cKO. A Mann-Whitney test was conducted ($p = 0.3803$).

B. Measurement of retrograde velocity in both genotypes. Similar to anterograde velocity, retrograde velocity only considers the fractions of movement when vesicles travel towards the cell body and no changes were detected in CCP1 cKO PV INs. The number of vesicles with retrograde movement in this analysis is 169 for WT and 110 for CCP1 cKO. A Mann-Whitney test was conducted ($p = 0.2339$).

C. Measurement of the fraction of time spent moving in both genotypes. This analysis includes all vesicles tracked, including motile and stationary vesicles and measures the percentage of time in movement for each vesicle. A threshold of 0.1 µm/s was established below which vesicles are considered immobile. Acidic vesicles are less motile in the CCP1 cKO condition as compared to WT. All vesicles that were tracked were included in this analysis for a total of 342 and 334 vesicles in WT and CCP1 cKO respectively. A Mann-Whitney test was conducted ($p < 0.0001$)
D. Measurement of the fraction of time pausing in motile vesicles of both genotypes. This measurement only considers vesicles that are motile for at least a portion of the movie and represents the percentage of time spent with a speed < 0.1 µm/s, which is considered as pausing. Motile acidic vesicles spend significantly more time pausing in CCP1 cKO PV INs. A total of 211 and 148 motile vesicles were included for the WT and CCP1 cKO conditions respectively. A Mann-Whitney test was conducted ($p = 0.006$).
E. Measurement of the percentage of immobile vesicles. Vesicles are considered as immobile if their instantaneous speed is < 0.1µm/s for the whole duration of the movie. For this analysis, the proportion of immobile vesicles in each neuron was calculated. Individual values on the graph represent single neurons. PV INs show a higher fraction of immobile vesicles in the CCP1 cKO condition. 8 and 7 PV^+ INs were recorded in the WT and CCP1 cKO conditions respectively, from 3 separate experiments. A Mann-Whitney test was conducted ($p = 0.0370$).
F-G. Representative kymographs for each genotype in PV^+ INs. Colored kymographs represent the tracks that were manually traced where blue lines correspond to time pausing, green lines anterograde movement and red lines retrograde movement.

We analyzed the same transport parameters in GFP^+ PV^- INs and found a different profile of lysosomal motility. Similar to PV^+ INs, anterograde and retrograde velocity was unchanged in CCP1 cKO PV^- INs (**Figure 27 A-B**). However, contrary to PV^+ INs, we did not find a significant reduction in the fraction of time in movement of lysosomes in CCP1 cKO PV^- INs (**Figure 27 C**). Interestingly, the fraction of time pausing was increased in CCP1 cKO PV^- INs, which may explain the trend towards a reduction of time in movement (**Figure 27 D**). However, PV^- INs showed no difference in the proportion of immobile lysosomes (**Figure 27 E**). These results suggest that PV^- INs show only minor lysosomal transport impairments with an increase in the pausing time of motile lysosomes but no change in the proportion of motile lysosomes. The hyperglutamylation of CCP1 cKO PV INs *in vivo* therefore correlates with a severe impairment of lysosomal transport.

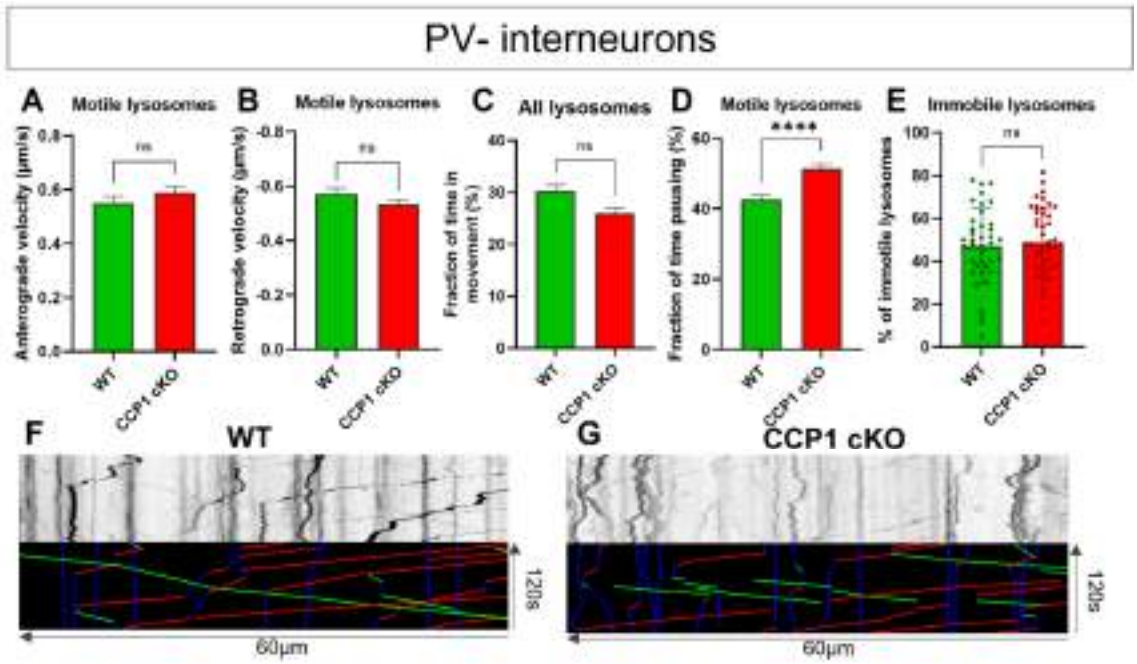

Figure 27: PV$^-$ INs only show a mild impairment in lysosome pausing time.

A-G. Axonal transport measurements from PV$^-$ INs recorded as part of the experiment presented in Figure 6.

A. Measurement of the anterograde velocity in both genotypes. Only the fractions of movement when vesicles travel away from the cell body are considered. When vesicles are moving in the anterograde direction, no change in velocity was detected in CCP1 cKO PV$^-$ INs. The number of vesicles with anterograde movement in this analysis is 363 for WT and 519 for CCP1 cKO. A Mann-Whitney test was conducted ($p = 0.2017$).

B. Measurement of retrograde velocity in both genotypes. Similar to anterograde velocity, retrograde velocity only considers the fractions of movement when vesicles travel towards the cell body and no changes were detected in CCP1 cKO PV$^-$ INs. The number of vesicles with retrograde movement in this analysis is 522 for WT and 604 for CCP1 cKO. A Mann-Whitney test was conducted ($p = 0.0699$).

C. Measurement of the fraction of time spent moving in both genotypes. This analysis takes into account all vesicles tracked, including motile and stationary vesicles and measures the percentage of time in movement for each vesicle. A threshold of 0.1 µm/s was established below which vesicles are considered immobile. Contrary to PV INs, CCP1 cKO PV$^-$ INs do not show a significant increase in the fraction of time spent in movement. All vesicles that were tracked were included in this analysis for a total of 1303 and 1506 vesicles in WT and CCP1 cKO respectively. A Mann-Whitney test was conducted ($p < 0.1107$)

D. Measurement of the fraction of time pausing in motile vesicles of both genotypes. This measurement only considers vesicles that are motile for at least a portion of the movie and represents the percentage of time spent with a speed < 0.1 µm/s, which is considered as pausing. Motile acidic vesicles spend significantly more time pausing in CCP1 cKO PV$^-$ INs. A total of 689 and 833 motile vesicles were included for the WT and CCP1 cKO conditions respectively. A Mann-Whitney test was conducted ($p < 0.0001$).

E. Measurement of the percentage of immobile vesicles. Vesicles are considered as immobile if their instantaneous speed is < 0.1µm/s for the whole duration of the movie. For this

analysis, the proportion of immobile vesicles in each neuron was calculated. Individual values on the graph represent single neurons. PV^- INs of both genotypes show similar fractions of immobile vesicles. 39 and 47 PV^+ INs were recorded in the WT and CCP1 cKO conditions respectively, from 3 separate experiments. An unpaired t-student test was conducted ($p = 0.7165$).
F-G. Representative kymographs for each genotype in PV^- INs. Colored kymographs represent the tracks that were manually traced where blue lines correspond to time pausing, green lines anterograde movement and red lines retrograde movement.

2.4 Assessment of IN neurodegeneration in CCP1 cKO hippocampus

Hyperglutamylation is associated with neurodegeneration in multiple cell types, including cortical neurons (Mullen, Eichert and Sidman, 1976; Landis and Mullen, 1978; Greer and Shepherd, 1982; O'Gorman, 1985; O'Gorman and Sidman, 1985; Magiera *et al.*, 2018). Additionally, hyperglutamylation triggered by CCP1 loss induces neurodegeneration of Purkinje Cells in a cell-autonomous manner since deletion of CCP1 under the control of a promoter specific to Purkinje Cells still leads to their degeneration (Magiera *et al.*, 2018). To test whether CCP1 loss leads to degeneration of INs in hippocampus, we crossed WT and CCP1 cKO mice with a ROSA-YFP reporter line to drive YFP expression in adult mice since GFP expression driven by Dlx5,6 subsides in the perinatal period. We then counted YFP^+ INs of the Dlx5,6 lineage at 3 month and did not highlight any differences in IN numbers in CCP1 cKO mice (**Figure 28 A-B**). We then assessed whether specific subtypes of INs may degenerate by counting the total number of PV and SST INs in the hippocampus. Despite the hyperglutamylation observed in PV^+ INs, we could not find any differences in the numbers of CCP1 cKO PV or SST INs in the hippocampi of 3 months old mice (**Figure 29 A-D**).

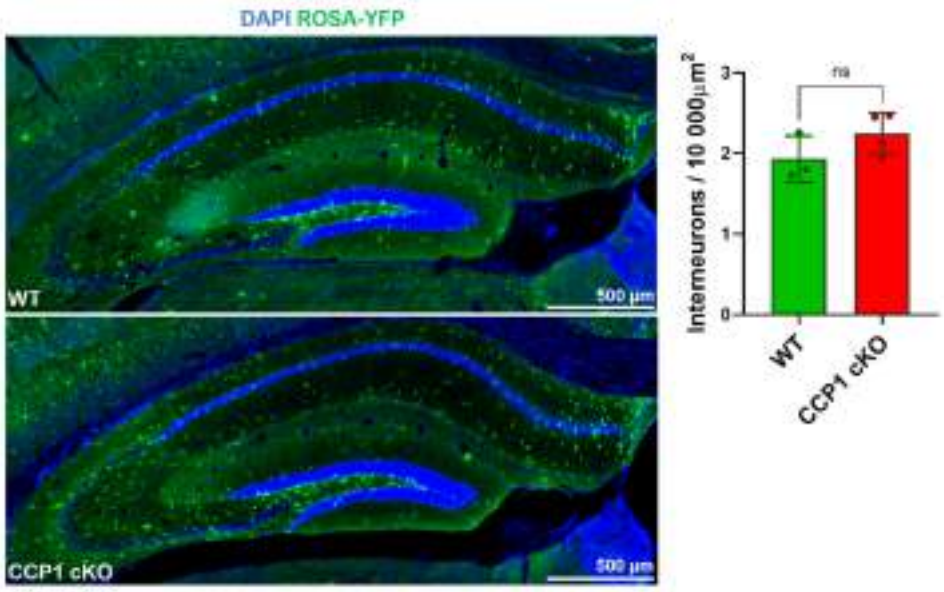

Figure 28: The total number of INs is unchanged in the hippocampi of 3 months old CCP1 cKO mice

A. Representative images of WT and CCP1 cKO hippocampi stained with GFP. WT and CCP1 cKO animals were crossed with ROSA-YFP to stain INs in adults.

B. Quantification of IN density. The total number of GFP^+ INs was divided by the area of the CA fields. nWT = 3 and ncKO = 4, a Mann-Whitney test was performed (p=0.2286).

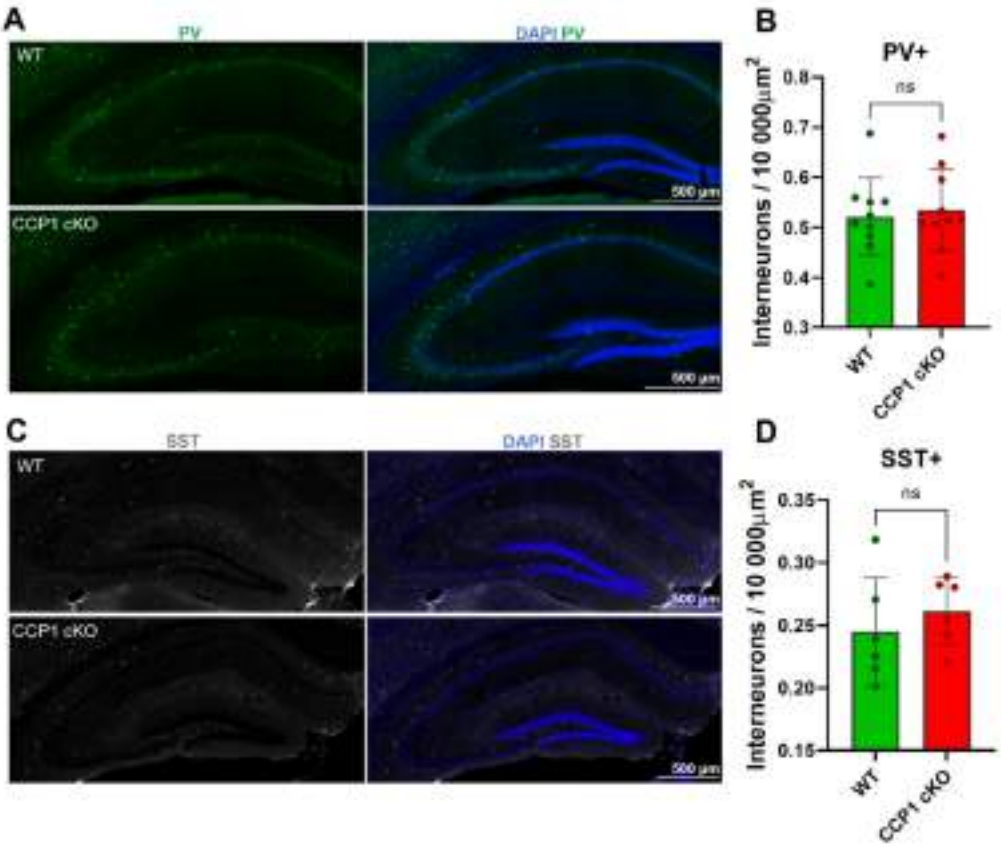

Figure 29: CCP1 loss does not trigger neurodegeneration of PV and SST INs at 3 months

A. Representative images of WT and CCP1 cKO hippocampi at 3 months showing the distribution of PV INs.

B. Quantification of the density of PV^+ INs in the CA fields normalized by the surface of the area analyzed. No differences were found in the density of PV INs in CCP1 cKO mice. n =10 mice for both conditions, an unpaired t-student test was performed (p = 0.7256).

C. Representative images of WT and CCP1 cKO hippocampi at 3 months showing the distribution of SST INs.

F-H. Quantification of the density of SST^+ INs in the CA fields normalized by the surface of the area analyzed. No differences were found in the density of PV INs in CCP1 cKO mice. n =6 mice for both conditions, an unpaired t-student test was performed (p = 0.4438).

These results suggest that at this age, neither PV INs, SST INs or other IN subtypes die in CCP1 cKO mice despite the hyperglutamylation observed in the PV INs. However, different timelines of neurodegeneration have been demonstrated in neurons suffering from hyperglutamylation. Purkinje Cells appear most sensitive to CCP1 loss and degenerate within a month (Mullen, Eichert and Sidman, 1976), while mitral cells degenerate between 2 and 3 months (Greer and Shepherd, 1982) and only a portion of hyperglutamylated cortical neurons have degenerated at 5 months (Magiera *et al.*, 2018). It is therefore possible that PV INs despite being hyperglutamylated do not degenerate at the relatively early stage that we have analyzed and additional experiments should be performed in older animals to address whether degeneration occurs in hyperglutamylated PV INs at later stages.

2.5 Analysis of synapse physiology and number in CCP1 cKO hippocampi

Although hyperglutamylation of PV INs does not induce neurodegeneration at 3 months, neuronal transport is crucial for the development, maintenance and function of synapses (Guedes-Dias and Holzbaur, 2019). Consequently, alterations in polyglutamylation levels have been linked to defects in the density of synaptic vesicles and in the transport of synaptic components such as gephyrin (Ikegami *et al.*, 2007; Maas *et al.*, 2009). Additionally, spastin depletion increases tubulin polyglutamylation and leads to a decrease of excitatory synapses (Lopes *et al.*, 2020). Whether INs are affected by spastin depletion and the consequences of hyperglutamylation on GABAergic synapses has not been assessed however. We therefore analyzed the number of hippocampal inhibitory synapses to uncover putative functional defects resulting from CCP1 loss in INs at 3 months. The vesicular GABA transporter (VGAT) is embedded in the membrane of synaptic vesicles at inhibitory pre-synaptic sites (Dobie and Craig, 2011), while gephyrin is a scaffolding protein expressed at the post-synaptic sites of

inhibitory synapses (Dobie and Craig, 2011). Co-staining of VGAT and gephyrin allows the identification of pre- and post-synaptic colocalization which corresponds to inhibitory synapses. We first performed co-immunolabeling of VGAT and gephyrin in DIV15 hippocampal cultures to assess the number of inhibitory synapses defined as the co-distribution of VGAT and gephyrin *punctae*. Inhibitory synapses along GFP$^+$ IN fibers were counted in the perisomatic sites of GFP- neurons which are likely PNs. We could therefore calculate the density of perisomatic inhibitory synapses *in vitro* and found a significant decrease in CCP1 cKO cultures (**Figure 30 A-C**).

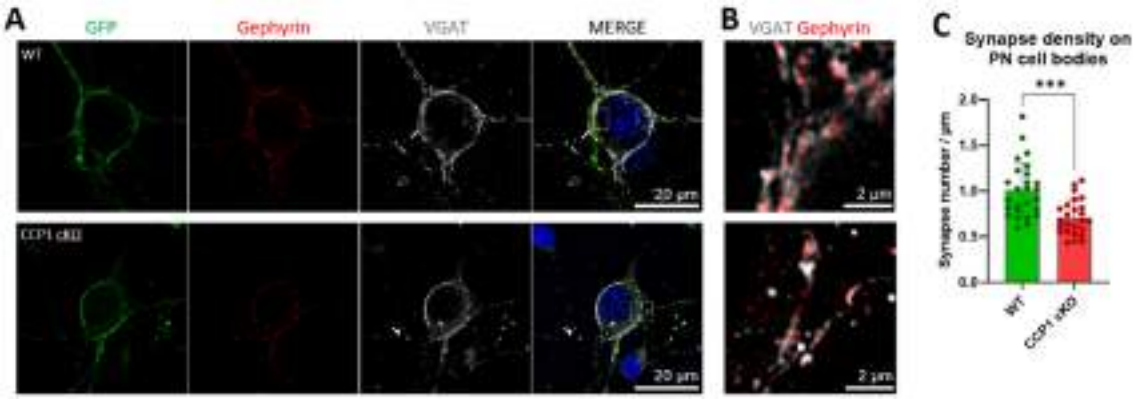

Figure 30: Quantification of inhibitory synapses at the soma of PNs *in vitro*

A. Representative images of WT or CCP1 cKO neurons innervated by GFP$^+$ IN axons lined with VGAT/Gephyrin *punctae* at DIV 15. Only GFP- neurons (presumably PNs) whose cell body were innervated by GFP$^+$ fibers were considered in this analysis.

B. Magnification of the yellow dotted square in panel (C) showing the colocalization of VGAT/Gephyrin *punctae*.

C. Quantification of the density of inhibitory synapses along GFP$^+$ fibers innervating the cell body of PNs. The number of gephyrin *punctae* colocalizing with VGAT was normalized to the length of GFP$^+$ fibers that innervate the cell body. A total of 26 and 25 cell bodies were analyzed in WT and CCP1 cKO respectively, from 3 independent experiments. An unpaired t-student test was conducted ($p < 0.0001$).

Next, we performed co-immunolabeling of VGAT and gephyrin in hippocampal slices of 3 months old WT and CCP1 cKO mice. To account for the specific patterns of inhibitory synapse across hippocampal layers and CA fields (Pelkey *et al.*, 2017; Booker and Vida, 2018), we analyzed 3 large regions within the CA1, CA2 and CA3 fields which were further subdivided in *stratum oriens* (SO), *stratum pyramidale* (SP) and *stratum radiatum/lacunosum* (SRL) *(***Material and methods, Figure 33 C***)*. We developed a semi-automatic method to count

synapses which limited biases and enabled the analysis of large regions containing thousands of synapses (described in Material and Methods).

We found a significant reduction of inhibitory synapses specific to the SO and SP but not SRL of the CA2 field (**Figure 31 A, E-G**). Although other hippocampal layers in CA1 and CA3 showed less inhibitory synapses, this reduction did not reach statistical significance (**Figure 31 B-D, H-J**). Interestingly, PV INs project mainly to the SP and SO through axonal projections of PV basket cells and PV axo-axonic cells respectively (Pelkey *et al.*, 2017; Booker and Vida, 2018). In addition, the CA2 region harbors the highest density of PV INs in the whole hippocampus (Botcher *et al.*, 2014). The decrease of inhibitory synapses in the SO and SP of CA2 may therefore be mainly driven by PV cells which is the subtype of IN that appears particularly sensitive to hyperglutamylation induced by CCP1 loss.

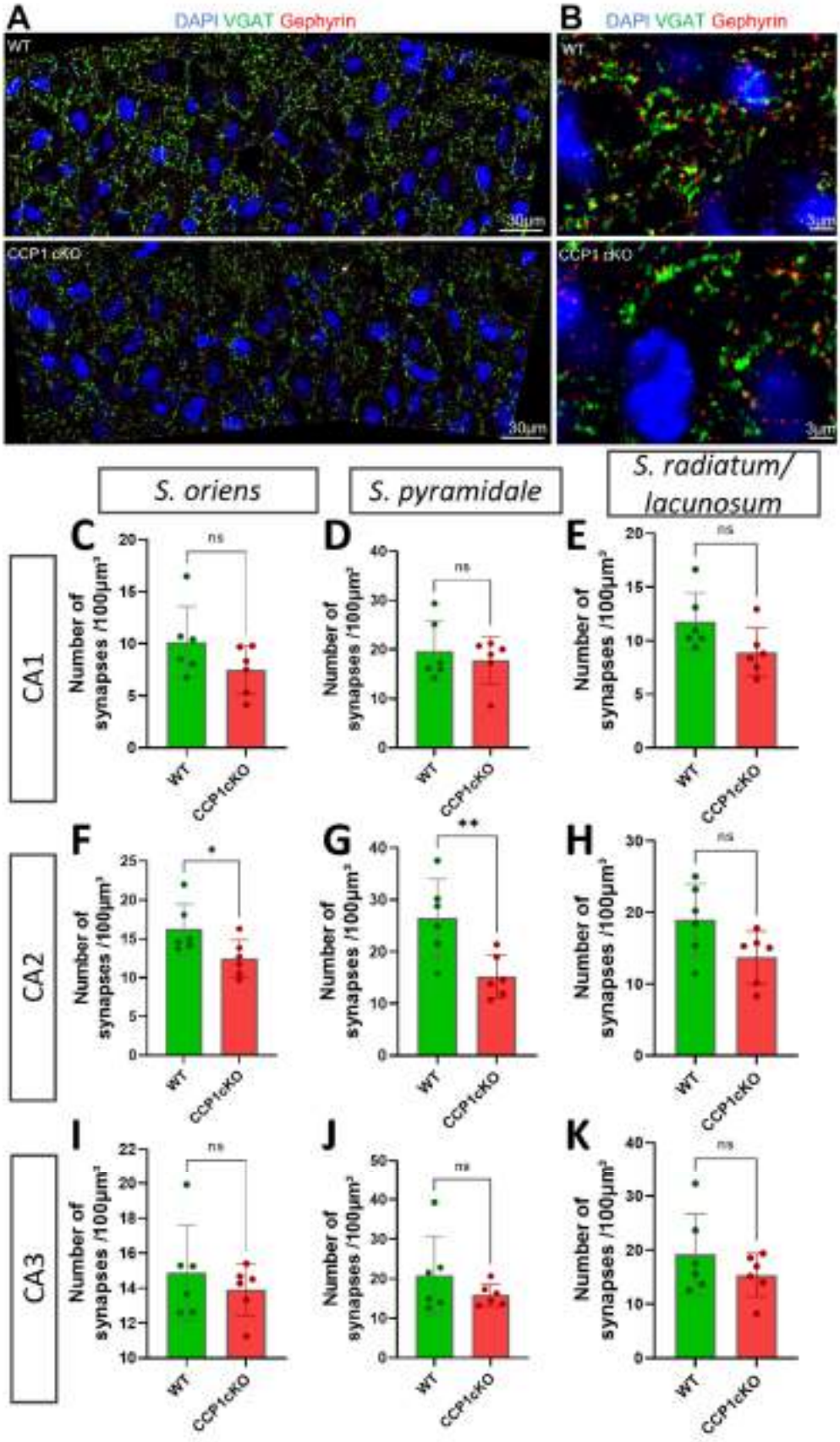
A
DAPI VGAT Gephyrin
WT
30μm
CCP1 cKO
30μm
B
DAPI VGAT Gephyrin
WT
3μm
CCP1 cKO
3μm
S. oriens
S. pyramidale
S. radiatum/ lacunosum
CA1
CA2
CA3
C
D
E
F
G
H
I
J
K
Number of synapses /100μm³
ns
*
**
WT
CCP1cKO

Figure 31: CCP1 loss is responsible for a decrease of inhibitory synapses specific to the CA2 field

A. Representative images of inhibitory synapses in the *stratum pyramidale* (SP) of the CA2 region from WT and CCP1 cKO 3 months old mice. Synapses were stained with the pre and postsynaptic markers VGAT and Gephyrin.
B. Higher magnification within the CA2 SP of WT and CCP1 cKO.
C-K. Quantification of the density of inhibitory synapses in the *stratum oriens*, SP and *stratum radiatum/lacunosum* of each CA field. The colocalization of one gephyrin *puncta* with one VGAT *puncta* was considered as an inhibitory synapse. This analysis was performed on 6 WT and 6 CCP1 cKO animals, an unpaired t-student test was conducted. p=0.1429 (C), p=0.5655 (D), p=0.0769 (E), p=0.0428 (F), p=0.0093 (G), p= 0.0650 (H), p= 0.4545 (I), p=0.2719 (J), p=0.2958 (K).

To assess whether the decrease in inhibitory synapses correlates with a decreased release of GABA vesicles, we performed whole-cell patch clamp on the soma of CA2 PNs in 8-10 weeks old WT or CCP1 cKO mice. Biocytin was injected in the patched cells and RGS1S4 staining combined with morphology and position of the neuron were used to confirm that all cells included in the analysis were CA2 PNs (**Figure 32 A**). Miniature inhibitory post-synaptic currents (mIPSCs) represent the spontaneous (without action potential) release of GABA-containing vesicles at inhibitory synapses. mIPSC were measured by blocking action potentials with tetrodotoxine (TTX). We found that the frequency of mIPSCs but not the amplitude, was significantly reduced on the soma of CCP1 cKO CA2 PNs (**Figure 32 B-G**). These results complement our observation that inhibitory synapses are reduced in the SP of CA2, suggesting that the reduced number of GABAergic synapses may result in a decreased probability of spontaneous GABA-vesicle release (in absence of axon potentials).

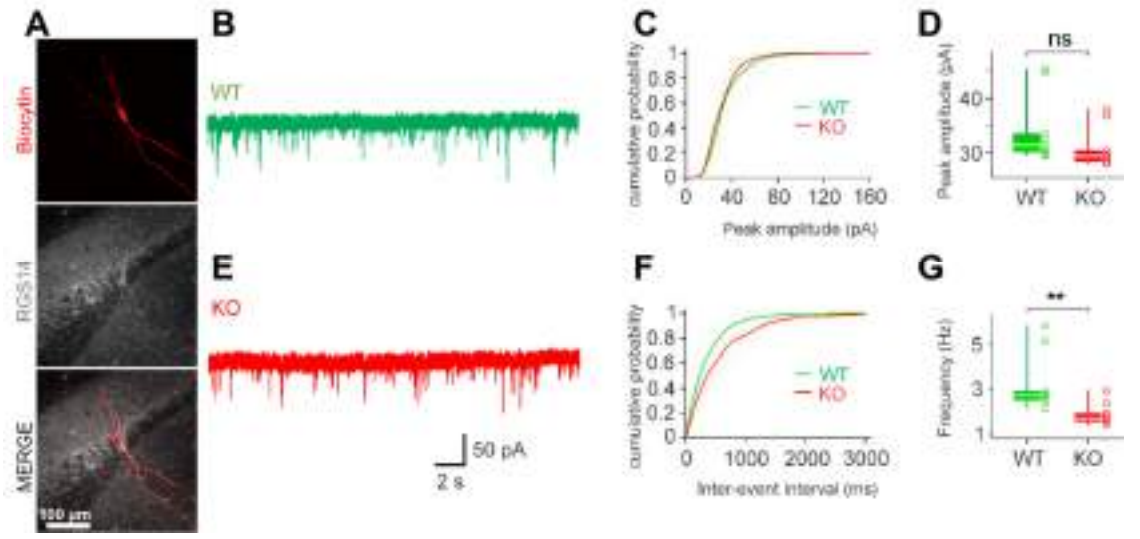

Figure 32: mIPSC frequency is reduced on the soma of CCP1 cKO CA2 PNs

A. Representative image of a CA2 PN that was patched and injected with biocytin in a horizontal hippocampal slice from an 8 weeks mouse. The yellow doted shape outlines the cell body of the biocytin+ cell to highlight the colocalization with the CA2 PN marker RGS14.
B, E. Current traces showing spontaneous miniature IPSCs at -70 mV in slices from control (WT) mice (top, green trace) and from KO mice (bottom, red trace). External solution contained 10 µM CNQX and 20 µM AP5 to block NMDA and AMPA receptors and 1 µM TTX to block action potentials.
C, F. Cumulative distributions of mIPSC amplitude **(C)** and inter-event intervals **(D)**. Thick lines are average cumulative distributions from PNs in WT- (green) and CCP1 cKO (red) mice, respectively. Thin lines are from individual cells. Data are from 9 and 8 individual PNs, respectively.
D, G. Boxplots of EPSC peak amplitude **(E)** and frequency **(F)** for WT mice and CCP1 cKO mice. Open circles indicate data from individual recordings, 9 PNs (WT) and 8 PNs (CCP1 cKO). T-student test or a Mann-Whitney test was conducted, depending on the normal or non-normal distribution of data, respectively p=0.0921 **(D)** and p=0.00814 **(G)**.

3. Material and methods

Animals

All animals were housed under standard conditions in a 12h light/12h dark cycle, with ad libitum access to food and water, constant temperature (19-22°C) and humidity (40-50%). Animals were treated according to the guidelines of the Belgian Ministry of Agriculture in agreement with the European Community Laboratory Animal Care and Use Regulations (86/609/CEE, Journal Official des Communautés Européennes L358, 18 December 1986). The animal work in this chapter was approved by the ethical committee of the University of Liège under the protocols 1912, 2177 and 2455.

Mice used in this study were all males of CD1 genetic background (Janvier Labs, Saint-Berthevin, France). Dlx5,6 CRE-GFP, CCP1 lox/lox (Muñoz-Castañeda *et al.*, 2018; Silva *et al.*, 2018) and ROSA-FloxStop YFP (Srinivas *et al.*, 2001) transgenic lines were all backcrossed in CD1 background before being bred for experiments. Transgenic colonies were regularly bred with CD1 mice purchased from Janvier Labs to prevent inbreeding. In this chapter, WT mice refer to Dlx5,6 $^{CRE\text{-}GFP/+}$ male mice, CCP1 cKO mice are Dlx5,6 $^{CRE\text{-}GFP/+}$; CCP1 $^{lox/lox}$ male mice. In CCP1 cKO mice, exons 20 and 21 of the CCP1 genes are excised by CRE recombination in the Dlx5,6 lineage therefore specifically targeting INs in the cortex and hippocampus. WT mice control for the expression of CRE and GFP in the Dlx5,6 lineage but have intact CCP1 alleles.

For the counting of INs from the Dlx5,6 lineage in adult hippocampus, we crossed WT and CCP1 cKO mice with homozygous ROSA-FloxStop YFP CD1 mice in order to report expression of INs at 3 months.

Genotyping

Transgenic animals were genotyped to maintain the colony and select experimental animals. A 1mm biopsy was performed at the tail and was then digested with proteinase K (200µg/mL, Promega, Cat. #MC5005) in 300 µL of TENS solution (100 mM Tris-HCl; 5 mM EDTA; 200 mM NaCl; 0.2% SDS, pH 8.2), for at least 4h at 55°C under agitation. The DNA was then precipitated by the addition of -20°C 300 µL isopropanol and centrifugation at 12 000g for 10 minutes. The supernatant was discarded and the DNA pellet is washed with 300µL -20°C ethanol 70% and a subsequent 12 000g centrifugation for 10 minutes. The supernatant was discarded and the DNA was then dissolved in 600µL of autoclaved water.

The genotype was then determined by polymerase chain reaction (PCR). A mix was prepared with 5x reaction buffer (Promega, M791A), dNTP (0.2 mM, New England Biolabs, N0447S), primers (0.2µM, IDT, **Table 2**), GoTaq polymerase (33U/mL, Promega – M7841). One reaction per animal was carried out with 24µL of mix and 1µL of DNA extracted in the previous step. The PCR was performed in a Labcycler SensoQuest (Reference 0499/9) with an amplification program specific to each transgene (**Table 3**). The PCR products were then visualized by electrophoresis on a 1% agarose gel.

Genes	Primers (5' – 3')	Amplicon size (bp)
Dlx5,6 CRE-GFP	Fw: ATC|CGA|AAA|GAA|AAC|GTT|GA	WT = no band Cre = 500 bp
	Rv: ATC|CAG|GTT|ACG|GAT|ATA|GT	
CCP1 lox	Fw: CAT|AAG|AAC|CAG|GTT|CAT|TCT|GTC|C	WT = 407 bp Lox = 485 bp
	Rv: TAG|CAT|CAT|GTT|AAA|ACT|CCC|TCC|T	
ROSA-YFP	R1: AAA|GTC|GCT|CTG|AGT|TGT|TAT	WT = 650 bp ROSA-YFP = 340 bp
	R2: GCG|AAG|AGT|TTG|TCC|TCA|ACC	
	R3: GGA|GCG|GGA|GAA|ATG|GAT|ATG	

Table 2: Primers used for genotyping.

Genes	PCR program	
Dlx5,6 CRE-GFP	Temperature	94°C – 94°C – 53°C – 72°C – 72°C – 10°C
	Time	3m – 30s – 45s – 1m – 5m - ∞
	Cycle	— 30 —
CCP1 lox	Temperature	94°C – 94°C – 63°C – 72°C – 72°C – 10°C
	Time	5m – 30s – 30s – 45s – 5m - ∞
	Cycle	— 33 —
ROSA-YFP	Temperature	94°C – 94°C – 60°C – 72°C – 72°C – 10°C
	Time	5m – 30s – 30s – 1m – 5m - ∞
	Cycle	— 35 —

Table 3: PCR programs.

Immunohistochemistry

For collection of the brain, mice were anesthetized by intra-peritoneal injection of pentobarbital (Euthasol 150mg/kg). Unconscious mice were then perfused intracadially with 4% paraformaldehyde solution (PFA) in phosphate buffered saline (PBS, 137 mM NaCl; 2,7 mM KCl; 10mM Na_2HPO_4; 1.76 mM KH_2PO_4, pH 7.4). The brain was then extracted and immersed in 4% PFA overnight at 4°C. The next day, brains were rinsed with PBS and cryoprotected overnight at 4°C in a solution of 30% sucrose diluted in PBS. Cryoprotected brains were then embedded in optimal cutting temperature (OCT) media (Richard-Allan Scientific Neg50), frozen on dry ice and stored at -80°C until further processing.

For immunohistochemistry experiments on brain tissue, 30µm coronal slices were cut using a LEICA cryostat (LEICA – CM30505) and placed in PBS. For some experiments, antigen retrieval was performed using citrate buffer (Agilent DAKO, S169984-2). Floating sections were placed in a hermetic container with antigen retrieval solution and incubated in a water bath at 80°C for 25min. For details on which experiments required antigen retrieval, see **Table 4**. Floating sections were permeabilized and blocked in PBS, 0,3% Triton X-100 (Sigma Aldrich, T8787), 10% normal donkey serum (NDS, Jackson ImmunoResearch, RRID: AB_2337258) for 1h under light agitation at room temperature (RT). Primary antibodies were diluted in antibody solution (PBS, 0,3% Triton X-100, 5% NDS) and slices were incubated overnight at 4°C or RT (**Table 4**). Three 15 minute washes with PBS, 0,3% Triton X-100 were performed and were followed by incubation in DAPI (2µg/mL, Sigma Aldrich, D9542) and adequate secondary antibodies

(Thermofisher Scientific or Jackson ImmunoResearch, 1:500) diluted in antibody solution for two hours at RT. Two washes in PBS, 0,3% Triton X-100 and a last wash in PBS were performed before slices were mounted on superfrost slides (Fisher Scientific, Epredia J1800AMNZ) using pencil brushes. 1h after mounting, when slices were dried, excess salt was removed by rapid immersion in MilliQ water and slides were covered with a glass coverslip using Fluoromount aqueous mounting medium (Sigma Aldrich, F4680).

Sample preparation for the immunohistochemistry of synapses *in vivo* was performed using a protocol adapted from (Schneider Gasser *et al.*, 2006). Brains were quickly extracted after euthanasia with intra peritoneal injection of pentobarbital (Euthasol) and immediately placed in -80°C isopropanol. They were then stored at -80°C until cryosectioning. 12µm coronal slices were cut and collected on superfrost slides and quickly placed at -20°C to prevent degradation of the unfixed tissue. After cryosectioning, slices were briefly fixed with 0.4% PFA solution in PBS by irradiation in a microwave oven (900W for 30s). Slides were then washed in PBS and the immunohistochemistry protocol described in the previous protocol was used for subsequent steps.

For immunohistochemistry of primary hippocampal cultures, cells were cultured on 12mm coverslips and a protocol identical to the one described above was used.

Confocal images were captured with airyscan on a Zeiss LSM 880 or Zeiss LSM 980 (GIGA-Imaging Platform) depending on experiments. All immunohistochemistries were performed simultaneously for a single experiment and were imaged with the same imaging equipment and settings to ensure reproducibility. Image analysis was conducted using Fiji (Image J) or QuPath depending on experiments.

Experiment	Antibodies	Host	Antigen retrieval	Dilution/ Incubation	Reference
Figure 22	Parvalbumin	Guinea pig	From Basescope protocol	1:300, O/N 4°C	Synaptic systems, 106 104
	Somatostatin	Rabbit		1:300, O/N 4°C	Peninsula laboratories, T-4102
Figure 23	Parvalbumin	Guinea pig	DAKO, 80°C, 25min	1:500, O/N RT	Synaptic systems, 106 104
	PolyE	Rabbit		1:1000, O/N RT	Adipogen, AG-25B-0030
	Somatostatin	Mouse		1:300, O/N RT	Santa Cruz, sc-55565
Figure 24	Parvalbumin	Guinea pig	No	1:500, O/N RT	Synaptic systems, 106 104

	PolyE	Rabbit		1:1000, O/N RT	Adipogen, AG-25B-0030
	RGS14	Mouse		1:500, O/N RT	Neuromab, 75-170
Figure 25 A	GFP	Rat	No	1:1000, O/N 4°C	Nacalai tesque, 04404-26
	Parvalbumin	Guinea pig		1:500, O/N 4°C	Synaptic systems, 106 104
	NeuN	Rabbit		1:1500, O/N 4°C	Cell signaling, 12943
Figure 25 F	GFP	Rat	No	1:1000, O/N 4°C	Nacalai tesque, 04404-26
	PolyE	Rabbit		1:5000, O/N 4°C	Adipogen, AG-25B-0030
	Parvalbumin	Guinea pig		1:500, O/N 4°C	Synaptic systems, 106 104
Figure 28	GFP	Goat	No	1:500, O/N 4°C	Abcam, ab6673
Figure 29 A	Parvalbumin	Guinea pig	No	1:500, O/N 4°C	Synaptic systems, 106 104
Figure 29 C	Somatostatin	Rabbit	No	1:500, O/N 4°C	Peninsula laboratories, T-4102
Figure 30	GFP	Rat	No	1:1000, O/N 4°C	Nacalai tesque, 04404-26
	Gephyrin	Guinea Pig		1:200, O/N 4°C	Synaptic systems, 147 318
	VGAT	Chicken		1:500, O/N 4°C	Synaptic systems, 131 006
Figure 31	Gephyrin	Guinea Pig	See methods	1:200, O/N 4°C	Synaptic systems, 147 318
	VGAT	Chicken		1:500, O/N 4°C	Synaptic systems, 131 006
Figure 32	RGS14	Mouse	No	1:500, O/N RT	Neuromab, 75-170

Table 4: Primary antibodies used for each experiment

Semi-automated analysis of inhibitory synapses *in vivo*

The method of tissue preparation for synapses described above improves the detection of pre and post-synaptic sites but decreases the quality of cytoplasmic stainings (Schneider Gasser *et al.*, 2006). As such, the RGS14 and PCP4 markers of CA2 PNs showed poor quality in this experiment. The CA1/CA2 boundary was therefore delineated based on the DAPI staining which shows a clear enlargement of the pyramidal layer at the CA1/CA2 border (**Figure 33 A-B**).

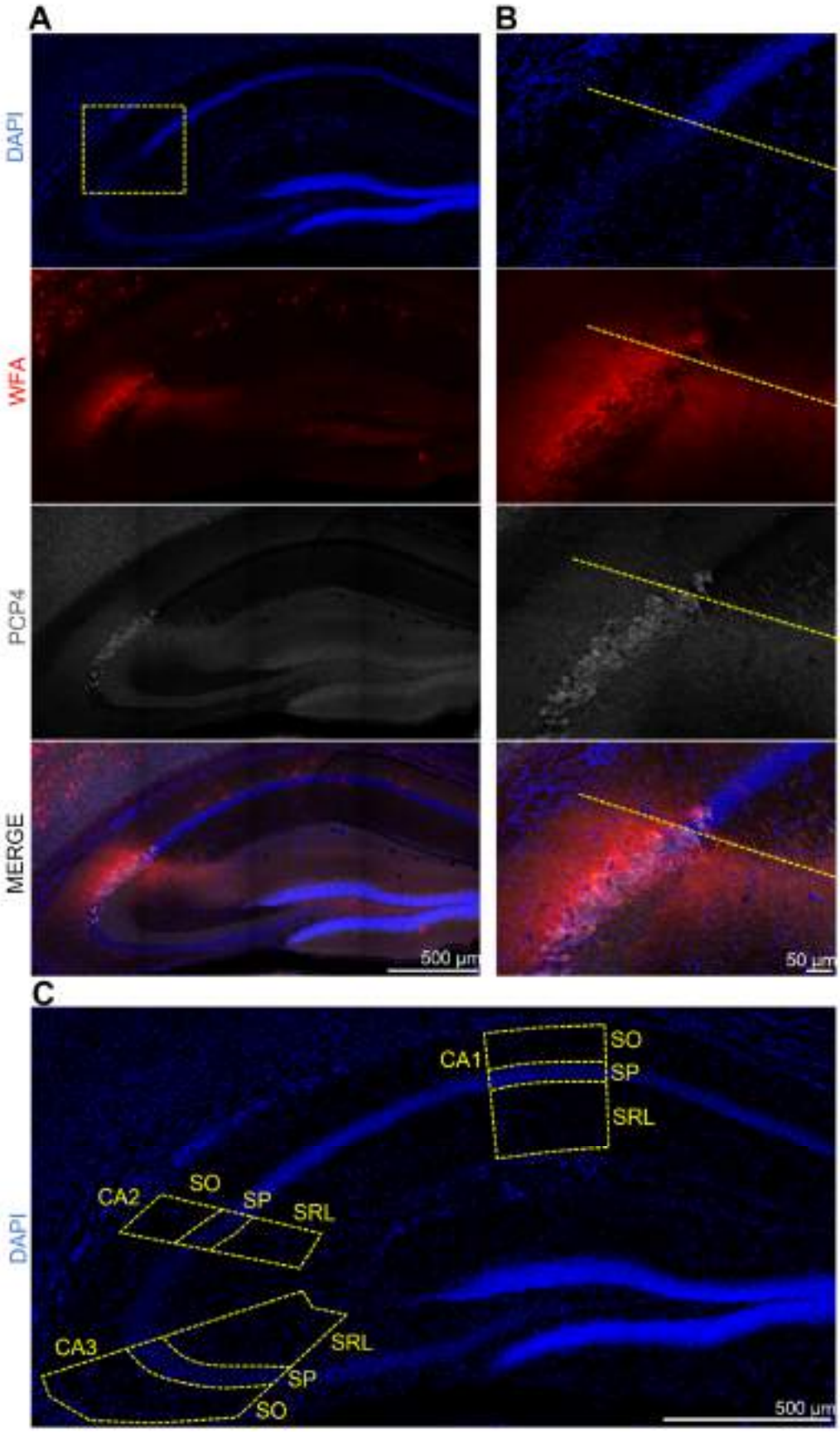
A
B
DAPI
WFA
PCP4
MERGE
500 µm
50 µm
C
CA1
SO
SP
SRL
CA2
SO
SP
SRL
CA3
SRL
SP
SO
DAPI
500 µm

Figure 33: CA1, CA2 and CA3 regions analyzed for inhibitory synapses

A. Wisteria Floribunda lectin (WFA) reveals the dense extracellular matrix proteoglycans in the CA2 region. WFA staining colocalizes with the CA2 PN marker PCP4. Yellow dotted square represents the area zoomed on panel **(B).**

B. The CA1/CA2 boundary (yellow dotted line) exhibits a clear shift in the pattern of DAPI staining that coincides with WFA and PCP4 staining.

C. Tile-scan images of synapse settings were captured in portions of the CA1, CA2 and CA3 fields (Yellow dotted lines). The CA1/CA2 boundary was determined based on DAPI staining as shown in panel **(B).** CA1, CA2 and CA3 subregions were then divided in *stratum oriens* (*SO*), *stratum pyramidale* (*SP*) and *stratum radiatum/lacunosum* (*SRL*) for synapse analysis.

CA1, CA2 and CA3 regions as shown in (**Figure 33 C**) were captured as tile images with a 63x oil objective, Zeiss LSM880 in airyscan mode. The SO, SP and SRL were cropped as shown in (**Figure 33 C**). Semi-automated analysis of gephyrin *punctae* colocalizing with VGAT *punctae* was then performed using the Imaris v9 software (**Figure 34**). Images were blinded to prevent experimenter bias in the manual step of the analysis. Background subtraction (1 sigma) was applied to each channel and the spot detection function was used to detect gephyrin and VGAT *punctae*. For each image, the estimated size of spots was defined as 400nm and a threshold for spot detection was manually established using the mean intensity filter. Inhibitory synapses were defined as a gephyrin spot within 400nm of a VGAT spot and were filtered using the "shortest distance to spots" function.

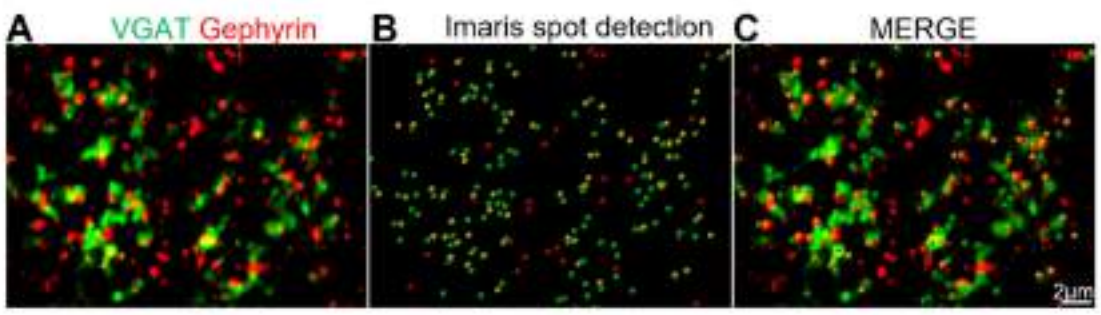

Figure 34: Spot detection of inhibitory synapses in imaris

A. Magnification of inhibitory synapses stained with VGAT and Gephyrin in the hippocampus of WT mice at 3 months.

B. Spots were created based on VGAT and gephyrin signal with the Imaris software. Green and red spots are generated based on VGAT and gephyrin staining respectively. Yellow spots correspond to gephyrin spots that are within 400nm of a VGAT spot. The number of yellow spots was considered as the number of inhibitory synapses and biologically corresponds to the number of post-synaptic sites that co-distribute with pre-synaptic sites.

C. Merged image representing the accurate detection of synapses using the Imaris method of quantification.

BaseScope

Brains were perfused and fixed overnight in PFA as described in the "immunohistochemistry" paragraph. 12µm slices were cut at the cryostat, collected on superfrost slides and stored at -80°C before experiments. Custom probes were designed to detect Ccp1 (Advanced Cell Diagnostics, Cat. No. 1113561-C1), Ccp6 (Advanced Cell Diagnostics, Cat. No. 1143731-C1) and Ttll1 (Advanced Cell Diagnostics, Cat. No. 1158941-C1) mRNA using the BaseScope v2 detection kit RED™ (Advanced cell diagnostics, Cat. No. 323900) according to manufacturer instructions. Concomitant detection of PV and SST via immunohistochemistry was performed using the RNA-Protein Co-detection Ancillary kit (Advanced cell diagnostics, Cat. No. 323180). The Ccp1 probe was designed to hybridize only to exons 20 and 21 of Ccp1 which are removed in CCP1 cKO animals therefore controlling for adequate excision of these exons in CCP1 cKO INs.

Slides were first washed with PBS, baked for 30min at 60°C, post-fixed with 4% PFA for 15min at 4°C and the tissue was then dehydrated with successive ethanol baths (50%-70%-100%-100%) for 5min at room temperature. RNAscope™ Hydrogen Peroxide was applied to the sections for 10min at RT and target retrieval was then performed by immersion of the slides in 100°C Co-detection Target Retrieval (Advanced Cell Diagnostics, Cat. No. 323180) for 5min. Slides were washed in water and once in PBS-T (PBS with 0,1% Tween-20). Slices were dried and primary antibodies diluted in Co-detection Antibody Diluent (Advanced Cell Diagnostics, Cat. No. 323180) were applied at 4°C overnight. The next day, slides were washed with PBS-T for 2 minutes twice and fixed with 4% PFA for 30min at RT. Additional PBS-T washes were performed and slices were treated with RNAscope™ Protease III (Advanced Cell Diagnostics, Cat. No. 322337) for 30min at 40°C in an HybEZ™ Oven (Advanced Cell Diagnostics, Cat. No. 310010). Slides were washed with distilled water and probes were hybridized for 2h, followed by serial amplifications (BaseScope v2 detection kit RED™, Advanced cell diagnostics, Cat. No. 323900). Two washes with wash buffer reagent (Advanced Cell Diagnostics, Cat. No. 310091) were performed between each step. Probe hybridization and amplification steps 1-6 were all performed at 40°C in HybEZ™ oven while amplification steps 7 and 8 were performed at RT. The signal was then revealed by incubating slides with BaseScope™ Fast RED for 10min at RT. Finally, slides were wash buffer reagent and Co-Detection Blocker (Advanced Cell Diagnostics, Cat. No. 323180) was applied for 15min at 40°C and washed in wash buffer and PBS-T. DAPI

(2µg/mL, Sigma, D9542) and secondary antibodies diluted 1:300 in Co-Detection Antibody Diluent were incubated for 1h at RT. Slides were washed in PBS-T several times and coverslips were mounted using Fluoromount^{TM} aqueous mounting media.

Primary hippocampal cultures

Hippocampal cultures were performed with a protocol adapted from (Falzone and Stokin, 2012). For immunohistochemistry and axonal transport recordings, we respectively used 24 well plates with 12mm glass coverslips and 35mm glass-bottom petri dishes (Mattek, P35G-1.5-14-CGRD-D). Coverslips and dishes were coated by a 45min incubation in poly-ornithine (0,1mg/mL in water, Sigma Aldrich #P4638) at 37°C, followed by three washes in water and incubation with laminin (5µg/mL in PBS, Sigma Aldrich #L2020) overnight at 4°C. Dishes were washed three times in PBS before seeding of dissociated hippocampal cells.

E17.5 hippocampi of WT or CCP1 cKO mice were micro-dissected in Hank's balanced saline solution (HBSS, Biowest, L0612-500) and meninges were removed. Hippocampi were then dissociated at 37°C for 25min by replacing HBSS with 1:10 DNAse (0,1% , Sigma, D5025) 9:10 Papain (CellSystems, #LK003178) in a volume adjusted to the number of hippocampi in the Eppendorf. Hippocampi were rinsed twice with 500µL Dulbecco's modified Eagle medium (DMEM) with 10% fetal bovine serum (FBS) and 1:100 penicillin/streptomycin (biowest, L0022-100). Hippocampi were then dissociated mechanically with a 1000µL micropipette and filtered on a 40µm mesh (Greiner, 542040). Finally, cells were counted and 30 000 cells were seeded per well of 24 well plates or glass-bottom petri dishes (Mattek, P35G-1.5-14-CGRD-D) for live-imaging. 2h after plating, complete neurobasal media was added (Neurobasal Medium (Thermo Fisher, 12348017), GlutaMAX supplement 1:100 (Thermo Fisher, 35050038), B-27 Supplement 1:50 (Thermo Fisher, 17504044), penicillin/streptomycin 1:100. Half of the media was replaced by fresh complete neurobasal every 2-3 days. Cultures were maintained until DIV15 when they were either fixed with 4% PFA for 10min at RT or used for neuronal transport recording.

Neuronal transport recording and analysis

Live-recording of lysosomal transport was conducted on DIV 15 WT and CCP1 cKO hippocampal cultures. INs of WT and CCP1 cKO express GFP under the control of the Dlx5,6

enhancer. To identify PV INs, we cultures neurons in glass-bottom dishes with an embedded grid (Mattek, P35G-1.5-14-CGRD-D) that can be viewed under a microscope (**Figure 35 A**). Hippocampal cultures were seeded for 15 days as detailed in the previous section and the days prior to imaging, complete neurobasal media without phenol red was used to limit autofluorescence. On the day of imaging, LysoTracker^{TM} Red (100nM, L7528) was added directly to the media for 30min at 37°C and transport was immediately recorded using a 63x oil objective on a confocal Zeiss LSM 980 microscope with a chamber maintained at 37°C and 5% CO_2. Transport was only recorded in proximal neurites of GFP$^+$ INs and a reference image in the green channel was taken for each neuron, together with its position on the grid (**Figure 35 B**). 2min movies in Fast Airyscan mode with a framerate of 600ms were acquired to record lysosome motility (**Figure 35 C**). Multiple neurites for one neuron were sometimes analyzed, 25 neurons from 3 independent cultures were acquired per genotype. After the imaging session, dishes were immediately fixed with PFA 4% at RT for 10min and rinsed 3 times with PBS. An immunohistochemistry for GFP and parvalbumin was then conducted with the protocol described above (**Figure 35 D**). Using the position marked on the grid and the neuronal morphology captured in the reference image, PV signal was captured for the GFP$^+$ INs in which transport was recorded. Few neurons could not be found following immunohistochemistry and were therefore excluded from the analysis since their PV expression status was unknown. The PV signal intensity within the soma was measured with Fiji to classify INs as PV$^-$ or PV$^+$. Transport was then analyzed using the KymoToolBox plugin according to the method described in (Turchetto *et al.*, 2022). Briefly, kymographs were generated for each movie and the entire path of lysosomes was traced with a segmented line. The path of a single lysosome may therefore include multiple runs with changes in direction and velocity. Summary data for each track was then exported to extract the anterograde velocity, retrograde velocity and pausing time of single vesicles.

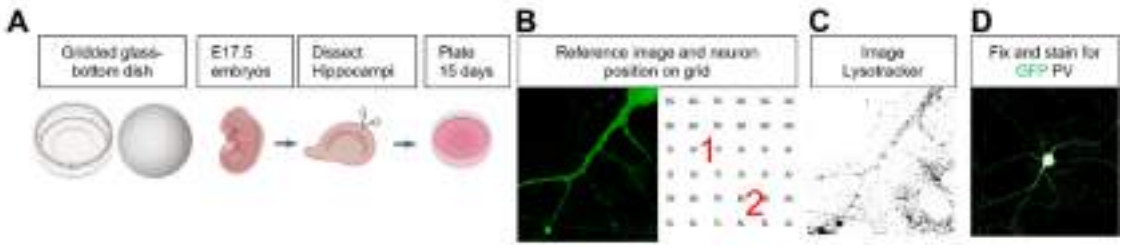

Figure 35: Experimental paradigm for analysis of neuronal transport in PV INs

A Glass-bottom dishes with a gridded coverslip were used to seed dissociated hippocampi of E17.5 WT or CCP1 cKO embryos for 15 days.
B At DIV15 GFP^+ INs were randomly selected and their position on the grid was recorded as represented by the red numbers.
C Neurons were labelled with LysoTracker™ and one or several movies was recorded in proximal neurites for each neuron.
D Neurons were fixed and stained for GFP and PV after the recording session. Using the annotated positions on the grid, each movie was then assigned to its corresponding neuron and sorted based on PV expression.

Electrophysiological recordings

Slice preparation

Slices were prepared from the brains of 8-10 week-old male WT or CCP1 cKO mice. Animals were kept in an oxygenated chamber for at least 10 minutes before being anaesthetized with isoflurane (Forene, Abbott, Belgium; 4% added to the inspiration air flow). After decapitation, the brain was rapidly dissected and immersed in ice-cold slicing solution containing: 87 NaCl, 25 NaHCO3, 10 D-glucose, 75 sucrose, 2.5 KCl, 1.25 NaH2PO4, 0.5 CaCl2 and 7 MgCl2, equilibrated with 95 % O2 / 5 % CO2 (pH 7.4, ~325 mOsm) as previously described (Bischofberger *et al.*, 2006). Sagittal 300-µm-thick slices were cut from the dorsal level of the hippocampus at 2-4 mm from midline using a vibratome (Leica VT-1200, Nussloch, Germany). Slices were stored in a reserve chamber containing slicing solution at ~34°C for ~30 min and subsequently at room temperature (20 – 25°C).

Patch-clamp recordings

Neurons were visualized using infrared IR–Dodt gradient contrast (IR–DGC) optics on a Zeiss FS microscope equipped with an IR camera (Newvicon tube in NC-70 Dage-MTI). In hippocampal slices, the CA2 region was visually identified and pyramidal cells were selected in CA2 close to the transition of CA2 to CA1. Biocytin was injected in the recorded neurons and the correct localization of the recorded pyramidal neurons in CA2 was validated using post hoc immunohistochemistry of RGS14 combined with morphological features of PNs. For recordings, the slices were perfused with saline containing in mM: 125 NaCl, 25 NaHCO3, 25 D-glucose, 2.5 KCl, 1.25 NaH2PO4, 2 CaCl2 and 1 MgCl2 (equilibrated with 95% O2/5% CO2 gas mixture, pH 7.4, ~315 mOsm) and maintained at room temperature. Patch pipettes were pulled from thick-walled borosilicate glass tubing (outer diameter: 2 mm, inner diameter: 1 mm; Hilgenberg, Germany) with a horizontal puller (P-97, Sutter Instruments). The

composition of the internal solution was, in mM: 110 KCl, 30 K-gluconate, 2 MgCl2, 2 Na2ATP, 10 EGTA, 10 HEPES and 0.2% biocytin (pH = 7.2, osmolarity: ~315 mOsm). Pipette resistance was 2.4 – 4.3 MΩ. Series resistance (6 – 12.5 MΩ) was not compensated in voltage-clamp, but carefully monitored during the experiments using 5 mV, 40 ms depolarizing test pulses. Synaptic currents were recorded in the voltage-clamp configuration with a holding potential of -70 mV. Neurons with a holding current larger than -130 pA were not included in the analysis. Miniature IPSCs were pharmacologically isolated in the presence of 10 µM 6-cyano-7-nitroquinoxaline-2,3-dione (CNQX), 20 µM D-2-amino-5-phosphonopentanoic acid (D-AP5) and 1 µM tetrodotoxin (TTX). Recordings were performed at room temperature (20 – 25°C).

Chemicals

Chemicals were as follows: tetrodotoxin citrate (TTX, Tocris) and biocytin (Life Technologies). The remaining chemicals were purchased from Sigma-Aldrich (Belgium).

Data acquisition and analysis

Recordings were performed using an Axopatch 200B amplifier (Molecular devices, Palo Alto, CA) connected to a PC via a Digidata 1440A interface (Molecular devices). Data were acquired with pClamp 10.4 (Molecular devices). Capacitive currents were recorded in voltage-clamp and filtered at 10 kHz. Membrane potential and firing were examined in current-clamp. Currents were low-pass filtered (Bessel) at 10 kHz and acquired at 10 kHz. The liquid junction potential was not corrected.

Miniature IPSCs in CA2 pyramidal neurons were collected using Minianalysis (version 6.0.7). All detected events were visually examined and subsequently validated by the user. Traces in the figures were digitally low-pass filtered with a Gaussian filter at 1 kHz. Cumulative distributions typically contained ~200 events. Further analysis was performed in clampFit 10.4 (Molecular devices), Stimfit 0.14 (Christoph Schmidt-Hieber, Institut Pasteur, https://github.com/neurodroid/stimfit; Guzman et al., 2014), Excel (Microsoft) and Mathematica 9 (Wolfram Research, Champaign, IL).

Statistical analysis

Statistical analysis was conducted using Graphpad Prism v9, normal distribution of the data was tested with the d'Agostino & Pearson test to perform appropriate parametric or non-

parametric tests. For post-hoc analysis of two-way ANOVA, Tukey's multiple comparison test was performed. Details for the statistical tests, n numbers and p-values are given in the figure legends.

4. Discussion

Our study aimed at uncovering whether CCP1 loss in INs is sufficient to induce hyperglutamylation and alter microcircuits in adult mice. We find that PV and SST INs express different levels of the main enzymes regulating polyglutamylation and consequently, CCP1 depletion in INs leads to a selective hyperglutamylation of PV INs in the adult hippocampus. We then show that hyperglutamylated PV INs develop severe neuronal transport defects reminiscent of those observed in hyperglutamylated PNs (Magiera *et al.*, 2018; Bodakuntla *et al.*, 2020, 2021). Although IN numbers remained unchanged at the time point of our analysis, we found a reduction of inhibitory synapses localized to the CA2 SO and SP that correlated with a decreased frequency of mIPSCs. Since PV cells are particularly dense in the CA2 region and mainly project to the SO and SP, it is likely that the reduction in inhibitory synapses is mainly driven by hyperglutamylated PV INs (Botcher *et al.*, 2014; Pelkey *et al.*, 2017; Booker and Vida, 2018). Together, these results suggest that specific neuronal subtypes cannot compensate for CCP1 loss and therefore accumulate protein polyglutamylation leading to cellular alterations. Our conclusions extend the scope of cell-types affected by CCP1 loss and suggest that hyperglutamylation is responsible for a spectrum of alterations to the neuronal circuitry, ranging from synaptic loss to neurodegeneration. We therefore highlight the need to address cell-type diversity in the pcd mouse and other CCP1 KO models since meaningful changes to the circuitry can potentially arise from one cell-type sensitive to CCP1 loss.

4.1 Subtype-specific sensitivity to CCP1 loss and hyperglutamylation

Despite its ubiquitous expression in the mouse brain (Kalinina *et al.*, 2007; Rogowski *et al.*, 2010), loss of CCP1 in the pcd mouse only leads to the neurodegeneration of specific cell types such as Purkinje cells, cerebellar granule neurons, mitral cells, retinal photoreceptors and subpopulations of thalamic neuron (Mullen, Eichert and Sidman, 1976; Landis and Mullen, 1978; Greer and Shepherd, 1982; O'Gorman, 1985; O'Gorman and Sidman, 1985). This observation suggests that some neuronal cell types particularly rely on CCP1 expression to

maintain their homeostasis which could be explained by: **1)** an extreme sensitivity to hyperglutamylation; **2)** differential regulation by the enzymes regulating polyglutamylation.

In support of this first hypothesis, it was described that concomitant CCP1 and CCP6 loss induces massive MT hyperglutamylation of cortical neurons. However, only about 20% of cortical neurons degenerate at 5 months in double-KO mice whereas Purkinje cells all degenerate before 1 month in the pcd mouse (Mullen, Eichert and Sidman, 1976; Magiera *et al.*, 2018). These findings suggest that Purkinje cells may be especially sensitive to MT hyperglutamylation, possibly owing to their extremely complex morphology, dense synapse network, long axonal projection and high electrical activity (McKay and Turner, 2005). Purkinje cells may therefore heavily rely on MT polyglutamylation for the regulation of cell homeostasis. It was suggested that the sensitivity of Purkinje cells to CCP1 loss may be mediated by mitochondria defects that could alter energy distribution (Gilmore-Hall *et al.*, 2019). On one hand, MT hyperglutamylation induces transport defects of mitochondria (Magiera *et al.*, 2018; Gilmore-Hall *et al.*, 2019; Bodakuntla *et al.*, 2020) and on the other hand mitochondrial fusion-fission dynamics are altered in pcd mutants (Gilmore-Hall *et al.*, 2019). Interestingly, mitochondria fusion-fission dynamics have been implicated in the establishment of dendritic arborization in Purkinje cells, a process that occurs post-natally (McKay and Turner, 2005; Fukumitsu *et al.*, 2016). These alterations in mitochondrial function may therefore synergize to induce neurodegeneration in Purkinje cells that have high energy demands and rely on mitochondria fusion-fission for their dendritogenesis.

Additionally, numerous studies support a differential regulation of MT polyglutamylation enzymes that may underpin sensitivity to CCP1 loss and MT hyperglutamylation. It was demonstrated that CCP6 which catalyzes the removal of glutamate from polyglutamylated side chains has varying levels of expression in the brain (Kalinina *et al.*, 2007; Rogowski *et al.*, 2010). CCP1, CCP4 and CCP6 may have a redundant enzymatic activity but CCP4 is expressed at very low levels in the brain, CCP1 is ubiquitous and CCP6 is mostly absent from the olfactory bulb and cerebellum (Kalinina *et al.*, 2007; Rogowski *et al.*, 2010). Interestingly, low expression of CCP6 in the olfactory bulb and cerebellum correlates with the neurodegeneration observed in mitral cells, Purkinje cells and cerebellar granule neurons (Mullen, Eichert and Sidman, 1976; Greer and Shepherd, 1982). Consistent with this, concomitant CCP1 and CCP6 loss in the cortex results in MT hyperglutamylation of

hippocampal and cortical neurons, and subsequent defects in axonal transport followed by neurodegeneration (Magiera *et al.*, 2018). Additionally, while granule cells of the cerebellum also express very low levels of CCP6, they are less sensitive to CCP1 loss as compared to Purkinje cells and consequently only degenerate partially and progressively in mice (Triarhou, 1998). This may be explained by the low levels of *Ttll1* expression in cerebellar granule cells compared to Purkinje Cells, which may prevent massive accumulation of MT hyperglutamylation in granule cells (Li *et al.*, 2020). Studies in retinal photoreceptor also found a particular sensitivity of these cells to loss of TTLL5 (Bedoni *et al.*, 2016; Smirnov *et al.*, 2021). TTLL5 catalyzes the addition of branching point glutamates and can therefore initiate the polyglutamate side chains on tubulin (van Dijk *et al.*, 2007). TTLL5 mutations in humans correlates with neurodegeneration of retinal photoreceptors (Bedoni *et al.*, 2016; Smirnov *et al.*, 2021). Concomitant loss of TTLL5 and CCP1 synergizes to aggravate the neurodegeneration of retinal photoreceptors in mice but this double-KO does not accelerate the neurodegeneration of mitral and Purkinje cells (Wu *et al.*, 2022). These findings suggest that retinal photoreceptors rely on TTLL5 expression for the regulation of MT polyglutamylation levels while other cell-types may compensate for its loss. Together, these studies highlight different expression patterns of polyglutamylation enzymes which correlate with their sensitivity to MT hyperglutamylation and neurodegeneration. It is therefore likely that different patterns of polyglutamylation are generated across cell-types and some neurons may rely more strongly on specific polyglutamylation enzymes therefore predicting sensitivity to specific mutations.

Along this line, we found that PV INs expressed higher levels of *Ccp1, Ccp6* and *Ttll1* mRNA compared to SST INs in the hippocampus. We then showed that PV INs but not SST INs are hyperglutamylated in the adult hippocampus. CCP1 loss may therefore alter the balance of polyglutamylation/deglutamylation in PV INs but not SST INs, therefore highlighting a cell-type specific regulation of polyglutamylation responsible for a sensitivity to CCP1 loss in PV cells (**Figure 36**). These findings extend the range of cell-types affected by CCP1 loss and highlight the need to study the effects of CCP1 loss at the cellular level since a minority of neurons within a brain region may be affected. Interestingly, neurodegeneration of cortical neurons in CCP1, CCP6 KO mice was demonstrated by the lower numbers of MAP2+ neurons in layer V and reduced density of MAP2+ apical dendrites in layer IV (Magiera *et al.*, 2018). PV

INs express MAP2 and are particularly concentrated in layers IV and V of the neocortex (Tremblay, Lee and Rudy, 2016; Franchi *et al.*, 2018). It would therefore be interesting to assess whether the partial neurodegeneration observed in the cortex at 5 months specifically targets some neuronal subtypes, with PV INs being a prime candidate.

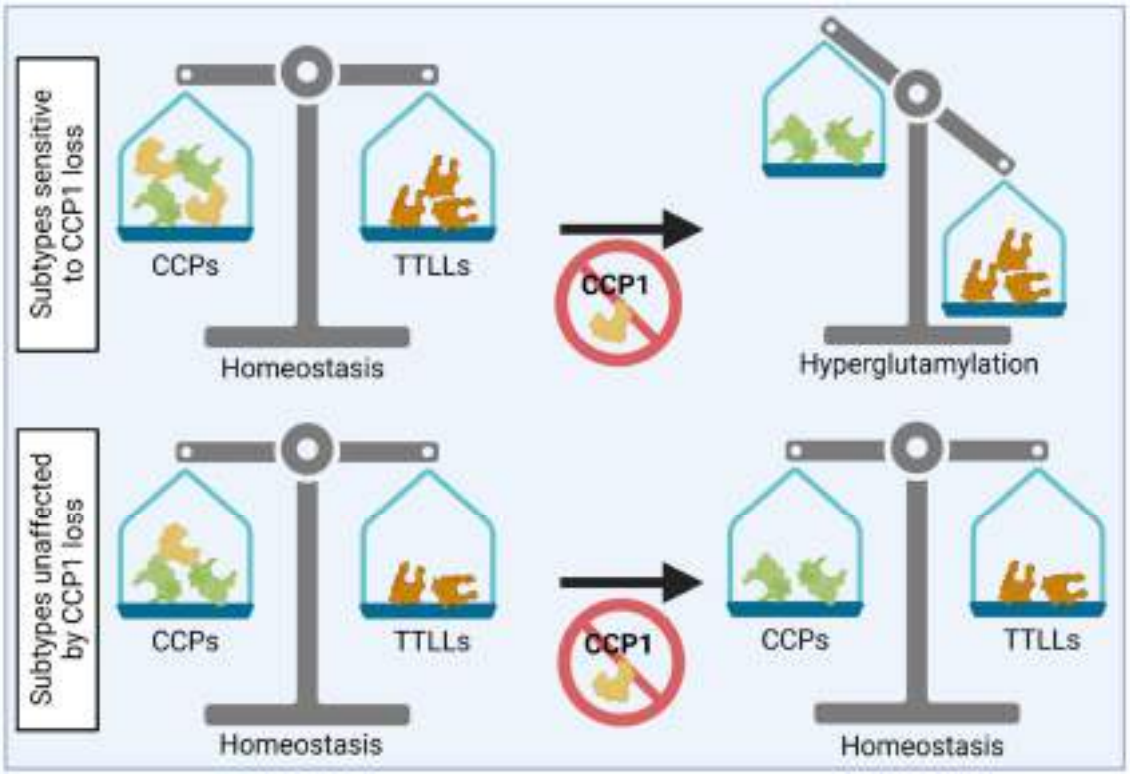

Figure 36: Proposed model for subtype-specific sensitivity to CCP1 loss.
We found that CCP1 loss induces hyperglutamylation in some neurons but not others. We propose that some neuron subtypes heavily rely on CCP1 expression to maintain homeostasis in physiological conditions. When CCP1 is lost, the equilibrium is shifted towards polyglutamylation by TTLLs therefore inducing hyperglutamylation. Neurons that maintain normal polyglutamylation levels following CCP1 loss may not rely as heavily on CCP1 for deglutamylation, compensate through other CCPs or downregulate TTLLs expression and activity.

4.2 Hyperglutamylation perturbs axonal transport across subtypes

Early studies demonstrated a potential effect of MT polyglutamylation on neuronal transport using *in vitro* motility assays where some kinesins showed increased processivity and velocity on polyglutamylated MTs (Larcher *et al.*, 1996; Sirajuddin, Rice and Vale, 2014). Since then, the link between MT polyglutamylation and neuronal transport has been confirmed in hippocampal PNs and cerebellar granule neurons (Magiera *et al.*, 2018; Gilmore-Hall *et al.*,

2019; Bodakuntla *et al.*, 2020). Hippocampal PNs in culture show altered motility of mitochondria, lysosomes, LAMP1 endosomes and BDNF vesicles following CCP1 loss (Bodakuntla *et al.*, 2020). These cargoes are transported by different motors and adaptor proteins and defects in both the anterograde and retrograde direction arise, suggesting that MT polyglutamylation is a general regulator of transport in hippocampal PNs (Maday *et al.*, 2014a; Bodakuntla *et al.*, 2020). Interestingly, similar mitochondrial transport defects occur in cultured cerebellar granule neurons however, lysosomal transport is unaffected, suggesting cell-type specific regulation of transport by polyglutamylation (Gilmore-Hall *et al.*, 2019).

Here, we found that CCP1 cKO PV but not SST INs were hyperglutamylated in the hippocampus *in vivo*. Analysis of lysosomal transport in neurites of hippocampal CCP1 cKO PV^+ and PV^- INs *in vitro* revealed significant transport defects in PV^+ INs that were remarkably similar to those described in hippocampal PNs (Magiera *et al.*, 2018; Bodakuntla *et al.*, 2020). Indeed, CCP1 cKO PV^+ INs showed a marked reduction in overall motility with increased pausing time and proportion of stationary vesicles but the anterograde and retrograde velocity was unchanged. This suggests that hyperglutamylation perturbs the initiation of cargo movement or induces motor inactivity/detachment. Interestingly, CCP1 cKO PV^- INs only showed an increase in the pausing time of motile vesicles but no difference in the proportion of stationary vesicles. Since polyglutamylation levels are higher in CCP1 cKO PV^+ INs, it is possible that vesicles are stopped for longer periods of time therefore increasing the proportion of vesicles that are stationary for the whole duration of the movie. The phenotype in CCP1 cKO PV^- INs may therefore reflect a milder alteration of transport albeit regulated by the same mechanisms as in CCP1 cKO PV^+ INs. CCP1 cKO PV^- INs showed no increase in polyglutamylation levels *in vivo* at 3 months but the transport analysis was performed at DIV15. Similar to cortical neurons, it is possible that glutamylation levels are elevated in the perinatal period due to lack of compensation by other CCPs, which may explain the mild transport defects seen in PV^- INs (Rogowski *et al.*, 2010; Magiera *et al.*, 2018). Although previous studies focused their analysis in the axon, we considered neurites irrespective of their identity. Since neurons have only one axon and multiple dendrites and since more than one neurite was often recorded for each neuron, the majority of neurites we analyzed must be dendrites. Despite the differences in the MT network of dendrites and axons, we find

similar transport defects as those described in axons, suggesting that polyglutamylation may regulate transport in a similar manner in both axons and dendrites.

Our results suggest that hyperglutamylation may control transport across neuronal subtypes, including hippocampal INs. However, subtle differences in IN subtypes may result in specific sensitivity to CCP1 loss and hyperglutamylation which cascades into severe transport defects. These findings once again highlight the need to address the diversity of neuronal subtypes when assessing the effects of CCP1 loss and hyperglutamylation.

4.3 How can tubulin polyglutamylation modulate neuronal transport ?

Recent studies begin to shed light on how tubulin polyglutamylation modulates neuronal transport, however, the exact mechanisms are still unknown and deserve further consideration. The neurodegeneration of Purkinje Cells in the pcd mouse can be prevented by downregulating the expression of TTLL1 but not TTLL7 (Rogowski *et al.*, 2010; Bodakuntla *et al.*, 2021). This may be due to the specific patterns of polyglutamylation generated by these two enzymes since TTLL1 and TTLL7 primarily add glutamate residues to the side chains of α and β-tubulin, respectively (Janke *et al.*, 2005; van Dijk *et al.*, 2007; Bodakuntla *et al.*, 2021). Interestingly, knockdown of TTLL1 but not TTLL7 increases the overall motility of mitochondria in hippocampal PNs, suggesting that the levels of α-tubulin polyglutamylation negatively correlate with the overall motility of mitochondria (Magiera *et al.*, 2018; Bodakuntla *et al.*, 2021).

Contrary to MT acetylation which affects both cargo velocity and motility, only the time spent in movement is regulated by MT polyglutamylation (Even *et al.*, 2019). This suggests that MT polyglutamylation is particularly important for the initiation and maintenance of cargo movement. Several hypotheses have been proposed to explain the transport defects observed in models of hyperglutamylation (Bodakuntla *et al.*, 2020; Bodakuntla, Janke and Magiera, 2021; Genova *et al.*, 2023).

First, MT polyglutamylation may affect the binding of motors or adaptor proteins thereby regulating the overall motility of cargoes (**Figure 37 A**). Polyglutamylation can indeed modify the velocity and processivity of kinesin-1 and kinesin-2 *in vitro* (Sirajuddin, Rice and Vale, 2014). Additionally, it was suggested that the pausing of KIF1A, from the kinesin-3 family, is

controlled by the polyglutamylation levels on tubulin (Lessard *et al.*, 2019). These observations were performed by comparing MTs from Hela cells or bovine brain which differ in their polyglutamylation status but may also exhibit other differences (Lessard *et al.*, 2019). A recent study found that the interaction time and run length of KIF5B was controlled by β but not α-tubulin polyglutamylation (Genova *et al.*, 2023). This finding is surprising considering that TTLL1 but not TTLL7 knockdown affects the overall motility of mitochondria (Bodakuntla *et al.*, 2021). Additional studies are therefore required to shed light on the contribution of MT polyglutamylation to the binding and processivity of molecular motors.

Next, MT polyglutamylation may affect transport through the regulation of MAP binding (**Figure 37 B**). The MAP tau which is associated to Alzheimer's disease and neurodegeneration (Dixit *et al.*, 2008; Wang and Mandelkow, 2016; Goedert, Eisenberg and Crowther, 2017; Chang, Shao and Mucke, 2021) inhibits the binding of kinesin 1 and 3 (Trinczek *et al.*, 1999; Dixit *et al.*, 2008). Tau interacts with the outer surface of MTs and blocks the interactions with the MT domains of kinesin (Trinczek *et al.*, 1999; Kellogg *et al.*, 2018). Therefore, motors tend to detach when they encounter patches of tau bound to MTs (Trinczek *et al.*, 1999; Dixit *et al.*, 2008). Another study also suggested that tau reduces the motor reattachment rates (Goedert, Eisenberg and Crowther, 2017). Interestingly, α and β-tubulin polyglutamylation both increase the affinity of tau for MTs (Genova *et al.*, 2023), which could create "roadblocks" in hyperglutamylated neurons to promote detachment and impede reattachment of cargoes. Other neuronal MAPs have been implicated in the regulation of transport but further studies are required to understand whether their affinity for MTs is regulated by polyglutamylation (Mandelkow *et al.*, 2004; Jiménez-Mateos *et al.*, 2006).

MT polyglutamylation levels regulate the activity of the severing enzymes katanin and spastin (Lacroix *et al.*, 2010; Szczesna *et al.*, 2022; Genova *et al.*, 2023). By remodeling the MT network, severing enzymes may regulate the transport of cargoes (McDermott *et al.*, 2003). Interestingly, spastin depletion increases tubulin polyglutamylation and impairs KIF5C-mediated transport. However, rescuing polyglutamylation levels through TTLL1 inhibition restores the transport of KIF5C, suggesting than MT polyglutamylation and not spastin on its own regulates KIF5C motility (Lopes *et al.*, 2020). Additionally, tau binding can increase the space between MTs therefore disrupting mitochondrial transport, possibly by decreasing the efficiency of track-switching (Shahpasand *et al.*, 2012). These observations suggest that MT

hyperglutamylation may remodel the MT network and thus contribute to the regulation of transport (**Figure 37 C**). Recent evidence also suggests that polyglutamylation levels regulate MT dynamics (Chen and Roll-mecak, 2023). This study shows that, *in vitro*, higher glutamylation correlates with decreased microtubule growth rate and increased catastrophes. In addition, removal of glutamate by CCP1 and CCP5 preferentially occurs on soluble tubulin whereas addition of glutamates by TTLLs preferentially occurs on polymerized MTs (Chen and Roll-mecak, 2023). Loss of function of CCPs may therefore impair microtubule polymerization and increase the rate of catastrophe by maintaining polymerized and free tubulin in an hyperglutamylated state.

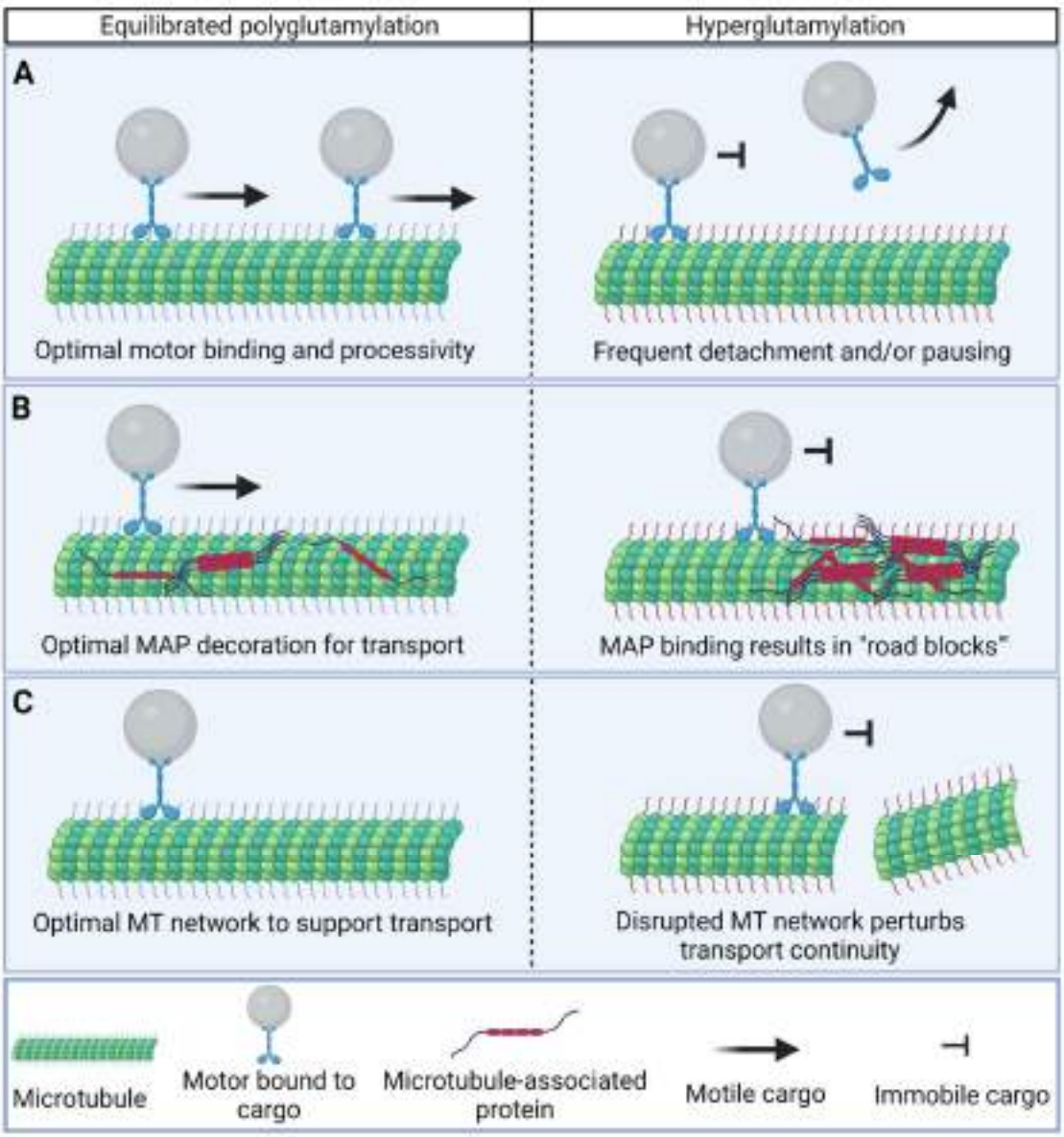

Figure 37: Potential mechanisms of transport impairment in hyperglutamylated neurons.
A. Binding and processivity of several motors has been shown to be influenced by the polyglutamylation state of tubulin side-chains. It is therefore possible that hyperglutamylation perturbs motor motility and induces frequent detachment or pausing that result in decreased overall motility of cargoes.
B. MT hyperglutamylation affects the binding of MAPs and in particular increases the binding of tau. Accumulation of tau on microtubules can cause "road blocks" that result in cargo arrest or detachment.
C. The MT network is finely regulated by severing enzymes and other MAPs to ensure transport continuity. Hyperglutamylation can alter the activity of severing enzymes and other potential MAPs that may alter the MT network. Transport could subsequently be interrupted by lack of continuity in the MT network.
This figure is inspired from (Bodakuntla *et al.*, 2020).

4.4 Tubulin polyglutamylation regulates synapse function and integrity

We found that CCP1 loss induces hyperglutamylation of PV INs but we could not detect significant degeneration at 3 months. However, inhibitory synapses are reduced in the adult hippocampus, especially in the SO and SP of the CA2 field. Since we detected inhibitory synapses based on the colocalization of VGAT and gephyrin, all GABAergic synapses were considered irrespective of IN subtype (Dobie and Craig, 2011). However, the highest density of PV INs is found in the CA2 field of the hippocampus and PV INs project to the SO and SP layers via axo-axonic cells and basket cells respectively (Botcher *et al.*, 2014; Pelkey *et al.*, 2017; Booker and Vida, 2018). It is therefore possible that the reduction of inhibitory synapses in CCP1 cKO is mainly driven by hyperglutamylated PV INs. Loss of inhibitory synapses in the CA2 region of the hippocampus correlates with a reduced frequency of mIPSCs on the soma of CA2 PNs.

Previous studies already suggested at a role for MT polyglutamylation on synapse integrity and function. Hypoglutamylation is linked to mislocalization of the synaptic vesicle motor KIF1A which fails to enter neurites (Ikegami *et al.*, 2007). Consequently, synaptic terminals show reduced synaptic vesicle density and rapid vesicle depletion upon stimulation (Ikegami *et al.*, 2007). Activation of hippocampal neurons also leads to increased tubulin polyglutamylation and accumulation of gephyrin-containing vesicles in the soma. Interestingly, Pgs1 inhibition (a TTLL1 subunit) prevents mislocalization of gephyrin-vesicles suggesting that high MT polyglutamylation levels also precludes entry of synaptic vesicles to neurites (Maas *et al.*, 2009). A new CCP1 KO model in which the exon 3 is depleted also

exhibits reduced levels of the glutamine receptor (GluA2) and kinesin-1 in hippocampal synaptosomes that correlates with a mild decrease in anxiety and impairments in context-dependent learning (Zhou *et al.*, 2022). Of note, deletion of the exon 3 induces a frameshift but truncated CCP1 proteins are detected, suggesting the presence of multiple translation start sites. Consequently, MT polyglutamylation is mildly increased but does not lead to the typical pcd phenotype of cerebellar degeneration (Zhou *et al.*, 2022). Depletion of spastin increases tubulin polyglutamylation and is linked to transport defects and reduction of excitatory synapses in hippocampal cultures and in the CA1 region of the hippocampus at 3 months (Lopes *et al.*, 2020). The reduction of excitatory synapses also correlates with a reduced frequency of miniature excitatory postsynaptic currents, reminiscent of our findings in CCP1 cKO mice. TTLL1 inhibition rescues transport defects but its effect on synapses was not assessed. It remains therefore unclear whether the loss of excitatory synapses is mediated by spastin depletion itself or by the increased polyglutamylation that ensued (Lopes *et al.*, 2020). Our findings demonstrate a loss of inhibitory synapses in the hippocampus of CCP1 cKO mice and therefore strongly suggest that MT hyperglutamylation can lead to synaptic alterations. Neuronal transport is crucial for synapse maintenance and it is therefore likely that transport defects in CCP1 cKO mice are involved in the loss of synapses (Guedes-Dias and Holzbaur, 2019).

4.5 Synaptic loss may precede neurodegeneration

Axonal transport defects have been previously associated to neurodegenerative disorders (Millecamps and Julien, 2013; Brady and Morfini, 2017; Sleigh *et al.*, 2019b). Although much attention has been given to the process of neurodegeneration itself, the loss of the soma is often preceded by axonal degeneration also coined as “dying back” (Vickers *et al.*, 2009; Adalbert and Coleman, 2013) (**Figure 38**). Clinical symptoms are sometimes concurrent with altered neuronal connectivity which develops before visible signs of neuronal loss (Vickers *et al.*, 2009; Adalbert and Coleman, 2013). Synaptic loss is therefore a significant factor in the pathogenesis of multiple neurodegenerative diseases such as Alzheimer, Parkinson, Huntington’s disease or multiple sclerosis (Wishart, Parson and Gillingwater, 2006; Henstridge, Pickett and Spires-Jones, 2016).

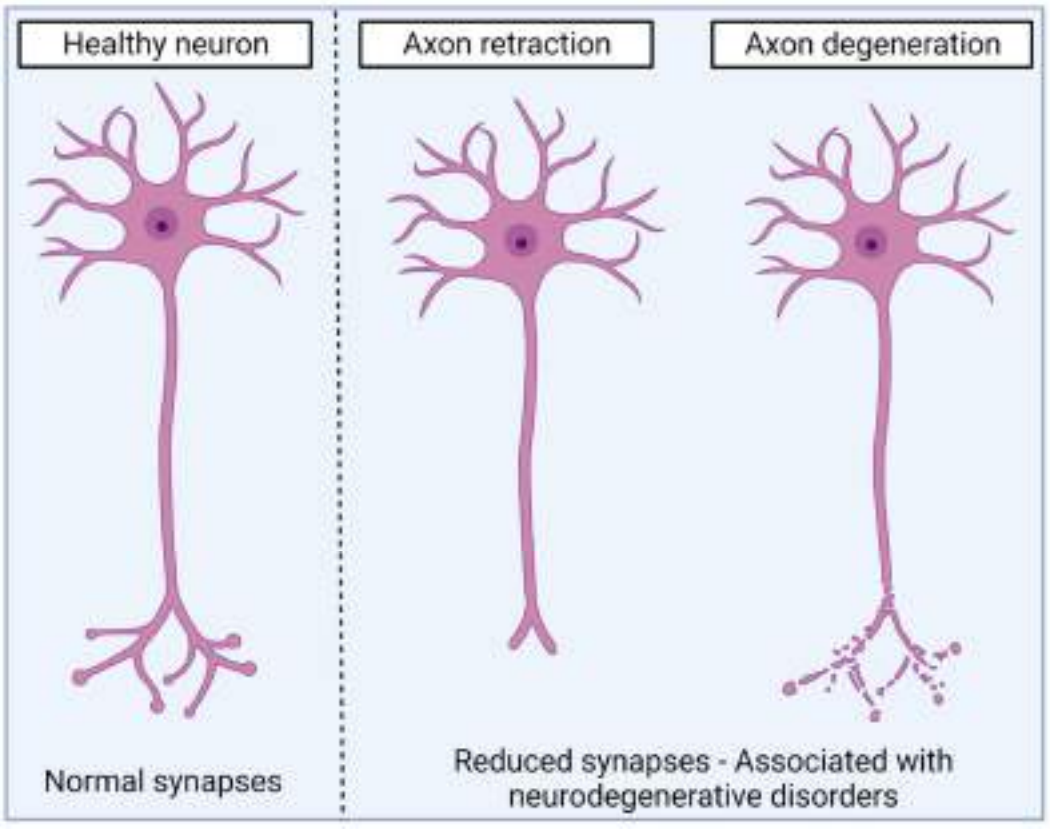

Figure 38: Axonal impairments in neurodegenerative disorders.
Axonal impairments arise in various neurodegenerative disorder such as Parkinson's disease and Alzheimer and can precede neuronal death. Both axonal retraction and axonal degeneration have been observed and result in loss of synapses and circuit alterations (Neukomm and Freeman, 2014; Salvadores *et al.*, 2017).

In the cortex of mice with concomitant deletion of CCP1 and CCP6, axons show signs of degeneration with organelle accumulation and axonal swelling (Magiera *et al.*, 2018). Although only about 20% of cortical neurons are lost at 5 months, some of the surviving neurons may also suffer from axonal degeneration and perturbed neuronal connectivity (Magiera *et al.*, 2018). Similarly, a reduction in myelinated axons is observed in the femoral quadriceps nerves of CCP1 KO mice, suggesting axonal degeneration of spinal cord motor neurons (Shashi *et al.*, 2018; Bodakuntla *et al.*, 2021). Our findings combined with the observation that excitatory synapses are reduced in hyperglutamylated hippocampal neurons following spastin depletion (Lopes *et al.*, 2020), suggests that axonal degeneration and synaptic loss may precede neurodegeneration and lead to meaningful alterations in neuronal connectivity. Additional studies assessing the viability of INs and especially the PV subtype in the hippocampus of CCP1 cKO mice are required to understand whether synaptic loss is an

early sign of neurodegeneration in this model. The functional and behavioral consequences of synaptic loss should also be studied to determine whether the reduction in inhibitory synapses may be pathologic.

4.6 How is neurodegeneration induced in CCP1 KO models?

Although CCP1 loss induces neurodegeneration in select neuron subtypes of the pcd mouse, it remains challenging to pinpoint the exact mechanisms that lead to neuronal death (Bodakuntla, Janke and Magiera, 2021). MT polyglutamylation regulates the activity of the severing enzymes spastin and katanin (Lacroix *et al.*, 2010; Valenstein and Roll-Mecak, 2016; Szczesna *et al.*, 2022). However, spastin deletion in CCP1 KO mice does not rescue neurodegeneration (Magiera *et al.*, 2018). Although MT polyglutamylation regulates spastin activity, it does so in a non-linear fashion where low and high levels of polyglutamylation both decrease spastin activity (Valenstein and Roll-Mecak, 2016). It is therefore possible that the levels of spastin activity are similar or even reduced in CCP1 KO mice as compared to controls. Additional studies to assess the role of spastin and katanin activity in CCP1 models are necessary to better understand the contribution of severing enzymes to neurodegeneration.

Axonal transport defects are a robust phenotype arising in CCP1 KO models and may also be involved in the process of neurodegeneration. Axonal transport defects are often associated with neurodegenerative disorders although it remains difficult to assess whether they are the cause or consequence of neurodegeneration (Millecamps and Julien, 2013; Brady and Morfini, 2017; Sleigh *et al.*, 2019b). Some studies have suggested that axonal transport defects precede neurodegeneration and may therefore be a causative factors in some diseases (Bilsland *et al.*, 2010; Small *et al.*, 2017). Interestingly, neurodegeneration induced by CCP1 loss is rescued by TTLL1 but not TTLL7 knockdown. Since TTLL1 and TTLL7 are tubulin specific and preferentially polyglutamylate α and β-tubulin respectively, these results suggest that α-tubulin polyglutamylation is the main driver of neurodegeneration (Rogowski *et al.*, 2010; Magiera *et al.*, 2018; Bodakuntla *et al.*, 2021). Additionally, knockdown of TTLL1 but not TTLL7 increases the overall motility of mitochondria hinting that neurodegeneration may be rescued through a restoration of transport (Bodakuntla *et al.*, 2021). Further supporting the role of transport in CCP1-induced neurodegeneration, organelle accumulation and axonal swelling in the axons of hyperglutamylated cortical neurons is reminiscent of the axonal

degeneration induced by transport defects (Magiera *et al.*, 2018). However, a causal link between transport alterations and neurodegeneration remains to be established in CCP1 KO models.

Additional mechanisms may contribute to neurodegeneration induced by CCP1 loss such as the regulation of MAPs by polyglutamylation (Genova *et al.*, 2023). Additionally, CCP1 can also catalyze the removal of glutamates from substrates other than tubulin, including gene-encoded glutamates and may therefore affect cell viability though mechanisms that have not yet been discovered (Tanco *et al.*, 2015; Silva *et al.*, 2018). However, since neurodegeneration is fully rescued by TTLL1 knockdown, it suggests that removal of gene-encoded glutamates by CCP1 does not play a major role in the phenotype (Magiera *et al.*, 2018). In addition, TTLL1 appears to specifically polyglutamylate tubulin, which further suggests that neurodegeneration is induced by MT hyperglutamylation and other substrates of CCP1 may therefore play only a minor role in the degeneration phenotype (Rogowski *et al.*, 2010; Magiera *et al.*, 2018).

5. Perspectives

Some complementary experiments could be performed to build upon our findings. Although our results suggest that PV INs are particularly sensitive to CCP1 loss and hyperglutamylation, additional experiments could strengthen these findings. We find that the expression levels of *Ccp1, Ttll1* and *Ccpp6* mRNA are higher in WT PV compared to WT SST INs. Additional experiments looking at the expression levels of other TTLLs and CCPs as well as their level of activity may help understand why PV INs but not SST INs are hyperglutamylated in adult mice. Although PV INs are hyperglutamylated at 3 months in CCP1 cKO mice, we do not find evidence of neurodegeneration. Assessment of IN numbers at later time points would reveal whether hyperglutamylation of PV INs would eventually lead to neurodegeneration as it does in the cortex at 5 months (Magiera *et al.*, 2018)

The use of a PV-CRE transgenic mice to drive CCP1 loss could also help in dissecting the synaptic defect that we have observed. Indeed, the decrease in inhibitory synapses and frequency of mIPSCs is phenocopied in the PV-CRE; $CCP1^{lox/lox}$ model, it would strongly suggest that PV INs are the main driver of the synaptic alterations. One caveat with this approach is

that PV expression is post-natal and CCP1 recombination would therefore occur later than in the Dlx5,6 model where CRE is expressed at embryonic stages around the time of terminal division of GE progenitors. A GAD2-CRE-ERT2 mouse could be used to drive CRE expression in GABAergic neurons at embryonic stages or post-natal stages. Bypassing the developmental period would reveal whether the histological defects we have observed are the result of altered developmental processes or rather accumulation of polyglutamylation postnatally.

The synaptic defects in CCP1 cKO may result in functional and behavioral alterations. Since the loss of synapses is mainly restricted to the CA2 region of the hippocampus, it is tempting to hypothesize that social memory would be impaired in CCP1 cKO mice (Hitti and Siegelbaum, 2014; Stevenson and Caldwell, 2014). A more thorough electrophysiological analysis could be performed to probe the function of inhibitory microcircuits through stimulation of the Schaffer collateral for instance. PV INs are known to receive strong afferents from CA3 PNs which subsequently inhibit CA2 PNs through feedforward inhibition (Piskorowski and Chevaleyre, 2013). A behavioral screen to assess spatial and social memory could also be conducted in CCP1 cKO mice to assess whether putative defects in the microcircuitry lead to broad alterations in memory encoding.

TTLL1 knockdown has been shown to increase mitochondria motility and rescue Purkinje cell degeneration (Rogowski *et al.*, 2010; Bodakuntla *et al.*, 2021). It would therefore be tempting to rescue polyglutamylation levels in PV INs through TTLL1 depletion to attempt a rescue of transport and synaptic defects as well as putative behavioral alterations in CCP1 cKO mice.

CHAPTER 2:

Uncovering the role of organelles in the regulation of microtubule acetylation and axonal transport dynamics

1. Summary of the results

In this section, I will summarize and discuss the results of two published manuscripts that address the question of how PTMs, notably MT acetylation regulates axonal transport. Both studies result from a collaborative work and my contribution mostly consisted in performing measurements of MT acetylation levels and axonal transport parameters in *Drosophila* larvae. I will detail my exact contribution to the two publications and then provide a summary of the full studies.

1.1 ATAT1-enriched vesicles promote MT acetylation via axonal transport

1.1.1 Contribution

This work was published in Science Advances in 2019 (**doi: 10.1126/sciadv.aax2705**). Most of my contribution pertains to the fly work.

I performed the transport and peristaltic waves rescue experiments using the HDAC6 inhibitor tubastatin as well as the measurements of MT acetylation levels in third instar larvae (Figure 2, panels G-L and P-Q). I also performed the experiments to assess MT acetylation and transport in third instar larvae following treatment with ciliobrevin D (Figure 5, panels D-I). Finally, I stained the neuromuscular junction of third instar larvae to assess the number of boutons (Figure S2, panels G and H). For all these experiments, I performed the dissections (when necessary), imaging, staining and analysis.

In Figure 4, I differentiated human induced pluripotent stem cells into glutamatergic neurons to study the colocalization of αTAT1 with LAMP1, SV2C and synaptophysin. Although I generated the neurons, immunostaining, imaging and analysis was performed by Silvia Turchetto (Figure 4, panel B). I cloned the truncated αTAT1 constructs with the help of Ivan Gladwyn-Ng for the experiments in Figure 4, panels I-M.

1.1.2 Summary of the results

A link between MT acetylation and axonal transport has been demonstrated and multiple studies showed that increasing levels of MT acetylation by inhibiting the deacetylating enzyme HDAC6 increases transport velocity (Reed *et al.*, 2006; Jim P Dompierre *et al.*, 2007; d'Ydewalle *et al.*, 2011; Godena *et al.*, 2014). However, HDAC6 catalytic activity is not specific

to MTs and may therefore affect axonal transport through the deacetylation of other substrates (Hai and Christianson, 2016; Varga *et al.*, 2022). Assessing neuronal transport dynamics following complete loss of acetylation induced by αTAT1 KO was therefore important to help deciphering the link between MT acetylation and transport.

Here, we characterized MT acetylation and axonal transport parameters of various cargoes following αTAT1 loss in mice or αTAT1 and αTAT2 loss in *Drosophila* third instar larvae. We found a complete loss of this PTM in murine neurons lacking αTAT1, as expected from previous reports showing that this enzyme is the main if not the only acetyltransferase in mammals. In *Drosophila*, residual MT acetylation remained, which likely resulted from the partial downregulation via RNAi-mediated αTAT1 and αTAT2 knockdown. In both mice and flies, a marked bidirectional reduction of cargo velocity was observed, accompanied by reduced run length and increased pausing time. Similarly, *in vitro* reconstitution assays show that cargo velocity is reduced in neuronal MTs lacking acetylation as compared to WT MTs. Interestingly, transfection of the acetylation-mimicking mutated α-tubulin K40Q in mouse neurons rescued transport defects. Similarly, HDAC6 RNAi-mediated knockdown or inhibition with tubastatin also rescued acetylation levels and transport defects in *Drosophila* larvae. These results are the first detailed analysis of axonal transport induced by loss of the MT acetylating enzymes and strengthen the link between MT acetylation and regulation of axonal transport. They also demonstrate that the regulation of transport by αTAT enzymes is mostly mediated by its α-tubulin acetyltransferase activity and they highlight the evolutionary conservation of MT acetylation as a regulator of cargo motility.

The acetylation of αK40 of tubulin occurs in MT, from inside the lumen and therefore αTAT1 must enter MTs to promote tubulin acetylation. The mechanisms underlying αTAT1 entry in MTs remain unclear. It was suggested that αTAT1 could enter MTs via both open ends and openings in the lattice to then diffuse within the MT lumen (Coombes *et al.*, 2016; Ly *et al.*, 2016). Because of its specificity for MTs and the requirement to be near the lattice to enter the lumen, we hypothesized that motile vesicles may deliver αTAT1 to the MTs. To test this hypothesis, we performed a proteomic screen on the vesicular pool of mouse cortical neurons which revealed the presence of αTAT1 but not HDAC6. We confirmed these results by showing with immunoblots that αTAT1 is enriched in the vesicular fraction following subcellular fractionation. In addition, αTAT1 partially colocalized with vesicular markers and

was co-transported with lysosomes and BDNF-vesicles. We then showed that the vesicular enrichment of αTAT1 is impaired following the loss of a domain in its C-terminal end, downstream of the catalytic site. This truncation was associated with reduced acetylation of MTs in HEK cells. Finally, proteinase K digestion reduced αTAT1 levels in vesicles but not the intravesicular protein α-synuclein. Together, these results suggested that αTAT1 binds to the cytoplasmic side of vesicles through a domain in its C-terminal tail which subsequently improves its acetylation efficiency.

We therefore hypothesized that the vesicular pool of αTAT1 may be delivered to MTs by vesicular transport. We found that inhibiting transport with ciliobrevin D or knockdown of Lis1 also resulted in reduced acetylation, suggesting that vesicular transport itself is required for the proper acetylation of MTs. To test whether the vesicular pool of αTAT1 can promote MT acetylation, we co-incubated non-acetylated MTs with WT vesicles and found a time-dependent increase in MT acetylation. This effect was lost when MTs were incubated with vesicles lacking αTAT1. These results suggest that vesicular transport promotes MT acetylation via its pool of αTAT1.

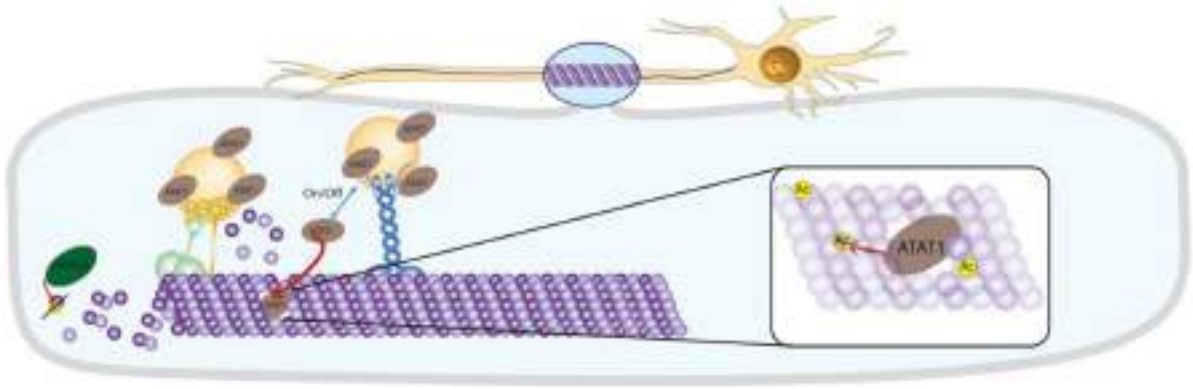

Figure 16: Proposed model of αTAT1 delivery to the MT lumen by vesicular transport.
Recent findings show that vesicular transport causes mechanical breaks in the MT lattice induced by the pulling forces of molecular motors. We propose a model in which the vesicular pool of αTAT1 is ideally positioned to enter the MT lumen through dynamic mechanical breaks induced by the transport of the vesicle on which αTAT1 resides. This model would suggest that MT acetylation and axonal transport dynamics have a bilateral association whereby MT acetylation promotes vesicular transport and vice versa. Figure from (Even *et al.*, 2019).

1.2 ATP-citrate lyase promotes axonal transport across species

1.2.1 Contribution

This work was published in *Nature Communications* in 2021 (**doi: 10.1038/s41467-021-26998-y**). In this paper, my contribution also pertains to the fly work.

I performed the quantification of MT acetylation levels in dissected third instar larvae (Figure 1, panel f). I quantified MT acetylation levels and transport parameters following **1)** Acly knockdown and rescue by HDAC6 knockdown **2)** Elp3 knockdown and rescue by Acly overexpression (Figure 3, panels e-h and m-p).

I crossed the flies and collected the material for the qPCR and immunoblot of Figure S1, panels p-r. I performed the staining for HRP (Horseradish peroxidase) and CSP (Cysteine string protein) in dissected third instar larvae (Figure S1, panels u and v). I generated the flies and collected the material for the immunoblot in Figure S3, panel h. I performed the experiment of crawling speed rescue by Acly overexpression (Figure S3, panel j) and generated the animals used for the analysis of the climbing index (Figure S3, panel k).

1.2.2 Summary of the results

The Elongator complex has previously been involved in the regulation of MT acetylation, however, despite harboring an acetyltransferase domain, Elongator does not appear to directly acetylate MTs (Creppe *et al.*, 2009; Kalebic, Sorrentino, *et al.*, 2013). In addition, despite the established link between MT acetylation and neuronal transport, no study so far demonstrated altered transport in models where Elongator function is impaired. Here, we provide evidence on the mechanism through which Elongator regulates MT acetylation and we establish a link between Elongator loss and axonal transport defects in mouse and fly neurons.

As we previously reported, we found that Elongator loss resulted in decreased MT acetylation in the mouse cortex, primary cultures of cortical neurons and third instar larvae motor neurons. Similar to defects in acetylation caused by αTAT1 loss, Elongator loss led to decreased bilateral transport velocity, and increased pausing time of lysosomes and mitochondria in mouse projection neurons. Similar results were also found for the transport of synaptotagmin-GFP in fly motor neurons, where transport defects were also associated

with reduced crawling speed in larvae and reduced climbing index in adult flies. MT acetylation, transport defects and locomotion were all rescued by HDAC6 knockdown in flies, suggesting that these alterations originate from the reduction in MT acetylation induced by Elongator loss. Interestingly, in murine neurons, αTAT1 KO combined with Elp3 KD did not result in a more severe transport phenotype as compared to αTAT1 KO alone, suggesting that Elp3 might act upstream of αTAT1. Together, these results suggest that Elp3 may act as an upstream regulator of MT acetylation and consistent with previous studies, they strengthen the link between reduced MT acetylation and axonal transport alterations.

To understand how loss of Elongator activity may affect MT acetylation, we tested whether Elongator regulated the expression or activity of HDAC6 and αTAT1 but found no difference between WT and Elp3 cKO. Since acetylation of MTs by αTAT1 requires acetyl-CoA as a substrate, we checked whether Elongator could affect the expression levels of the two enzymes that produce cytoplasmic acetyl-CoA, Acly and Acss2. We found a reduction in the expression of both proteins following Elp3 loss, which may explain how Elongator helps regulating MT acetylation levels. Since we have previously shown that αTAT1 is enriched at vesicles to promote MT acetylation, we performed subcellular fractionation of cortical lysates to assess the relative abundance of Acly and Acss2 in the cytoplasm or at vesicles. We found that Acly is largely enriched at vesicles while conversely Acss2 is mostly located in the cytoplasm. Consistently with this, in an *in vitro* assay, Acly activity was higher in the vesicular fraction compared to the cytoplasmic fraction. Mass spectrometry analysis revealed that acetyl-CoA levels are lower in the Elp3 cKO brain lysates as compared to WT. We found that Acly mRNA levels are not changed in ELP3 cKO mice and neither are translation dynamics, assessed by puromycin-ligation assay (PLA). Instead, cycloheximide assay showed that the stability of Acly is reduced in Elp3 cKO as compared to controls, which correlated with an interaction of Elongator with Acly, demonstrated by immuno-precipitation. Together, these results suggest that Elongator modulates Acly levels by increasing its stability and therefore adjusts acetyl-CoA availability. Elongator may therefore control MT acetylation by providing acetyl-CoA to αTAT1 through the regulation of vesicular Acly expression.

Since we hypothesized that Acly is an Elongator target, we tested whether Acly downregulation could phenocopy the alterations induced by Elongator loss. Pharmacological inhibition of Acly in mouse neurons and RNAi-mediated knockdown in fly motor neurons

induced a reduction of MT acetylation correlated with decreased transport velocity and increased pausing time, which was rescued by HDAC6 inhibition in flies. These results were consistent with our observations in models in which Elongator was lost and we therefore tested whether Acly overexpression could rescue the defects in these models. Acly overexpression following Elongator loss rescued MT acetylation and transport defects in both mouse and flies and it also ameliorated the impaired locomotion in flies. Together, these results suggest that restoring acetyl-CoA levels through the upregulation of Acly rescues physiological levels of MT acetylation and subsequently improved transport and locomotion defects.

To assess whether these findings are relevant in the context of FD, a developmental disease caused by Elp1 mutation in humans, we tested whether our findings are recapitulated in human FD fibroblasts. We found that fibroblasts isolated from FD patients show lower levels of MT acetylation and impaired lysosomal transport compared to controls. Similarly to mouse and fly neurons, Acly overexpression rescued both MT acetylation levels and transport defects, suggesting that the regulation of acetyl-CoA levels by Elongator is conserved in human fibroblasts and may therefore be a pathophysiological mechanism in FD patients.

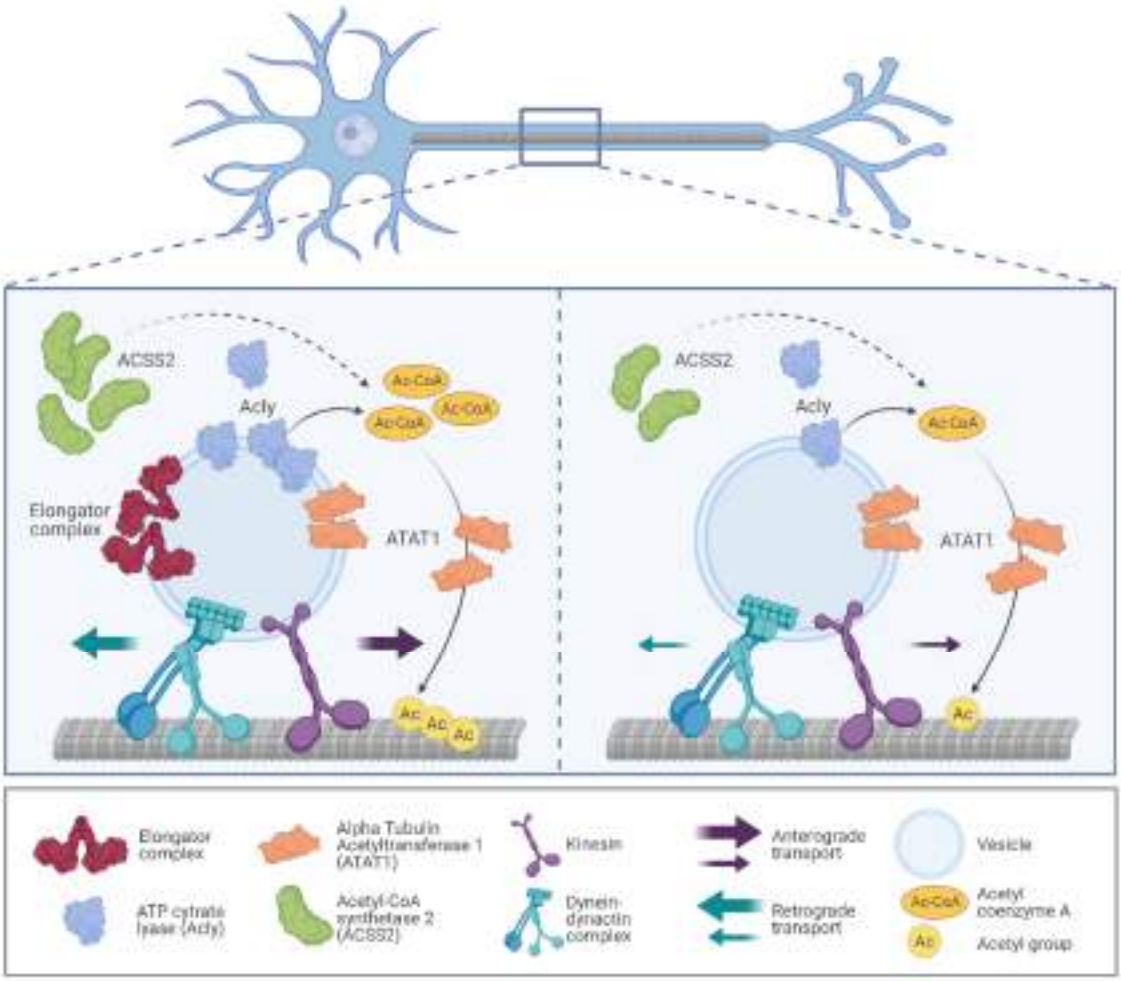

Figure 17: Proposed model for the regulation of MT acetylation and transport by Elongator.
We propose that loss of Elongator reduces the levels of Acly and Acss2 which are the two enzymes responsible for the production of cytosolic Acetyl-CoA. Acss2 is mostly localized in the cytoplasm while Acly is enriched at vesicles and therefore the latter may be a privileged source of acetyl-CoA to promote MT acetylation by the vesicular pool of αTAT1. Acetyl-CoA reduction following loss of Elongator therefore leads to reduced MT acetylation which correlates with a reduction of axonal transport velocity and increased pausing time. Figure from (Even *et al.*, 2021).

2. ATAT1-enriched vesicles promote MT acetylation via axonal transport

3. ATP-citrate lyase promotes axonal transport across species

4. Supplementary material and methods

The supplementary materials provided here concern the experiments I performed in flies for both manuscripts.

4.1 Immunohistochemistry of dissected larvae

The description of the immunohistochemistry procedure is adapted from my master thesis manuscript (https://hdl.handle.net/2268/235914).

4.1.1 3rd instar larvae dissection

3rd instar larvae were dissected and fixed for the immunostaining of motor neurons and NMJ. The dissection protocol is adapted from (Brent, Werner and McCabe, 2009; Devireddy *et al.*, 2014).

Materials:

Dissection microscope (Leica M80) with incident illumination
Vannas iris scissors (Aesculap OC498R)
Two pairs of forceps (Fine Science Tools - Dumostar #55)
Minutien insect pins (Fine Science Tools #26002-10)
Homemade Sylgard plate with small edges (Sylgard 184 Silicone Elastomer Kit from Dow Corning)
PBS buffer
PFA 4%
10% sucrose solubilized in distilled water

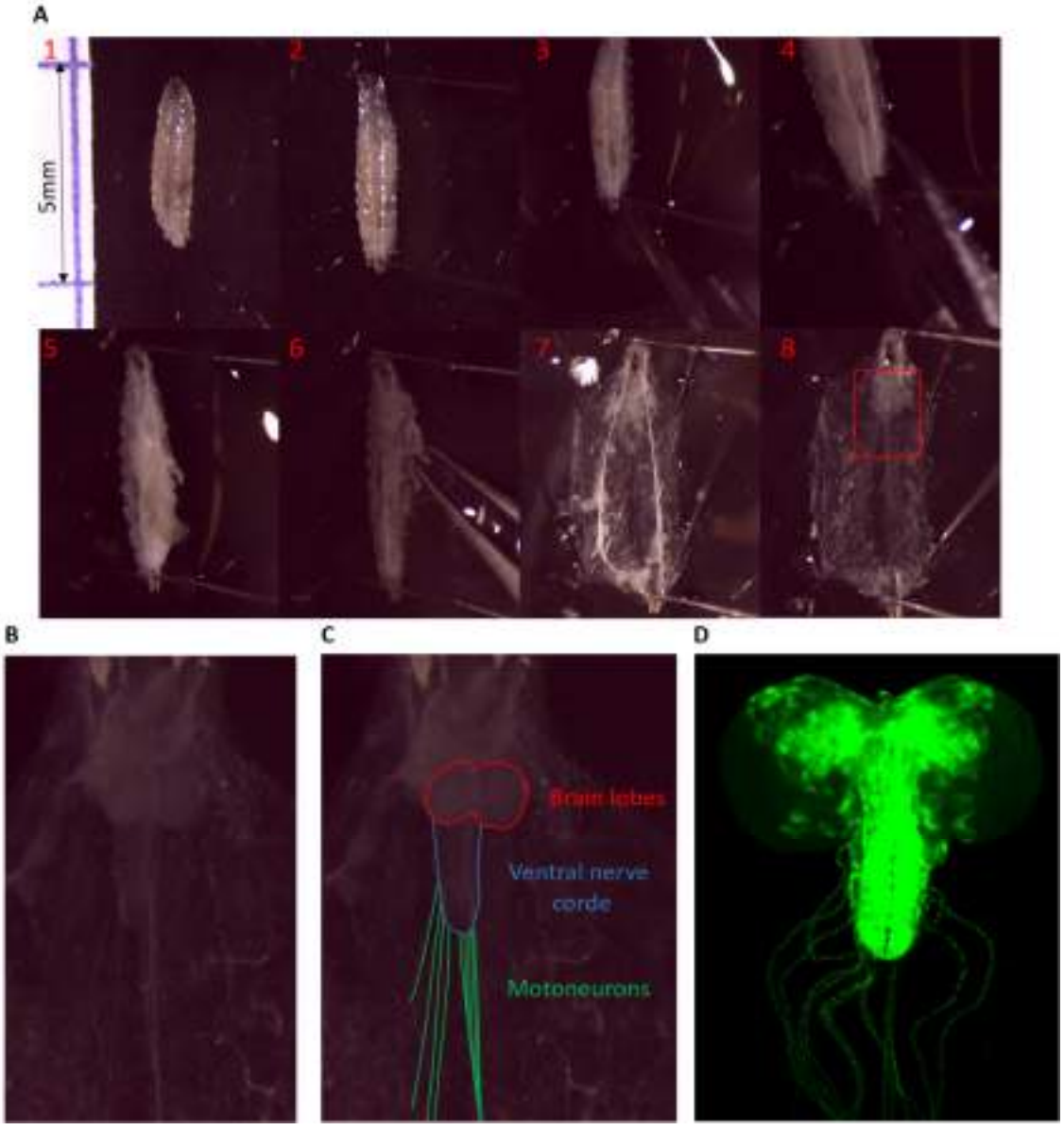

Figure 18: Critical steps of larval dissection and CNS representation

A. Critical steps of the larva dissection, in all frames the anterior part is up. In order, the larva is placed on the dissection plate **(1)**, it is then pinned at its anterior and posterior extremity **(2)**. PBS is added and a hole is pierced adjacent to the posterior pin **(3)** and a longitudinal cut from the posterior to the anterior end is performed **(4)**. The organs are floating in PBS **(5),** making it easier to remove those using fine forceps **(6).** When most organs have been removed, 4 pins are inserted to flatten the body walls **(7)** and the remaining organs are removed **(8).**

B. Magnification of the frame drawn in **(A8)**.

C. Annotated version of **(B)** highlighting the brain lobes, ventral nerve cord and motoneurons.

D. Confocal image of a 3rd instar larva D42 > *mito*GFP brain at 20x after dissection.

1mL of the sucrose solution at room temperature was added in each well of a 12-wells plate and 3rd instar larvae were segregated in the wells according to their genotype. Larvae were usually kept for a maximum of one hour in this solution before a new batch was collected. Once in the sucrose solution, the GFP expression was checked with a binocular epifluorescent microscope. The larvae exhibiting no GFP in the nervous system and salivary glands were excluded.

The description of the procedure is illustrated with 8 key frames in (**Figure 18 A**) which are referred to only by their number in the following text. A larva was transferred from a well to the Sylgard plate with the ventral part of the body facing downwards to make the pharyngeal tubes apparent **(1).** An insect pin was then inserted through the posterior part of the body between the pharynges. A second pin was inserted in the anterior part between the mouth hooks to slightly stretch the larva and hold it in place **(2)**. 100µL of PBS was added to submerge the larva to make internal organs float which facilitated their removal **(5)**. Using a larger pin, a small hole was created by gently pulling on the skin that was pierced at the posterior end **(3)**. A longitudinal cut along the midline was then performed starting from the posterior end to the anterior end **(4)**. This step is critical as the integrity of the nervous system must be preserved. To avoid damaging motoneurons or the brain, the cut must be made just underneath the larval body wall. Organs (fat, salivary glands, intestine, pharyngeal tubes) were grossly removed with fine forceps **(6)** while avoiding strong pulling forces on the segmental nerves. 4 pins were then placed on the 4 extremities of the body wall to flatten the larva and stretch it in a horizontal and vertical manner **(7).** The remaining organs were then carefully removed to leave only the CNS and peripheral nerves **(8)**. Higher magnifications of the brain revealed by the dissection are shown in (**Figure 18 B-D**). The PBS was removed using a micropipette and 100µL of PFA 4% was added. After 20 minutes at room temperature, the PFA was removed and the larva was washed 3 times with PBS. The pins were then gently pulled while holding the body of the larva to prevent ripping. The dissected larvae can either be used for immunostaining directly or they can be stored at 4°C for a few weeks in a plastic container filled with PBS.

4.1.2 Immunohistochemistry

Immunochemistry experiments were performed in glass dishes with a spherical bottom. The antibodies used were tubulin 1:150 from sheep (Cytoskeleton ATNO2), acetylated-tubulin

1:5000 from mouse (Sigma, T6793), HRP 1:1000 from rabbit (Sigma) and CSP 1:10 from mouse, kindly gifted by S. Benzer. Secondary antibodies against the appropriate species were used with a 1:500 dilution.

Larvae were washed 3 times in PBS 0.3% Triton X-100 for 5 minutes and incubated for 30 minutes in the blocking solution of PBS 0.3% Triton X-100 and 1% bovine serum albumin (BSA). Larvae were incubated at 4° over-night in the primary antibodies diluted in the blocking solution. To prevent evaporation of the solution, the dish was covered with parafilm. Larvae were then washed 3 times in PBS 0.3% Triton X-100 for 5 minutes and incubated for 2 hours at room temperature in the secondary antibodies diluted in the blocking solution. Larvae were washed 3 times in PBS 0.3% Triton X-100 for 5 minutes and immediately mounted on glass slides with the nervous system facing upwards. A maximum of 3 larvae were mounted per slide using 100µL of the mounting medium Mowiol. The slides were kept at room temperature for a few hours for the Mowiol to dry and then stored at 4°C until imaging.

This protocol was used for tubulin/acetylated tubulin stainings. The protocol for CSP/HRP staining is identical but PBS 0.2% Triton X-100 was used at each step.

Larvae were imaged using a Nikon A1Ti inverted confocal microscope. For quantitative analysis, laser power, gain and offset were optimized to avoid surexposition while maintaining adequate sensitivity. The optimized settings were used throughout experiments to ensure samples were comparable. Imaging of tubulin/acetylated tubulin stainings was performed using the 60x oil-immersed objective while the 40x oil-immersed was used for CSP/HRP.

4.2 Live-imaging of transport in larvae

I wrote a methods article together with Silvia Turchetto which thoroughly explains the procedure for the live-imagine of transport in larvae as well as the analysis of transport parameters. This article is attached in annex and can be used as a reference for the method of live-imaging in 3rd instar larvae (Turchetto *et al.*, 2022).

4.3 Drug administration

Tubastatin A 1mM (Sigma Aldrich, SML0044) or Ciliobrevin D 800µM (EMD Millipore 250401) or an equivalent amount of dimethyl sulfoxide (DMSO) were diluted in a 10% sucrose solution. The solution was distributed in a 24 well plate with 500µL per well and a single larva was placed in each well. Larvae were fed the solution for 30min and were then dried properly and

dissected immediately for immunohistochemistry or anesthetized for time-lapse imaging of transport.

5. Discussion

Our understanding of the regulation of MT acetylation keeps growing, fueled by the discovery of αTAT1, HDAC6 and SIRT2 enzyme functions. The link between MT acetylation and neuronal transport has also emerged in multiple studies (Reed *et al.*, 2006; Jim P Dompierre *et al.*, 2007; d'Ydewalle *et al.*, 2011; Godena *et al.*, 2014; Guo *et al.*, 2017; Morelli *et al.*, 2018). However, some questions remain unanswered due to the atypical nature of MT acetylation which occurs within the lumen. In the two studies presented in this chapter, we provide further evidence of the link between MT acetylation and neuronal transport. We also shed light on some mechanisms that act upstream of αTAT1 to regulate acetylation. Finally, we provide evidence that the vesicular localization of key acetylation regulators may endow vesicles with the ability to regulate MT acetylation. This would imply that the relationship between MT acetylation and neuronal transport is bidirectional, with cargoes and MT acetylation able to influence each other. Here we discuss and contextualize our findings and reflect on outstanding questions in the field of MT acetylation and transport.

5.1 Is there a causal link between MT acetylation and neuronal transport ?

Early studies that established a link between MT acetylation and neuronal transport rely on **1)** studying transport in pathological models that correlate with low MT acetylation and **2)** evaluating the impact of HDAC6 inhibition on transport dynamics (Jim P Dompierre *et al.*, 2007; d'Ydewalle *et al.*, 2011; Godena *et al.*, 2014; Guo *et al.*, 2017). Although these studies are informative, the observations come from pathological models whose etiology is probably complex. In each of these studies MT acetylation is reduced and axonal transport defects arise but some other pathological mechanisms may contribute to axonal transport defects, such as protein aggregation, which can arise in some disease models and affect axonal transport independently of MT acetylation (Lee, Yoshihara and Littleton, 2004). In those studies, HDAC6 inhibition was carried out pharmacologically or genetically using trichostatin A (TSA), a general HDAC inhibitor, tubastatin A (TBA), a selective HDAC6 inhibitor or RNAi mediated KD of HDAC6 (Shukla and Tekwani, 2020). Since TSA inhibits multiple HDACs, it affects the

acetylation levels of a broad range of substrates including histones, and therefore its positive effect on axonal transport defect may also be in part mediated by increased acetylation of other proteins. TBA and HDAC6 KD partially overcome this issue by selectively inhibiting HDAC6 and therefore reducing the range of substrates, however, HDAC6 is not selective to α-tubulin and may also regulate transport through the deacetylation of other substrates (Hai and Christianson, 2016; Varga *et al.*, 2022). For instance, the MAP tau is a substrate of HDAC6 and its acetylation state can influence MT dynamics (Sohn *et al.*, 2016).

The discovery that αTAT1 is the main α-tubulin acetyltransferase, if not the only one, provided researchers with a new approach to manipulate MT acetylation (Shida *et al.*, 2010; Kalebic, Sorrentino, *et al.*, 2013). Some studies suggest that αTAT1 is specific to αK40 and does not acetylate other substrates (Shida *et al.*, 2010; Friedmann *et al.*, 2012), which provides a unique opportunity to assess the specific effect of αK40 acetylation on transport. Surprisingly, loss of αTAT1 has yielded controversial results. In *C. elegans*, αTAT1 loss disrupted axonal transport but this effect was independent of its catalytic activity. Indeed, the axonal degeneration induced by loss of αTAT1 could be rescued by the expression of a transgene lacking the catalytic site (Neumann and Hilliard, 2014). However, in *C. elegans*, αTAT2 seems to be responsible for the major part of αK40 acetylation (Shida *et al.*, 2010). It is therefore possible that non-canonical functions of αTAT1 regulate transport in *C. elegans*, but it does not exclude a contribution of αK40 acetylation. Additionally, loss of αTAT1 in primary cultures of mouse dorsal root ganglion or hippocampal neurons did not result in transport deficits (Morley *et al.*, 2016; Wei *et al.*, 2018). Our findings suggest that αTAT1 loss in mouse cortical neurons or αTAT1 and αTAT2 loss in fly motor neurons both result in robust axonal transport alterations. Substitution of αK40 by a glycine residue has been shown to mimic acetylation due to the similarity in the structure of glycine compared to acetylated lysine (Li *et al.*, 2002). Consistent with this, we found that K40Q substitution on α-tubulin rescues transport defects following loss of acetylation in αTAT1 KO mice. This suggests that in mouse cortical neurons, αK40 acetylation is a regulator of cargo motility. Interestingly, we also found that in mouse cortical neurons and fly motor neurons, MT acetylation seems to regulate the trafficking of multiple cargoes (Morelli *et al.*, 2018; Even *et al.*, 2019). These contradictory findings may reflect a cell-type specific regulation of cargo motility through MT acetylation whereby some cell-types rely more on MT acetylation than others for the regulation of axonal transport.

5.2 How does MT acetylation affect cargo transport ?

It remains unclear how MT acetylation modulates cargo transport. It may do so by: **1)** regulating the binding of motor/adaptor proteins to MT tracks; **2)** changing the structure and dynamics of the MT lattice; **3)** promoting MT bundling.

One way through which acetylation may affect motor transport is through MT bundling, a process that consists in the aggregation of MT arrays through crosslinking (Walczak and Shaw, 2010). Kinesin-1 motility is improved on bundled MTs (Conway *et al.*, 2014). Interestingly, MT networks isolated from cells are partially bundled and αK40 acetylation strongly co-distributes with MT bundles (Balabanian, Berger and Hendricks, 2017). Although acetylation on single MTs does not affect kinesin-1 binding and run length, those parameters are significantly increased upon MT bundling (Balabanian, Berger and Hendricks, 2017). The increased run length may be due to the ability of kinesin-1 to quickly switch MT tracks when the network is bundled, however these findings are correlative. It would be interesting to test whether acetylation can promote bundling of MTs to regulate kinesin-1 transport as it would help explain the discrepancy between *in vitro* reconstitution and cellular assays. In addition, although these findings may explain the higher run length that we observed in our experiments, additional mechanisms may take place to regulate the increased cargo velocity that we have observed on acetylated MTs.

The binding affinity of molecular motors is in part dependent on their interaction with the C-terminal tail of tubulins which are prone to modification by various PTMs. Since αK40 acetylation occurs inside the MT lumen, it cannot interact directly with molecular motors. Interestingly however, in cells, kinesin-1 binding is improved on acetylated MTs (Reed *et al.*, 2006; J. P. Dompierre *et al.*, 2007) and consistent with this, kinesin-1 preferentially moves along acetylated MTs (Cai *et al.*, 2009; Katrukha *et al.*, 2017). *In vitro* reconstitution assays with purified MTs did not find changes in the binding or processivity of kinesin-1 motors to MTs (Walter *et al.*, 2012; Kaul, Soppina and Verhey, 2014). This indicates that MT acetylation alone is not sufficient to induce changes in motor binding, and consistent with this, MT acetylation does not seem to significantly affect the MT structure apart from loosening the interactions between protofilaments (Howes *et al.*, 2014; Xu *et al.*, 2017). However, these studies are performed with *in vitro* reconstitution assays that aim to compare acetylated and

non-acetylated MTs in a controlled setting and therefore may not account for the full complexity of an *in vivo* system. Although acetylation may not affect motors directly, it could help to recruit proteins or alter MT structure and dynamics in a cellular environment, which may subsequently alter motor binding and processivity. If true, it would reconcile contradictory findings in cells and reconstitution assays.

In cells, MTs have luminal particles that have yet to be identified but likely are microtubule inner proteins (MIPs) (Garvalov *et al.*, 2006; Bouchet-Marquis *et al.*, 2007) since they have a size similar to large globular proteins (Erickson, 2009). In the axoneme of *Chlamydomonas reinhardtii*, researchers have managed to elucidate the identity and distribution of 33 MIPs. This important study reveals that a complex regulation of the intraluminal make-up of MTs may regulate its functions since MIPs can alter the interaction between the lateral contacts of protofilaments (Ichikawa *et al.*, 2017). Intriguingly, some MIPs even partially protrude outside of the MT lattice by extending through openings in the lattice, therefore opening the possibility of protein interactions across the lattice (Ichikawa *et al.*, 2017; Ma *et al.*, 2019).

The characterization of MIPs in neurons is still underway and it remains unclear whether they play a critical role in the regulation of MT function. In *C. elegans*, loss of MT acetylation in neurons results in the disappearance of intraluminal particles, suggesting a potential role of αK40 acetylation for the recruitment of MIPs (Topalidou *et al.*, 2012) Interestingly, knockout of MAP6 in mouse neurons results in a strong reduction of MIPs. Intraluminal MAP6 appears to induce coiling of the MT lattice into an helix which subsequently creates openings in the lattice (Cuveillier *et al.*, 2020). MAP6 KO mice suffer from schizophrenia which is correlated to axonal transport defects. Treatment with MT-stabilizing molecule can rescue axonal transport defects and alleviate the symptoms in mice (Daoust *et al.*, 2014). Together, these results suggest that αK40 acetylation may help the recruitment of MIPs which subsequently alter the conformation of the MT lattice. It is still unclear whether additional MIPs are present in neuronal MTs and whether they affect transport. Additional studies are required to shed light on the nature and function of MIPs and whether they can modify the interaction of extra-luminal MAPs. Elucidating the nature and function of these intraluminal particles may shed light on the regulation of motor binding by MT acetylation (**Figure 19**).

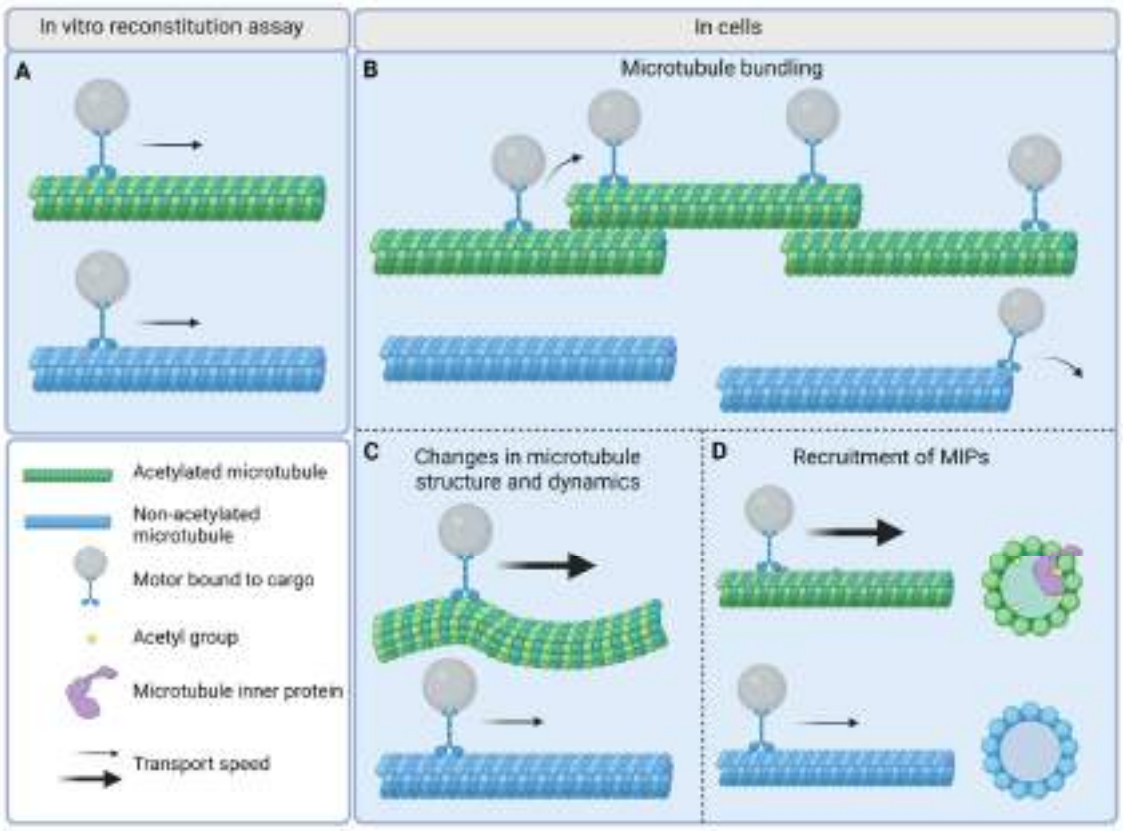

Figure 19: Potential mechanisms through which MT acetylation regulates transport

A. Using *in vitro* reconstitution assays, the motility of motors appears to be the same on acetylated MTs (green) and unacetylated MTs (blue).

B-D. In cells, changes in the motility of motors and their cargos have been highlighted, which may be due to the higher complexity of the MT network and its interactors.

B. Acetylated MTs tend to bundle and motors are preferentially recruited to bundled MTs where they have a longer run length. This may be due to an easy switch between bundled tracks whereas motors would fall off single MTs more frequently thereby inducing pausing time.

C. Acetylation increases the flexibility of MTs by weakening protofilament interactions which may change the way motors interact with the MT lattice.

D. MT acetylation may recruit proteins to the lumen which may further alter the structure and dynamics of the lattice. Additionally, some MIPs protrude to the cytoplasm and may therefore interact with motors or other proteins.

5.3 How can proteins enter the MT lumen ?

The combined observation that the αK40 of α-tubulin is positioned within the MT lumen and that αTAT1 mainly acetylates polymerized MTs begs the question of how the enzyme can enter inside the MT lumen to reach its lysine substrate. The two main hypothesis which are not mutually exclusive are that αTAT1 enters through the open ends of MTs and/or through openings in the MT lattice (Coombes *et al.*, 2016; Ly *et al.*, 2016). Recent evidence supports

entry through MT extremities and defects in the lattice simultaneously and it is likely that both these mechanisms coexist in cells (Nihongaki, Matsubayashi and Inoue, 2021).

In support of the hypothesis that acetylation starts through MT extremities, it was found that αTAT1 accumulates at MT ends and that acetylation accumulates preferentially at MT ends *ex vivo* (Coombes *et al.*, 2016; Ly *et al.*, 2016) (**Figure 20 A**). Entry through transient lattice openings is also supported by several studies. Acetylation itself can affect the structure of the lattice by weakening the lateral bonds between protofilaments and increasing MT flexibility, which opens gaps between protofilaments and therefore could enable αTAT1 entry (Portran *et al.*, 2017; Xu *et al.*, 2017) (**Figure 20 B**). MTs can also exhibit breaks within their lattice through which proteins may enter (Jiang *et al.*, 2017). Accumulation of these breaks can lead to MT crushing but tubulin dimers can be included within the lattice to repair damage and stabilize MTs (Schaedel *et al.*, 2015; Jiang *et al.*, 2017; Triclin *et al.*, 2021). Interestingly, removal of some tubulin dimers can be caused by molecular motors exerting forces on the C-terminal tails of tubulins as they travel along MTs (Triclin *et al.*, 2021; Andreu-Carbó *et al.*, 2022; Budaitis *et al.*, 2022; Kuo *et al.*, 2022). αTAT1 is well positioned to enter through breaks induced by motors since there is evidence of αTAT1 bound to the exterior of MTs (Howes *et al.*, 2014; Ly *et al.*, 2016). In addition, we found that αTAT1 is enriched on the cytoplasmic side of vesicles, which may help deliver it to MT openings. This suggests that openings are created as vesicles travel along MTs and αTAT1, primely positioned at the surface of the cargoes could then enter the lumen to regulate acetylation (**Figure 20 C**).

Since HDAC6 also deacetylates polymerized MTs (Hubbert *et al.*, 2002), the deacetylating enzymes also needs to enter the MT lumen. Similar to αTAT1, HDAC6 may enter from MT ends or breaks in the lattice. Deacetylation seems to occur homogenously along MT tracks, suggesting that entry through breaks is likely (Miyake *et al.*, 2016).

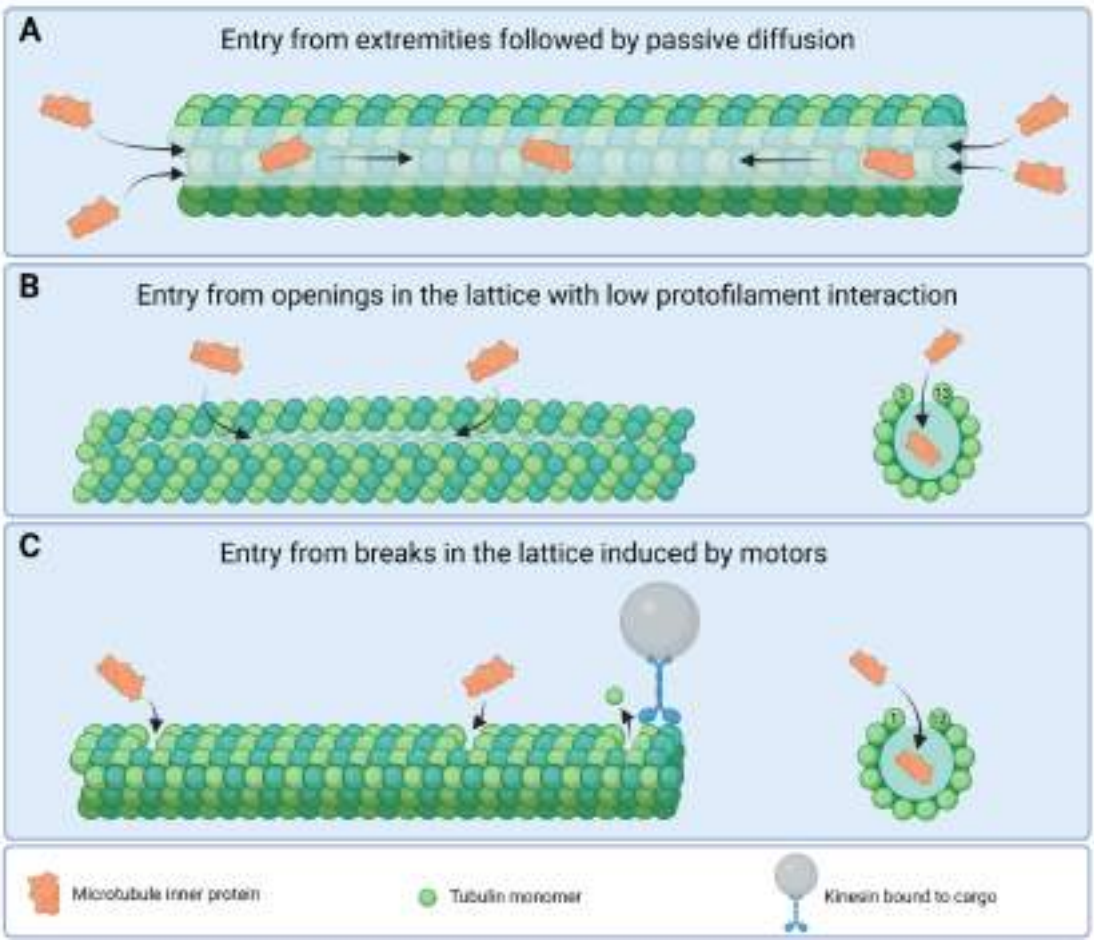

Figure 20: Potential mechanisms of entry in the MT lumen

A. MT inner proteins (MIPs) may enter the lumen through the extremities of MTs and then passively diffuse inside the lattice

B. MIPs may enter through openings in the lattice created by a low interaction between protofilaments. MT acetylation has been shown to weaken protofilament interaction and the MIP MAP6 also generates openings by inducing coiling of the MT lattice.

C. MIPs may enter the lumen through breaks in the lattice which create openings along MTs. It was recently shown that breaks in the lattice can be induced from the forces exerted by molecular motors.

5.4 Can vesicles autonomously modulate their transport ?

In the two studies presented here, we found that αTAT1 and Acly are enriched in vesicles. This suggests that the machinery to acetylate MTs travels together with vesicles, which may increase the efficiency of acetylation by delivering these enzymes where they are required. Indeed, we found that inhibiting vesicular transport with Ciliobrevin D or shRNA targeting Lis1 resulted in a significant reduction of MT acetylation. This suggests a bidirectional interplay between MT acetylation and axonal transport whereby the efficiency of cargo motility is

increased by acetylation and cargoes also increase MT acetylation. In favor of this hypothesis, a recent preprint shows that mitochondria promote MT acetylation by recruiting αTAT1 at sites of mitochondrial contacts through mitofusin-2 (MFN2), a mitochondrial fusion protein that resides in the outer mitochondrial membrane (Atul *et al.*, 2023). MFN2 KO cells show reduced acetylation and motility defects which are rescued by HDAC6 inhibitors. Interestingly, two common mutations of MFN2 in CMT show higher binding affinity with αTAT1 and expression of those mutant forms in MFN2 KO cells fails to rescue acetylation levels, suggesting that deficient acetylation contributes to the pathogenesis. In support of this, MFN2 KO leads to a dying-back phenotype in DRG neurons which is rescued by HDAC6 inhibition. Together, these results suggest that MFN2 helps deliver αTAT1 to MTs to promote acetylation and MFN2 mutations can lead to degeneration of DRG neurons by disrupting acetylation (Atul *et al.*, 2023). In our analysis of vesicular proteins, we did not find an enrichment of HDAC6 in vesicles, which may be explained by the fact that deacetylases activity targets both soluble tubulin dimers and MTs, therefore delivery of deacetylating enzymes to MTs by cargoes may be less crucial than delivery of αTAT1 (Hubbert *et al.*, 2002; Skultetyova *et al.*, 2017).

ATP is the energy source that powers the movement of kinesins and dynein along MTs (Hackney, 1994; Mallik *et al.*, 2004; Ross *et al.*, 2006). Interestingly, vesicles may at least partially produce their own energy while moving since motile glycolytic enzymes are enriched in vesicles and produce ATP (M. V. Hinckelmann *et al.*, 2016) . In an *in vitro* reconstitution assay, addition of ATP is required to promote vesicular motion. However, the substrates of pyruvate kinase, the last enzyme in the glycolysis reaction which produces ATP from phosphoenolpyruvate and adenosine diphosphate, are enough to promote vesicular transport (M.-V. Hinckelmann *et al.*, 2016). In addition, silencing of glyceraldehyde-3-phosphate dehydrogenase (GAPDH) reduces axonal transport velocity of vesicles but not mitochondria in neurons (Zala, Hinckelmann and Saudou, 2013). These results suggest that vesicles can produce their own ATP through glycolytic enzymes to fuel their own transport. Together with our observations, these studies suggests that vesicles have an on-board enzymatic machinery that: **1)** fuels their energy requirements; **2)** modulates their own transport by changing levels of MT acetylation.

5.5 Evolutionary conservation of MT acetylation regulation

The enzymes that acetylate and deacetylate α-tubulin are broadly conserved across species. In the mouse, αTAT1 is responsible for the acetylation of αK40 acetyltransferase in mammals (Kalebic, Sorrentino, *et al.*, 2013). In invertebrates, the paralogs αTAT1 and αTAT2 acetylate αK40 together as it was demonstrated in *C. elegans* and in our work in Drosophila *melanogaster* (Shida *et al.*, 2010). Interestingly, sensory neurons are particularly sensitive to the loss of MT αK40 acetylation which results in defects in touch sensation in *C.* elegans, Drosophila and mouse, highlighting the conserved regulation of touch sensation by αK40 acetylation (Shida *et al.*, 2010; Morley *et al.*, 2016; Yan *et al.*, 2018).

The αK40 deacetylation mediated by HDAC6 was first discovered in a cell-line of mouse fibroblasts (Hubbert *et al.*, 2002). The other αK40 deacetylating enzyme, SIRT2, was discovered in human immortal cell lines (North *et al.*, 2003). Since these original discoveries, orthologs have been described across species and their expression has been manipulated to modulate MT acetylation. HDAC6 appears to be the main αK40 deacetylase in invertebrates and mammals. In *Drosophila* melanogaster, αK40 acetylation is elevated by the knockdown of HDAC6 but not any of the two SIRT2 orthologs, Sirt1 and Sirt2 (Yan *et al.*, 2018). Similarly in mice, SIRT2 KO does not affect the levels of αK40 acetylation in the brain (Bobrowska *et al.*, 2012). However, the function of HDAC6 seems largely conserved in invertebrates and mammals. HDAC6 inhibition consistently results in an increase of MT acetylation and transport velocity in *Drosophila melanogaster*, mouse and hIPSC-derived neurons (Jim P Dompierre *et al.*, 2007; d'Ydewalle *et al.*, 2011; Godena *et al.*, 2014; Guo *et al.*, 2017).

Similarly, the upstream regulators of acetylation appear to be largely conserved. Loss of Elongator results in decreased MT acetylation and transport defects in *C. Elegans*, *Drosophila*, mouse and human fibroblasts derived from FD patients (Creppe *et al.*, 2009; Solinger *et al.*, 2010). We found that these alterations are likely to result from the decreased expression of Acly following loss of Elongator, thereby diminishing the supply of acetyl-CoA to promote αK40 acetylation. This regulatory mechanism is conserved in the fly, mouse and human fibroblasts. Similarly, we previously demonstrated that in mice, $p27^{kip1}$ loss results in decreased αK40 acetylation and transport defects and loss of its ortholog dacapo in *Drosophila* larvae led to the same alterations. Interestingly, the phenotype induced by $p27^{kip1}$

KO in mouse neurons could be rescued by the expression of the fly ortholog dacapo, highlighting the remarkable evolutionary conservation of this protein from invertebrates to vertebrates (G. Morelli *et al.*, 2018). Together these studies suggest that the machinery regulating αK40 acetylation is remarkably conserved and contributes to the modulation of cargo transport across species.

5.6 Implications for neurological diseases

We show that loss of acetylation mediated by αTAT1 KO in mice results in transport defects but surprisingly, these alterations seem to result in only mild phenotypes. αTAT1 KO has been linked to impaired migration of cortical neurons, mild hippocampal malformation and increased cortico-cortical projections (Li *et al.*, 2012; Kim *et al.*, 2013; Wei *et al.*, 2018) but no severe behavioral defects have been found in αTAT1 KO mice apart from reduced mechanosensation and mild anxiety (Kalebic, Sorrentino, *et al.*, 2013; Morley *et al.*, 2016; Wei *et al.*, 2018). This suggests that αK40 acetylation is not crucial for brain development. However, acetylation may help to provide resilience to injury. Axonal degeneration can occur after brain hemorrhage and is associated with persistent functional disabilities in patients (Tao *et al.*, 2017; Jiang *et al.*, 2019). αK40 acetylation is significantly reduced as a result of brain hemorrhage and interestingly, increasing acetylation by HDAC6 inhibition rescues mitochondria transport defects and protects from axonal degeneration (Yang *et al.*, 2018, 2022).

In addition, αK40 may play a critical role in disorders acquired through aging and potentialize neurodegeneration. In a mouse model of Charcot-Marie-Tooth disease, αK40 acetylation was reduced and correlated with axonal transport defects. HDAC6 inhibition restored MT acetylation levels and corrected the transport defects which subsequently prevented axonal loss (d'Ydewalle *et al.*, 2011). Similar findings emerged from a study on neurons derived from hIPSC of patients with the disease (Kim *et al.*, 2016). Amyotrophic lateral sclerosis is a lethal disease that affects motor function after the loss of upper and lower motor neurons (Hardiman *et al.*, 2017). In this disease, αK40 acetylation levels are also reduced and associated with transport defects which are both rescued by HDAC6 inhibition in mouse and neurons derived from patients (Taes *et al.*, 2013; Guo *et al.*, 2017). This intervention delays disease progression in mouse (Taes *et al.*, 2013). Patients suffering from Huntington's disease

(HD) show lower levels of αK40 acetylation in the brain and consistently, HDAC6 inhibition restores acetylation levels and corrects transport defects in a disease mouse model (Jim P Dompierre *et al.*, 2007). However, in another mouse model of HD, acetylation levels are normal and HDAC6 inhibition does not affect disease progression (Bobrowska *et al.*, 2011). This finding suggests that HDAC6 inhibition may be beneficial only in specific disease contexts where αK40 acetylation is reduced.

HDAC6 inhibitors have shown promise in preclinical studies to delay disease progression in several neurodegenerative disorders (Simões-Pires *et al.*, 2013; Lopresti, 2021). Therefore, HDAC6 is being considered as a therapeutic target and clinical trials are beginning to emerge. A selective HDAC6 inhibitor, ricolinostat, has been proven safe in cancer patients and is currently undergoing phase II clinical trial for the treatment of neuropathy in diabetic patients (Clinicaltrials.gov identifier: NCT03176472). It is still unclear how HDAC6 inhibition can delay disease progression and it may be due to its effect on MT acetylation but also to increased acetylation of its other substrates (Hai and Christianson, 2016; Varga *et al.*, 2022). Interestingly, only one of the two catalytic domains of HDAC6 catalyzes the deacetylation of αK40, which may enable the development of pharmacological inhibitors that specifically target the inhibition of αK40 deacetylation (Miyake *et al.*, 2016). The development of more selective HDAC6 inhibitors would provide researchers with a tool to dissect the molecular functions of HDAC6 and may shed light on the therapeutic value of HDAC6 inhibition in neurological disorders.

5.7 Perspectives

Our results suggest that a vesicular pool of αTAT1 promotes MT acetylation and vesicular Acly provides the acetyl-CoA to catalyze the reaction. It was recently discovered that motors running along MT tracks induce damage to the lattice which may enable the entry of proteins in the lumen (Triclin *et al.*, 2021; Andreu-Carbó *et al.*, 2022; Budaitis *et al.*, 2022; Kuo *et al.*, 2022). Additional studies are needed to uncover whether acetylating/deacetylating enzymes can enter through breaks induced by motor movement. Such a mechanism may allow vesicles to locally regulate acetylation levels by delivering enzymes to the lumen along their path.

Although the link between MT acetylation and neuronal transport is robust, it is still unclear how MT αK40 acetylation can affect cargo motility. Studies have mostly focused on the kinesin-1 family of anterograde motors but we find that αK40 acetylation affects the motility of a broad range of cargoes in both the anterograde and retrograde direction (G. Morelli *et al.*, 2018). Synaptic vesicles and dense core vesicles, mainly transported by kinesin-3 and late endosomes and lysosomes transported by kinesin-2 are also affected in our experiments (Maday *et al.*, 2014b). Similarly, the retrograde transport of every cargo we analyzed was impaired, suggesting that dynein motility is also regulated by αK40 acetylation. Additional studies are therefore required to shed light on how MT acetylation can act as a general modulator of cargo transport.

It was recently discovered that three methyl groups can be added to αK40, therefore competing with αTAT1 for the modification of αK40 (Park, Chowdhury, *et al.*, 2016; Park, Powell, *et al.*, 2016). The function of αK40 trimethylation requires further research but a recent study found that this modification is enriched in the developing cortex and influences neuronal polarization and migration of cortical neurons (Xie *et al.*, 2021). It is hypothesized that methylated αK40 enhances MT polymerization and consistent with this, reducing αK40 methylation results in a reduction of MT ends (Xie *et al.*, 2021). Interestingly, cortical neuron migration is also impaired in αTAT1 KO mice and it can be partially rescued by increasing αK40 trimethylation (Li *et al.*, 2012; Xie *et al.*, 2021). This suggests that these two modifications may compensate for one another during development, possibly because acetylation improves MT stability while methylation improves MT polymerization (Portran *et al.*, 2017; Xu *et al.*, 2017; Xie *et al.*, 2021). However, loss of αTAT1 results in overbranching of cortico-cortical projections, possibly by affecting the MT +end dynamics and this effect is not compensated by increased αK40 methylation (Xie *et al.*, 2021). Further studies are needed to clarify the function and regulation of this newly discovered PTM and how it may interact with αK40 acetylation.

REFERENCES

Adalbert, R. and Coleman, M.P. (2013) 'Review: Axon pathology in age-related neurodegenerative disorders', *Neuropathology and Applied Neurobiology*, 39(2), pp. 90–108. Available at: https://doi.org/10.1111/j.1365-2990.2012.01308.x.

Ahmad, F.J. *et al.* (1999) 'An Essential Role for Katanin in Severing Microtubules in the Neuron', *Journal of Cell Biology*, 145(2), pp. 305–315. Available at: https://doi.org/10.1083/jcb.145.2.305.

Aiken, J. *et al.* (2017) 'The α-tubulin gene TUBA1A in brain development: A key ingredient in the neuronal isotype blend', *Journal of Developmental Biology*, 5(3). Available at: https://doi.org/10.3390/jdb5030008.

Aiken, J. *et al.* (2020) 'Tubulin mutations in brain development disorders: Why haploinsufficiency does not explain TUBA1A tubulinopathies', *Cytoskeleton*, 77(3–4), pp. 40–54. Available at: https://doi.org/10.1002/cm.21567.

Aiken, J., Moore, J.K. and Bates, E.A. (2019) 'TUBA1A mutations identified in lissencephaly patients dominantly disrupt neuronal migration and impair dynein activity', *Human Molecular Genetics*, 28(8), pp. 1227–1243. Available at: https://doi.org/10.1093/hmg/ddy416.

Aillaud, C. *et al.* (2017) 'Vasohibins/SVBP are tubulin carboxypeptidases (TCPs) that regulate neuron differentiation', *Science*, 358(6369), pp. 1448–1453. Available at: https://doi.org/10.1126/science.aao4165.

Akella, J.S. *et al.* (2010) 'MEC-17 is an α-tubulin acetyltransferase', *Nature*, 467(7312), pp. 218–222. Available at: https://doi.org/10.1038/nature09324.

Akhmanova, A. and Steinmetz, M.O. (2008) 'Tracking the ends: a dynamic protein network controls the fate of microtubule tips.', *Nature reviews. Molecular cell biology*, 9(4), pp. 309–322. Available at: https://doi.org/10.1038/nrm2369.

Akhmanova, A. and Steinmetz, M.O. (2015) 'Control of microtubule organization and dynamics: two ends in the limelight', *Nature Reviews Molecular Cell Biology*, 16(12), pp. 711–726. Available at: https://doi.org/10.1038/nrm4084.

Alata, M. *et al.* (2021) 'Longitudinal Evaluation of Cerebellar Signs of H-ABC Tubulinopathy in a Patient and in the taiep Model', *Frontiers in Neurology*, 12. Available at: https://doi.org/10.3389/fneur.2021.702039.

Alcantara, S., Ferrer, I. and Soriano, E. (1993) 'Postnatal development of parvalbumin and calbindin D28K immunoreactivities in the cerebral cortex of the rat', *Anatomy and Embryology*, 188(1). Available at: https://doi.org/10.1007/BF00191452.

Alves-Silva, J. *et al.* (2012) 'Spectraplakins Promote Microtubule-Mediated Axonal Growth by Functioning As Structural Microtubule-Associated Proteins and EB1-Dependent +TIPs (Tip Interacting Proteins)', *Journal of Neuroscience*, 32(27), pp. 9143–9158. Available at: https://doi.org/10.1523/JNEUROSCI.0416-12.2012.

Anderson, S.L. *et al.* (2001) 'Familial Dysautonomia Is Caused by Mutations of the IKAP Gene', *The American Journal of Human Genetics*, 68(3), pp. 753–758. Available at: https://doi.org/10.1086/318808.

Andreu-Carbó, M. *et al.* (2022) 'Motor usage imprints microtubule stability along the shaft', *Developmental Cell*, 57(1), pp. 5-18.e8. Available at: https://doi.org/10.1016/j.devcel.2021.11.019.

Arce, C.A. *et al.* (1975) 'Incorporation of l-Tyrosine, l-Phenylalanine and l-3,4-Dihydroxyphenylalanine as Single Units into Rat Brain Tubulin', *European Journal of Biochemistry*, 59(1), pp. 145–149. Available at:

https://doi.org/10.1111/j.1432-1033.1975.tb02435.x.
Arce, C.A. and Barra, H.S. (1985) 'Release of C -terminal tyrosine from tubulin and microtubules at steady state', *Biochemical Journal*, 226(1), pp. 311–317. Available at: https://doi.org/10.1042/bj2260311.
Atul, K. *et al.* (2023) 'MFN2-dependent recruitment of ATAT1 coordinates mitochondria motility with alpha-tubulin acetylation and is disrupted in CMT2A', *bioRxiv*, pp. 1–39.
Avalos, C.B., Brugmann, R. and Sprecher, S.G. (2019) 'Single cell transcriptome atlas of the drosophila larval brain', *eLife*, 8, pp. 1–25. Available at: https://doi.org/10.7554/eLife.50354.
Ayala, R., Shu, T. and Tsai, L.H. (2007) 'Trekking across the Brain: The Journey of Neuronal Migration', *Cell*, 128(1), pp. 29–43. Available at: https://doi.org/10.1016/j.cell.2006.12.021.
Baas, P.W. *et al.* (1988) 'Polarity orientation of microtubules in hippocampal neurons: uniformity in the axon and nonuniformity in the dendrite.', *Proceedings of the National Academy of Sciences*, 85(21), pp. 8335–8339. Available at: https://doi.org/10.1073/pnas.85.21.8335.
Bahi-buisson, N. *et al.* (2013) 'New insights into genotype–phenotype correlations for the doublecortin-related lissencephaly spectrum', *Brain* [Preprint]. Available at: https://doi.org/10.1093/brain/aws323.
Baker, A.-M. *et al.* (2017) 'Robust RNA-based in situ mutation detection delineates colorectal cancer subclonal evolution', *Nature Communications*, 8(1), p. 1998. Available at: https://doi.org/10.1038/s41467-017-02295-5.
Balabanian, L., Berger, C.L. and Hendricks, A.G. (2017) 'Acetylated Microtubules Are Preferentially Bundled Leading to Enhanced Kinesin-1 Motility', *Biophysical Journal*, 113(7), pp. 1551–1560. Available at: https://doi.org/10.1016/j.bpj.2017.08.009.
Baldassarre, G. *et al.* (2005) 'p27Kip1-stathmin interaction influences sarcoma cell migration and invasion', *Cancer Cell*, 7(1), pp. 51–63. Available at: https://doi.org/10.1016/j.ccr.2004.11.025.
Barisic, M. *et al.* (2015) 'Microtubule detyrosination guides chromosomes during mitosis', *Science*, 348(6236), pp. 799–803. Available at: https://doi.org/10.1126/science.aaa5175.
Bart, H. and Jean-Pierre, B. (1996) 'Reduction of Acetylated a-Tubulin Immunoreactivity in Neurofibrillary Tangle-bearing Neurons in Alzheimer's Disease', *Journal of neuropathology and experimental neurology*, 55(9), pp. 964–972. Available at: https://doi.org/https://doi.org/10.1097/00005072-199609000-00003.
Beaudoin, G.M.J. *et al.* (2012) 'Culturing pyramidal neurons from the early postnatal mouse hippocampus and cortex', *Nature Protocols*, 7(9), pp. 1741–1754. Available at: https://doi.org/10.1038/nprot.2012.099.
Bedoni, N. *et al.* (2016) 'Mutations in the polyglutamylase gene TTLL5 , expressed in photoreceptor cells and spermatozoa, are associated with cone-rod degeneration and reduced male fertility', *Human Molecular Genetics*, p. ddw282. Available at: https://doi.org/10.1093/hmg/ddw282.
Beltramo, D.M., Arce, C.A. and Barra, H.S. (1987) 'Tubulin, but not microtubules, is the substrate for tubulin:tyrosine ligase in mature avian erythrocytes.', *Journal of Biological Chemistry*, 262(32), pp. 15673–15677. Available at:

https://doi.org/10.1016/S0021-9258(18)47779-4.
Belvindrah, R. *et al.* (2017) 'Mutation of the α-tubulin Tuba1a leads to straighter microtubules and perturbs neuronal migration', *Journal of Cell Biology*, 216(8), pp. 2443–2461. Available at: https://doi.org/10.1083/jcb.201607074.
Bencivenga, D. *et al.* (2021) 'p27Kip1, an Intrinsically Unstructured Protein with Scaffold Properties', *Cells*, 10(9), p. 2254. Available at: https://doi.org/10.3390/cells10092254.
Bento-Abreu, A. *et al.* (2018) 'Elongator subunit 3 (ELP3) modifies ALS through tRNA modification', *Human Molecular Genetics*, 27(7), pp. 1276–1289. Available at: https://doi.org/10.1093/hmg/ddy043.
Berezniuk, I. *et al.* (2013) 'Cytosolic Carboxypeptidase 5 Removes α- and γ-Linked Glutamates from Tubulin', *Journal of Biological Chemistry*, 288(42), pp. 30445–30453. Available at: https://doi.org/10.1074/jbc.M113.497917.
Berni, J. *et al.* (2012) 'Autonomous circuitry for substrate exploration in freely moving drosophila larvae', *Current Biology*, 22(20), pp. 1861–1870. Available at: https://doi.org/10.1016/j.cub.2012.07.048.
Beuter, S. *et al.* (2016) 'Receptor tyrosine kinase EphA7 is required for interneuron connectivity at specific subcellular compartments of granule cells', *Scientific Reports*, 6(1), p. 29710. Available at: https://doi.org/10.1038/srep29710.
Bezaire, M.J. and Soltesz, I. (2013) 'Quantitative assessment of CA1 local circuits: Knowledge base for interneuron-pyramidal cell connectivity', *Hippocampus*, 23(9), pp. 751–785. Available at: https://doi.org/10.1002/hipo.22141.
Bienkiewicz, E.A., Adkins, J.N. and Lumb, K.J. (2002) 'Functional Consequences of Preorganized Helical Structure in the Intrinsically Disordered Cell-Cycle Inhibitor p27 Kip1', *Biochemistry*, 41(3), pp. 752–759. Available at: https://doi.org/10.1021/bi015763t.
Bilsland, L.G. *et al.* (2010) 'Deficits in axonal transport precede ALS symptoms in vivo', *Proceedings of the National Academy of Sciences*, 107(47), pp. 20523–20528. Available at: https://doi.org/10.1073/pnas.1006869107.
Bischofberger, J. *et al.* (2006) 'Patch-clamp recording from mossy fiber terminals in hippocampal slices', *Nature Protocols*, 1(4), pp. 2075–2081. Available at: https://doi.org/10.1038/nprot.2006.312.
Blumkin, L. *et al.* (2014) 'Expansion of the spectrum of TUBB4A-related disorders: a new phenotype associated with a novel mutation in the TUBB4A gene', *neurogenetics* [Preprint]. Available at: https://doi.org/10.1007/s10048-014-0392-2.
Bobrowska, A. *et al.* (2011) 'Hdac6 Knock-Out Increases Tubulin Acetylation but Does Not Modify Disease Progression in the R6/2 Mouse Model of Huntington's Disease', *PLoS ONE*. Edited by K.M. Iijima, 6(6), p. e20696. Available at: https://doi.org/10.1371/journal.pone.0020696.
Bobrowska, A. *et al.* (2012) 'SIRT2 ablation has no effect on tubulin acetylation in brain, cholesterol biosynthesis or the progression of Huntington's disease phenotypes in vivo.', *PloS one*, 7(4), p. e34805. Available at: https://doi.org/10.1371/journal.pone.0034805.
Bodakuntla, S. *et al.* (2019) 'Microtubule-Associated Proteins: Structuring the Cytoskeleton', *Trends in Cell Biology*, 29(10), pp. 804–819. Available at: https://doi.org/10.1016/j.tcb.2019.07.004.
Bodakuntla, S. *et al.* (2020) 'Tubulin polyglutamylation is a general traffic control mechanism

in hippocampal neurons', *Journal of Cell Science*, 133(3). Available at: https://doi.org/10.1242/jcs.241802.

Bodakuntla, S. *et al.* (2021) 'Distinct roles of α- and β-tubulin polyglutamylation in controlling axonal transport and in neurodegeneration', *The EMBO Journal*, 40(17). Available at: https://doi.org/10.15252/embj.2021108498.

Bodakuntla, S., Janke, C. and Magiera, M.M. (2021) 'Tubulin polyglutamylation, a regulator of microtubule functions, can cause neurodegeneration', *Neuroscience Letters*, 746(November 2020), p. 135656. Available at: https://doi.org/10.1016/j.neulet.2021.135656.

Bolus, H. *et al.* (2020) 'Modeling Neurodegenerative Disorders in Drosophila melanogaster', *International Journal of Molecular Sciences*, 21(9), p. 3055. Available at: https://doi.org/10.3390/ijms21093055.

Bond, A.M. *et al.* (2020) 'Differential timing and coordination of neurogenesis and astrogenesis in developing mouse hippocampal subregions', *Brain Sciences*, 10(12), pp. 1–14. Available at: https://doi.org/10.3390/brainsci10120909.

Bonner, J.M. and Boulianne, G.L. (2011) 'Drosophila as a model to study age-related neurodegenerative disorders: Alzheimer's disease', *Experimental Gerontology*, 46(5), pp. 335–339. Available at: https://doi.org/10.1016/j.exger.2010.08.004.

Bonnet, C. *et al.* (2001) 'Differential Binding Regulation of Microtubule-associated Proteins MAP1A, MAP1B, and MAP2 by Tubulin Polyglutamylation', *Journal of Biological Chemistry*, 276(16), pp. 12839–12848. Available at: https://doi.org/10.1074/jbc.M011380200.

Booker, S.A. and Vida, I. (2018) 'Morphological diversity and connectivity of hippocampal interneurons', *Cell and Tissue Research*, 373(3), pp. 619–641. Available at: https://doi.org/10.1007/s00441-018-2882-2.

Botcher, N.A. *et al.* (2014) 'Distribution of interneurons in the CA2 region of the rat hippocampus', *Frontiers in Neuroanatomy*, 8(SEP), pp. 1–16. Available at: https://doi.org/10.3389/fnana.2014.00104.

Boucher, D. *et al.* (1994) 'Polyglutamylation of Tubulin as a Progressive Regulator of in Vitro Interactions between the Microtubule-Associated Protein Tau and Tubulin', *Biochemistry*, 33(41), pp. 12471–12477. Available at: https://doi.org/10.1021/bi00207a014.

Bouchet-Marquis, C. *et al.* (2007) 'Visualization of cell microtubules in their native state', *Biology of the Cell*, 99(1), pp. 45–53. Available at: https://doi.org/10.1042/BC20060081.

Brady, S.T. and Morfini, G.A. (2017) 'Regulation of motor proteins, axonal transport deficits and adult-onset neurodegenerative diseases', *Neurobiology of Disease*, 105, pp. 273–282. Available at: https://doi.org/10.1016/j.nbd.2017.04.010.

Bre, M.H. *et al.* (1996) 'Axonemal tubulin polyglycylation probed with two monoclonal antibodies: widespread evolutionary distribution, appearance during spermatozoan maturation and possible function in motility', *Journal of Cell Science*, 109(4), pp. 727–738. Available at: https://doi.org/10.1242/jcs.109.4.727.

Brent, J., Werner, K. and McCabe, B.D. (2009) 'Drosophila larval NMJ immunohistochemistry.', *Journal of visualized experiments : JoVE*, pp. 4–5. Available at: https://doi.org/10.3791/1108.

Bubb, E.J., Kinnavane, L. and Aggleton, J.P. (2017) 'Hippocampal–diencephalic–cingulate

networks for memory and emotion: An anatomical guide', *Brain and Neuroscience Advances*, 1, p. 239821281772344. Available at: https://doi.org/10.1177/2398212817723443.

Budaitis, B.G. *et al.* (2022) 'A kinesin-1 variant reveals motor-induced microtubule damage in cells', *Current Biology*, 32(11), pp. 2416-2429.e6. Available at: https://doi.org/10.1016/j.cub.2022.04.020.

Bunda, A. and Andrade, A. (2022) 'BaseScope™ Approach to Visualize Alternative Splice Variants in Tissue', in, pp. 185–196. Available at: https://doi.org/10.1007/978-1-0716-2521-7_11.

Burgess, N., Maguire, E.A. and O'Keefe, J. (2002) 'The Human Hippocampus and Spatial and Episodic Memory', *Neuron*, 35(4), pp. 625–641. Available at: https://doi.org/10.1016/S0896-6273(02)00830-9.

Cai, D. *et al.* (2009) 'Single Molecule Imaging Reveals Differences in Microtubule Track Selection Between Kinesin Motors', *PLoS Biology*. Edited by M. Schliwa, 7(10), p. e1000216. Available at: https://doi.org/10.1371/journal.pbio.1000216.

Cai, L. *et al.* (2011) 'Acetyl-CoA Induces Cell Growth and Proliferation by Promoting the Acetylation of Histones at Growth Genes', *Molecular Cell*, 42(4), pp. 426–437. Available at: https://doi.org/10.1016/j.molcel.2011.05.004.

Carstens, K.E. *et al.* (2016) 'Perineuronal Nets Suppress Plasticity of Excitatory Synapses on CA2 Pyramidal Neurons', *The Journal of Neuroscience*, 36(23), pp. 6312–6320. Available at: https://doi.org/10.1523/JNEUROSCI.0245-16.2016.

Cason, S.E. and Holzbaur, E.L.F. (2022) 'Selective motor activation in organelle transport along axons', *Nature Reviews Molecular Cell Biology*, 23(11), pp. 699–714. Available at: https://doi.org/10.1038/s41580-022-00491-w.

Cembrowski, M.S. *et al.* (2016) 'Spatial Gene-Expression Gradients Underlie Prominent Heterogeneity of CA1 Pyramidal Neurons', *Neuron*, 89(2), pp. 351–368. Available at: https://doi.org/10.1016/j.neuron.2015.12.013.

Chakraborti, S. *et al.* (2016) 'The emerging role of the tubulin code: From the tubulin molecule to neuronal function and disease', *Cytoskeleton*, 73(10), pp. 521–550. Available at: https://doi.org/10.1002/cm.21290.

Chang, B.S. (2015) 'Tubulinopathies and their brain malformation syndromes: Every TUB on its own bottom', *Epilepsy Currents*, 15(2), pp. 65–67. Available at: https://doi.org/10.5698/1535-7597-15.2.65.

Chang, C.-W., Shao, E. and Mucke, L. (2021) 'Tau: Enabler of diverse brain disorders and target of rapidly evolving therapeutic strategies', *Science*, 371(6532). Available at: https://doi.org/10.1126/science.abb8255.

Chen, C. *et al.* (2011) 'Elongator Complex Influences Telomeric Gene Silencing and DNA Damage Response by Its Role in Wobble Uridine tRNA Modification', *PLoS Genetics*. Edited by H.D. Madhani, 7(9), p. e1002258. Available at: https://doi.org/10.1371/journal.pgen.1002258.

Chen, C., Tuck, S. and Byström, A.S. (2009) 'Defects in tRNA Modification Associated with Neurological and Developmental Dysfunctions in Caenorhabditis elegans Elongator Mutants', *PLoS Genetics*. Edited by S.E. Mango, 5(7), p. e1000561. Available at: https://doi.org/10.1371/journal.pgen.1000561.

Chen, J. *et al.* (1992) 'Projection domains of MAP2 and tau determine spacings between microtubules in dendrites and axons', *Nature*, 360(6405), pp. 674–677. Available at: https://doi.org/10.1038/360674a0.

Chen, J. and Roll-mecak, A. (2023) 'Glutamylation is a negative regulator of microtubule growth', *Molecular Biology of the Cell*, pp. 1–39.

Choudhary, C. *et al.* (2014) 'The growing landscape of lysine acetylation links metabolism and cell signalling', *Nature Reviews Molecular Cell Biology*, 15(8), pp. 536–550. Available at: https://doi.org/10.1038/nrm3841.

Chu, C.-W. *et al.* (2011) 'A novel acetylation of β-tubulin by San modulates microtubule polymerization via down-regulating tubulin incorporation', *Molecular Biology of the Cell*. Edited by E.L.F. Holzbaur, 22(4), pp. 448–456. Available at: https://doi.org/10.1091/mbc.e10-03-0203.

Conway, L. *et al.* (2014) 'Microtubule orientation and spacing within bundles is critical for long-range kinesin-1 motility', *Cytoskeleton*, 71(11), pp. 595–610. Available at: https://doi.org/10.1002/cm.21197.

Coombes, C. *et al.* (2016) 'Mechanism of microtubule lumen entry for the α-tubulin acetyltransferase enzyme αTAT1', *Proceedings of the National Academy of Sciences of the United States of America*, 113(46), pp. E7176–E7184. Available at: https://doi.org/10.1073/pnas.1605397113.

Corbet, C. and Feron, O. (2017) 'Cancer cell metabolism and mitochondria: Nutrient plasticity for TCA cycle fueling', *Biochimica et Biophysica Acta (BBA) - Reviews on Cancer*, 1868(1), pp. 7–15. Available at: https://doi.org/10.1016/j.bbcan.2017.01.002.

Corrales, M. *et al.* (2022) 'A single-cell transcriptomic atlas of complete insect nervous systems across multiple life stages', *Neural Development*, 17(1), pp. 1–23. Available at: https://doi.org/10.1186/s13064-022-00164-6.

Cosker, K.E. and Segal, R.A. (2014) 'Neuronal Signaling through Endocytosis', *Cold Spring Harbor Perspectives in Biology*, 6(2), pp. a020669–a020669. Available at: https://doi.org/10.1101/cshperspect.a020669.

Cowan, N.J. *et al.* (1988) 'Tubulin isotypes and their interaction with microtubule associated proteins', *Protoplasma*, 145(2–3), pp. 106–111. Available at: https://doi.org/10.1007/BF01349346.

Creppe, C. *et al.* (2009) 'Elongator Controls the Migration and Differentiation of Cortical Neurons through Acetylation of α-Tubulin', *Cell*, 136(3), pp. 551–564. Available at: https://doi.org/10.1016/j.cell.2008.11.043.

Cuajungco, M.P. *et al.* (2003) 'Tissue-Specific Reduction in Splicing Efficiency of IKBKAP Due to the Major Mutation Associated with Familial Dysautonomia', *The American Journal of Human Genetics*, 72(3), pp. 749–758. Available at: https://doi.org/10.1086/368263.

Cueva, J.G. *et al.* (2012) 'Posttranslational Acetylation of α-Tubulin Constrains Protofilament Number in Native Microtubules', *Current Biology*, 22(12), pp. 1066–1074. Available at: https://doi.org/10.1016/j.cub.2012.05.012.

Cui, Z., Gerfen, C.R. and Young, W.S. (2013) 'Hypothalamic and other connections with dorsal CA2 area of the mouse hippocampus', *Journal of Comparative Neurology*, 521(8), pp. 1844–1866. Available at: https://doi.org/10.1002/cne.23263.

Cuveillier, C. *et al.* (2020) 'MAP6 is an intraluminal protein that induces neuronal microtubules to coil', *Science Advances*, 6(14). Available at: https://doi.org/10.1126/sciadv.aaz4344.

d'Ydewalle, C. *et al.* (2011) 'HDAC6 inhibitors reverse axonal loss in a mouse model of mutant HSPB1–induced Charcot-Marie-Tooth disease', *Nature Medicine*, 17(8), pp. 968–974. Available at: https://doi.org/10.1038/nm.2396.

Dalwadi, U. and Yip, C.K. (2018) 'Structural insights into the function of Elongator', *Cellular and Molecular Life Sciences*, 75(9), pp. 1613–1622. Available at: https://doi.org/10.1007/s00018-018-2747-6.

Daoust, A. *et al.* (2014) 'Neuronal transport defects of the MAP6 KO mouse – a model of schizophrenia – and alleviation by Epothilone D treatment, as observed using MEMRI', *NeuroImage*, 96, pp. 133–142. Available at: https://doi.org/10.1016/j.neuroimage.2014.03.071.

Davie, K. *et al.* (2018) 'A Single-Cell Transcriptome Atlas of the Aging Drosophila Brain', *Cell*, 174(4), pp. 982-998.e20. Available at: https://doi.org/10.1016/j.cell.2018.05.057.

Denarier, E. *et al.* (2021) 'Modeling a disease-correlated tubulin mutation in budding yeast reveals insight into MAP-mediated dynein function', *Molecular Biology of the Cell*. Edited by T. Surrey, 32(20), p. ar10. Available at: https://doi.org/10.1091/mbc.E21-05-0237.

Deng, W., Aimone, J.B. and Gage, F.H. (2010) 'New neurons and new memories: How does adult hippocampal neurogenesis affect learning and memory?', *Nature Reviews Neuroscience*, 11(5), pp. 339–350. Available at: https://doi.org/10.1038/nrn2822.

Desai, A. and Mitchison, T.J. (1997) 'Microtubule polymerization dynamics', *Annual Review of Cell and Developmental Biology*, 13, pp. 83–117. Available at: https://doi.org/10.1146/annurev.cellbio.13.1.83.

Devireddy, S. *et al.* (2014) *Analysis of mitochondrial traffic in drosophila*. 1st edn, *Methods in Enzymology*. 1st edn. Elsevier Inc. Available at: https://doi.org/10.1016/B978-0-12-801415-8.00008-4.

van Dijk, J. *et al.* (2007) 'A Targeted Multienzyme Mechanism for Selective Microtubule Polyglutamylation', *Molecular Cell*, 26(3), pp. 437–448. Available at: https://doi.org/10.1016/j.molcel.2007.04.012.

van Dijk, J. *et al.* (2008) 'Polyglutamylation Is a Post-translational Modification with a Broad Range of Substrates', *Journal of Biological Chemistry*, 283(7), pp. 3915–3922. Available at: https://doi.org/10.1074/jbc.M705813200.

Dimitrov, A. *et al.* (2008) 'Detection of GTP-Tubulin Conformation in Vivo Reveals a Role for GTP Remnants in Microtubule Rescues', *Science*, 322(5906), pp. 1353–1356. Available at: https://doi.org/10.1126/science.1165401.

Dixit, R. *et al.* (2008) 'Differential Regulation of Dynein and Kinesin Motor Proteins by Tau', *Science*, 319(5866), pp. 1086–1089. Available at: https://doi.org/10.1126/science.1152993.

Dobie, F.A. and Craig, A.M. (2011) 'Inhibitory synapse dynamics: Coordinated presynaptic and postsynaptic mobility and the major contribution of recycled vesicles to new synapse formation', *Journal of Neuroscience*, 31(29), pp. 10481–10493. Available at: https://doi.org/10.1523/JNEUROSCI.6023-10.2011.

Dompierre, Jim P *et al.* (2007) 'Histone deacetylase 6 inhibition compensates for the transport deficit in Huntington's disease by increasing tubulin acetylation.', *The Journal of neuroscience : the official journal of the Society for Neuroscience*, 27(13), pp. 3571–3583. Available at: https://doi.org/10.1523/JNEUROSCI.0037-07.2007.

Dompierre, J. P. *et al.* (2007) 'Histone Deacetylase 6 Inhibition Compensates for the Transport Deficit in Huntington's Disease by Increasing Tubulin Acetylation', *Journal of Neuroscience*, 27(13), pp. 3571–3583. Available at:

https://doi.org/10.1523/JNEUROSCI.0037-07.2007.
Dunn, S. *et al.* (2008) 'Differential trafficking of Kif5c on tyrosinated and detyrosinated microtubules in live cells', *Journal of Cell Science*, 121(7), pp. 1085–1095. Available at: https://doi.org/10.1242/jcs.026492.
Ebneth, A. *et al.* (1998) 'Overexpression of Tau Protein Inhibits Kinesin-dependent Trafficking of Vesicles, Mitochondria, and Endoplasmic Reticulum: Implications for Alzheimer's Disease', *Journal of Cell Biology*, 143(3), pp. 777–794. Available at: https://doi.org/10.1083/jcb.143.3.777.
Eddé, B. *et al.* (1990) 'Posttranslational Glutamylation of α-tubulin', *Science*, 247(4938), pp. 83–85. Available at: https://doi.org/10.1126/science.1967194.
Erck, C. *et al.* (2005) 'A vital role of tubulin-tyrosine-ligase for neuronal organization', *Proceedings of the National Academy of Sciences*, 102(22), pp. 7853–7858. Available at: https://doi.org/10.1073/pnas.0409626102.
Erickson, H.P. (2009) 'Size and Shape of Protein Molecules at the Nanometer Level Determined by Sedimentation, Gel Filtration, and Electron Microscopy', *Biological Procedures Online*, 11(1), pp. 32–51. Available at: https://doi.org/10.1007/s12575-009-9008-x.
Esberg, A. *et al.* (2006) 'Elevated Levels of Two tRNA Species Bypass the Requirement for Elongator Complex in Transcription and Exocytosis', *Molecular Cell*, 24(1), pp. 139–148. Available at: https://doi.org/10.1016/j.molcel.2006.07.031.
Eshun-Wilson, L. *et al.* (2019) 'Effects of α-tubulin acetylation on microtubule structure and stability', *Proceedings of the National Academy of Sciences of the United States of America*, 116(21), pp. 10366–10371. Available at: https://doi.org/10.1073/pnas.1900441116.
Even, A. *et al.* (2019) 'ATAT1-enriched vesicles promote microtubule acetylation via axonal transport', *Science Advances*, 5(12). Available at: https://doi.org/10.1126/sciadv.aax2705.
Even, A. *et al.* (2021) 'ATP-citrate lyase promotes axonal transport across species', *Nature Communications*, 12(1), pp. 1–14. Available at: https://doi.org/10.1038/s41467-021-25786-y.
Falzone, T.L. and Stokin, G.B. (2012) 'Imaging Amyloid Precursor Protein In Vivo: An Axonal Transport Assay', in, pp. 295–303. Available at: https://doi.org/10.1007/978-1-61779-536-7_25.
Fame, R.M., MacDonald, J.L. and Macklis, J.D. (2011) 'Development, specification, and diversity of callosal projection neurons', *Trends in Neurosciences*, 34(1), pp. 41–50. Available at: https://doi.org/10.1016/j.tins.2010.10.002.
Fenlon, L.R., Suárez, R. and Richards, L.J. (2017) 'The anatomy, organisation and development of contralateral callosal projections of the mouse somatosensory cortex', *Brain and Neuroscience Advances*, 1, p. 239821281769488. Available at: https://doi.org/10.1177/2398212817694888.
Fernandez-Gonzalez, A. (2002) 'Purkinje cell degeneration (pcd) Phenotypes Caused by Mutations in the Axotomy-Induced Gene, Nna1', *Science*, 295(5561), pp. 1904–1906. Available at: https://doi.org/10.1126/science.1068912.
Fertuzinhos, S. *et al.* (2022) 'A dominant tubulin mutation causes cerebellar neurodegeneration in a genetic model of tubulinopathy', *Science Advances*, 8(7), pp. 1–17. Available at: https://doi.org/10.1126/sciadv.abf7262.
Fiore, M., Goulas, C. and Pillois, X. (2017) 'A new mutation in TUBB1 associated with

thrombocytopenia confirms that C-terminal part of β1-tubulin plays a role in microtubule assembly', *Clinical Genetics*, 91(6), pp. 924–926. Available at: https://doi.org/10.1111/cge.12879.

Fourniol, F.J. *et al.* (2010) 'Template-free 13-protofilament microtubule–MAP assembly visualized at 8 Å resolution', *Journal of Cell Biology*, 191(3), pp. 463–470. Available at: https://doi.org/10.1083/jcb.201007081.

Franchi, S.A. *et al.* (2018) 'A Method to Culture GABAergic Interneurons Derived from the Medial Ganglionic Eminence', *Frontiers in Cellular Neuroscience*, 11. Available at: https://doi.org/10.3389/fncel.2017.00423.

Friedmann, D.R. *et al.* (2012) 'Structure of the α-tubulin acetyltransferase, αTAT1, and implications for tubulin-specific acetylation', *Proceedings of the National Academy of Sciences*, 109(48), pp. 19655–19660. Available at: https://doi.org/10.1073/pnas.1209357109.

Fu, C. *et al.* (2012) 'GABAergic Interneuron Development and Function Is Modulated by the Tsc1 Gene', *Cerebral Cortex*, 22(9), pp. 2111–2119. Available at: https://doi.org/10.1093/cercor/bhr300.

Fukumitsu, K. *et al.* (2016) 'Mitochondrial fission protein Drp1 regulates mitochondrial transport and dendritic arborization in cerebellar Purkinje cells', *Molecular and Cellular Neuroscience*, 71, pp. 56–65. Available at: https://doi.org/10.1016/j.mcn.2015.12.006.

Gadadhar, S., Bodakuntla, S., *et al.* (2017) 'The tubulin code at a glance', *Journal of Cell Science*, 130(8), pp. 1347–1353. Available at: https://doi.org/10.1242/jcs.199471.

Gadadhar, S., Dadi, H., *et al.* (2017) 'Tubulin glycylation controls primary cilia length', *Journal of Cell Biology*, 216(9), pp. 2701–2713. Available at: https://doi.org/10.1083/jcb.201612050.

Gadadhar, S. *et al.* (2021) 'Tubulin glycylation controls axonemal dynein activity, flagellar beat, and male fertility', *Science*, 371(6525). Available at: https://doi.org/10.1126/science.abd4914.

Gaik, M. *et al.* (2022) 'Elongator and the role of its subcomplexes in human diseases', pp. 4–7. Available at: https://doi.org/10.15252/emmm.202216418.

Garvalov, B.K. *et al.* (2006) 'Luminal particles within cellular microtubules', *The Journal of Cell Biology*, 174(6), pp. 759–765. Available at: https://doi.org/10.1083/jcb.200606074.

Genova, M. *et al.* (2023) 'Tubulin polyglutamylation differentially regulates microtubule-interacting proteins', *The EMBO Journal*, pp. 1–17. Available at: https://doi.org/10.15252/embj.2022112101.

Geyer, E.A. *et al.* (2015) 'A mutation uncouples the tubulin conformational and GTPase cycles, revealing allosteric control of microtubule dynamics', *eLife*, 4. Available at: https://doi.org/10.7554/eLife.10113.

Ghosh, S., Laxmi, T.R. and Chattarji, S. (2013) 'Functional Connectivity from the Amygdala to the Hippocampus Grows Stronger after Stress', *Journal of Neuroscience*, 33(17), pp. 7234–7244. Available at: https://doi.org/10.1523/JNEUROSCI.0638-13.2013.

Gilmore-Hall, S. *et al.* (2019) 'CCP1 promotes mitochondrial fusion and motility to prevent Purkinje cell neuron loss in pcd mice', *Journal of Cell Biology*, 218(1), pp. 206–219. Available at: https://doi.org/10.1083/jcb.201709028.

Gleeson, J.G. *et al.* (1999) 'Doublecortin Is a Microtubule-Associated Protein and Is Expressed Widely by Migrating Neurons', *Neuron*, 23, pp. 257–271.

Godena, V.K. *et al.* (2014) 'Increasing microtubule acetylation rescues axonal transport and locomotor deficits caused by LRRK2 Roc-COR domain mutations', *Nature Communications*, 5, p. 5245. Available at: https://doi.org/10.1038/ncomms6245.

Godin, J.D. *et al.* (2012) 'P27Kip1 Is a Microtubule-Associated Protein that Promotes Microtubule Polymerization during Neuron Migration', *Developmental Cell*, 23(4), pp. 729–744. Available at: https://doi.org/10.1016/j.devcel.2012.08.006.

Godin, J.D. and Nguyen, L. (2014) *Novel functions of core cell cycle regulators in neuronal migration*, *Advances in Experimental Medicine and Biology*. Available at: https://doi.org/10.1007/978-94-7-7687-6_4.

Goedert, M., Eisenberg, D.S. and Crowther, R.A. (2017) 'Propagation of Tau Aggregates and Neurodegeneration', *Annual Review of Neuroscience*, 40(1), pp. 189–210. Available at: https://doi.org/10.1146/annurev-neuro-072116-031153.

Gomes, I.D., Ariyaratne, U. V. and Pflum, M.K.H. (2021) 'HDAC6 Substrate Discovery Using Proteomics-Based Substrate Trapping: HDAC6 Deacetylates PRMT5 to Influence Methyltransferase Activity', *ACS Chemical Biology*, 16(8), pp. 1435–1444. Available at: https://doi.org/10.1021/acschembio.1c00303.

Govindarajan, N. *et al.* (2013) 'Reducing HDAC6 ameliorates cognitive deficits in a mouse model for Alzheimer's disease', *EMBO Molecular Medicine*, 5(1), pp. 52–63. Available at: https://doi.org/10.1002/emmm.201201923.

Grau, M.B. *et al.* (2013) 'Tubulin glycylases and glutamylases have distinct functions in stabilization and motility of ependymal cilia', *Journal of Cell Biology*, 202(3), pp. 441–451. Available at: https://doi.org/10.1083/jcb.201305041.

Greenspan, R.J. (1997) *Fly Pushing: The Theory and Practice of Drosophila genetics*. Cold Sprin. Plain-view, New York.

Greer, C.A. and Shepherd, G.M. (1982) 'Mitral cell degeneration and sensory function in the neurological mutant mouse Purkinje cell degeneration (PCD)', *Brain Research*, 235(1), pp. 156–161. Available at: https://doi.org/10.1016/0006-8993(82)90206-2.

Grove, E.A. *et al.* (1998) 'The hem of the embryonic cerebral cortex is defined by the expression of multiple Wnt genes and is compromised in Gli3-deficient mice', *Development*, 125(12), pp. 2315–2325. Available at: https://doi.org/10.1242/dev.125.12.2315.

Guedes-Dias, P. *et al.* (2019) 'Kinesin-3 Responds to Local Microtubule Dynamics to Target Synaptic Cargo Delivery to the Presynapse', *Current Biology*, 29(2), pp. 268-282.e8. Available at: https://doi.org/10.1016/j.cub.2018.11.065.

Guedes-Dias, P. and Holzbaur, E.L.F. (2019) 'Axonal transport: Driving synaptic function', *Science*, 366(6462). Available at: https://doi.org/10.1126/science.aaw9997.

Gunawardena, S. *et al.* (2003) 'Disruption of axonal transport by loss of huntingtin or expression of pathogenic polyQ proteins in Drosophila', *Neuron*, 40(1), pp. 25–40. Available at: https://doi.org/10.1016/S0896-6273(03)00594-4.

Guo, W. *et al.* (2017) 'HDAC6 inhibition reverses axonal transport defects in motor neurons derived from FUS-ALS patients', *Nature Communications*, 8(1), pp. 1–14. Available at: https://doi.org/10.1038/s41467-017-00911-y.

Gupta, A., Tsai, L.-H. and Wynshaw-Boris, A. (2002) 'Life Is a Journey: a Genetic Look At

Neocortical Development', *Nature Reviews Genetics*, 3(5), pp. 342–355. Available at: https://doi.org/10.1038/nrg799.

Hackney, D.D. (1994) 'Evidence for alternating head catalysis by kinesin during microtubule-stimulated ATP hydrolysis.', *Proceedings of the National Academy of Sciences*, 91(15), pp. 6865–6869. Available at: https://doi.org/10.1073/pnas.91.15.6865.

Hai, Y. and Christianson, D.W. (2016) 'Histone deacetylase 6 structure and molecular basis of catalysis and inhibition', *Nature Chemical Biology*, 12(9), pp. 741–747. Available at: https://doi.org/10.1038/nchembio.2134.

Hall, J.L. and Cowan, N.J. (1985) 'Structural features and restricted expression of a human α-tubulin gene', *Nucleic Acids Research*, 13(1), pp. 207–223. Available at: https://doi.org/10.1093/nar/13.1.207.

Hallak, M.E. *et al.* (1977) 'Release of tyrosine from tyrosinated tubulin. Some common factors that affect this process and the assembly of tubulin', *FEBS Letters*, 73(2), pp. 147–150. Available at: https://doi.org/10.1016/0014-5793(77)80968-X.

Hammond, J.W. *et al.* (2010) 'Posttranslational Modifications of Tubulin and the Polarized Transport of Kinesin-1 in Neurons', *Molecular Biology of the Cell*. Edited by E. Holzbaur, 21(4), pp. 572–583. Available at: https://doi.org/10.1091/mbc.e09-01-0044.

Hardiman, O. *et al.* (2017) 'Amyotrophic lateral sclerosis', *Nature Reviews Disease Primers*, 3(1), p. 17071. Available at: https://doi.org/10.1038/nrdp.2017.71.

Hebebrand, M. *et al.* (2019) 'The mutational and phenotypic spectrum of TUBA1A-associated tubulinopathy', *Orphanet Journal of Rare Diseases*, 14(1), pp. 1–13. Available at: https://doi.org/10.1186/s13023-019-1020-x.

Hempel, C.M., Sugino, K. and Nelson, S.B. (2007) 'A manual method for the purification of fluorescently labeled neurons from the mammalian brain', *Nature Protocols*, 2(11), pp. 2924–2929. Available at: https://doi.org/10.1038/nprot.2007.416.

Henstridge, C.M., Pickett, E. and Spires-Jones, T.L. (2016) 'Synaptic pathology: A shared mechanism in neurological disease', *Ageing Research Reviews*, 28, pp. 72–84. Available at: https://doi.org/10.1016/j.arr.2016.04.005.

Hinckelmann, M.-V. *et al.* (2016) 'Self-propelling vesicles define glycolysis as the minimal energy machinery for neuronal transport', *Nature Communications*, 7, p. 13233. Available at: https://doi.org/10.1038/ncomms13233.

Hinckelmann, M.V. *et al.* (2016) 'Self-propelling vesicles define glycolysis as the minimal energy machinery for neuronal transport', *Nature Communications*, 7. Available at: https://doi.org/10.1038/ncomms13233.

Hitti, F.L. and Siegelbaum, S.A. (2014) 'The hippocampal CA2 region is essential for social memory', *Nature*, 508(1), pp. 88–92. Available at: https://doi.org/10.1038/nature13028.

Howes, S.C. *et al.* (2014) 'Effects of tubulin acetylation and tubulin acetyltransferase binding on microtubule structure.', *Molecular biology of the cell*, 25(2), pp. 257–66. Available at: https://doi.org/10.1091/mbc.E13-07-0387.

Huang, B., Joanhsson, M.J.O. and Byström, A.S. (2005) 'An early step in wobble uridine tRNA modification requires the Elongator complex', *RNA*, 11(4), pp. 424–436. Available at: https://doi.org/10.1261/rna.7247705.

Hubbert, C. *et al.* (2002) 'HDAC6 is a microtubule-associated deacetylase', *Nature*, 417(6887), pp. 455–458. Available at: https://doi.org/10.1038/417455a.

Ichikawa, M. *et al.* (2017) 'Subnanometre-resolution structure of the doublet microtubule

reveals new classes of microtubuleassociated proteins', *Nature Communications*, 8(May), pp. 1–12. Available at: https://doi.org/10.1038/ncomms15035.

Ikegami, K. *et al.* (2007) 'Loss of α-tubulin polyglutamylation in ROSA22 mice is associated with abnormal targeting of KIF1A and modulated synaptic function', *Proceedings of the National Academy of Sciences of the United States of America*, 104(9), pp. 3213–3218. Available at: https://doi.org/10.1073/pnas.0611547104.

Ikegami, K. and Setou, M. (2009) 'TTLL10 can perform tubulin glycylation when co-expressed with TTLL8', *FEBS Letters*, 583(12), pp. 1957–1963. Available at: https://doi.org/10.1016/j.febslet.2009.05.003.

Jablonowski, D. *et al.* (2001) 'Kluyveromyces lactis zymocin mode of action is linked to RNA polymerase II function via Elongator', *Molecular Microbiology*, 42(4), pp. 1095–1105. Available at: https://doi.org/10.1046/j.1365-2958.2001.02705.x.

Jacobson, C., Schnapp, B. and Banker, G.A. (2006) 'A Change in the Selective Translocation of the Kinesin-1 Motor Domain Marks the Initial Specification of the Axon', *Neuron*, 49(6), pp. 797–804. Available at: https://doi.org/10.1016/j.neuron.2006.02.005.

Janke, C. *et al.* (2005) 'Biochemistry: Tubulin polyglutamylase enzymes are members of the TTL domain protein family', *Science*, 308(5729), pp. 1758–1762. Available at: https://doi.org/10.1126/science.1113010.

Janke, C. and Magiera, M.M. (2020) 'The tubulin code and its role in controlling microtubule properties and functions', *Nature Reviews Molecular Cell Biology*, 21(6), pp. 307–326. Available at: https://doi.org/10.1038/s41580-020-0214-3.

Janning, D. *et al.* (2014) 'Single-molecule tracking of tau reveals fast kiss-and-hop interaction with microtubules in living neurons', *Molecular Biology of the Cell*. Edited by J. Lippincott-Schwartz and J. Lippincott-Schwartz, 25(22), pp. 3541–3551. Available at: https://doi.org/10.1091/mbc.e14-06-1099.

Janssens, K. *et al.* (2014) 'Human Rab7 mutation mimics features of Charcot-Marie-Tooth neuropathy type 2B in drosophila', *Neurobiology of Disease*, 65, pp. 211–219. Available at: https://doi.org/10.1016/j.nbd.2014.01.021.

Jiang, N. *et al.* (2017) 'Modeling the effects of lattice defects on microtubule breaking and healing', *Cytoskeleton*, 74(1), pp. 3–17. Available at: https://doi.org/10.1002/cm.21346.

Jiang, Y. *et al.* (2019) 'White matter repair and treatment strategy after intracerebral hemorrhage', *CNS Neuroscience & Therapeutics*, 25(10), pp. 1113–1125. Available at: https://doi.org/10.1111/cns.13226.

Jiang, Y. and Ehlers, M.D. (2013) 'Modeling Autism by SHANK Gene Mutations in Mice', *Neuron*, 78(1), pp. 8–27. Available at: https://doi.org/10.1016/j.neuron.2013.03.016.

Jiménez-Mateos, E.-M. *et al.* (2006) 'Role of MAP1B in axonal retrograde transport of mitochondria', *Biochemical Journal*, 397(1), pp. 53–59. Available at: https://doi.org/10.1042/BJ20060205.

Johansson, M.J.O., Xu, F. and Byström, A.S. (2018) 'Elongator—a tRNA modifying complex that promotes efficient translational decoding', *Biochimica et Biophysica Acta (BBA) - Gene Regulatory Mechanisms*, 1861(4), pp. 401–408. Available at: https://doi.org/10.1016/j.bbagrm.2017.11.006.

Johnson, A.A. *et al.* (2013) 'Increasing Tip60 HAT Levels Rescues Axonal Transport Defects and Associated Behavioral Phenotypes in a Drosophila Alzheimer's Disease Model',

Journal of Neuroscience, 33(17), pp. 7535–7547. Available at: https://doi.org/10.1523/JNEUROSCI.3739-12.2013.

Johnston, D. and Amaral, D.G. (2004) 'Hippocampus', in *The Synaptic Organization of the Brain*. Oxford University Press, pp. 455–498. Available at: https://doi.org/10.1093/acprof:oso/9780195159561.003.0011.

Jurgensen, S. and Castillo, P.E. (2015) 'Selective Dysregulation of Hippocampal Inhibition in the Mouse Lacking Autism Candidate Gene CNTNAP2', *Journal of Neuroscience*, 35(43), pp. 14681–14687. Available at: https://doi.org/10.1523/JNEUROSCI.1666-15.2015.

Kalebic, N., Martinez, C., *et al.* (2013) 'Tubulin Acetyltransferase αTAT1 Destabilizes Microtubules Independently of Its Acetylation Activity', *Molecular and Cellular Biology*, 33(6), pp. 1114–1123. Available at: https://doi.org/10.1128/mcb.01044-12.

Kalebic, N., Sorrentino, S., *et al.* (2013) 'αTAT1 is the major α-tubulin acetyltransferase in mice', *Nature Communications*, 4. Available at: https://doi.org/10.1038/ncomms2962.

Kalinina, E. *et al.* (2007) 'A novel subfamily of mouse cytosolic carboxypeptidases', *The FASEB Journal*, 21(3), pp. 836–850. Available at: https://doi.org/10.1096/fj.06-7329com.

Kalinski, A.L. *et al.* (2019) 'Deacetylation of Miro1 by HDAC6 blocks mitochondrial transport and mediates axon growth inhibition', *Journal of Cell Biology*, 218(6), pp. 1871–1890. Available at: https://doi.org/10.1083/jcb.201702187.

Kapitein, L.C. *et al.* (2010) 'Mixed Microtubules Steer Dynein-Driven Cargo Transport into Dendrites', *Current Biology*, 20(4), pp. 290–299. Available at: https://doi.org/10.1016/j.cub.2009.12.052.

Karlsborn, T. *et al.* (2014) 'Elongator, a conserved complex required for wobble uridine modifications in Eukaryotes', *RNA Biology*, 11(12), pp. 1519–1528. Available at: https://doi.org/10.4161/15476286.2014.992276.

Kasher, P.R. *et al.* (2009) 'Direct evidence for axonal transport defects in a novel mouse model of mutant spastin-induced hereditary spastic paraplegia (HSP) and human HSP patients', *Journal of Neurochemistry*, 110(1), pp. 34–44. Available at: https://doi.org/10.1111/j.1471-4159.2009.06104.x.

Katrukha, E.A. *et al.* (2017) 'Probing cytoskeletal modulation of passive and active intracellular dynamics using nanobody-functionalized quantum dots', *Nature Communications*, 8(1), p. 14772. Available at: https://doi.org/10.1038/ncomms14772.

Kaul, N., Soppina, V. and Verhey, K.J. (2014) 'Effects of α-tubulin K40 acetylation and detyrosination on kinesin-1 motility in a purified system', *Biophysical Journal*, 106(12), pp. 2636–2643. Available at: https://doi.org/10.1016/j.bpj.2014.05.008.

Kellogg, E.H. *et al.* (2018) 'Near-atomic model of microtubule-tau interactions', *Science*, 360(6394), pp. 1242–1246. Available at: https://doi.org/10.1126/science.aat1780.

Khawaja, S., Gundersen, G.G. and Bulinski, J.C. (1988) 'Enhanced stability of microtubules enriched in detyrosinated tubulin is not a direct function of detyrosination level.', *Journal of Cell Biology*, 106(1), pp. 141–149. Available at: https://doi.org/10.1083/jcb.106.1.141.

Khodiyar, V.K. *et al.* (2007) 'A revised nomenclature for the human and rodent α-tubulin gene family', *Genomics*, 90(2), pp. 285–289. Available at: https://doi.org/10.1016/j.ygeno.2007.04.008.

Kim, C. *et al.* (2012) 'HDAC6 Inhibitor Blocks Amyloid Beta-Induced Impairment of Mitochondrial Transport in Hippocampal Neurons', *PLoS ONE*. Edited by S.T. Ferreira, 7(8), p. e42983. Available at: https://doi.org/10.1371/journal.pone.0042983.

Kim, G.W. *et al.* (2013) 'Mice lacking α-tubulin acetyltransferase 1 are viable but display α-tubulin acetylation deficiency and dentate gyrus distortion', *Journal of Biological Chemistry*, 288(28), pp. 20334–20350. Available at: https://doi.org/10.1074/jbc.M113.464792.

Kim, J.-Y. *et al.* (2016) 'HDAC6 Inhibitors Rescued the Defective Axonal Mitochondrial Movement in Motor Neurons Derived from the Induced Pluripotent Stem Cells of Peripheral Neuropathy Patients with HSPB1 Mutation', *Stem Cells International*, 2016, pp. 1–14. Available at: https://doi.org/10.1155/2016/9475981.

Kimura, Y. *et al.* (2010) 'Identification of Tubulin Deglutamylase among Caenorhabditis elegans and Mammalian Cytosolic Carboxypeptidases (CCPs)', *Journal of Biological Chemistry*, 285(30), pp. 22936–22941. Available at: https://doi.org/10.1074/jbc.C110.128280.

Knabbe, J. *et al.* (2018) 'Secretory vesicle trafficking in awake and anaesthetized mice: differential speeds in axons versus synapses', *The Journal of Physiology*, 596(16), pp. 3759–3773. Available at: https://doi.org/10.1113/JP276022.

Knabbe, J., Protzmann, J. and Kuner, T. (2022) 'In Vivo Imaging of Axonal Organelle Transport in the Mouse Brain', in, pp. 95–109. Available at: https://doi.org/10.1007/978-1-0716-1990-2_5.

Kohara, K. *et al.* (2014) 'Cell type-specific genetic and optogenetic tools reveal hippocampal CA2 circuits', *Nature Neuroscience*, 17(2), pp. 269–279. Available at: https://doi.org/10.1038/nn.3614.

Kolaj-Robin, O. and Séraphin, B. (2017) 'Structures and Activities of the Elongator Complex and Its Cofactors', in *Enzymes*, pp. 117–149. Available at: https://doi.org/10.1016/bs.enz.2017.03.001.

Komarova, Y.A. *et al.* (2002) 'Cytoplasmic linker proteins promote microtubule rescue in vivo', *Journal of Cell Biology*, 159(4), pp. 589–599. Available at: https://doi.org/10.1083/jcb.200208058.

Konishi, Y. and Setou, M. (2009) 'Tubulin tyrosination navigates the kinesin-1 motor domain to axons', *Nature Neuroscience*, 12(5), pp. 559–567. Available at: https://doi.org/10.1038/nn.2314.

Konstantinides, N. *et al.* (2018) 'Phenotypic Convergence: Distinct Transcription Factors Regulate Common Terminal Features', *Cell*, 174(3), pp. 622-635.e13. Available at: https://doi.org/10.1016/j.cell.2018.05.021.

Krogan, N.J. and Greenblatt, J.F. (2001) 'Characterization of a Six-Subunit Holo-Elongator Complex Required for the Regulated Expression of a Group of Genes in Saccharomyces cerevisiae', *Molecular and Cellular Biology*, 21(23), pp. 8203–8212. Available at: https://doi.org/10.1128/MCB.21.23.8203-8212.2001.

Kumar, N. and Flavin, M. (1981) 'Preferential action of a brain detyrosinolating carboxypeptidase on polymerized tubulin.', *Journal of Biological Chemistry*,

256(14), pp. 7678–7686. Available at: https://doi.org/10.1016/S0021-9258(19)69014-9.

Kuo, Y.W. *et al.* (2022) 'The force required to remove tubulin from the microtubule lattice by pulling on its α-tubulin C-terminal tail', *Nature Communications*, 13(1). Available at: https://doi.org/10.1038/s41467-022-31069-x.

Kurmangaliyev, Y.Z. *et al.* (2020) 'Transcriptional Programs of Circuit Assembly in the Drosophila Visual System', *Neuron*, 108(6), pp. 1045-1057.e6. Available at: https://doi.org/10.1016/j.neuron.2020.10.006.

L'Hernault, S.W. and Rosenbaum, J.L. (1985) 'Chlamydomonas .alpha.-tubulin is posttranslationally modified by acetylation on the .epsilon.-amino group of a lysine', *Biochemistry*, 24(2), pp. 473–478. Available at: https://doi.org/10.1021/bi00323a034.

Lacroix, B. *et al.* (2010) 'Tubulin polyglutamylation stimulates spastin-mediated microtubule severing', *Journal of Cell Biology*, 189(6), pp. 945–954. Available at: https://doi.org/10.1083/jcb.201001024.

Lacy, E.R. *et al.* (2004) 'p27 binds cyclin–CDK complexes through a sequential mechanism involving binding-induced protein folding', *Nature Structural & Molecular Biology*, 11(4), pp. 358–364. Available at: https://doi.org/10.1038/nsmb746.

Laguesse, S. *et al.* (2015) 'A Dynamic Unfolded Protein Response Contributes to the Control of Cortical Neurogenesis', *Developmental Cell*, 35(5), pp. 553–567. Available at: https://doi.org/10.1016/j.devcel.2015.11.005.

Laguesse, S. *et al.* (2017) 'Loss of Elp3 Impairs the Acetylation and Distribution of Connexin-43 in the Developing Cerebral Cortex', *Frontiers in Cellular Neuroscience*, 11. Available at: https://doi.org/10.3389/fncel.2017.00122.

Landis, S.C. and Mullen, R.J. (1978) 'The development and degeneration of Purkinje cells in pcd mutant mice', *Journal of Comparative Neurology*, 177(1), pp. 125–143. Available at: https://doi.org/10.1002/cne.901770109.

Landskron, L. *et al.* (2022) 'Posttranslational modification of microtubules by the MATCAP detyrosinase', *Science*, 376(6595). Available at: https://doi.org/10.1126/science.abn6020.

Larcher, J.C. *et al.* (1996) 'Interaction of kinesin motor domains with α- and β-tubulin subunits at a tau-independent binding site: Regulation by polyglutamylation', *Journal of Biological Chemistry*, 271(36), pp. 22117–22124. Available at: https://doi.org/10.1074/jbc.271.36.22117.

Latremoliere, A. *et al.* (2018) 'Neuronal-Specific TUBB3 Is Not Required for Normal Neuronal Function but Is Essential for Timely Axon Regeneration', *Cell Reports*, 24(7), pp. 1865-1879.e9. Available at: https://doi.org/10.1016/j.celrep.2018.07.029.

Lazarus, J.E. *et al.* (2013) 'Dynactin Subunit p150Glued Is a Neuron-Specific Anti-Catastrophe Factor', *PLoS Biology*. Edited by D. Pellman, 11(7), p. e1001611. Available at: https://doi.org/10.1371/journal.pbio.1001611.

Leca, I. *et al.* (2020) 'A proteomic survey of microtubule-associated proteins in a R402H TUBA1A mutant mouse', *PLOS Genetics*. Edited by E.A. Bates, 16(11), p. e1009104. Available at: https://doi.org/10.1371/journal.pgen.1009104.

Lecea, L. de, del Ri´o, J. and Soriano, E. (1995) 'Developmental expression of parvalbumin mRNA in the cerebral cortex and hippocampus of the rat', *Molecular Brain Research*, 32(1), pp. 1–13. Available at: https://doi.org/10.1016/0169-328X(95)00056-X.

LeDizet, M. and Piperno, G. (1986) 'Cytoplasmic microtubules containing acetylated alpha-tubulin in Chlamydomonas reinhardtii: spatial arrangement and properties.', *The Journal of Cell Biology*, 103(1), pp. 13–22. Available at: https://doi.org/10.1083/jcb.103.1.13.

LeDizet, M. and Piperno, G. (1987) 'Identification of an acetylation site of Chlamydomonas alpha-tubulin.', *Proceedings of the National Academy of Sciences*, 84(16), pp. 5720–5724. Available at: https://doi.org/10.1073/pnas.84.16.5720.

Lee, E., Lee, J. and Kim, E. (2017) 'Excitation/Inhibition Imbalance in Animal Models of Autism Spectrum Disorders', *Biological Psychiatry*, 81(10), pp. 838–847. Available at: https://doi.org/10.1016/j.biopsych.2016.05.011.

Lee, J. V. *et al.* (2014) 'Akt-dependent metabolic reprogramming regulates tumor cell Histone acetylation', *Cell Metabolism*, 20(2), pp. 306–319. Available at: https://doi.org/10.1016/j.cmet.2014.06.004.

Lee, S.E. *et al.* (2010) 'RGS14 is a natural suppressor of both synaptic plasticity in CA2 neurons and hippocampal-based learning and memory', *Proceedings of the National Academy of Sciences*, 107(39), pp. 16994–16998. Available at: https://doi.org/10.1073/pnas.1005362107.

Lee, S.M. *et al.* (2000) 'A local Wnt-3a signal is required for development of the mammalian hippocampus', *Development*, 127(3), pp. 457–467. Available at: https://doi.org/10.1242/dev.127.3.457.

Lee, W.-C.M., Yoshihara, M. and Littleton, J.T. (2004) 'Cytoplasmic aggregates trap polyglutamine-containing proteins and block axonal transport in a Drosophila model of Huntington's disease', *Proceedings of the National Academy of Sciences*, 101(9), pp. 3224–3229. Available at: https://doi.org/10.1073/pnas.0400243101.

De León Reyes, N.S., Bragg-Gonzalo, L. and Nieto, M. (2020) 'Development and plasticity of the corpus callosum', *Development*, 147(18), pp. 1–15. Available at: https://doi.org/10.1242/dev.189738.

Lessard, D. V. *et al.* (2019) 'Polyglutamylation of tubulin's C-terminal tail controls pausing and motility of kinesin-3 family member KIF1A', *Journal of Biological Chemistry*, 294(16), pp. 6353–6363. Available at: https://doi.org/10.1074/jbc.RA118.005765.

Lévy, J. *et al.* (2021) 'EPHA7 haploinsufficiency is associated with a neurodevelopmental disorder', *Clinical Genetics*, 100(4), pp. 396–404. Available at: https://doi.org/10.1111/cge.14017.

Lewis, S.A., Gu, W. and Cowan, N.J. (1987) 'Free intermingling of mammalian β-tubulin isotypes among functionally distinct microtubules', *Cell*, 49(4), pp. 539–548. Available at: https://doi.org/10.1016/0092-8674(87)90456-9.

Lewis, T.L. *et al.* (2016) 'Progressive Decrease of Mitochondrial Motility during Maturation of Cortical Axons In Vitro and In Vivo', *Current Biology*, 26(19), pp. 2602–2608. Available at: https://doi.org/10.1016/j.cub.2016.07.064.

Li, H. *et al.* (2022) 'Fly Cell Atlas: A single-nucleus transcriptomic atlas of the adult fruit fly', *Science*, 375(6584). Available at: https://doi.org/10.1126/science.abk2432.

Li, J. *et al.* (2020) 'Nna1 gene deficiency triggers Purkinje neuron death by tubulin hyperglutamylation and ER dysfunction', *JCI Insight*, 5(19). Available at: https://doi.org/10.1172/jci.insight.136078.

Li, L. *et al.* (2012) 'MEC-17 deficiency leads to reduced α-tubulin acetylation and impaired

migration of cortical neurons', *Journal of Neuroscience*, 32(37), pp. 12673–12683. Available at: https://doi.org/10.1523/JNEUROSCI.0016-12.2012.

Li, M. *et al.* (2002) 'Acetylation of p53 Inhibits Its Ubiquitination by Mdm2', *Journal of Biological Chemistry*, 277(52), pp. 50607–50611. Available at: https://doi.org/10.1074/jbc.C200578200.

Lim, L. *et al.* (2018) 'Development and Functional Diversification of Cortical Interneurons', *Neuron*, 100(2), pp. 294–313. Available at: https://doi.org/10.1016/j.neuron.2018.10.009.

Liu, N., Xiong, Y., Li, S., *et al.* (2015) 'New HDAC6-mediated deacetylation sites of tubulin in the mouse brain identified by quantitative mass spectrometry', *Scientific Reports*, 5(1), p. 16869. Available at: https://doi.org/10.1038/srep16869.

Liu, N., Xiong, Y., Ren, Y., *et al.* (2015) 'Proteomic Profiling and Functional Characterization of Multiple Post-Translational Modifications of Tubulin', *Journal of Proteome Research*, 14(8), pp. 3292–3304. Available at: https://doi.org/10.1021/acs.jproteome.5b00308.

Long, J.E. *et al.* (2009) 'Dlx1&2 and Mash1 Transcription Factors Control MGE and CGE Patterning and Differentiation through Parallel and Overlapping Pathways', *Cerebral Cortex*, 19(suppl_1), pp. i96–i106. Available at: https://doi.org/10.1093/cercor/bhp045.

Lopes, A.T. *et al.* (2020) 'Spastin depletion increases tubulin polyglutamylation and impairs kinesin-mediated neuronal transport, leading to working and associative memory deficits', *PLoS Biology*, 18(8), pp. 1–29. Available at: https://doi.org/10.1371/journal.pbio.3000820.

Lopresti, P. (2021) 'Hdac6 in diseases of cognition and of neurons', *Cells*, 10(1), pp. 1–15. Available at: https://doi.org/10.3390/cells10010012.

Lundby, A. *et al.* (2012) 'Proteomic Analysis of Lysine Acetylation Sites in Rat Tissues Reveals Organ Specificity and Subcellular Patterns', *Cell Reports*, 2(2), pp. 419–431. Available at: https://doi.org/10.1016/j.celrep.2012.07.006.

Luong, A. *et al.* (2000) 'Molecular Characterization of Human Acetyl-CoA Synthetase, an Enzyme Regulated by Sterol Regulatory Element-binding Proteins', *Journal of Biological Chemistry*, 275(34), pp. 26458–26466. Available at: https://doi.org/10.1074/jbc.M004160200.

Ly, N. *et al.* (2016) 'αtAT1 controls longitudinal spreading of acetylation marks from open microtubules extremities', *Scientific Reports*, 6(July), pp. 1–10. Available at: https://doi.org/10.1038/srep35624.

Ma, M. *et al.* (2019) 'Structure of the Decorated Ciliary Doublet Microtubule', *Cell*, 179(4), pp. 909-922.e12. Available at: https://doi.org/10.1016/j.cell.2019.09.030.

Maas, C. *et al.* (2009) 'Synaptic activation modifies microtubules underlying transport of postsynaptic cargo', *Proceedings of the National Academy of Sciences of the United States of America*, 106(21), pp. 8731–8736. Available at: https://doi.org/10.1073/pnas.0812391106.

Maday, S. *et al.* (2014a) 'Axonal Transport: Cargo-Specific Mechanisms of Motility and Regulation', *Neuron*, 84(2), pp. 292–309. Available at: https://doi.org/10.1016/j.neuron.2014.10.019.

Maday, S. *et al.* (2014b) 'Axonal Transport: Cargo-Specific Mechanisms of Motility and Regulation', *Neuron*, 84(2), pp. 292–309. Available at: https://doi.org/10.1016/j.neuron.2014.10.019.

Magiera, M.M. *et al.* (2018) 'Excessive tubulin polyglutamylation causes neurodegeneration and perturbs neuronal transport', *The EMBO Journal*, 37(23), pp. 1–14. Available at: https://doi.org/10.15252/embj.2018100440.

Mallik, R. *et al.* (2004) 'Cytoplasmic dynein functions as a gear in response to load', *Nature*, 427(6975), pp. 649–652. Available at: https://doi.org/10.1038/nature02293.

Mandelkow, E.-M. *et al.* (2004) 'MARK/PAR1 kinase is a regulator of microtubule-dependent transport in axons', *Journal of Cell Biology*, 167(1), pp. 99–110. Available at: https://doi.org/10.1083/jcb.200401085.

Mandelkow, E. (2003) 'Clogging of axons by tau, inhibition of axonal traffic and starvation of synapses', *Neurobiology of Aging*, 24(8), pp. 1079–1085. Available at: https://doi.org/10.1016/j.neurobiolaging.2003.04.007.

Mangale, V.S. *et al.* (2008) 'Lhx2 Selector Activity Specifies Cortical Identity and Suppresses Hippocampal Organizer Fate', *Science*, 319(5861), pp. 304–309. Available at: https://doi.org/10.1126/science.1151695.

Mao, W. *et al.* (2015) 'Shank1 regulates excitatory synaptic transmission in mouse hippocampal parvalbumin-expressing inhibitory interneurons', *European Journal of Neuroscience*, 41(8), pp. 1025–1035. Available at: https://doi.org/10.1111/ejn.12877.

Marissal, T. *et al.* (2018) 'Restoring wild-type-like CA1 network dynamics and behavior during adulthood in a mouse model of schizophrenia', *Nature Neuroscience*, 21(10), pp. 1412–1420. Available at: https://doi.org/10.1038/s41593-018-0225-y.

Martinez-Losa, M. *et al.* (2018) 'Nav1.1-Overexpressing Interneuron Transplants Restore Brain Rhythms and Cognition in a Mouse Model of Alzheimer's Disease', *Neuron*, 98(1), pp. 75-89.e5. Available at: https://doi.org/10.1016/j.neuron.2018.02.029.

Mayer, C. *et al.* (2018) 'Developmental diversification of cortical inhibitory interneurons', *Nature*, 555(7697), pp. 457–462. Available at: https://doi.org/10.1038/nature25999.

McDermott, C.J. *et al.* (2003) 'Hereditary spastic paraparesis: Disrupted intracellular transport associated with spastin mutation', *Annals of Neurology*, 54(6), pp. 748–759. Available at: https://doi.org/10.1002/ana.10757.

McGurk, L., Berson, A. and Bonini, N.M. (2015) 'Drosophila as an In Vivo Model for Human Neurodegenerative Disease', *Genetics*, 201(2), pp. 377–402. Available at: https://doi.org/10.1534/genetics.115.179457.

McKay, B.E. and Turner, R.W. (2005) 'Physiological and morphological development of the rat cerebellar Purkinje cell', *The Journal of Physiology*, 567(3), pp. 829–850. Available at: https://doi.org/10.1113/jphysiol.2005.089383.

McKay, L.K. and White, J.P. (2021) 'The AMPK/p27Kip1 Pathway as a Novel Target to Promote Autophagy and Resilience in Aged Cells', *Cells*, 10(6), p. 1430. Available at: https://doi.org/10.3390/cells10061430.

McKenney, R.J. *et al.* (2016) 'Tyrosination of α-tubulin controls the initiation of processive dynein–dynactin motility', *The EMBO Journal*, 35(11), pp. 1175–1185. Available at: https://doi.org/10.15252/embj.201593071.

McNally, F.J. and Roll-Mecak, A. (2018) 'Microtubule-severing enzymes: From cellular functions to molecular mechanism', *Journal of Cell Biology*, 217(12), pp. 4057–4069. Available at: https://doi.org/10.1083/jcb.201612104.

Mehlgarten, C. *et al.* (2010) 'Elongator function in tRNA wobble uridine modification is conserved between yeast and plants', *Molecular Microbiology*, 76(5), pp. 1082–

1094. Available at: https://doi.org/10.1111/j.1365-2958.2010.07163.x.
Meira, T. *et al.* (2018) 'A hippocampal circuit linking dorsal CA2 to ventral CA1 critical for social memory dynamics', *Nature Communications*, 9(1), pp. 1–14. Available at: https://doi.org/10.1038/s41467-018-06501-w.
Mi, D. *et al.* (2018) 'Early emergence of cortical interneuron diversity in the mouse embryo', *Science*, 360(6384), pp. 81–85. Available at: https://doi.org/10.1126/science.aar6821.
Millecamps, S. and Julien, J.-P. (2013) 'Axonal transport deficits and neurodegenerative diseases', *Nature Reviews Neuroscience*, 14(3), pp. 161–176. Available at: https://doi.org/10.1038/nrn3380.
Miśkiewicz, K. *et al.* (2011) 'ELP3 Controls Active Zone Morphology by Acetylating the ELKS Family Member Bruchpilot', *Neuron*, 72(5), pp. 776–788. Available at: https://doi.org/10.1016/j.neuron.2011.10.010.
Mitchison, T. and Kirschner, M. (1984) 'Dynamic instability of microtubule growth.', *Nature*, 312(5991), pp. 237–42. Available at: https://doi.org/10.1038/312237a0.
Miyake, Y. *et al.* (2016) 'Structural insights into HDAC6 tubulin deacetylation and its selective inhibition', *Nature Chemical Biology*, 12(9), pp. 748–754. Available at: https://doi.org/10.1038/nchembio.2140.
Mizuno, H., Hirano, T. and Tagawa, Y. (2007) 'Evidence for activity-dependent cortical wiring: Formation of interhemispheric connections in neonatal mouse visual cortex requires projection neuron activity', *Journal of Neuroscience*, 27(25), pp. 6760–6770. Available at: https://doi.org/10.1523/JNEUROSCI.1215-07.2007.
Mizuno, H., Hirano, T. and Tagawa, Y. (2010) 'Pre-synaptic and post-synaptic neuronal activity supports the axon development of callosal projection neurons during different post-natal periods in the mouse cerebral cortex', *European Journal of Neuroscience*, 31(3), pp. 410–424. Available at: https://doi.org/10.1111/j.1460-9568.2009.07070.x.
Moore, S.A. and Iulianella, A. (2021) 'Development of the mammalian cortical hem and its derivatives: The choroid plexus, Cajal-Retzius cells and hippocampus', *Open Biology*, 11(5). Available at: https://doi.org/10.1098/rsob.210042.
Morelli *et al.* (2018) 'p27Kip1 Modulates Axonal Transport by Regulating α-Tubulin Acetyltransferase 1 Stability', *Cell Reports*, 23(8), pp. 2429–2442. Available at: https://doi.org/10.1016/j.celrep.2018.04.083.
Morelli, G. *et al.* (2018) 'p27^{Kip1} Modulates Axonal Transport by Regulating α-Tubulin Acetyltransferase 1 Stability', *Cell Reports*, 23(8). Available at: https://doi.org/10.1016/j.celrep.2018.04.083.
Morley, S.J. *et al.* (2016) 'Acetylated tubulin is essential for touch sensation in mice', *eLife*, 5(DECEMBER2016), p. 25. Available at: https://doi.org/10.7554/eLife.20813.
Mullen, R.J., Eichert, E.M. and Sidman, R.L. (1976) 'Purkinje cell degeneration, a new neurological mutation in the mouse (cerebellar development/cellular pathology in brain/retinal degeneration/behavioral correlates/sperm)', *Genetics*, 73(1), pp. 208–212. Available at: https://doi.org/10.1073/pnas.73.1.208.
Muñoz-Castañeda, R. *et al.* (2018) 'Cytoskeleton stability is essential for the integrity of the cerebellum and its motor- and affective-related behaviors', *Scientific Reports*, 8(1), p. 3072. Available at: https://doi.org/10.1038/s41598-018-21470-2.
Murofushi, H. (1980) 'Purification and Characterization of Tubulin-Tyrosine Ligase from Porcine Brain1', *The Journal of Biochemistry*, 87(3), pp. 979–984. Available at:

https://doi.org/10.1093/oxfordjournals.jbchem.a132828.
Murphy, F. V *et al.* (2004) 'The role of modifications in codon discrimination by tRNALysUUU', *Nature Structural & Molecular Biology*, 11(12), pp. 1186–1191. Available at: https://doi.org/10.1038/nsmb861.
Murray, E.A., Wise, S.P. and Graham, K.S. (2018) 'Representational specializations of the hippocampus in phylogenetic perspective', *Neuroscience Letters*, 680, pp. 4–12. Available at: https://doi.org/10.1016/j.neulet.2017.04.065.
Nakata, T. *et al.* (2011) 'Preferential binding of a kinesin-1 motor to GTP-tubulin-rich microtubules underlies polarized vesicle transport', *Journal of Cell Biology*, 194(2), pp. 245–255. Available at: https://doi.org/10.1083/jcb.201104034.
Nakata, T. and Hirokawa, N. (2003) 'Microtubules provide directional cues for polarized axonal transport through interaction with kinesin motor head', *Journal of Cell Biology*, 162(6), pp. 1045–1055. Available at: https://doi.org/10.1083/jcb.200302175.
Nassif, C., Noveen, A. and Hartenstein, V. (2003) 'Early development of the Drosophila brain: III. The pattern of neuropile founder tracts during the larval period', *Journal of Comparative Neurology*, 455(4), pp. 417–434. Available at: https://doi.org/10.1002/cne.10482.
Neukomm, L.J. and Freeman, M.R. (2014) 'Diverse cellular and molecular modes of axon degeneration', *Trends in Cell Biology*, 24(9), pp. 515–523. Available at: https://doi.org/10.1016/j.tcb.2014.04.003.
Neumann, B. and Hilliard, M.A. (2014) 'Loss of MEC-17 leads to microtubule instability and axonal degeneration', *Cell Reports*, 6(1), pp. 93–103. Available at: https://doi.org/10.1016/j.celrep.2013.12.004.
Nguyen, L. *et al.* (2010) 'Elongator - an emerging role in neurological disorders', *Trends in Molecular Medicine*, 16(1), pp. 1–6. Available at: https://doi.org/10.1016/j.molmed.2009.11.002.
Nieuwenhuis, J. *et al.* (2017) 'Vasohibins encode tubulin detyrosinating activity', *Science*, 358(6369), pp. 1453–1456. Available at: https://doi.org/10.1126/science.aao5676.
Nieuwenhuis, J. and Brummelkamp, T.R. (2019) 'The Tubulin Detyrosination Cycle: Function and Enzymes', *Trends in Cell Biology*, 29(1), pp. 80–92. Available at: https://doi.org/10.1016/j.tcb.2018.08.003.
Nihongaki, Y., Matsubayashi, H.T. and Inoue, T. (2021) 'A molecular trap inside microtubules probes luminal access by soluble proteins', *Nature Chemical Biology*, 17(8), pp. 888–895. Available at: https://doi.org/10.1038/s41589-021-00791-w.
Niven, J.E., Graham, C.M. and Burrows, M. (2008) 'Diversity and Evolution of the Insect Ventral Nerve Cord', *Annual Review of Entomology*, 53(1), pp. 253–271. Available at: https://doi.org/10.1146/annurev.ento.52.110405.091322.
Noguchi, A. *et al.* (2017) 'Juvenile Hippocampal CA2 Region Expresses Aggrecan', *Frontiers in Neuroanatomy*, 11. Available at: https://doi.org/10.3389/fnana.2017.00041.
North, B.J. *et al.* (2003) 'The human Sir2 ortholog, SIRT2, is an NAD+-dependent tubulin deacetylase', *Molecular Cell*, 11(2), pp. 437–444. Available at: https://doi.org/10.1016/S1097-2765(03)00038-8.
O'Gorman, S. (1985) 'Degeneration of thalamic neurons in "Purkinje cell degeneration" mutant mice. II. Cytology of neuron loss', *Journal of Comparative Neurology*, 234(3), pp. 298–316. Available at: https://doi.org/10.1002/cne.902340303.

O'Gorman, S. and Sidman, R.L. (1985) 'Degeneration of thalamic neurons in "Purkinje cell degeneration" mutant mice. I. Distribution of neuron loss', *Journal of Comparative Neurology*, 234(3), pp. 277–297. Available at: https://doi.org/10.1002/cne.902340302.

Okada, Y. *et al.* (2010) 'A role for the elongator complex in zygotic paternal genome demethylation', *Nature*, 463(7280), pp. 554–558. Available at: https://doi.org/10.1038/nature08732.

Okuyama, T. *et al.* (2016) 'Ventral CA1 neurons store social memory', *Science*, 353(6307), pp. 1536–1541. Available at: https://doi.org/10.1126/science.aaf7003.

Özel, M.N. *et al.* (2021) 'Neuronal diversity and convergence in a visual system developmental atlas', *Nature*, 589(7840), pp. 88–95. Available at: https://doi.org/10.1038/s41586-020-2879-3.

Palazzo, A., Ackerman, B. and Gundersen, G.G. (2003) 'Tubulin acetylation and cell motility', *Nature*, 421(6920), pp. 230–230. Available at: https://doi.org/10.1038/421230a.

Panda, D. *et al.* (1994) 'Microtubule dynamics in vitro are regulated by the tubulin isotype composition.', *Proceedings of the National Academy of Sciences*, 91(24), pp. 11358–11362. Available at: https://doi.org/10.1073/pnas.91.24.11358.

Panganiban, G. and Rubenstein, J.L.R. (2002) 'Developmental functions of the Distal-less /Dlx homeobox genes', *Development*, 129(19), pp. 4371–4386. Available at: https://doi.org/10.1242/dev.129.19.4371.

Park, I.Y., Powell, R.T., *et al.* (2016) 'Dual Chromatin and Cytoskeletal Remodeling by SETD2', *Cell*, 166(4), pp. 950–962. Available at: https://doi.org/10.1016/j.cell.2016.07.005.

Park, I.Y., Chowdhury, P., *et al.* (2016) 'Methylated α-tubulin antibodies recognize a new microtubule modification on mitotic microtubules', *mAbs*, 8(8), pp. 1590–1597. Available at: https://doi.org/10.1080/19420862.2016.1228505.

Paturle-Lafanechere, L. *et al.* (1991) 'Characterization of a major brain tubulin variant which cannot be tyrosinated', *Biochemistry*, 30(43), pp. 10523–10528. Available at: https://doi.org/10.1021/bi00107a022.

Peet, D.R., Burroughs, N.J. and Cross, R.A. (2018) 'Kinesin expands and stabilizes the GDP-microtubule lattice', *Nature Nanotechnology*, 13(5), pp. 386–391. Available at: https://doi.org/10.1038/s41565-018-0084-4.

Pelkey, K.A. *et al.* (2017) 'Hippocampal gabaergic inhibitory interneurons', *Physiological Reviews*, 97(4), pp. 1619–1747. Available at: https://doi.org/10.1152/physrev.00007.2017.

Peñagarikano, O. *et al.* (2011) 'Absence of CNTNAP2 Leads to Epilepsy, Neuronal Migration Abnormalities, and Core Autism-Related Deficits', *Cell*, 147(1), pp. 235–246. Available at: https://doi.org/10.1016/j.cell.2011.08.040.

Peris, L. *et al.* (2009) 'Motor-dependent microtubule disassembly driven by tubulin tyrosination', *Journal of Cell Biology*, 185(7), pp. 1159–1166. Available at: https://doi.org/10.1083/jcb.200902142.

Pero, M.E. *et al.* (2021) 'Pathogenic role of delta 2 tubulin in bortezomib-induced peripheral neuropathy', *Proceedings of the National Academy of Sciences*, 118(4). Available at: https://doi.org/10.1073/pnas.2012685118.

Perrimon, N., Pitsouli, C. and Shilo, B.-Z. (2012) 'Signaling Mechanisms Controlling Cell Fate and Embryonic Patterning', *Cold Spring Harbor Perspectives in Biology*, 4(8), pp. a005975–a005975. Available at: https://doi.org/10.1101/cshperspect.a005975.

Pietrocola, F. *et al.* (2015) 'Acetyl coenzyme A: A central metabolite and second messenger', *Cell Metabolism*, 21(6), pp. 805–821. Available at: https://doi.org/10.1016/j.cmet.2015.05.014.

Pilling, A.D. *et al.* (2006) 'Kinesin-1 and Dynein are the primary motors for fast transport of mitochondria in Drosophila motor axons.', *Molecular biology of the cell*, 17(4), pp. 2057–68. Available at: https://doi.org/10.1091/mbc.E05-06-0526.

Piskorowski, R.A. *et al.* (2016) 'Age-Dependent Specific Changes in Area CA2 of the Hippocampus and Social Memory Deficit in a Mouse Model of the 22q11.2 Deletion Syndrome', *Neuron*, 89(1), pp. 163–176. Available at: https://doi.org/10.1016/j.neuron.2015.11.036.

Piskorowski, R.A. and Chevaleyre, V. (2013) 'Delta-opioid receptors mediate unique plasticity onto parvalbumin-expressing interneurons in area CA2 of the hippocampus', *Journal of Neuroscience*, 33(36), pp. 14567–14578. Available at: https://doi.org/10.1523/JNEUROSCI.0649-13.2013.

Planelles-Herrero, V.J. *et al.* (2022) *Elongator stabilizes microtubules to control central spindle asymmetry and polarized trafficking of cell fate determinants*, *Nature Cell Biology*. Springer US. Available at: https://doi.org/10.1038/s41556-022-01020-9.

Portran, D. *et al.* (2017) 'Tubulin acetylation protects long-lived microtubules against mechanical ageing', *Nature Cell Biology*, 19(4), pp. 391–398. Available at: https://doi.org/10.1038/ncb3481.

Prota, A.E. *et al.* (2013) 'Structural basis of tubulin tyrosination by tubulin tyrosine ligase', *Journal of Cell Biology*, 200(3), pp. 259–270. Available at: https://doi.org/10.1083/jcb.201211017.

Pulipparacharuvil, S. *et al.* (2005) 'Drosophila Vps16A is required for trafficking to lysosomes and biogenesis of pigment granules', *Journal of Cell Science*, 118(16), pp. 3663–3673. Available at: https://doi.org/10.1242/jcs.02502.

Qiang, L. *et al.* (2006) 'Tau Protects Microtubules in the Axon from Severing by Katanin', *The Journal of Neuroscience*, 26(12), pp. 3120–3129. Available at: https://doi.org/10.1523/JNEUROSCI.5392-05.2006.

Qiang, L. *et al.* (2018) 'Tau Does Not Stabilize Axonal Microtubules but Rather Enables Them to Have Long Labile Domains', *Current Biology*, 28(13), pp. 2181-2189.e4. Available at: https://doi.org/10.1016/j.cub.2018.05.045.

Qin, J. *et al.* (2020) 'How kinesin-1 utilize the energy of nucleotide: The conformational changes and mechanochemical coupling in the unidirectional motion of kinesin-1', *International Journal of Molecular Sciences*, 21(18), pp. 1–18. Available at: https://doi.org/10.3390/ijms21186977.

Que, L. *et al.* (2021) 'Transcriptional and morphological profiling of parvalbumin interneuron subpopulations in the mouse hippocampus', *Nature Communications*, 12(1). Available at: https://doi.org/10.1038/s41467-020-20328-4.

Radwitz, J. *et al.* (2022) 'Tubb3 expression levels are sensitive to neuronal activity changes and determine microtubule growth and kinesin-mediated transport', *Cellular and Molecular Life Sciences*, 79(11), pp. 1–21. Available at: https://doi.org/10.1007/s00018-022-04607-5.

Ragot, A. *et al.* (2015) 'Genetic deletion of the Histone Deacetylase 6 exacerbates selected behavioral deficits in the R6/1 mouse model for Huntington's disease', *Brain and Behavior*, 5(9). Available at: https://doi.org/10.1002/brb3.361.

Rakic, P. (2009) 'Evolution of the neocortex: a perspective from developmental biology', *Nature Reviews Neuroscience*, 10(10), pp. 724–735. Available at: https://doi.org/10.1038/nrn2719.

Rapino, F. *et al.* (2018) 'Codon-specific translation reprogramming promotes resistance to targeted therapy', *Nature*, 558(7711), pp. 605–609. Available at: https://doi.org/10.1038/s41586-018-0243-7.

Reck-Peterson, S.L. *et al.* (2018) 'The cytoplasmic dynein transport machinery and its many cargoes', *Nature Reviews Molecular Cell Biology*, 19(6), pp. 382–398. Available at: https://doi.org/10.1038/s41580-018-0004-3.

Redeker, V. *et al.* (1994) 'Polyglycylation of Tubulin: a Posttranslational Modification in Axonemal Microtubules', *Science*, 266(5191), pp. 1688–1691. Available at: https://doi.org/10.1126/science.7992051.

Reed, N.A. *et al.* (2006) 'Microtubule Acetylation Promotes Kinesin-1 Binding and Transport', *Current Biology*, 16(21), pp. 2166–2172. Available at: https://doi.org/10.1016/j.cub.2006.09.014.

Regnard, C. *et al.* (2000) 'Polyglutamylation of Nucleosome Assembly Proteins', *Journal of Biological Chemistry*, 275(21), pp. 15969–15976. Available at: https://doi.org/10.1074/jbc.M000045200.

Reid, H.M.O. *et al.* (2021) 'Understanding Changes in Hippocampal Interneurons Subtypes in the Pathogenesis of Alzheimer's Disease: A Systematic Review', *Brain Connectivity*, 11(3), pp. 159–179. Available at: https://doi.org/10.1089/brain.2020.0879.

Reiter, L.T. *et al.* (2001) 'A Systematic Analysis of Human Disease-Associated Gene Sequences In Drosophila melanogaster', *Genome Research*, 11(6), pp. 1114–1125. Available at: https://doi.org/10.1101/gr.169101.

Reiter, L.T. (2001) 'A Systematic Analysis of Human Disease-Associated Gene Sequences In Drosophila melanogaster', *Genome Research*, 11(6), pp. 1114–1125. Available at: https://doi.org/10.1101/gr.169101.

Riley, C.M. and Day, R.L. (1949) 'Central autonomic dysfunction with defective lacrimation; report of five cases.', *Pediatrics*, 3(4), pp. 468–78. Available at: http://www.ncbi.nlm.nih.gov/pubmed/18118947.

Robert, V. *et al.* (2018) 'Hippocampal area CA2: properties and contribution to hippocampal function', *Cell and Tissue Research*, 373(3), pp. 525–540. Available at: https://doi.org/10.1007/s00441-017-2769-7.

Robert, V. *et al.* (2021) 'Local circuit allowing hypothalamic control of hippocampal area CA2 activity and consequences for CA1', *eLife*, 1, p. 2020.09.18.303693. Available at: http://biorxiv.org/content/early/2020/09/18/2020.09.18.303693.abstract.

Rodríguez-Tornos, F.M. *et al.* (2016) 'Cux1 Enables Interhemispheric Connections of Layer II/III Neurons by Regulating Kv1-Dependent Firing', *Neuron*, 89(3), pp. 494–506. Available at: https://doi.org/10.1016/j.neuron.2015.12.020.

Rogowski, K. *et al.* (2009) 'Evolutionary Divergence of Enzymatic Mechanisms for Posttranslational Polyglycylation', *Cell*, 137(6), pp. 1076–1087. Available at: https://doi.org/10.1016/j.cell.2009.05.020.

Rogowski, K. *et al.* (2010) 'A family of protein-deglutamylating enzymes associated with neurodegeneration', *Cell*, 143(4), pp. 564–578. Available at: https://doi.org/10.1016/j.cell.2010.10.014.

Ross, J.L. *et al.* (2006) 'Processive bidirectional motion of dynein–dynactin complexes in vitro',

Nature Cell Biology, 8(6), pp. 562–570. Available at: https://doi.org/10.1038/ncb1421.

Rubin, B.Y. and Anderson, S.L. (2017) 'IKBKAP/ELP1 gene mutations: Mechanisms of familial dysautonomia and gene-targeting therapies', *Application of Clinical Genetics*, 10, pp. 95–103. Available at: https://doi.org/10.2147/TACG.S129638.

Rüdiger, M. *et al.* (1992) 'Class II tubulin, the major brain β tubulin isotype is polyglutamylated on glutamic acid residue 435', *FEBS Letters*, 308(1), pp. 101–105. Available at: https://doi.org/10.1016/0014-5793(92)81061-P.

Rudy, J.W. and Matus-Amat, P. (2005) 'The Ventral Hippocampus Supports a Memory Representation of Context and Contextual Fear Conditioning: Implications for a Unitary Function of the Hippocampus.', *Behavioral Neuroscience*, 119(1), pp. 154–163. Available at: https://doi.org/10.1037/0735-7044.119.1.154.

Ruiz-Cañada, C. and Budnik, V. (2006) 'Introduction on The Use of The Drosophila Embryonic/Larval Neuromuscular Junction as A Model System to Study Synapse Development and Function, and A Brief Summary of Pathfinding and Target Recognition', *International Review of Neurobiology*, 75(06), pp. 1–31. Available at: https://doi.org/10.1016/S0074-7742(06)75001-2.

Russo, A.A. *et al.* (1996) 'Crystal structure of the p27Kip1 cyclin-dependent-kinase inibitor bound to the cyclin A–Cdk2 complex', *Nature*, 382(6589), pp. 325–331. Available at: https://doi.org/10.1038/382325a0.

Saillour, Y. *et al.* (2014) 'Beta tubulin isoforms are not interchangeable for rescuing impaired radial migration due to Tubb3 knockdown', *Human Molecular Genetics*, 23(6), pp. 1516–1526. Available at: https://doi.org/10.1093/hmg/ddt538.

Salvadores, N. *et al.* (2017) 'Axonal Degeneration during Aging and Its Functional Role in Neurodegenerative Disorders', *Frontiers in Neuroscience*, 11. Available at: https://doi.org/10.3389/fnins.2017.00451.

Saunders, H.A.J. *et al.* (2022) 'Acetylated α-tubulin K394 regulates microtubule stability to shape the growth of axon terminals', *Current Biology*, 32(3), pp. 614-630.e5. Available at: https://doi.org/10.1016/j.cub.2021.12.012.

Schacter, D.L. (1997) 'The cognitive neuroscience of memory: perspectives from neuroimaging research', *Philosophical Transactions of the Royal Society of London. Series B: Biological Sciences*, 352(1362), pp. 1689–1695. Available at: https://doi.org/10.1098/rstb.1997.0150.

Schaedel, L. *et al.* (2015) 'Microtubules self-repair in response to mechanical stress', *Nature Materials*, 14(11), pp. 1156–1163. Available at: https://doi.org/10.1038/nmat4396.

Schneider Gasser, E.M. *et al.* (2006) 'Immunofluorescence in brain sections: Simultaneous detection of presynaptic and postsynaptic proteins in identified neurons', *Nature Protocols*, 1(4), pp. 1887–1897. Available at: https://doi.org/10.1038/nprot.2006.265.

Schönfeld, P. and Reiser, G. (2017) 'Brain energy metabolism spurns fatty acids as fuel due to their inherent mitotoxicity and potential capacity to unleash neurodegeneration', *Neurochemistry International*, 109, pp. 68–77. Available at: https://doi.org/10.1016/j.neuint.2017.03.018.

Schönfeld, P. and Reiser, G. (2021) 'How the brain fights fatty acids' toxicity', *Neurochemistry International*, 148(April). Available at: https://doi.org/10.1016/j.neuint.2021.105050.

Schröder, H.C., Wehland, J. and Weber, K. (1985) 'Purification of brain tubulin-tyrosine ligase by biochemical and immunological methods.', *The Journal of Cell Biology*, 100(1), pp. 276–281. Available at: https://doi.org/10.1083/jcb.100.1.276.

Scoville, W.B. and Milner, B. (1957) 'Loss of recent memory after bilateral hippocampal lesions', *Journal of Neurology, Neurosurgery & Psychiatry*, 20(1), pp. 11–21. Available at: https://doi.org/10.1136/jnnp.20.1.11.

Shahpasand, K. *et al.* (2012) 'Regulation of Mitochondrial Transport and Inter-Microtubule Spacing by Tau Phosphorylation at the Sites Hyperphosphorylated in Alzheimer's Disease', *Journal of Neuroscience*, 32(7), pp. 2430–2441. Available at: https://doi.org/10.1523/JNEUROSCI.5927-11.2012.

Shashi, V. *et al.* (2018) 'Loss of tubulin deglutamylase CCP1 causes infantile-onset neurodegeneration', *The EMBO Journal*, 37(23), pp. 1–12. Available at: https://doi.org/10.15252/embj.2018100540.

Shida, T. *et al.* (2010) 'The major α-tubulin K40 acetyltransferase αTAT1 promotes rapid ciliogenesis and efficient mechanosensation', *Proceedings of the National Academy of Sciences*, 107(50), pp. 21517–21522. Available at: https://doi.org/10.1073/pnas.1013728107.

Shilian, M. *et al.* (2022) 'Elongator promotes neuritogenesis via regulation of tau stability through acly activity', *Frontiers in Cell and Developmental Biology*, 10(October), pp. 1–20. Available at: https://doi.org/10.3389/fcell.2022.1015125.

Shima, T. *et al.* (2018) 'Kinesin-binding–triggered conformation switching of microtubules contributes to polarized transport', *Journal of Cell Biology*, 217(12), pp. 4164–4183. Available at: https://doi.org/10.1083/jcb.201711178.

Shin, S.C. *et al.* (2019) 'Structural and Molecular Basis for Katanin-Mediated Severing of Glutamylated Microtubules', *Cell Reports*, 26(5), pp. 1357-1367.e5. Available at: https://doi.org/10.1016/j.celrep.2019.01.020.

Shukla, S. and Tekwani, B.L. (2020) 'Histone Deacetylases Inhibitors in Neurodegenerative Diseases, Neuroprotection and Neuronal Differentiation', *Frontiers in Pharmacology*, 11. Available at: https://doi.org/10.3389/fphar.2020.00537.

Silva, C.G. *et al.* (2018) 'Cell-Intrinsic Control of Interneuron Migration Drives Cortical Morphogenesis', *Cell*, 172(5), pp. 1063-1067.e19. Available at: https://doi.org/10.1016/j.cell.2018.01.031.

Silva, C.G., Peyre, E. and Nguyen, L. (2019) 'Cell migration promotes dynamic cellular interactions to control cerebral cortex morphogenesis', *Nature Reviews Neuroscience* [Preprint]. Available at: https://doi.org/10.1038/s41583-019-0148-y.

Silva, M. *et al.* (2017) 'Cell-Specific α-Tubulin Isotype Regulates Ciliary Microtubule Ultrastructure, Intraflagellar Transport, and Extracellular Vesicle Biology', *Current Biology*, 27(7), pp. 968–980. Available at: https://doi.org/10.1016/j.cub.2017.02.039.

Simões-Pires, C. *et al.* (2013) 'HDAC6 as a target for neurodegenerative diseases: What makes it different from the other HDACs?', *Molecular Neurodegeneration*, 8(1). Available at: https://doi.org/10.1186/1750-1326-8-7.

Simpson, C.L. *et al.* (2009) 'Variants of the elongator protein 3 (ELP3) gene are associated with motor neuron degeneration', *Human Molecular Genetics*, 18(3), pp. 472–481. Available at: https://doi.org/10.1093/hmg/ddn375.

Sirajuddin, M., Rice, L.M. and Vale, R.D. (2014) 'Regulation of microtubule motors by tubulin

isotypes and post-translational modifications', *Nature Cell Biology*, 16(4), pp. 335–344. Available at: https://doi.org/10.1038/ncb2920.

Siudeja, K. *et al.* (2011) 'Impaired Coenzyme A metabolism affects histone and tubulin acetylation in Drosophila and human cell models of pantothenate kinase associated neurodegeneration', *EMBO Molecular Medicine*, 3(12), pp. 755–766. Available at: https://doi.org/10.1002/emmm.201100180.

Sivanand, S., Viney, I. and Wellen, K.E. (2018) 'Spatiotemporal Control of Acetyl-CoA Metabolism in Chromatin Regulation', *Trends in Biochemical Sciences*, 43(1), pp. 61–74. Available at: https://doi.org/10.1016/j.tibs.2017.11.004.

Skultetyova, L. *et al.* (2017) 'Human histone deacetylase 6 shows strong preference for tubulin dimers over assembled microtubules', *Scientific Reports*, 7(1), pp. 1–13. Available at: https://doi.org/10.1038/s41598-017-11739-3.

Slaugenhaupt, S.A. *et al.* (2001) 'Tissue-Specific Expression of a Splicing Mutation in the Gene Causes Familial Dysautonomia', *The American Journal of Human Genetics*, 68(3), pp. 598–605. Available at: https://doi.org/10.1086/318810.

Sleigh, J.N. *et al.* (2019a) 'Axonal transport and neurological disease', *Nature Reviews Neurology*, 15(12), pp. 691–703. Available at: https://doi.org/10.1038/s41582-019-0257-2.

Sleigh, J.N. *et al.* (2019b) 'Axonal transport and neurological disease', *Nature Reviews Neurology*, 15(12), pp. 691–703. Available at: https://doi.org/10.1038/s41582-019-0257-2.

Slepecky, N.B., Henderson, C.G. and Saha, S. (1995) 'Post-translational modifications of tubulin suggest that dynamic microtubules are present in sensory cells and stable microtubules are present in supporting cells of the mammalian cochlea', *Hearing Research*, 91(1–2), pp. 136–147. Available at: https://doi.org/10.1016/0378-5955(95)00184-0.

Small, S.A. *et al.* (2017) 'Endosomal Traffic Jams Represent a Pathogenic Hub and Therapeutic Target in Alzheimer's Disease', *Trends in Neurosciences*, 40(10), pp. 592–602. Available at: https://doi.org/10.1016/j.tins.2017.08.003.

Smirnov, V. *et al.* (2021) 'Novel TTLL5 Variants Associated with Cone-Rod Dystrophy and Early-Onset Severe Retinal Dystrophy', *International Journal of Molecular Sciences*, 22(12), p. 6410. Available at: https://doi.org/10.3390/ijms22126410.

Smith, A.S. *et al.* (2016) 'Targeted activation of the hippocampal CA2 area strongly enhances social memory', *Molecular Psychiatry*, 21(8), pp. 1137–1144. Available at: https://doi.org/10.1038/mp.2015.189.

Sohn, P.D. *et al.* (2016) 'Acetylated tau destabilizes the cytoskeleton in the axon initial segment and is mislocalized to the somatodendritic compartment', *Molecular Neurodegeneration*, 11(1), pp. 1–13. Available at: https://doi.org/10.1186/s13024-016-0109-0.

Solinger, J.A. *et al.* (2010) 'The Caenorhabditis elegans Elongator Complex Regulates Neuronal α-tubulin Acetylation', *PLoS Genetics*. Edited by K. Shen, 6(1), p. e1000820. Available at: https://doi.org/10.1371/journal.pgen.1000820.

Sprick, U. (1995) 'Functional aspects of the involvement of the hippocampus in behavior and memory functions', *Behavioural Brain Research*, 66(1–2), pp. 61–64. Available at: https://doi.org/10.1016/0166-4328(94)00125-Y.

Squire, L.R. and Zola-Morgan, S. (1991) 'The Medial Temporal Lobe Memory System', *Science*, 253(5026), pp. 1380–1386. Available at:

https://doi.org/10.1126/science.1896849.
Srinivas, S. *et al.* (2001) 'Cre reporter strains produced by targeted insertion of EYFP and ECFP into the ROSA26 locus', *BMC Developmental Biology*, 1, pp. 1–8. Available at: https://doi.org/10.1186/1471-213X-1-4.
Stevenson, E.L. and Caldwell, H.K. (2014) 'Lesions to the CA2 region of the hippocampus impair social memory in mice', *European Journal of Neuroscience*, 40(9), pp. 3294–3301. Available at: https://doi.org/10.1111/ejn.12689.
Suárez, R. *et al.* (2014) 'Balanced interhemispheric cortical activity is required for correct targeting of the corpus callosum', *Neuron*, 82(6), pp. 1289–1298. Available at: https://doi.org/10.1016/j.neuron.2014.04.040.
Subramanian, L. and Tole, S. (2009) 'Mechanisms Underlying the Specification, Positional Regulation, and Function of the Cortical Hem', *Cerebral Cortex*, 19(suppl 1), pp. i90–i95. Available at: https://doi.org/10.1093/cercor/bhp031.
Sudo, H. and Baas, P.W. (2010) 'Acetylation of microtubules influences their sensitivity to severing by katanin in neurons and fibroblasts', *Journal of Neuroscience*, 30(21), pp. 7215–7226. Available at: https://doi.org/10.1523/JNEUROSCI.0048-10.2010.
Sultan, K.T., Brown, K.N. and Shi, S.-H. (2013) 'Production and organization of neocortical interneurons', *Frontiers in Cellular Neuroscience*, 7(November), pp. 1–14. Available at: https://doi.org/10.3389/fncel.2013.00221.
Svejstrup, J.Q. (2007) 'Elongator complex: how many roles does it play?', *Current Opinion in Cell Biology*, 19(3), pp. 331–336. Available at: https://doi.org/10.1016/j.ceb.2007.04.005.
Szczesna, E. *et al.* (2022) 'Combinatorial and antagonistic effects of tubulin glutamylation and glycylation on katanin microtubule severing', *Developmental Cell*, 57(21), pp. 2497-2513.e6. Available at: https://doi.org/10.1016/j.devcel.2022.10.003.
Taes, I. *et al.* (2013) 'Hdac6 deletion delays disease progression in the sod1g93a mouse model of als', *Human Molecular Genetics*, 22(9), pp. 1783–1790. Available at: https://doi.org/10.1093/hmg/ddt028.
Takemura, R. *et al.* (1992) 'Increased microtubule stability and alpha tubulin acetylation in cells transfected with microtubule-associated proteins MAP1B , MAP2 or tau', *Journal of Cell Science*, 964, pp. 953–964.
Tanco, S. *et al.* (2015) 'C-terminomics Screen for Natural Substrates of Cytosolic Carboxypeptidase 1 Reveals Processing of Acidic Protein C termini', *Molecular & Cellular Proteomics*, 14(1), pp. 177–190. Available at: https://doi.org/10.1074/mcp.M114.040360.
Tao, C. *et al.* (2017) 'White Matter Injury after Intracerebral Hemorrhage: Pathophysiology and Therapeutic Strategies', *Frontiers in Human Neuroscience*, 11. Available at: https://doi.org/10.3389/fnhum.2017.00422.
Tas, R.P. *et al.* (2017) 'Differentiation between Oppositely Oriented Microtubules Controls Polarized Neuronal Transport', *Neuron*, 96(6), pp. 1264-1271.e5. Available at: https://doi.org/10.1016/j.neuron.2017.11.018.
Ti, S.-C. *et al.* (2016) 'Mutations in Human Tubulin Proximal to the Kinesin-Binding Site Alter Dynamic Instability at Microtubule Plus- and Minus-Ends', *Developmental Cell*, 37(1), pp. 72–84. Available at: https://doi.org/10.1016/j.devcel.2016.03.003.
Tielens, S. *et al.* (2016) 'Elongator controls cortical interneuron migration by regulating actomyosin dynamics', *Cell Research*, 26(10), pp. 1131–1148. Available at:

https://doi.org/10.1038/cr.2016.112.
Tischfield, M.A. *et al.* (2010) 'Human TUBB3 Mutations Perturb Microtubule Dynamics, Kinesin Interactions, and Axon Guidance', *Cell*, 140(1), pp. 74–87. Available at: https://doi.org/10.1016/j.cell.2009.12.011.
Topalidou, I. *et al.* (2012) 'Genetically Separable Functions of the MEC-17 Tubulin Acetyltransferase Affect Microtubule Organization', *Current Biology*, 22(12), pp. 1057–1065. Available at: https://doi.org/10.1016/j.cub.2012.03.066.
Toyoshima, H. and Hunter, T. (1994) 'p27, a novel inhibitor of G1 cyclin-Cdk protein kinase activity, is related to p21', *Cell*, 78(1), pp. 67–74. Available at: https://doi.org/10.1016/0092-8674(94)90573-8.
Tremblay, R., Lee, S. and Rudy, B. (2016) 'GABAergic Interneurons in the Neocortex: From Cellular Properties to Circuits', *Neuron*, 91(2), pp. 260–292. Available at: https://doi.org/10.1016/j.neuron.2016.06.033.
Triarhou, L.C. (1998) 'Rate of neuronal fallout in a transsynaptic cerebellar model', *Brain Research Bulletin*, 47(3), pp. 219–222. Available at: https://doi.org/10.1016/S0361-9230(98)00076-8.
Triclin, S. *et al.* (2021) 'Self-repair protects microtubules from destruction by molecular motors', *Nature Materials*, 20(6), pp. 883–891. Available at: https://doi.org/10.1038/s41563-020-00905-0.
Trinczek, B. *et al.* (1999) 'Tau regulates the attachment/detachment but not the speed of motors in microtubule-dependent transport of single vesicles and organelles', *Journal of Cell Science*, 112(14), pp. 2355–2367. Available at: https://doi.org/10.1242/jcs.112.14.2355.
Tukker, J.J. *et al.* (2013) 'Distinct dendritic arborization and in vivo firing patterns of parvalbumin-expressing basket cells in the hippocampal area CA3', *Journal of Neuroscience*, 33(16), pp. 6809–6825. Available at: https://doi.org/10.1523/JNEUROSCI.5052-12.2013.
Turchetto, S. *et al.* (2022) 'Molecular Analysis of Axonal Transport Dynamics upon Modulation of Microtubule Acetylation', in *Methods in Molecular Biology*, pp. 207–224. Available at: https://doi.org/10.1007/978-1-0716-1990-2_10.
Turchetto, S., Broix, L. and Nguyen, L. (2020a) 'Ex Vivo Recording of Axonal Transport Dynamics on Postnatal Organotypic Cortical Slices', *STAR Protocols*, 1(3), p. 100131. Available at: https://doi.org/10.1016/j.xpro.2020.100131.
Turchetto, S., Broix, L. and Nguyen, L. (2020b) 'Ex Vivo Recording of Axonal Transport Dynamics on Postnatal Organotypic Cortical Slices', *STAR Protocols*, 1(3), p. 100131. Available at: https://doi.org/10.1016/j.xpro.2020.100131.
Urbán, N. and Guillemot, F. (2014) 'Neurogenesis in the embryonic and adult brain: Same regulators, different roles', *Frontiers in Cellular Neuroscience*, 8(NOV), pp. 1–19. Available at: https://doi.org/10.3389/fncel.2014.00396.
Vagnoni, A. and Bullock, S.L. (2016) 'A simple method for imaging axonal transport in aging neurons using the adult Drosophila wing', *Nature Protocols*, 11(9), pp. 1711–1723. Available at: https://doi.org/10.1038/nprot.2016.112.
Valenstein, M.L. and Roll-Mecak, A. (2016) 'Graded Control of Microtubule Severing by Tubulin Glutamylation', *Cell*, 164(5), pp. 911–921. Available at: https://doi.org/10.1016/j.cell.2016.01.019.
Vallee, R.B., McKenney, R.J. and Ori-Mckenney, K.M. (2012) 'Multiple modes of cytoplasmic dynein regulation', *Nature Cell Biology*, 14(3), pp. 224–230. Available at:

https://doi.org/10.1038/ncb2420.
Varga, J.K. *et al.* (2022) 'Structure-based prediction of HDAC6 substrates validated by enzymatic assay reveals determinants of promiscuity and detects new potential substrates', *Scientific Reports*, 12(1), p. 1788. Available at: https://doi.org/10.1038/s41598-022-05681-2.
Vickers, J.C. *et al.* (2009) 'Axonopathy and cytoskeletal disruption in degenerative diseases of the central nervous system', *Brain Research Bulletin*, 80(4–5), pp. 217–223. Available at: https://doi.org/10.1016/j.brainresbull.2009.08.004.
Vossel, K.A. *et al.* (2010) 'Tau Reduction Prevents Aβ-Induced Defects in Axonal Transport', *Science*, 330(6001), pp. 198–198. Available at: https://doi.org/10.1126/science.1194653.
Vu, H.T. *et al.* (2017) 'Increase in α-tubulin modifications in the neuronal processes of hippocampal neurons in both kainic acid-induced epileptic seizure and Alzheimer's disease', *Scientific Reports*, 7(1), p. 40205. Available at: https://doi.org/10.1038/srep40205.
Vulinovic, F. *et al.* (2018) 'Motor protein binding and mitochondrial transport are altered by pathogenic TUBB4A variants', *Human Mutation*, 39(12), pp. 1901–1915. Available at: https://doi.org/10.1002/humu.23602.
Walczak, C.E. and Shaw, S.L. (2010) 'A MAP for Bundling Microtubules', *Cell*, 142(3), pp. 364–367. Available at: https://doi.org/10.1016/j.cell.2010.07.023.
Walker, J. *et al.* (2011) 'Role of Elongator Subunit Elp3 in Drosophila melanogaster Larval Development and Immunity', *Genetics*, 187(4), pp. 1067–1075. Available at: https://doi.org/10.1534/genetics.110.123893.
Walter, W.J. *et al.* (2012) 'Tubulin Acetylation alone does not affect kinesin-1 velocity and run length in vitro', *PLoS ONE*, 7(8), pp. 1–5. Available at: https://doi.org/10.1371/journal.pone.0042218.
Wamsley, B. and Fishell, G. (2017) 'Genetic and activity-dependent mechanisms underlying interneuron diversity', *Nature Reviews Neuroscience*, 18(5), pp. 299–309. Available at: https://doi.org/10.1038/nrn.2017.30.
Wang, C.L. *et al.* (2007) 'Activity-dependent development of callosal projections in the somatosensory cortex', *Journal of Neuroscience*, 27(42), pp. 11334–11342. Available at: https://doi.org/10.1523/JNEUROSCI.3380-07.2007.
Wang, N. *et al.* (2019) 'Structural basis of tubulin detyrosination by the vasohibin–SVBP enzyme complex', *Nature Structural & Molecular Biology*, 26(7), pp. 571–582. Available at: https://doi.org/10.1038/s41594-019-0241-y.
Wang, Y. *et al.* (2010) 'Dlx5 and Dlx6 Regulate the Development of Parvalbumin-Expressing Cortical Interneurons', *Journal of Neuroscience*, 30(15), pp. 5334–5345. Available at: https://doi.org/10.1523/JNEUROSCI.5963-09.2010.
Wang, Y. *et al.* (2019) 'Alkaline phosphatase-based chromogenic and fluorescence detection method for BaseScope™ In Situ hybridization', *Journal of Histotechnology*, 42(4), pp. 193–201. Available at: https://doi.org/10.1080/01478885.2019.1620906.
Wang, Y. and Mandelkow, E. (2016) 'Tau in physiology and pathology', *Nature Reviews Neuroscience*, 17(1), pp. 22–35. Available at: https://doi.org/10.1038/nrn.2015.1.
Watson, J.A., Fang, M. and Lowenstein, J.M. (1969) 'Tricarballylate and hydroxycitrate: Substrate and inhibitor of ATP: Citrate oxaloacetate lyase', *Archives of Biochemistry and Biophysics*, 135, pp. 209–217. Available at:

https://doi.org/10.1016/0003-9861(69)90532-3.
Webster, D.D.R. and Borisy, G.G. (1989) 'Microtubules are acetylated in domains that turn over slowly', *J. Cell Sci.*, 92(1), pp. 57–65. Available at: http://jcs.biologists.org/content/92/1/57.short.
Webster, D.R. (1990) 'Detyrosination of alpha tubulin does not stabilize microtubules in vivo [published erratum appears in J Cell Biol 1990 Sep;111(3):1325-6]', *The Journal of Cell Biology*, 111(1), pp. 113–122. Available at: https://doi.org/10.1083/jcb.111.1.113.
Wei, D. *et al.* (2018) 'α-Tubulin acetylation restricts axon overbranching by dampening microtubule plus-end dynamics in neurons', *Cerebral Cortex*, 28(9), pp. 3332–3346. Available at: https://doi.org/10.1093/cercor/bhx225.
Weinert, B.T. *et al.* (2011) 'Proteome-Wide Mapping of the Drosophila Acetylome Demonstrates a High Degree of Conservation of Lysine Acetylation', *Science Signaling*, 4(183). Available at: https://doi.org/10.1126/scisignal.2001902.
Wellen, K.E. *et al.* (2009) 'ATP-citrate lyase links cellular metabolism to histone acetylation', *Science*, 324(5930), pp. 1076–1080. Available at: https://doi.org/10.1126/science.1164097.
Winkler, G.S. *et al.* (2002) 'Elongator is a histone H3 and H4 acetyltransferase important for normal histone acetylation levels in vivo', *Proceedings of the National Academy of Sciences*, 99(6), pp. 3517–3522. Available at: https://doi.org/10.1073/pnas.022042899.
Wishart, T.M., Parson, S.H. and Gillingwater, T.H. (2006) 'Synaptic vulnerability in neurodegenerative disease', *Journal of Neuropathology and Experimental Neurology*, 65(8), pp. 733–739. Available at: https://doi.org/10.1097/01.jnen.0000228202.35163.c4.
Wloga, D. *et al.* (2009) 'TTLL3 Is a Tubulin Glycine Ligase that Regulates the Assembly of Cilia', *Developmental Cell*, 16(6), pp. 867–876. Available at: https://doi.org/10.1016/j.devcel.2009.04.008.
Wolff, A. *et al.* (1992) 'Distribution of glutamylated alpha and beta-tubulin in mouse tissues using a specific monoclonal antibody, GT335.', *European journal of cell biology*, 59(2), pp. 425–32. Available at: http://www.ncbi.nlm.nih.gov/pubmed/1493808.
Wu, H.Y. *et al.* (2022) 'TTLL1 and TTLL4 polyglutamylases are required for the neurodegenerative phenotypes in pcd mice', *PLoS Genetics*, 18(4), pp. 1–25. Available at: https://doi.org/10.1371/journal.pgen.1010144.
Xia, L. *et al.* (2000) 'Polyglycylation of Tubulin Is Essential and Affects Cell Motility and Division in Tetrahymena thermophila', *Journal of Cell Biology*, 149(5), pp. 1097–1106. Available at: https://doi.org/10.1083/jcb.149.5.1097.
Xia, P. *et al.* (2014) 'Superresolution imaging reveals structural features of EB1 in microtubule plus-end tracking', *Molecular Biology of the Cell*. Edited by Y. Zheng, 25(25), pp. 4166–4173. Available at: https://doi.org/10.1091/mbc.e14-06-1133.
Xie, X. *et al.* (2021) 'α-TubK40me3 is required for neuronal polarization and migration by promoting microtubule formation', *Nature Communications*, 12(1), pp. 1–16. Available at: https://doi.org/10.1038/s41467-021-24376-2.
Xu, Z. *et al.* (2017) 'Microtubules acquire resistance from mechanical breakage through intralumenal acetylation', *Science*, 356(6335), pp. 328–332. Available at: https://doi.org/10.1126/science.aai8764.

Yan, C. *et al.* (2018) 'Microtubule Acetylation Is Required for Mechanosensation in Drosophila', *Cell Reports*, 25(4), pp. 1051-1065.e6. Available at: https://doi.org/10.1016/j.celrep.2018.09.075.

Yang, R. *et al.* (2019) 'A novel strategy to visualize vesicle-bound kinesins reveals the diversity of kinesin-mediated transport', *Traffic*, 20(11), pp. 851–866. Available at: https://doi.org/10.1111/tra.12692.

Yang, Y. *et al.* (2018) 'Epothilone B Benefits Nigrostriatal Pathway Recovery by Promoting Microtubule Stabilization After Intracerebral Hemorrhage', *Journal of the American Heart Association*, 7(2). Available at: https://doi.org/10.1161/JAHA.117.007626.

Yang, Y. *et al.* (2022) 'MEC17-induced α-tubulin acetylation restores mitochondrial transport function and alleviates axonal injury after intracerebral hemorrhage in mice', *Journal of Neurochemistry*, 160(1), pp. 51–63. Available at: https://doi.org/10.1111/jnc.15493.

Yarian, C. *et al.* (2000) 'Modified Nucleoside Dependent Watson−Crick and Wobble Codon Binding by tRNA Lys UUU Species', *Biochemistry*, 39(44), pp. 13390–13395. Available at: https://doi.org/10.1021/bi001302g.

Yogev, S. *et al.* (2016) 'Microtubule Organization Determines Axonal Transport Dynamics', *Neuron*, 92(2), pp. 449–460. Available at: https://doi.org/10.1016/j.neuron.2016.09.036.

Zaidi, N., Swinnen, J. V. and Smans, K. (2012) 'ATP-Citrate Lyase: A Key Player in Cancer Metabolism', *Cancer Research*, 72(15), pp. 3709–3714. Available at: https://doi.org/10.1158/0008-5472.CAN-11-4112.

Zala, D., Hinckelmann, M.-V. and Saudou, F. (2013) 'Huntingtin's function in axonal transport is conserved in Drosophila melanogaster.', *PloS one*, 8(3), p. e60162. Available at: https://doi.org/10.1371/journal.pone.0060162.

Zeisel, A. *et al.* (2015) 'Cell types in the mouse cortex and hippocampus revealed by single-cell RNA-seq', *Science*, 347(6226), pp. 1138–1142. Available at: https://doi.org/10.1126/science.aaa1934.

Zhang, Y. *et al.* (2014) 'An RNA-sequencing transcriptome and splicing database of glia, neurons, and vascular cells of the cerebral cortex', *Journal of Neuroscience*, 34(36), pp. 11929–11947. Available at: https://doi.org/10.1523/JNEUROSCI.1860-14.2014.

Zhang, Y.Q., Rodesch, C.K. and Broadie, K. (2002) 'Living synaptic vesicle marker: Synaptotagmin-GFP', *Genesis*, 34(1–2), pp. 142–145. Available at: https://doi.org/10.1002/gene.10144.

Zhao, M. *et al.* (2007) 'Synaptic Plasticity (and the Lack Thereof) in Hippocampal CA2 Neurons', *Journal of Neuroscience*, 27(44), pp. 12025–12032. Available at: https://doi.org/10.1523/JNEUROSCI.4094-07.2007.

Zhou, L. *et al.* (2022) 'Nna1, Essential for Purkinje Cell Survival, Is also Associated with Emotion and Memory', *International Journal of Molecular Sciences*, 23(21), p. 12961. Available at: https://doi.org/10.3390/ijms232112961.

ANNEX

1. Side project – Cortico-cortical projections in CCP1 cKO mice

1.1 Context of the experiments

We have previously demonstrated in our lab that loss of CCP1 in post-mitotic cortical INs (cINs) alters their mode of migration and results in an increased invasion of the cortex by migrating cINs in CCP1 cKO mice (Silva *et al.*, 2018). Although the increase in cINs is regulated by P8, migrating cINs crosstalk with the Tbr2+ intermediate progenitors of the cortex and stimulate their proliferation, thereby regulating the output of upper layer PNs (Silva *et al.*, 2018). However, it remains unclear whether the supernumerary layer 2-3 neurons develop a normal pattern of projections. In addition, several studies have shown that during perinatal critical periods, neuronal activity shapes callosal projections (Mizuno, Hirano and Tagawa, 2007, 2010; Wang *et al.*, 2007; Suárez *et al.*, 2014; Rodríguez-Tornos *et al.*, 2016). This raises the possibility that alterations in the microcircuits of CCP1 cKO mice could alter the development and refinement of callosal projections.

We therefore studied the anatomy of callosal projections at P7 and P21, which represent two critical developmental stages. At P7 callosal projections begin to invade the cortex and it is therefore an ideal time point to highlight any delay in corpus callosum development (Fame, MacDonald and Macklis, 2011; Fenlon, Suárez and Richards, 2017). By P21, excessive callosal projections have been refined and resemble adult PN projections, therefore constituting an optimal timepoint to assess whether cortico-cortical projections developed as expected (Fame, MacDonald and Macklis, 2011; Fenlon, Suárez and Richards, 2017).

1.2 Results

To analyze the callosal projections of upper layer PNs, we electroporated the cortex of WT and CCP1 cKO mice at E15.5, a time-point at which radial glial progenitors are committed to the generation of upper-layer pyramidal neurons that mostly project to the contralateral cortex via the corpus callosum (De León Reyes, Bragg-Gonzalo and Nieto, 2020). Mice were electroporated with plasmids expressing membrane-tagged fluorescent proteins for optimal visualization of axons. Since layer 2-3 projection neurons mostly project to contralateral homotypic regions, we measured the fluorescence intensity of contralateral projections from

the pia to the corpus callosum and normalized to the fluorescence of the homotypic ipsilateral layer 2/3 (L2/3) neurons to account for variability in the electroporation efficiency (e.g. fluorescence intensity).

We found no difference in contralateral projections at P7 in CCP1 cKO as compared to WT mice, suggesting that callosal projections develop normally until this time point despite the increase in L2/3 neurons (**Figure 39**). Since the fluorescence of contralateral projections is normalized to the ipsilateral electroporation site, only a change in the pattern of projection would be detected but not necessarily an increase in the number of L2/3 neurons projecting to the contralateral cortex.

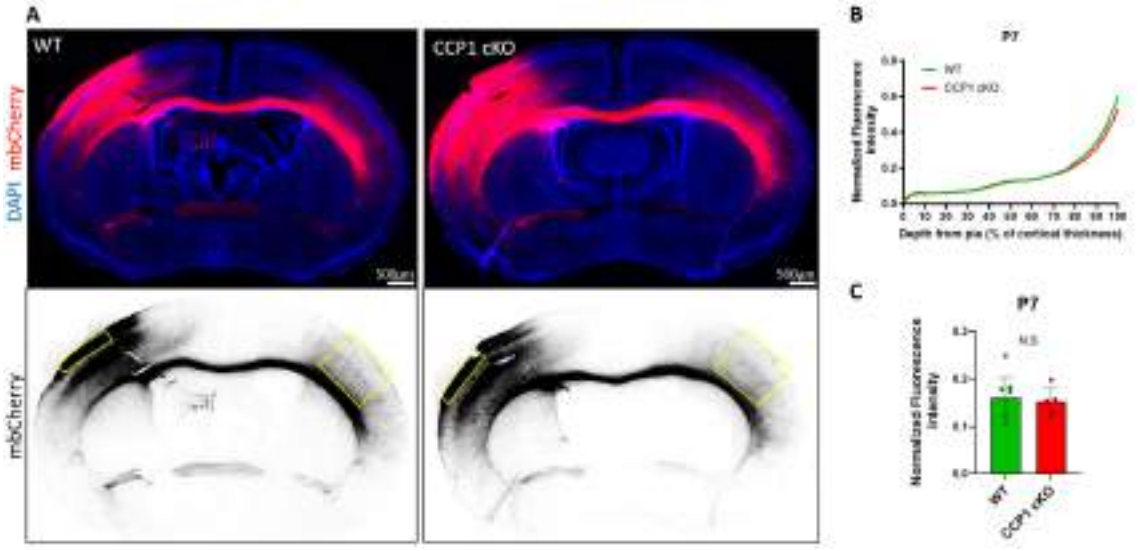

Figure 39: Cortico-cortical projections are unaltered in P7 CCP1 cKO mice.
A. Cortico-cortical axonal projections were labelled by in utero electroporation of mbCherry in the cortex of E15.5 WT or CCP1 cKO mice. On these representative images, mbCherry electroporated neurons (left hemisphere) project through the corpus callosum and send axonal projections in the contralateral cortex (right hemisphere).
B. The fluorescence intensity of mbCherry signal in the contralateral cortex was measured in a region showed by a yellow rectangle in panel (A). The fluorescence intensity was then normalized to the fluorescence intensity of the electroporated cells in the ipsilateral cortex to account for electroporation variability. The graph represents the average profile of fluorescence intensity of all animals analyzed, from the pia to corpus callosum.
C. The average normalized fluorescence intensity of the region shown in the yellow rectangle of panel (B) was measured and compared between WT and CCP1 cKO animals. nWT = 9, ncKO = 5. Unpaired t-student test, p = 0.7163.

At P21, callosal projections have acquired the adult pattern of connectivity and several tracts with dense projections can be visualized in the contralateral cortex. We analyzed the normalized fluorescence intensity of the medial and lateral tracts in the frontal brain and found a significant decrease for the former but not the latter in CCP1 cKO mice (**Figure 40**). We found a similar pattern of altered projections in a more caudal region of the brain of CCP1 cKO mice (**Figure 41**). These results suggest a putative disruption of callosal projection development or refinement. Since we found that PV INs are hyperglutamylated and inhibitory synapses are reduced in the CA2 region of the hippocampus, we hypothesize that similar mechanisms are at play in the cortex where a disruption in microcircuits could alter neuronal activity in the critical period of callosal projection refinement. We have not yet performed experiments to test this hypothesis and this remains an ongoing project in the lab.

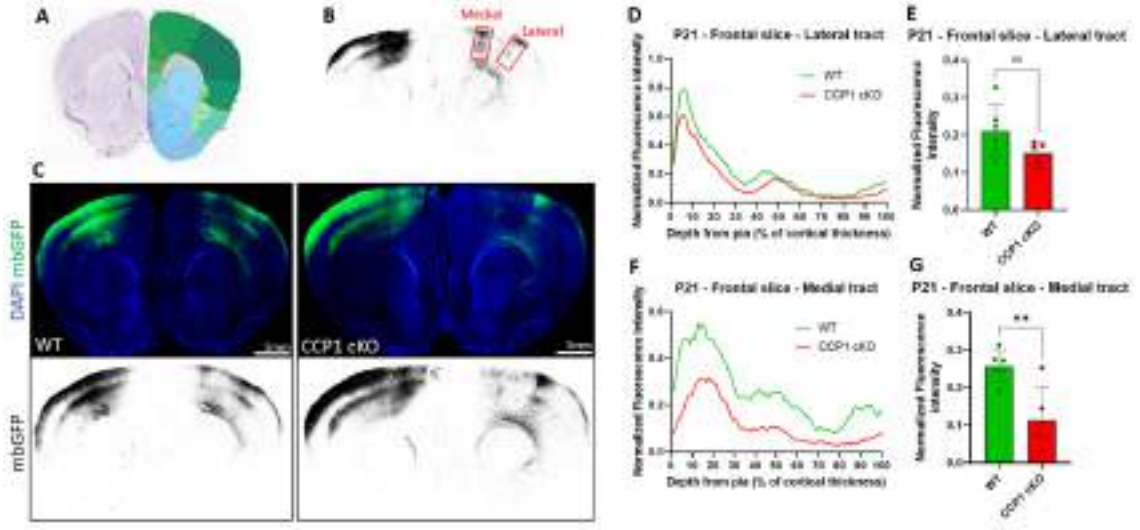

Figure 40: Cortico-cortical projections are reduced in the frontal brain of CCP1 cKO P21 mice.
A. Coronal slice from Allen Brain Atlas showing the rostro-caudal level considered in this analysis.
B. Coronal slice of a P21 brain electroporated with mbGFP at E15.5. The ispsilateral electroporation site is on the left in which layer 2-3 electroporated neurons project through the corpus callosum to the contralateral cortex (on the right). Two prominent projection tracts are visible and marked with with red boxes, the medial tract and the lateral tract that mainly project to the motor and the somatosensory cortex, respectively.
C. Representative images of WT and CCP1 cKO P21 coronal slices electroporated with mbGFP at E15.5. Contralateral projections are visible in the hemisphere on the right.
D and F. The fluorescence intensity of mGFP signal in the contralateral cortex was measured in the lateral tract **(D)** or medial tract **(F)** as shown in panel **(B)**. The fluorescence intensity was then normalized to the fluorescence intensity of the electroporated cells in the homotypic L2/3 of the ipsilateral cortex to account for electroporation variability. The graph represents

the average profile of fluorescence intensity of all animals analyzed, from the pia to corpus callosum.

E and G. The average normalized fluorescence intensity of the lateral tract **(E)** and medial tract **(G)** was measured and compared between WT and CCP1 cKO animals. $n_{WT} = 6$, $n_{cKO} = 5$. Unpaired t-student test, p = 0.1183 for lateral tract, p = 0.0060 for medial tract.

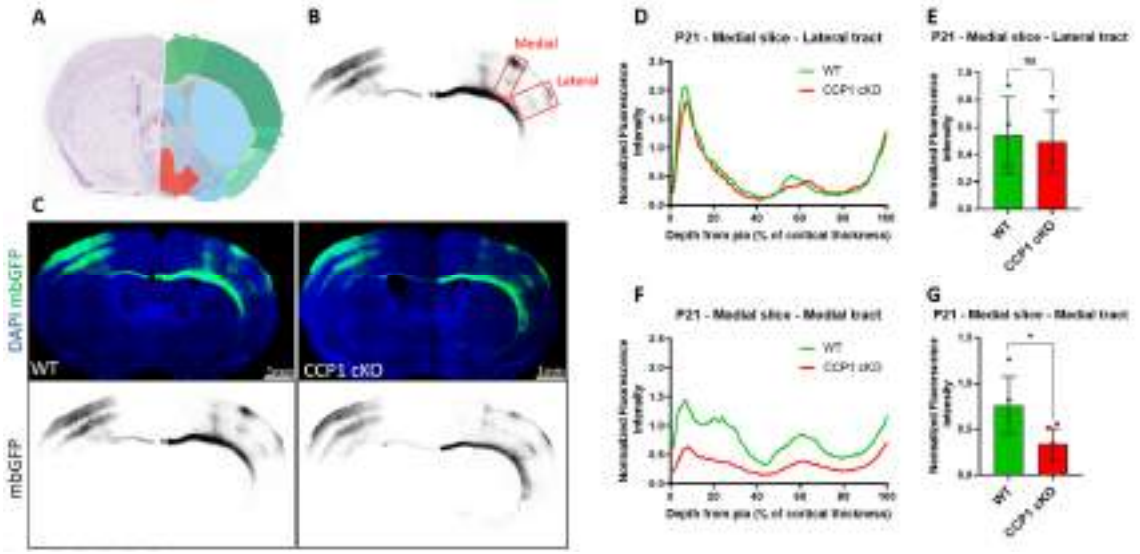

Figure 41: Cortico-cortical projections are reduced in the medial brain of CCP1 cKO P21 mice.

A. Coronal slice from Allen Brain Atlas showing the rostro-caudal level considered in this analysis.

B. Coronal slice of a P21 brain electroporated with mbGFP at E15.5. The ispsilateral electroporation site is on the left in which layer 2-3 electroporated neurons project through the corpus callosum to the contralateral cortex (on the right). Three prominent projection tracts are visible. For this analysis we considered the medial and the lateral tracts (marked by red boxes) since they were consistently present in electroporated animals.

C. Representative images of WT and CCP1 cKO P21 coronal slices electroporated with mbGFP at E15.5. Contralateral projections are visible in the hemisphere on the right.

D and F. The fluorescence intensity of mGFP signal in the contralateral cortex was measured in the lateral tract **(D)** or medial tract **(F)** as shown in panel **(B)**. The fluorescence intensity was then normalized to the fluorescence intensity of the electroporated cells in the homotypic L2/3 of the ipsilateral cortex to account for electroporation variability. The graph represents the average profile of fluorescence intensity of all animals analyzed, from the pia to corpus callosum.

E and G. The average normalized fluorescence intensity of the lateral tract **(E)** and medial tract **(G)** was measured and compared between WT and CCP1 cKO animals. $n_{WT} = 4$, $n_{cKO} = 4$ for lateral tract and $n_{WT} = 5$, $n_{cKO} = 6$. Only animals with robust electroporation in the homotypic L 2-3 of the medial or lateral tracts were included. Unpaired t-student test, p = 0.8134 for lateral tract, p = 0.0183 for medial tract.

To confirm our anatomical observations and understand whether they result in functional changes to cortico-cortical connectivity, we collaborated with the team of Jean-Bernard Manent (INMED Marseille) to probe interhemispheric connectivity by performing electrophysiological recordings on electroporated WT and CCP1 cKO animals. To this end, I co-electroporated WT and CCP1 cKO mice at E15.5 with a membrane-tagged fluorescent protein and Channel Rhodopsin 2 (ChR2), which can be excited with light to induce depolarization of the electroporated cells. The axon terminals of electroporated neurons were stimulated in the contralateral cortex where whole-cell patch clamp of pyramidal cells was performed simultaneously (**Figure 42 A**). A neuron was considered as responsive when a current could be measured following light stimulation (**Figure 42 B**). Interestingly, the proportion of neurons responsive to stimulation of axon terminals was significantly reduced in the medial tract and showed a trend towards a decrease in the lateral tract of CCP1 cKO mice (**Figure 42 C**). These results suggest that the reduction in callosal projections correlates with a decrease in inter-hemispheric connectivity, which may have consequences for behavior.

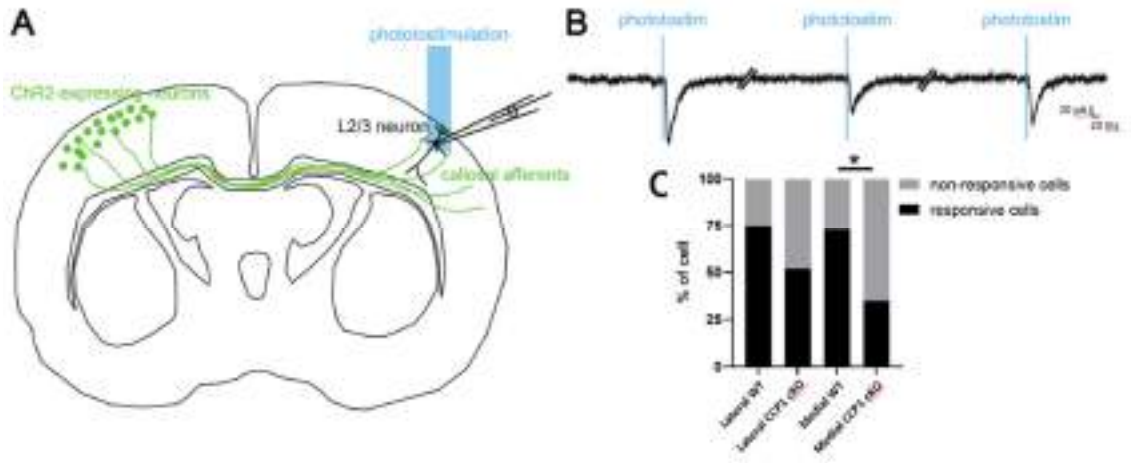

Figure 42: Callosal functional connectivity is altered in CCP1 cKO mice.
A. Schema of a coronal brain slice showing L2/3 neurons (Green) electroporated with Channel Rhodopsin 2 (ChR2) and projecting to homotypic contralateral regions through the corpus callosum. Whole-cell patch clamp of L2/3 contralateral pyramidal neurons was performed and the axon termini of electroporated neurons were photostimulated in the vicinity of the recorded neurons.
B. Representative trace of excitatory post-synaptic currents (EPSCs) evoked by callosal photostimulation (blue lines)
C. Proportion of recorded L2/3 neurons that showed EPSCs in response to photostimulation in the medial and lateral regions of WT and CCP1 cKO contralateral cortexes.

These results are promising and show that non-cell-autonomous alterations in callosal projections arise from CCP1 loss in cINs. Although we cannot yet explain the mechanism by which callosal projection are altered, we hypothesize that it may be due to a disruption of the inhibitory micro-circuitry which may subsequently alter the neuronal activity crucial for the development and refinement of callosal projections. Additional experiments to understand the crosstalk mechanism between cINs and callosal PNs are ongoing in the lab, in addition to an assessment of the behavioral alterations that may arise from disrupted interhemispheric connectivity.

1.3 Material and methods

Animals

The transgenic animals used in these experiments are Dlx5,6 CRE-GFP and CCP1 lox/lox (Muñoz-Castañeda *et al.*, 2018; Silva *et al.*, 2018), as described in **Chapter 1**. WT mice refer to Dlx5,6 $^{CRE\text{-}GFP/+}$ and CCP1 cKO mice are Dlx5,6 $^{CRE\text{-}GFP/+}$; CCP1 $^{lox/lox}$. WT mice control for the expression of CRE and GFP in the Dlx5,6 lineage but have intact CCP1 alleles. Both male and female pups were included in the experiments.

In utero electroporation

Electroporations were performed at E15.5 according to the protocol described in (Turchetto, Broix and Nguyen, 2020b). Briefly, 1µg/µL of mbCherry (for analysis at P7) or mbGFP (for analysis at P21) were injected with a glass capillary (Harvard Apparatus, 30-0016) and a microinjector (Eppendorf, 5252000013) in a single lateral ventricle. Embryos were then electroporated with 5 pulses of 50ms, 1s interval at 50V using bipolar electrodes (Sonidel, CUY650P3) and an electroporator (BTX, ECM 8305).

Immunohistochemistry

Tissue preparation and immunohistochemistry was performed according to the protocol described in the material and methods of **Chapter 1.** The primary antibodies used at P7 and P21 are respectively RFP (1:500, Rabbit, Rockland, 600-401-379) and GFP (1:500, Goat, Abcam, ab6673).

Imaging and analysis

At P7, slices were imaged using an Olympus VS200 slide scanner with a 20x objective. At P21, slices were imaged with Nikon A1R confocal microscope using a 20x objective. A large tile-scan was captured for the full cortex with laser and gain settings specific to each hemisphere in order to avoid over-exposition of the electroporated hemisphere. Although each hemisphere was captured with different settings, the settings remained consistent across individuals to ensure that the ratio of contra/ipsilateral fluorescence was comparable. The distribution of fluorescence intensity in the contralateral cortex was analyzed with Fiji by using the "Plot profile" function. A rectangular selection was made from the pia to the corpus callosum as shown in Figure 1A, Figure 2B and Figure 3B. The width of the rectangle was 1200µm at P7 and 300µm at P21. The Plot profile function bins the rectangle along its length and calculates the average pixel intensity for each bin, therefore generating a distribution of fluorescence intensity in the cortex. The average intensity for each bin was normalized by dividing each value with the mean intensity from the homotypic L2/3 electroporated cortex. Finally, the fluorescence intensity of adjacent bins was averaged to obtain a total of 100 bins for each individual and therefore allow the comparison of fluorescence intensity from the pia to the corpus callosum irrespective of cortical thickness. The average intensity of the full rectangular selection, normalized to the homotypic L2/3 electroporated cortex was used to perform statistical comparison between WT and CCP1 cKO mice.

Optogenetics and electrophysiological recordings

Mice were electroporated at E15.5 with 1µg/µL ChR2-Venus and 1µg/µL mbCherry. Successful electroporation was assessed under a fluorescent binocular at P0 and electroporated pups were sent to the INMED of Marseille at P21 (**Figure 43**).

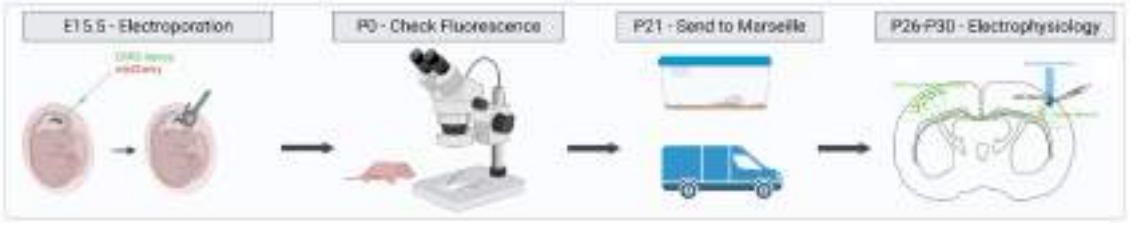

Figure 43: Schematic representation of the workflow for the characterization of functional connectivity
Mice were electroporated with ChR2-Venus and mbCherry at E15.5. Mice that showed fluorescence in the cortex at P0 were sent to the INMED of Marseille at P21. After a recovery

period, electrophysiology experiments were performed by stimulating ChR2 in contralateral axonal termini to measure the response of adjacent PNs. An excitatory post-synaptic current (EPSC) is evoked by light-stimulation if electroporated neurons establish functional synaptic connections with the recorded neuron. This paradigm therefore allows the quantification of interhemispheric functional connectivity between L2/3 PNs.

P28 to P35 mice were deeply anesthetized with tiletamine/zolazepam (Zoletil, 40 mg/kg) and medetomidine (Domitor, 0.6 mg/kg), and decapitated. The brain was then quickly removed and was placed in chilled and oxygenated ACSF containing the following (in mM): 25 NaHCO3, 1.25 NaH2PO4.H2O, 6.3 d-glucose, 2.5 KCl, 7 MgCl2.6H2O, 0.5 CaCl2.2H2O and 132.5 choline chloride. Coronal slices (250-µm-thick) were obtained using a vibrating microtome (Leica Biosystems). During the electrophysiological experiments, the slices were superfused with oxygenated ACSF at a rate of 2 ml/min containing the following (in mM): 126 NaCl, 26 NaHCO3, 1.2 NaH2PO4.H2O, 6.3 d-Glucose, 3.5 KCl, 1.3 MgCl2.6H2O, 2 CaCl2.2H2O. Recordings were amplified using a Multiclamp 700B amplifier (Molecular Devices) and digitized using a Digidata 1440A (Molecular Devices). Patch electrodes (ranging from 6 to 9 MΩ) were filled with intracellular solution containing (in mM): 120 KMeSO4, 10 KCl, 10 HEPES, 8 NaCl, 4 Mg-ATP, 0.3 Na-GTP, and 0.3 Tris-base. The intracellular solution was also supplemented with 5 mM of biocytin to ensure cell localization in the superficial layers. An optoLED system (Cairn Research) consisting of two LEDs was used to visualize fluorescence signals and stimulate ChR2-expressing callosal terminals. A white LED coupled to a TRITC/Cy3 filter cube was used to visualize the ChR2/mCherry-expressing axons. A 470 nm LED coupled to a GFP filter cube was used to activate ChR2-expressing terminals (10 sweeps of 2 x 3 ms-long light pulses with 50 ms interval). Whole-cell patch-clamp recordings of contra lateral or contra medial ChR2-non expressing pyramidal cells were performed in voltage-clamp configuration to test for short delay postsynaptic responses (monosynaptic < 10 ms). Light was delivered using a 40× objective, leading to a light spot size of ~1 mm, avoiding somatic stimulation of ChR2-expressing cells.

2. Molecular Analysis of Axonal Transport Dynamics upon Modulation of Microtubule Acetylation

3. Learning about cell lineage, cellular diversity and evolution of the human brain through stem cell models (Review)